AWARD NUMBER: W81XWH-16-1-0221

TITLE: Treating Duchenne Cardiomyopathy in the Mouse Model by Gene Repair

PRINCIPAL INVESTIGATOR: Dongsheng Duan

CONTRACTING ORGANIZATION: University of Missouri System
Columbia, MO 65211-3020

REPORT DATE: August 2017

TYPE OF REPORT: Annual

PREPARED FOR: U.S. Army Medical Research and Materiel Command
Fort Detrick, Maryland 21702-5012

REPORT DOCUMENTATION PAGE

Form Approved
OMB No. 0704-0188

1. REPORT DATE	**2. REPORT TYPE**	**3. DATES COVERED**
August 2017	Annual	1 Aug 2016 - 31 Jul 2017

4. TITLE AND SUBTITLE: Treating Duchenne Cardiomyopathy in the Mouse Model by Gene Repair

5a. CONTRACT NUMBER

5b. GRANT NUMBER
W81XWH-16-1-0221

5c. PROGRAM ELEMENT NUMBER

6. AUTHOR(S):
Dongsheng Duan, Nalinda Wasala, Yongping Yue, Gary Yao, Charles Gersbach

E-Mail: duand@missouri.edu

5d. PROJECT NUMBER

5e. TASK NUMBER

5f. WORK UNIT NUMBER

7. PERFORMING ORGANIZATION NAME(S) AND ADDRESS(ES)

University of Missouri System
316 University Hall Columbia,
MO 65211-3020

8. PERFORMING ORGANIZATION REPORT NUMBER

9. SPONSORING / MONITORING AGENCY NAME(S) AND ADDRESS(ES)

U.S. Army Medical Research and Materiel Command
Fort Detrick, Maryland 21702-5012

10. SPONSOR/MONITOR'S ACRONYM(S)

11. SPONSOR/MONITOR'S REPORT NUMBER(S)

12. DISTRIBUTION / AVAILABILITY STATEMENT

Approved for Public Release; Distribution Unlimited

13. SUPPLEMENTARY NOTES

14. ABSTRACT: The goal of this project is to test adeno-associated virus (AAV) CRISPR (clustered regularly interspaced palindromic repeat) gene editing therapy for Duchenne cardiomyopathy in the mdx model. In this funding period, we performed AAV CRISPR therapy in young adult mdx mice. We observed widespread dystrophin restoration in the heart on mmunostaining. However, western blot showed only ~5% dystrophin restoration. Nevertheless, we detected persistent gene editing till mice reached 18 months of age. Cardiac histology was not improved. Neither was the blood pumping function. Limited improvement was noticed in some ECG parameters. Surprisingly, mice treated at the young age showed a statistically significant body weight reduction despite the absence of off-target editing in the predicted locations. To determine therapeutic relevance of low-level dystrophin expression, we also examined mdx3cv mice. These mice expressed ~3.3% dystrophin in the heart on western blot. They showed characteristic cardiac pathology and abnormal ECG although their hemodynamic performance was better than dystrophin-null mice. In summary, our results suggest that the low-level dystrophin restoration obtained from the current AAV CRISPR technology is insufficient to substantially improve Duchenne cardiomyopathy. Unexpected weight loss cautions on potential side effects of this therapy. In next funding period, we will explore novel strategies to improve gene-editing efficiency. We will also examine whether weight loss is a real safety concern.

15. SUBJECT TERMS: Duchene muscular dystrophy, DMD, dystrophin, adeno-associated virus, AAV, cardiomyopathy, gene editing, clustered regularly interspaced palindromic repeat (CRISPR), CRISPR-associated endonuclease 9 (Cas9), heart

16. SECURITY CLASSIFICATION OF:			**17. LIMITATION OF ABSTRACT**	**18. NUMBER OF PAGES**	**19a. NAME OF RESPONSIBLE PERSON**
a. REPORT	**b. ABSTRACT**	**c. THIS PAGE**			USAMRMC
U Unclassified	U Unclassified	U Unclassified	UU Unclassified	115	**19b. TELEPHONE NUMBER** *(include area code)*

Standard Form 298 (Rev. 8-98)
Prescribed by ANSI Std. Z39.18

Table of Contents

Page

1. Introduction

Duchenne muscular dystrophy (DMD) is a progressive muscle wasting disease caused by the loss of dystrophin, an essential sub-sarcolemmal cytoskeleton protein in muscle. Repair of the mutated dystrophin gene offers the opportunity to express a near full-length dystrophin protein. We have recently published proof-of-principle data suggesting that gene editing with clustered regularly interspaced palindromic repeat (CRISPR)/ CRISPR-associated endonuclease 9 (Cas9) by adeno-associated virus (AAV) may ameliorate skeletal muscle disease. We now propose to evaluate AAV CRISPR gene therapy to treat DMD-associated cardiomyopathy, a leading cause of morbidity and mortality in DMD patients.

2. Keywords

Duchenne muscular dystrophy, DMD, dystrophin, adeno-associated virus, AAV, cardiomyopathy, gene editing, clustered regularly interspaced palindromic repeat (CRISPR), CRISPR-associated endonuclease 9 (Cas9), heart

3. Accomplishments

Major goal. We have three specific aims. Our first aim is to test if AAV CRISPR therapy can prevent Duchenne cardiomyopathy in neonatal mdx mice. Our second aim is to test if AAV CRISPR therapy can treat early stage Duchenne cardiomyopathy in young adult mdx mice. Our third aim is to test if AAV CRISPR therapy can treat symptomatic late-stage Duchenne cardiomyopathy in aged mdx mice.

Accomplishments.

Aim 1. Our initial plan is to perform systemic AAV CRISPR therapy in newborn mdx mice following the approval of the ACUC protocol and generation of highly pure AAV vectors. Before we perform the comprehensive systemic delivery study, we performed a pilot study. Despite detection of widespread dystrophin positive cells by immunofluorescence staining, the level of expression was fairly low (≤ 5%) on western blot. Our results are in line with these obtained by other groups such as the Chamberlain lab and Wagner lab (personal communication). Currently, it is not clear whether dystrophin expression at such a low level can benefit the heart. To this end, we feel it is necessary to determine whether low-level dystrophin expression in the heart has any protective effect. We have previously shown that mdx3cv mice express ~5% dystrophin in skeletal muscle and this level expression partially improved skeletal muscle function and the lifespan (Li et al, 2008; Li et al, 2010). Since we have these mice in the lab, we opted to evaluate cardiac dystrophin expression and function in these mice. Because mdx mice do not develop dystrophic cardiomyopathy until they reach 21 months of age (Bostick et al, 2008), we focused our study on 21-m-old mdx3cv mice. Since mdx3cv mice are on the C57Bl\6 (BL6) background, we used age and sex-matched BL6 mice as the wild type control. Mdx4cv mice are also on the BL6 background but they do not expression any dystrophin. So we used mdx4cv mice as the negative control. Below we summarize the results from this study.

The heart of aged mdx3cv mice expressed dystrophin at ~3.3% of the wild type level. We first performed dystrophin immunostaining in the heart **(Figure 1A)**. We observed robust, no and very low expression in the heart of BL6, mdx4cv and mdx3cv mice, respectively. To quantify dystrophin expression, we performed whole heart lysate western blot **(Figure 1B)**. Serially diluted BL6 heart lysate was used to show band intensity at 5, 25, 50 and 100% of the wild-type levels **(Figure 1B)**. As

expected, no dystrophin was detected in mdx4cv. Mdx3cv showed a faint band. On quantification, it reached approximately 3.3% of the wild-type level **(Figure 1B)**.

Low dystrophin expression in the mdx3cv heart had minimal impact on the expression of utrophin and components of dystrophin-associated glycoprotein (DGC) complex. We have previously found that the hearts of 21-m-old normal BL10 mice and BL10-background dystrophin-null mdx mice had similar levels of utrophin expression on western blot (Lai et al, 2014). Consistently, there was not much difference in the cardiac utrophin level among aged BL6, mdx3cv and mdx4cv mice **(Figure 1C)**. We also compared the expression level of representative DGC components including β-dystroglycan, α-sarcoglycan, syntrophin and dystrobrevin. Compared to that of the BL6 mouse heart, there appeared a slight reduction of the DGC components in the heart of mdx3cv and mdx4cv mice **(Figure 1C)**.

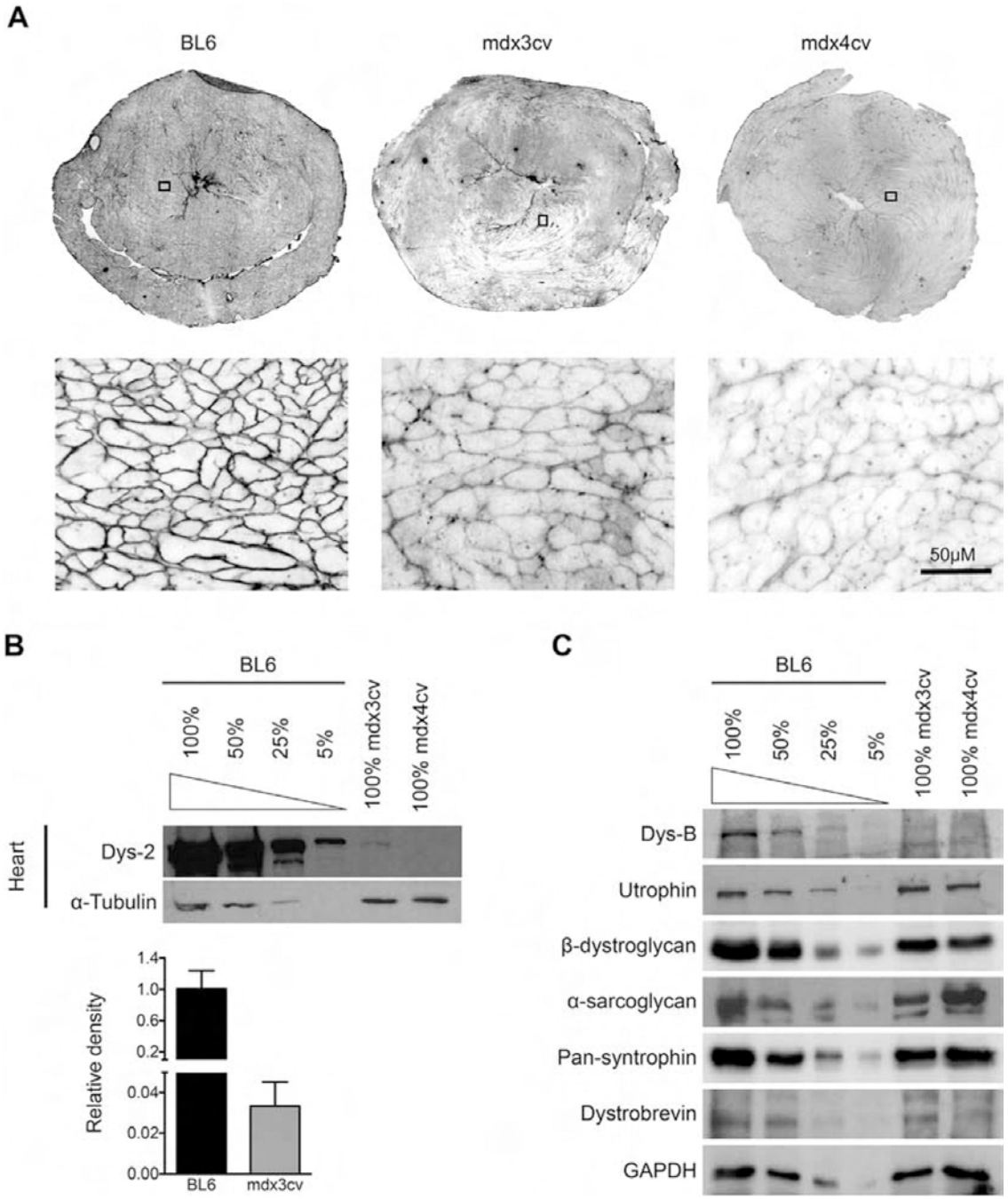

Figure 1. Mdx3cv mouse heart expressed low-level dystrophin. A, Representative photomicrographs of dystrophin immunofluorescence staining in BL6, mdx3cv and mdx4cv heart. Upper panel shows the whole heart view and the lower panel shows a higher magnification of the corresponding boxed region in the whole heart view. **B,** Top panel, Representative heart western blot from BL6, mdx3cv and mdx4cv mice. The BL6 heart lysate was loaded at 100%, 50%, 25% and 5%. The mdx3cv and mdx4cv heart lysate was loaded at 100%; Bottom panel, Densitometry quantification of cardiac dystrophin expression (N=3 for each group). Dys-2, a monoclonal antibody against the dystrophin C-terminal domain. The heart of mdx3cv mice showed uniform dystrophin expression at approximately 3.3% of the wild-type level. **C,** Representative cardiac western blots for utrophin and selected components of dystrophin-associated glycoprotein complex (β-dystroglycan, α-sarcoglycan, syntrophin and dystrobrevin). DysB, a monoclonal antibody against the dystrophin exons 10-12; GAPDH, glyceraldehyde 3-phosphate dehydrogenase.

Low-level dystrophin expression did not improve cardiac histopathology. On HE staining, BL6 mouse heart showed normal morphology **(Figure 2A)**. Some myocardial distortion and mononuclear cell infiltration were noted in both mdx3cv and mdx4cv heart. But there was no apparent difference between these two strains **(Figure 2A)**. Cardiac fibrosis was examined using Masson trichrome staining **(Figure 2B)**. The BL6 heart had no fibrosis. The hearts of mdx3cv and mdx4cv mice showed similar patchy myocardial fibrosis **(Figure 2B)**. Cardiac inflammation was examined by immunohistochemical staining **(Figure 2C)**. Abundant macrophages and neutrophils were detected in the heart of mdx3cv and mdx4cv mice but not BL6 mice **(Figure 2C)**.

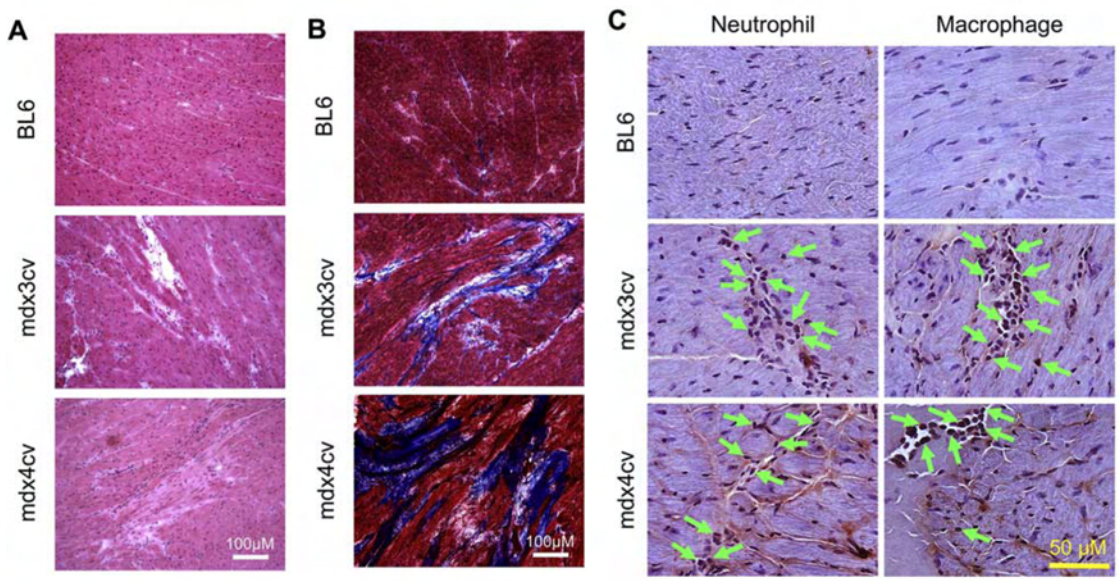

Figure 2. Low-level dystrophin expression did not ameliorate myocardial inflammation and fibrosis in mdx3cv mice. A, Representative heart HE staining photomicrographs from BL6, mdx3cv and mdx4cv mice. **B,** Representative Masson trichrome staining photomicrographs of the BL6, mdx3cv and mdx4cv heart. The blue color in Masson trichrome staining marks myocardial fibrosis. **C,** Representative macrophage and neutrophil immunohistochemical staining photomicrographs of the BL6, mdx3cv and mdx4cv heart. Arrow, dark brown stained macrophages and neutrophils.

The anatomic properties of the heart were similar between mdx3cv and mdx4cv mice. The absolute heart weight (HW) and ventricular weight (VW) were similar between mdx3cv and mdx4cv mice **(Table 1)**. Both were significantly lower than those of BL6 mice. For the tibial length (TL) and anterior tibialis muscle weight (TW) normalized heart weight and ventricular weight (HW/TL, HW/TW, VW/TL and VW/TW), we did not see a difference between mdx3cv and mdx4cv mice. These ratios were all significantly lower than those of BL6 mice **(Table 1)**. The body weight (BW) of BL6 and mdx3cv mice was comparable. However, the BW of mdx4cv mice was significantly reduced **(Table 1)**. Hypertrophy of anterior tibialis muscle was obvious in mdx3cv and mdx4cv mice. Interestingly, the TW of mdx3cv mice was significantly higher than that of mdx4cv mice **(Table 1)**.

Table 1
Anatomical measurements and ratios.

	BL6	mdx3cv	mdx4cv
Sample size (N)	11	28	19
Age (m)	21.67 ± 0.54	21.85 ± 0.33	20.76 ± 0.19
BW (g)	26.78 ± 0.79	27.60 ± 0.37	23.59 ± 0.91[a]
HW (mg)	117.80 ± 3.42	101.99 ± 2.73[b]	101.58 ± 3.22[b]
VW (mg)	111.49 ± 3.25	89.91 ± 2.52[b]	94.32 ± 3.10[b]
TL (mm)	18.51 ± 0.09	18.42 ± 0.08	18.94 ± 0.09[a]
TW (mg)	36.75 ± 1.14[a]	63.14 ± 2.02[a]	55.42 ± 2.32[a]
HW/BW (mg/g)	4.41 ± 0.11	3.71 ± 0.11[a]	4.38 ± 0.16
HW/TL (mg/mm)	6.36 ± 0.17	5.21 ± 0.10[b]	5.17 ± 0.16[b]
HW/TW (mg/g)	3.25 ± 0.16	1.81 ± 0.25[b]	1.89 ± 0.10[b]
VW/TL (mg/mm)	6.02 ± 0.16	4.81 ± 0.11[b]	4.78 ± 0.15[b]
VW/TW (mg/g)	3.08 ± 0.15	1.60 ± 0.23[b]	1.76 ± 0.09[b]

Abbreviations: BW, body weight; HW, heart weight; VW, ventricle weight; TL, tibia length; TW, anterior tibialis muscle weight.
[a] Significantly different from other two groups.
[b] Significantly different from BL6 mice.

Mdx3cv mice showed improved QRS duration. To study cardiac electrophysiology, we performed 12-lead ECG recordings using our published protocol (Bostick et al, 2011b; Wasala et al, 2013). Compared with BL6, mdx4cv showed characteristic dystrophic ECG changes such as tachycardia, PR-interval reduction, QRS duration and QT interval prolongation, and a significant increase in the cardiomyopathy index **(Figure 3)** (Bostick et al, 2011a; Bostick et al, 2012; Bostick et al, 2010; Bostick et al, 2008). Surprisingly, we did not detect a significant change in the amplitude of Q wave among three strains **(Figure 3)**. Compared to those of mdx4cv, several ECG parameters (the heart rate, QT interval and cardiomyopathy index) showed a trend of improvement in mdx3cv mice but did not reach statistical significance. The only ECG parameter that was significantly improved in mdx3cv mice was the QRS duration. It was significantly reduced compared to that of mdx4cv mice **(Figure 3)**.

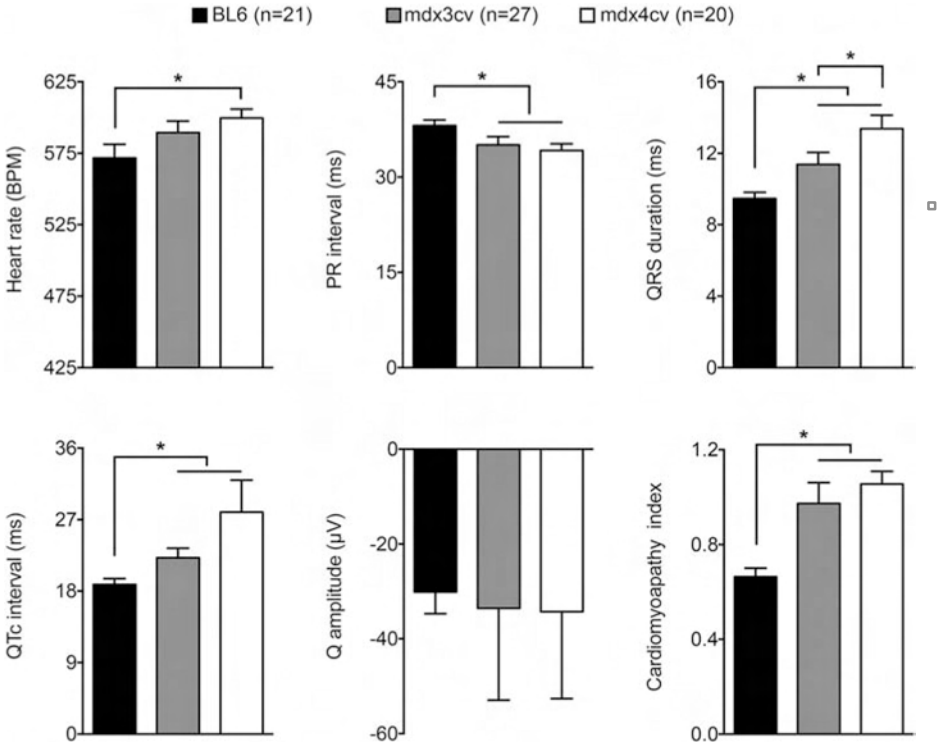

Figure 3. Low-level dystrophin expression improved QRS duration but not other ECG parameters in mdx3cv mice. Quantitative evaluation of the heart rate, PR interval, QRS duration, Mitchell corrected QT interval (QTc), cardiomyopathy index and the Q wave amplitude (Q Amp). Asterisk, statistically significant ($p<0.05$).

Low-level dystrophin in the heart normalized diastolic function in mdx3cv mice. We next examined the pump function of the heart using an ultra-miniature Millar ventricular catheter (Bostick et al, 2011b; Wasala et al, 2013). Compared with BL6, mdx4cv showed the characteristic profile of dilated cardiomyopathy **(Figure 4)**. Specifically, the end-systolic volume was significantly increased **(Figure 4A)**. The end-diastolic volume also showed an apparent increase though not statistically significant **(Figure 4B)**. Cardiac contractility (as reflexed by the maximum pressure, absolute values of dP/dt max and dP/dt min) was significantly reduced. The isovolumic relaxation time constant during diastole (tau) was prolonged **(Figure 4B)**. As a result, the stroke volume, ejection fraction and cardiac output were all significantly decreased in mdx4cv mice **(Figure 4C)**. Low-level dystrophin expression in mdx3cv mice completely normalized diastolic parameters including the end diastolic volume, tau and dP/dt min **(Figure 4B)**. The end systolic volume showed a trend of reduction **(Figure 4A)**. However, overall heart performance (stroke volume, ejection fraction and cardiac output) was not significantly improved in mdx3cv mice.

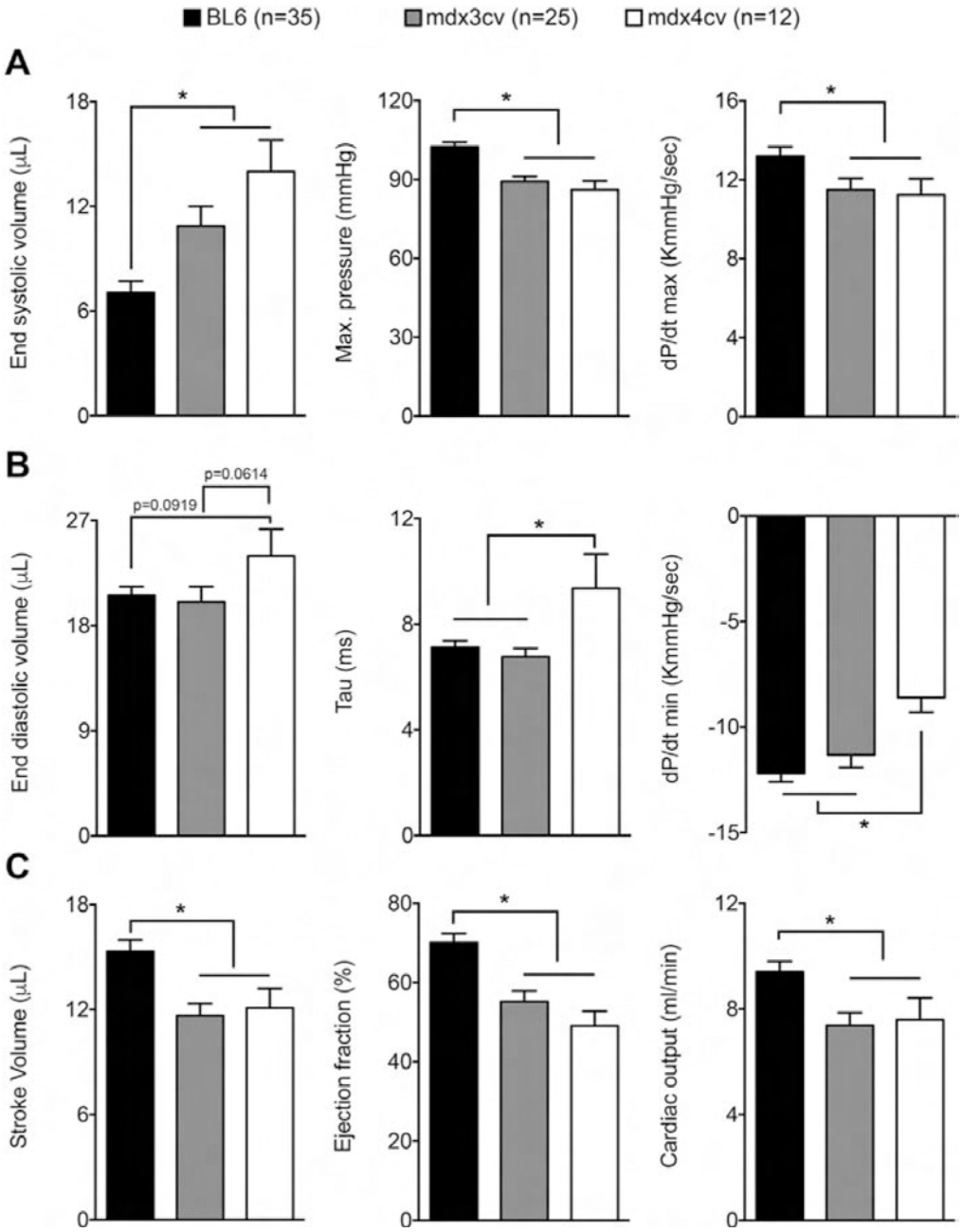

Figure 4. Low-level dystrophin expression partially improved hemodynamics in mdx3cv mice. **A,** Quantitative evaluation of systolic hemodynamic parameters. **B,** Quantitative evaluation of diastolic hemodynamic parameters. End-diastolic volume, tau and dP/dt min were all normalized in mdx3cv mice. **C,** Quantitative evaluation of overall heart function. Asterisk, statistically significant ($p<0.05$). The heart rate at the hemodynamic assay was 616.9± 9.10 bpm, 619.9± 25.5 bpm and 629.3± 8.3 bpm for BL6, mdx3cv and mdx4cv, respectively. There is no statistically significance difference.

In summary, we found that marginal level (approximately 3.3% of the wild-type level) homogenous dystrophin expression in the myocardium of aged mdx3cv mice **(Figure 1)**. This residual level expression did not change the anatomic properties of the heart **(Table 1)**. Neither did it reduce histological lesions in the heart **(Figure 2)**. However, some aspects of heart function measures were significantly improved **(Figures 3 and 4)**. Specifically, the abnormally elongated QRS duration was shortened and deficiencies in diastolic hemodynamics were completely prevented **(Figures 3 and 4)**. Our data suggest that uniform low-level dystrophin expression may have therapeutic implications for preventing and/or treating Duchenne cardiomyopathy. The results from this study are published in **Journal of Molecular and Cellular Cardiology** 102:45-52, **2017** (Wasala et al, 2017).

Aims 2 and 3. Our eventual goal is to treat DMD-associated cardiomyopathy with CRISPR gene editing therapy. Since the vast majority of patients are diagnosed at ages of 3 to 5 years and most of them are likely going to be treated when they are young. In the **aim 2** of our proposal, we plan to treat early stage Duchenne cardiomyopathy in young adult mdx mice with CRISPR/Cas9. The age of young adult mdx mice will be most comparable to the age of human patients that will receive the gene editing therapy. For this reason, we decided to focus our effort in this aim during this funding period.

Many existing DMD patients have reached the terminal stage of their disease course. In the **aim 3** of our proposal, we plan to treat terminal age mdx mice (16-m-old) by tail vein injection. As a prelude to the therapy in very old mice, we opted to do a pilot study in in this funding period to see if CRISPR therapy can be performed in 8-m-old mdx mice. Results from this pilot study will shed light on the design of the study in very old mice. Below we summarize the results from these studies.

A single intravenous injection of the CRISPR editing vectors with AAV-9 resulted in persistent myocardial dystrophin expression in both young and old mdx mice. The mdx mouse carries a nonsense point mutation in exon 23. Removal of the mutated exon restores the reading frame and leads to the production of a near full-length dystrophin protein. We have previously characterized a pair of gRNAs targeting introns 22 and 23 of the mouse dystrophin gene (Nelson et al, 2016). Co-expression of these gRNAs and SaCas9 in young mdx mice resulted in robust genome editing with minimal off-target cutting (Nelson et al, 2016). Since we are interested in studying the cardiac benefits of the CRISPR therapy, we packaged gRNAs and SaCas9 expression cassettes in two vectors in cardiotropic AAV-9. These two vectors were then co-injected intravenously to 6-week-old and 8-month-old mdx mice at the dose of 3.6×10^{12} viral genome (vg) particles per mouse for the gRNA vector and 7.2×10^{12} vg particles per mouse for the SaCas9 vector **(Fig. 5A)**.

One mouse injected at 6 weeks of age was harvested at the age of 8 months to evaluate dystrophin restoration. On immunostaining and western blot, robust dystrophin expression was detected in the heart but not in skeletal muscle **(Fig. 6)**. Remaining experimental subjects were harvested at 18 months of age. Widespread dystrophin expression was found throughout the entire heart cross-section by immunostaining irrespective of the age of the injection **(Fig. 5B, Fig. 7)**. By

western blot, dystrophin reached ~ 5% of the wild type level in the heart in both age groups **(Fig. 5D, Fig. 8)**. Compared to levels in the heart, dystrophin expression in skeletal muscle was low in both age groups although there were substantial individual differences **(Fig. 5C, Fig. 6 and 7)**.

Consistent with the pattern of dystrophin expression, higher levels of AAV genome copy numbers (both gRNA vector and Cas9 vector) were detected in the heart than in skeletal muscle in both age groups **(Fig. 5E, Fig. 9)**. Interestingly, bodywide comparison of the AAV genome copy number showed that there were more AAV vectors at 18 months in mice injected at 8 months of age compared to mice treated at 6 weeks of age. In several tissues, the difference reached statistical significance **(Fig. 5E, Fig. 9)**. Similarly, mice injected at 8 months appeared to have more Cas9 in the heart by western blot **(Fig. 5D)**.

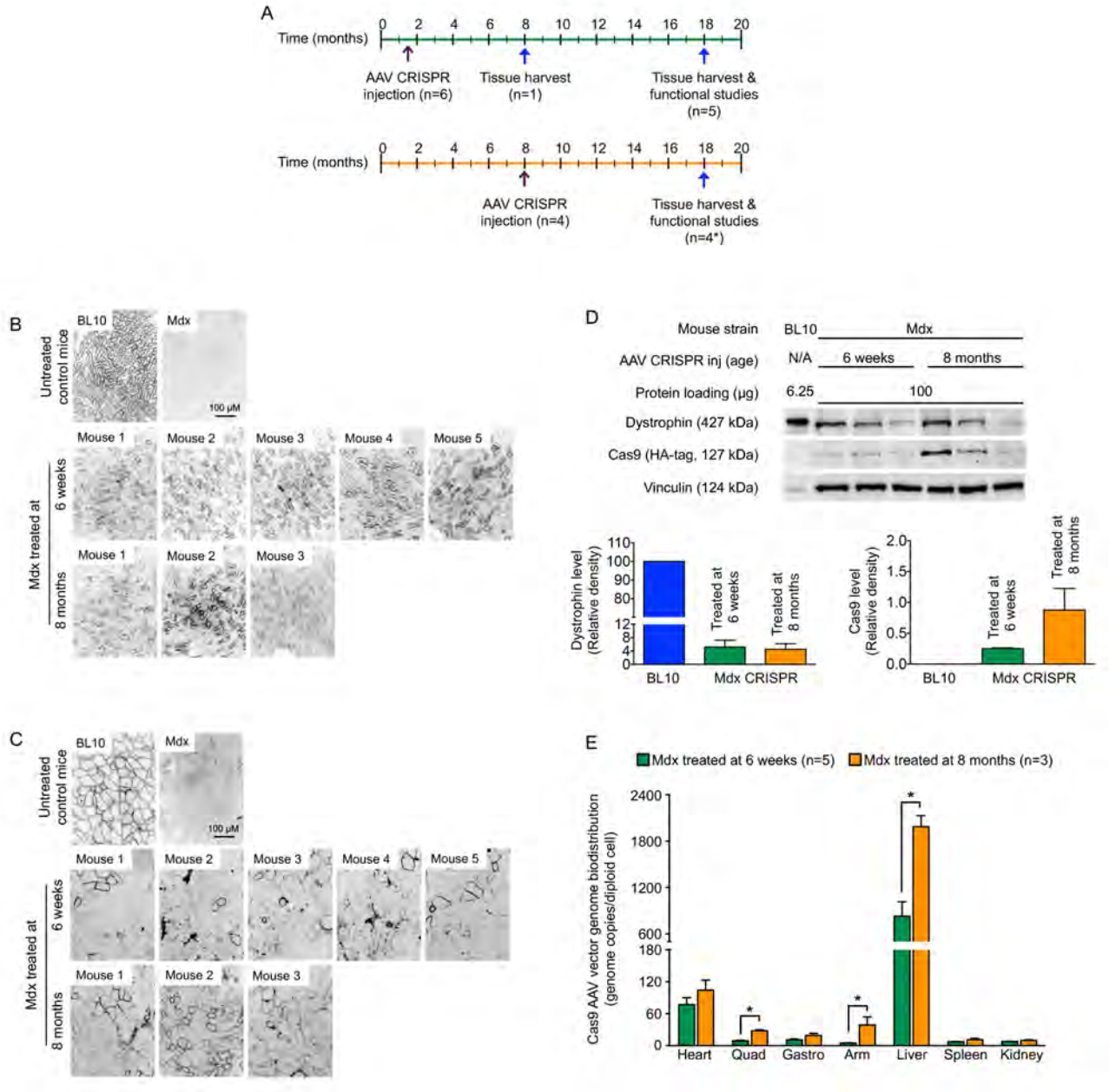

Figure 5. Systemic AAV CRISPR editing resulted in long-term dystrophin expression in young and old mdx mice. A, Schematic overview of the study. Top panel, mdx mice treated at 6 weeks of the age. Bottom panel, mdx mice treated at 8 months of age. The age of AAV injection and tissue harvest are marked. Sample size is provided in bracket. Asterisk, one mouse died at night (likely from arrhythmic sudden cardiac death) two days after ECG measurement. Cardiac catheterization was not performed and tissue not harvested from this mouse. Of the remaining three mice from this group, successful cardiac catheterization was achieved in two. **B,** Representative myocardial dystrophin immunostaining from tissues harvested at 18 months of age. **C,** Representative quadriceps muscle dystrophin immunostaining from tissues harvested at 18 months of age. **D,** Representative dystrophin and Cas9 western blot from the heart harvested at 18 months of age. Vinculin is the loading control. Bottom panels are normalized LICOR quantifications of dystrophin and Cas9 in each experimental group. **E,** TaqMan PCR quantification of the Cas9 vector genome copy number in AAV CRISPR treated mdx mice. Gastro, gastrocnemius; Quad, quadriceps. Asterisk, $p<0.05$.

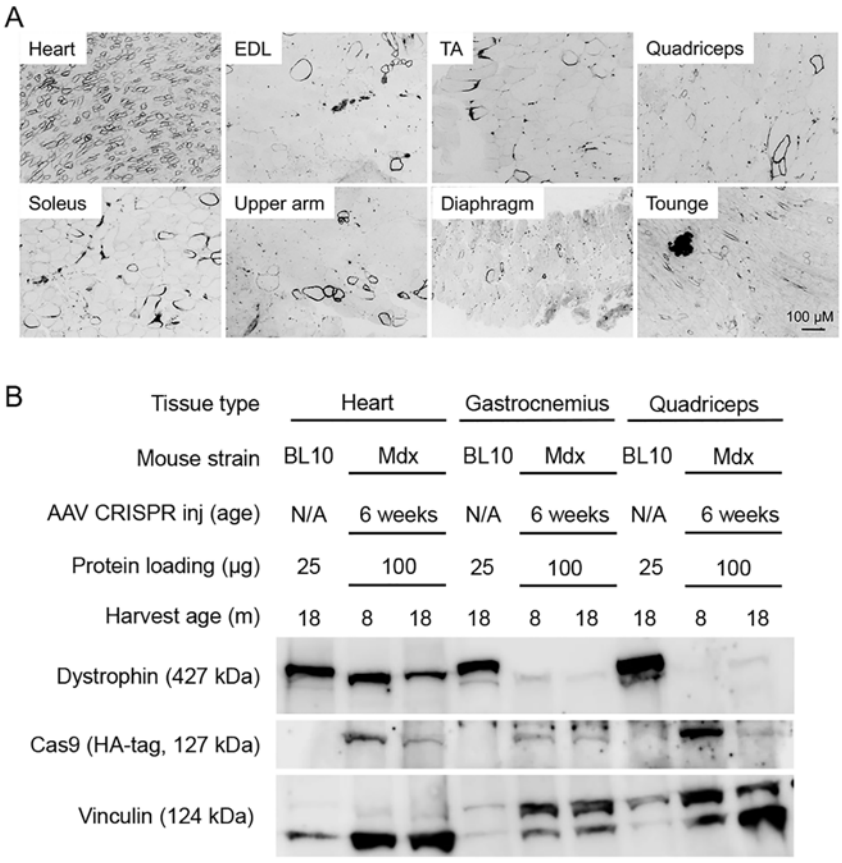

Figure 6. Evaluation of dystrophin expression following systemic AAV CRISPR therapy. A, Representative muscle and heart dystrophin immunostaining photomicrographs from a mouse treated at 6 weeks of age and harvested at 8 months of age. **B,** Representative dystrophin and Cas9 western blot from the heart, gastrocnemius and quadriceps harvested from two mice that were treated at 6 weeks of age. One of the mice was harvested at 8 months of the age and the other at 18 months of age. Tissue from an 18-month-old BL10 mouse was used as the wild type control. Vinculin is the loading control.

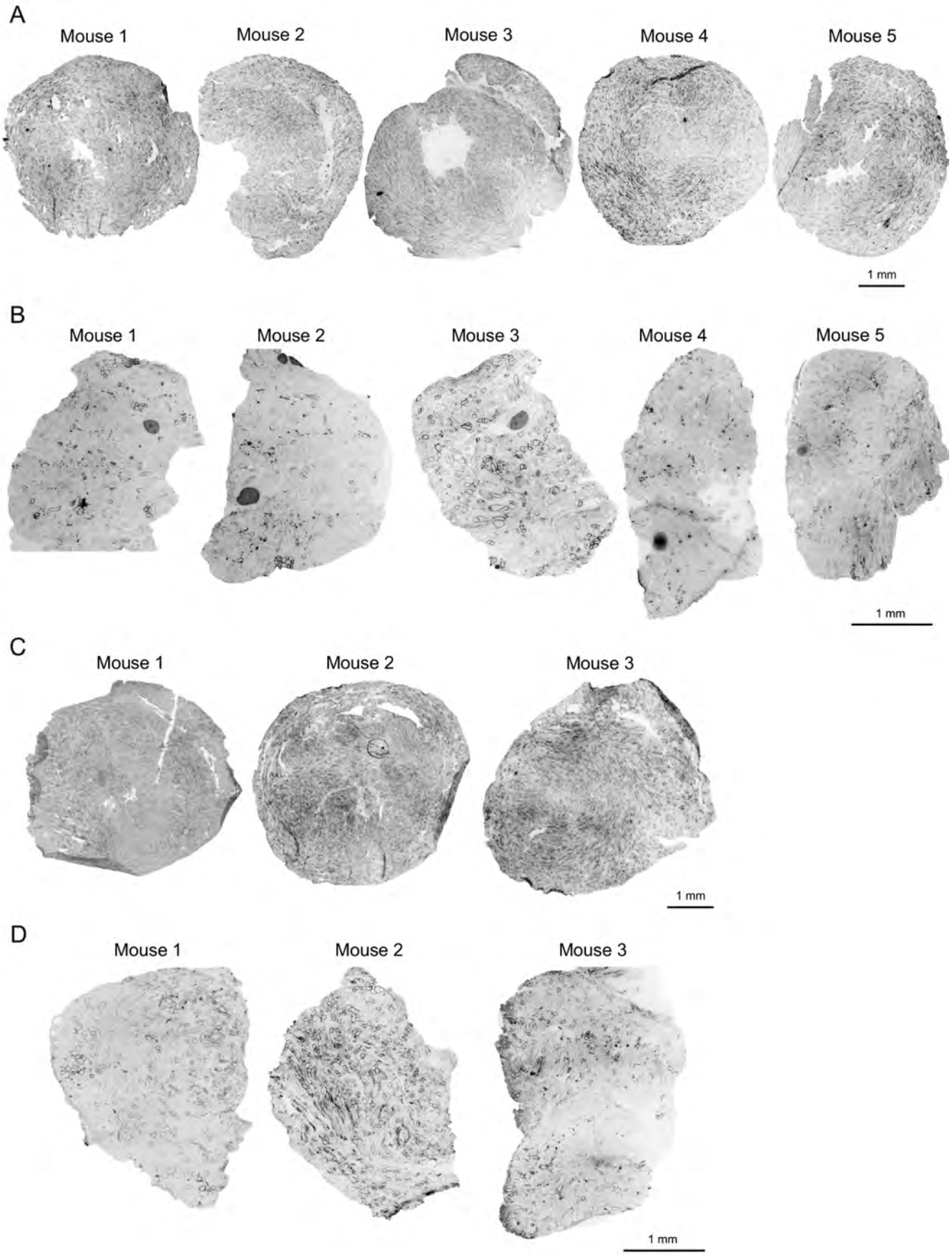
A
Mouse 1
Mouse 2
Mouse 3
Mouse 4
Mouse 5
1 mm
B
Mouse 1
Mouse 2
Mouse 3
Mouse 4
Mouse 5
1 mm
C
Mouse 1
Mouse 2
Mouse 3
1 mm
D
Mouse 1
Mouse 2
Mouse 3
1 mm

Figure 7. Representative full-view of dystrophin immunofluorescence staining photomicrographs from AAV CRISPR treated mice that were harvested at 18 months of age. **A,** Heart dystrophin staining photomicrographs from five mice treated at 6 weeks of age. **B,** Quadriceps muscle dystrophin staining photomicrographs from five mice treated at 6 weeks of age. **C,** Heart dystrophin staining photomicrographs from three mice treated at 18 months of age. **D,** Quadriceps muscle dystrophin staining photomicrographs from three mice treated at 18 months of age.

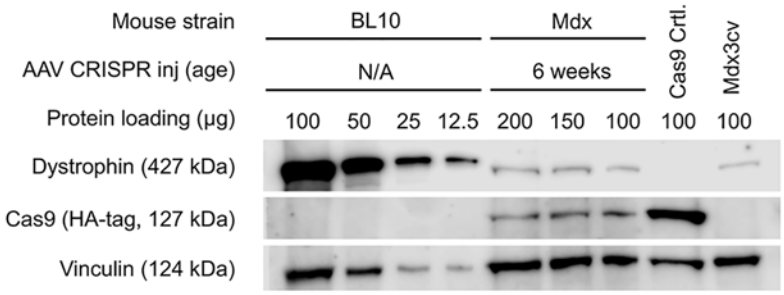

Figure 8. Titration of dystrophin expression on western blot. Representative dystrophin western blot from the heart of an 18-m-old BL10 mouse, the heart of an 18-m-old mdx mouse that received AAV CRISPR treatment at 6 weeks of age, the tibialis anterior muscle of a 3-m-old mdx mouse that received local Cas9 AAV vector injection at 6 weeks of age (Cas9 control), and the heart of an 18-m-old mdx3cv mouse. Mdx3cv mouse heart expresses a near full-length dystrophin at ~3.3% of the wild type level (Wasala et al *Journal of Molecular and Cellular Cardiology* 102:45-52, 2017). Vinculin is the loading control.

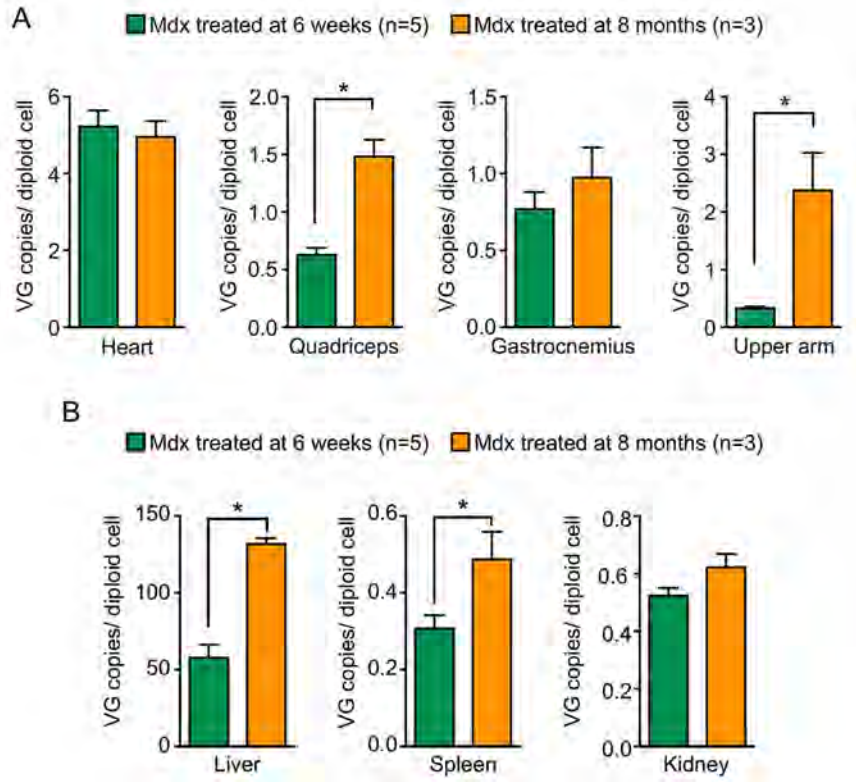

Figure 9. TaqMan PCR quantification of the gRNA vector genome copy number in AAV CRISPR treated mdx mice. Similar results were obtained from intron 22 gRNA PCR and intron 23 gRNA PCR. The data in the bar graph represent the mean value from both PCR reactions. **A,** Results from mdx mice treated at 6 weeks of age and harvested at 18 months of age. **B,** Results from mdx mice treated at 8 months of age and harvested at 18 months of age. Asterisk, statistically significant ($p<0.05$).

Systemic CRISPR therapy improved ECG but not myocardial pathology and hemodynamic deficiency. Dystrophin assembles a set of transmembrane and cytosolic proteins into the dystrophin-associated glycoprotein complex (DGC). The DGC is the structural basis for dystrophin to serve as a shock absorber and signaling hub in muscle. Compared to that of the age-matched untreated mdx heart, DGC expression in the heart of CRISPR-treated mdx mice was minimally changed **(Fig. 10)**. Hematoxylin-eosin (HE) staining and Masson trichrome staining revealed similar pathology and fibrosis in the hearts of treated and untreated mdx mice **(Fig. 11A)**.

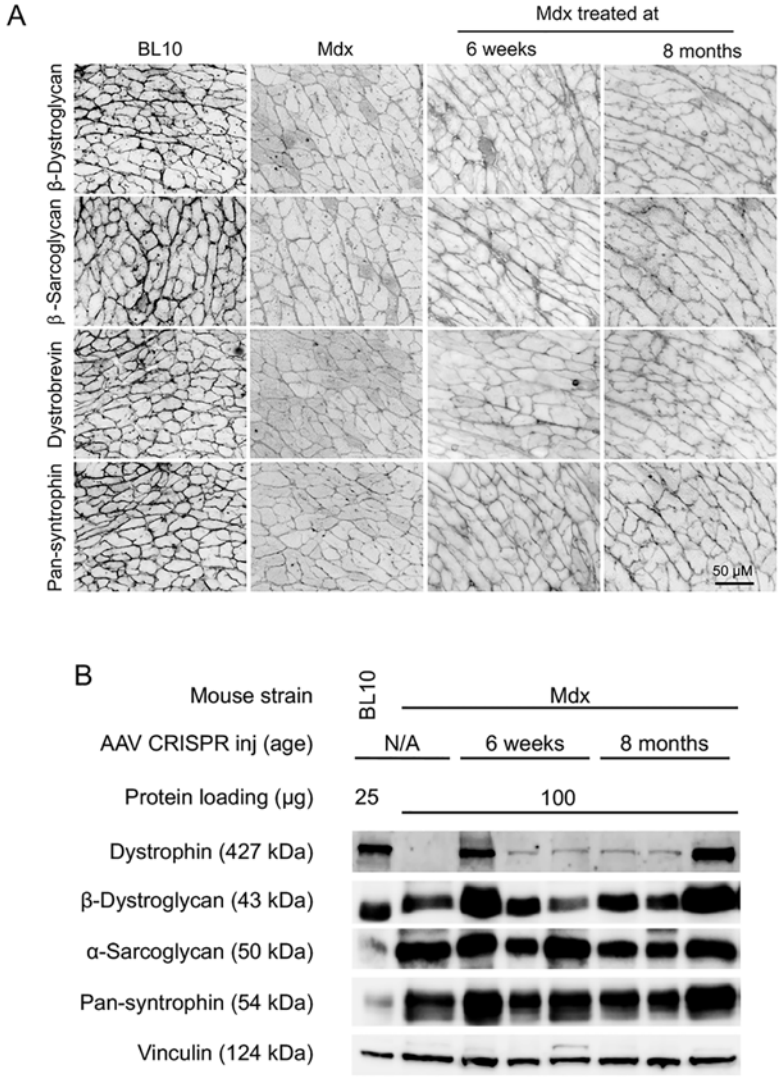

Figure 10. Evaluation of dystrophin-associated glycoprotein complex in the heart of 18-m-old experimental mice. **A,** Representative photomicrographs of β-dystroglycan, β-sarcoglycan, dystrobrevin and pan-syntrophin. **B,** Representative western blot of dystrophin, β-dystroglycan, α-sarcoglycan, and pan-syntrophin. Vinculin is the loading control.

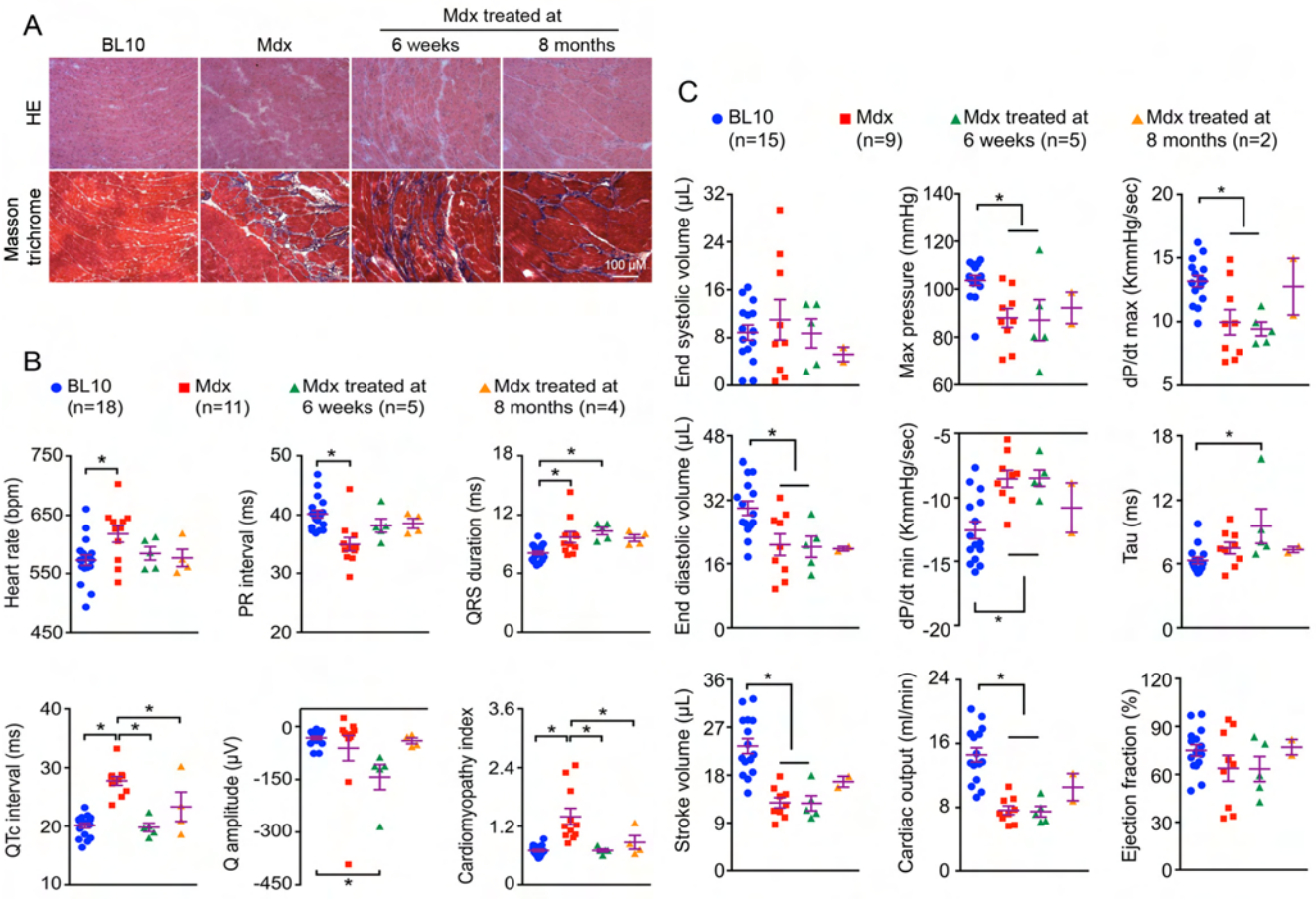

Figure 11. CRISPR therapy improved ECG performance in old mdx mice. **A,** Representative HE and Masson trichrome staining of the heart harvested at 18 months of age. **B,** Quantitative evaluation of the heart rate, PR interval, QRS duration, Mitchell corrected QT interval (QTc), Q amplitude and cardiomyopathy index. Asterisk, statistically significant ($p<0.05$). **C,** Quantitative evaluation of the left ventricle hemodynamics by cardiac catheterization. Statistical analysis was performed among BL10, mdx and mdx treated at 6 weeks of age but not mdx treated at 8 months of age due to the low sample size in this group. Asterisk, statistically significant ($p<0.05$)

DMD patients and dystrophic animals show characteristic ECG changes such as tachycardia, PR interval reduction, QRS prolongation, QT prolongation and a higher cardiomyopathy index (Bostick et al, 2008; Fine et al, 2011; Nigro et al, 1984). The heart rate and PR interval of CRISPR-treated mdx mice showed a trend towards normalization but did not reach statistical significance **(Fig. 11B, Fig. 12)**. However, significant improvement was observed in the QT interval and the

cardiomyopathy index in CRISPR-treated mdx mice **(Fig. 11B, Fig. 12)**. Consistent with our findings on dystrophin expression **(Fig. 5-8)**, mice treated at 6 weeks and 8 months showed comparable improvement in these two ECG parameters **(Fig. 11B)**.

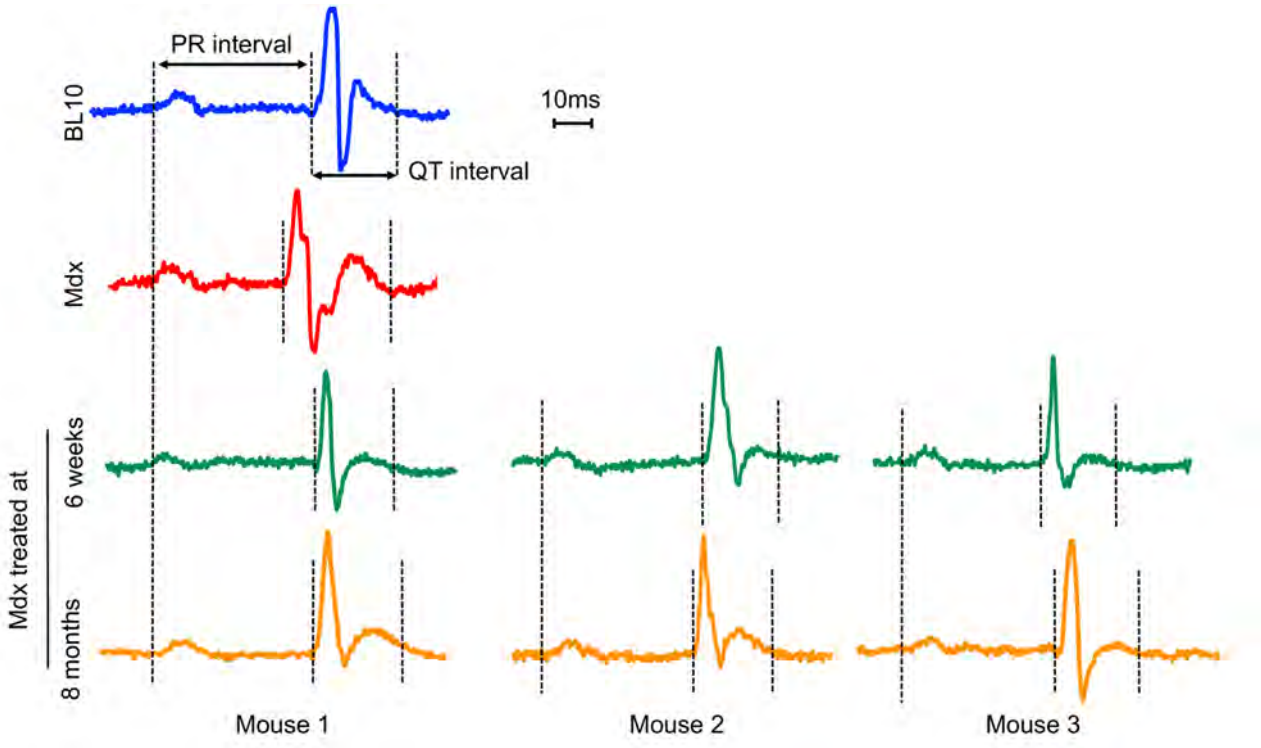

Figure 12. Representative ECG tracing from 18-m-old experimental mice. The PR interval was reduced but the QT interval was prolonged in mdx ECG tracing. These defects were corrected in AAV CRISPR treated mdx mice. Representative tracing from three mice are presented for each group of treated mdx mice.

We quantified left ventricular hemodynamics by cardiac catheterization and did not detect improvement in CRISPR-treated mdx mice **(Fig. 11C)**. Quantification of the anatomic properties of the heart was unremarkable as well **(Table 2)**.

Table 2. Anatomical property of control and AAV CRISPR treated mice

	BL10	Mdx	Mdx CRISPR (6-wk-old)	Mdx CRISPR (8-m-old)
Sample Size (n)	15	16	5	3
Age (m)	18.77 ± 0.35	18.85± 0.32	18.90 ± 0.05	18.20 ± 1.48
BW (g)	33.33 ± 0.63	31.58 ± 0.95	23.74 ± 0.42[a]	28.43 ± 2.77
HW (mg)	136.26 ± 2.45	132.68 ± 3.78	122.62 ± 8.71	120.50 ± 14.59
VW (mg)	129.09 ± 2.46	122.67 ± 3.03	116.60 ± 8.40	115.93 ± 14.19
TW (mg)	42.03 ± 1.05	52.84 ± 2.92[b]	44.45 ± 2.59	44.90 ± 5.26
HW/BW (mg/g)	4.11 ± 0.11	4.30 ± 0.12	5.15 ± 0.29[a]	4.28 ± 0.48
TW/BW (mg/g)	1.26 ± 0.03	1.61 ± 0.14	1.87 ± 0.08[b]	1.59 ± 0.16
HW/TW (mg/g)	3.28 ± 0.12	2.68 ± 0.17[b]	2.77 ± 0.16	2.68 ± 0.05
VW/BW (mg/g)	3.89 ± 0.11	3.98± 0.12	4.90 ± 0.28[a]	4.12 ± 0.46
VW/TW (mg/g)	3.10 ± 0.11	2.47 ± 0.15[b]	2.63 ± 0.16	2.58 ± 0.04

Abbreviations
BW, body weight
HW, heart weight
VW, ventricle weight
TW, tibialis anterior muscle weight
[a], significantly different from both BL10 and mdx
[b], significantly different from BL10 only

AAV CRISPR therapy in young mdx mice resulted in unexpected weight loss. The body weight (BW), heart weight (HW), ventricle weight (VW) and tibialis anterior muscle weight (TW) were recorded at the time of harvest **(Table 2)**. Compared to those of untreated mdx mice, the weights of CRISPR-treated mdx mice appeared to have reduced **(Table 2)**. Notably, the BW of mdx mice treated at 6 weeks of age was significantly decreased compared to that of BL10 and untreated mdx mice **(Fig. 13A, Table 2)**.

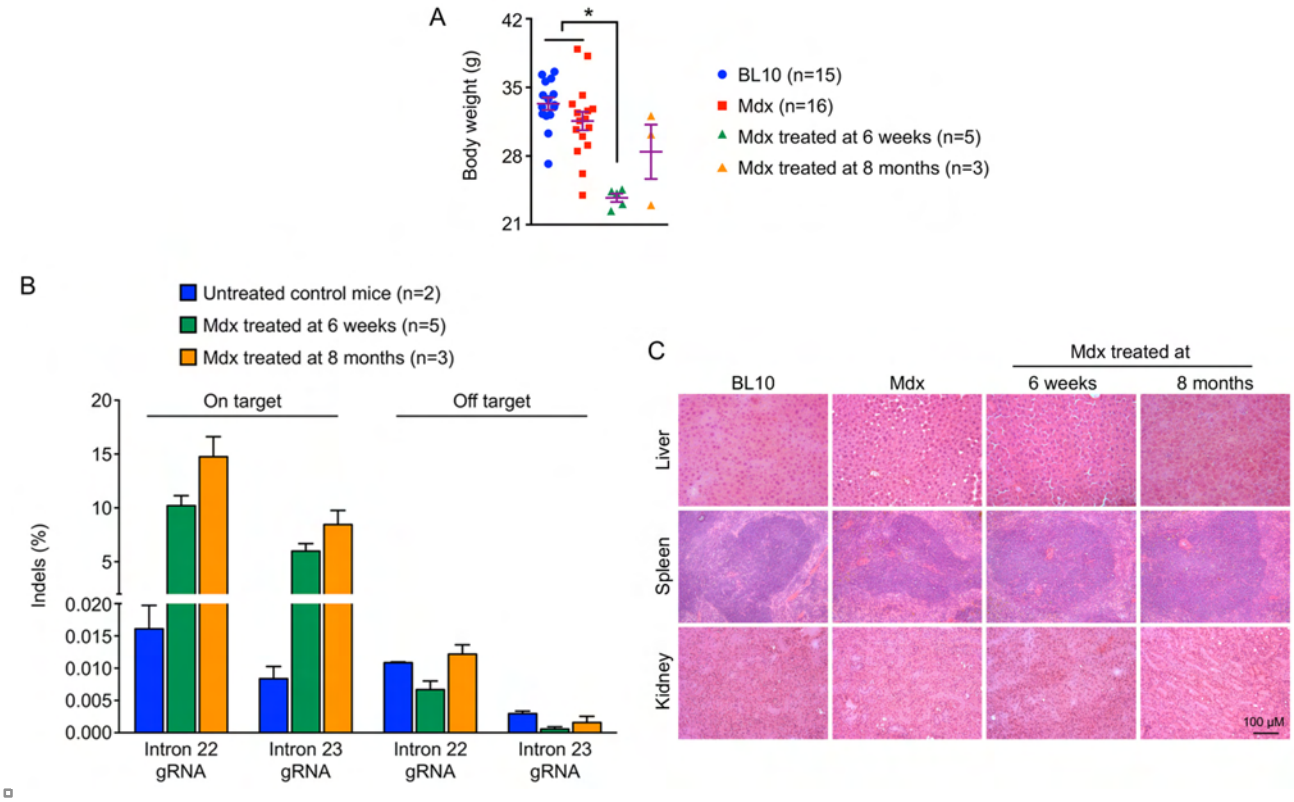

Figure 13. Systemic AAV CRISPR therapy in young mdx mice resulted in unexpected body weight reduction. A, Body weight at 18 months of age in different study groups. Asterisk, statistically significant ($p<0.05$). **B,** Deep sequencing quantification of indels in untreated control mice and AAV CRISPR treated mice. **C,** Representative liver, spleen and kidney HE staining photomicrographs from mice harvested at 18 months of age.

The weight loss seen in mice treated at 6-week-old has never been observed following systemic AAV-9 injection in mdx mice (Bostick et al, 2011a; Ghosh et al, 2009; Shin et al, 2011; Zhang et al, 2013). Since the BW of these mice at the time of AAV injection was comparable to the colony average **(Fig. 14)**, we concluded that the low body weight was not because our experimental mice were

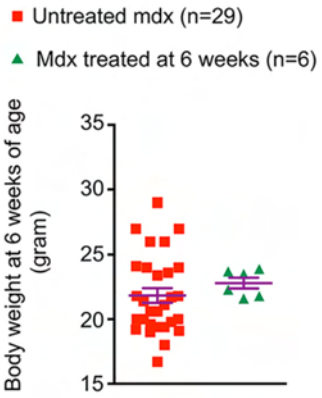

Figure 14. Body weight of 6-week-old male mdx mice. One group received AAV CRIPSPR therapy. The other group did not receive any therapy.

inherently smaller. It is possible that the weight loss is related to the CRISPR therapy. To determine whether long-term Cas9 expression increased off-target editing, we performed deep sequencing on both the target sites and predicted off-target sites, including an off-target site in which we previously observed low levels of activity following local intramuscular injection (Nelson et al, 2016). At the intended location for the intron 22 gRNA, we detected 0.0%, 10.2% and 14.9% indel formation in untreated control mice, mice treated at 6 weeks, and mice treated at 8 months, respectively **(Fig. 13B)**. At the intended location for the intron 23 gRNA, we detected 0.0%, 6.1% and 8.6% indel formation in untreated control mice, mice treated at 6 weeks and mice treated at 8 months, respectively **(Fig. 13B)**. Despite the high levels of indel formation at the target sites, we did not find off-target editing with either gRNA **(Fig. 13B)**. To determine whether long-term CRISPR therapy resulted in tissue toxicity, we examined major internal organs. At necropsy, no gross abnormalities were noted. No obvious abnormalities were detected by HE staining either **(Fig. 13C)**.

In summary, we show that a single intravenous AAV-9 CRISPR therapy in 6-week-old and 8-month-old dystrophic mice resulted in persistent cardiac dystrophin rescue till 18 months at levels comparable to those achieved in short-term studies. Moreover, therapy significantly attenuated characteristic ECG defects.

While we have answered some outstanding questions, our study also revealed several critical but yet not fully appreciated issues. The first is whether AAV CRISPR therapy can result in sufficient dystrophin production to fundamentally improve the outcome in patients. Systemic CRISPR therapy has been tested in two different DMD mouse models using AAV-6, 8 and 9 delivery of SaCas9 and Streptococcus pyogenes Cas9 at a wide range of doses (from $1x10^{12}$ to $1x10^{13}$ vg/mouse) in newborn to 11-week-old mice (Bengtsson et al, 2017; Long et al, 2016; Nelson et al, 2016; Tabebordbar et al, 2016). In these studies, variable levels of dystrophin rescue were detected in the heart and skeletal muscles on immunostaining. However, by western blot the dystrophin quantity was consistently below, or at best equal to 5% of the wild type level (Bengtsson et al, 2017; Long et al, 2016; Nelson et al, 2016; Tabebordbar et al, 2016). Similar levels of dystrophin restoration were observed in our study when treated mice were followed to 18 months of age. Previous studies suggest that this level of expression can improve skeletal muscle force, heart function, and even significantly prolong the life expectancy in severely affected dystrophin/utrophin double knock out mice. However, it does not improve muscle and heart histology (Godfrey et al, 2015; Li et al, 2008; Li et al, 2010; van Putten et al, 2013; Wasala et al, 2016; Wasala et al, 2017). In DMD patients, some marginal benefits have been reported with ≤ 5% dystrophin expression but the disease course was not greatly altered (Muntoni et al, 2017; Nicholson, 1993; Nicholson et al, 1993; Unger & Califf, 2017; van den Bergen et al, 2014). In our study, ~5% dystrophin expression did not significantly enhance DGC restoration in the heart. Heart histology and pump function were not improved either. **Clearly, there is an urgent need to develop new strategies to enhance the editing efficiency.** We would like to set this as a major focus in our studies in the years 2 and 3 of this project.

The second issue is the potential toxicity of CRISPR therapy. It is hypothesized that off-target cutting at important genes will cause deleterious consequences. A number of Cas9 transgenic mice have been generated (Carroll et al, 2016; Chu et al, 2016; Dow et al, 2015; Platt et al, 2014). A mouse line that constitutively expresses Cas9 has been commercialized and propagated for many generations (Platt et al, 2014). This line has also been crossed to the mdx background (Xu et al, 2016). Interestingly, there have been no reports showing severe untoward events in these Cas9 mice. In our study, we used the AAV-9 vector to ensure robust Cas9 expression from the circularized episomal vector genome (Bostick et al, 2007; Duan et al, 1998). Under the regulation of the cytomegalovirus

promoter, Cas9 was expressed for 10 months (in mice injected at 8 months of age) and more than 16 months (in mice injected at 6 weeks of age). While we did not see any adverse effects in treated mice, surprisingly, the body weight of the mice that had the longest Cas9 expression was significantly decreased. However we did not detect genome editing at the highest-ranking off-target sites by deep sequencing, where we previously observed low levels of off-target activity when a relatively higher dose of AAV was injected to muscle locally (Nelson et al, 2016). Histological examination of major internal organs was unremarkable. The behavior, activity, feeding and drinking of these mice were not different from other mice in the colony. We are puzzled by the observed weight loss. It is possible that **the observed weight loss could be a direct consequence of prolonged Cas9 expression** from the AAV vector. **Extensive additional studies are warranted to address this critical safety concern**. In this regard, we would like to set this as a major focus in our studies in the years 2 and 3 of this project. Specifically, we will determine whether the weight loss is a reproducible finding and if yes, how can we minimize this untoward side effect.

The results from this study will be presented in September 2017 at the **4th Ottawa International Conference on Neuromuscular Disease and Biology.** Ottawa, Ontario, Canada.

Additional accomplishments that have benefited from this grant.

Accomplishment benefit from this grant 1. In this study, we have proposed to use intravenous injection to deliver AAV vectors. We published a review article on the current state-of-art on systemic AAV delivery in animal models (Duan, 2016).

Accomplishment benefit from this grant 2. A potential concern of CRISPR therapy for DMD is the loss of AAV CRISPR vectors and loss of dystrophin expression over time. We published an original research article to evaluate whether the loss of therapeutic gene later would affect the outcome of the therapy. We conclude the DMD therapy requires persistent presence of the therapeutic gene and persistent dystrophin expression (Wasala et al, 2016).

Accomplishment benefit from this grant 3. In this study, we have proposed to use optical imaging technology to evaluate heart remodeling. We published one research article on the fine-tuning and optimization of the protocol. We show that optical polarization tractography technology that we have developed represents an excellent tool to study DMD cardiomyopathy in mice (Wang et al, 2017).

Accomplishment benefit from this grant 4. In this study, we have proposed to use AAV vectors as the delivery tool. AAV is a bio-nanoparticle. We published a review article on the current state-of-art on nanotherapy (both viral and noviral) for DMD (Nance et al, 2017).

Accomplishment benefit from this grant 5. An important concern of CRISPR therapy is off-target. Improving gRNA design may improve on-target efficiency and reduce off-target events. We collaborated with Dr. Shi-jie Chen lab and developed a new algorithm that showed superior performance (Xu et al, 2017). We will use this new tool to help design gRNA in the future.

Accomplishment benefit from this grant 6. During this funding period, we published a commentary article on CRISPR gene therapy for DMD (Duan, 2017).

Training and professional development opportunities. Nothing to report.

Dissemination of the results. Above mentioned studies and review articles have been either published in peer-reviewed scientific journals or presented in academic conferences.

Plan for the next reporting period.

In this funding period, we made two critical observations. First, we found that the current AAV CRISPR technology can only result in limited amount of dystrophin production on western blot. This low level of expression is unlikely to significantly change the disease course of Duchenne cardiomyopathy. Second, we found the long-term AAV-mediated Cas9 expression may cause body weight reduction. This is a significant safety concern. In light of these new findings, we would like to propose major changes in the specific aims (see Section 5). In the next funding period, we will focus on the following studies

(1). We will repeat the AAV CRISPR study in young adult mdx mice to see if the body weight reduction seen in the current report can be reproduced. If yes, it will be a critical warning to the entire DMD CRISPR therapy filed. We will then test new strategies to see if we can overcome this safety concern.

(2). We will test whether alteration in the Cas9 vector to gRNA vector ratio can significantly enhance the level of dystrophin restoration and improve heart function in mdx mice. Since we already have these constructs in our lab, we can start this study immediately. As we move forward, we will also explore other strategies (see Section 5 for details) such as using Cpf1 and the single gRNA vector. For these studies, we will need to design new constructs and we will begin to test them in mdx mice once we have cloned and confirmed the constructs.

References for Section 3

Bengtsson NE, Hall JK, Odom GL, Phelps MP, Andrus CR, Hawkins RD, Hauschka SD, Chamberlain JR, Chamberlain JS (2017) Muscle-specific CRISPR/Cas9 dystrophin gene editing ameliorates pathophysiology in a mouse model for Duchenne muscular dystrophy. *Nat Commun* **8:** 14454

Bostick B, Ghosh A, Yue Y, Long C, Duan D (2007) Systemic AAV-9 transduction in mice is influenced by animal age but not by the route of administration. *Gene Ther* **14:** 1605-1609

Bostick B, Shin J-H, Yue Y, Duan D (2011a) AAV-microdystrophin therapy improves cardiac performance in aged female mdx mice. *Mol Ther* **19:** 1826-1832

Bostick B, Shin JH, Yue Y, Wasala NB, Lai Y, Duan D (2012) AAV micro-dystrophin gene therapy alleviates stress-induced cardiac death but not myocardial fibrosis in >21-m-old mdx mice, an end-stage model of Duchenne muscular dystrophy cardiomyopathy. *J Mol Cell Cardiol* **53:** 217-222

Bostick B, Yue Y, Duan D (2010) Gender influences cardiac function in the mdx model of Duchenne cardiomyopathy. *Muscle Nerve* **42:** 600-603

Bostick B, Yue Y, Duan D (2011b) Phenotyping cardiac gene therapy in mice. *Methods Mol Biol* **709:** 91-104

Bostick B, Yue Y, Long C, Duan D (2008) Prevention of dystrophin-deficient cardiomyopathy in twenty-one-month-old carrier mice by mosaic dystrophin expression or complementary dystrophin/utrophin expression. *Circ Res* **102:** 121-130

Carroll KJ, Makarewich CA, McAnally J, Anderson DM, Zentilin L, Liu N, Giacca M, Bassel-Duby R, Olson EN (2016) A mouse model for adult cardiac-specific gene deletion with CRISPR/Cas9. *Proc Natl Acad Sci U S A* **113:** 338-343

Chu VT, Weber T, Graf R, Sommermann T, Petsch K, Sack U, Volchkov P, Rajewsky K, Kuhn R (2016) Efficient generation of Rosa26 knock-in mice using CRISPR/Cas9 in C57BL/6 zygotes. *BMC Biotechnol* **16:** 4

Dow LE, Fisher J, O'Rourke KP, Muley A, Kastenhuber ER, Livshits G, Tschaharganeh DF, Socci ND, Lowe SW (2015) Inducible in vivo genome editing with CRISPR-Cas9. *Nature biotechnology* **33:** 390-394

Duan D (2016) Systemic delivery of adeno-associated viral vectors. *Current opinion in virology* **21:** 16-25

Duan D (2017) A new kid on the playground of CRISPR DMD therapy. *Human gene therapy Clinical development* **28:** 62-64

Duan D, Sharma P, Yang J, Yue Y, Dudus L, Zhang Y, Fisher KJ, Engelhardt JF (1998) Circular intermediates of recombinant adeno-associated virus have defined structural characteristics responsible for long term episomal persistence In muscle. *J Virol* **72:** 8568-8577

Fine DM, Shin JH, Yue Y, Volkmann D, Leach SB, Smith BF, McIntosh M, Duan D (2011) Age-matched comparison reveals early electrocardiography and echocardiography changes in dystrophin-deficient dogs. *Neuromuscul Disord* **21:** 453-461

Ghosh A, Yue Y, Shin J-H, Duan D (2009) Systemic trans-splicing AAV delivery efficiently transduces the heart of adult mdx mouse, a model for Duchenne muscular dystrophy. *Hum Gene Ther* **20:** 1319-1328

Godfrey C, Muses S, McClorey G, Wells KE, Coursindel T, Terry RL, Betts C, Hammond S, O'Donovan L, Hildyard J, El Andaloussi S, Gait MJ, Wood MJ, Wells DJ (2015) How much dystrophin is enough: the physiological consequences of different levels of dystrophin in the mdx mouse. *Hum Mol Genet* **24:** 4225-4237

Lai Y, Zhao J, Yue Y, Wasala NB, Duan D (2014) Partial restoration of cardiac function with ΔPDZ nNOS in aged mdx model of Duchenne cardiomyopathy. *Hum Mol Genet* **23:** 3189-3199

Li D, Yue Y, Duan D (2008) Preservation of muscle force in mdx3cv mice correlates with low-level expression of a near full-length dystrophin protein. *Am J Pathol* **172:** 1332-1341

Li D, Yue Y, Duan D (2010) Marginal level dystrophin expression improves clinical outcome in a strain of dystrophin/utrophin double knockout mice. *PLoS ONE* **5:** e15286

Long C, Amoasii L, Mireault AA, McAnally JR, Li H, Sanchez-Ortiz E, Bhattacharyya S, Shelton JM, Bassel-Duby R, Olson EN (2016) Postnatal genome editing partially restores dystrophin expression in a mouse model of muscular dystrophy. *Science* **351:** 400-403

Makarova KS, Wolf YI, Alkhnbashi OS, Costa F, Shah SA, Saunders SJ, Barrangou R, Brouns SJ, Charpentier E, Haft DH, Horvath P, Moineau S, Mojica FJ, Terns RM, Terns MP, White MF, Yakunin AF, Garrett RA, van der Oost J, Backofen R, Koonin EV (2015) An updated evolutionary classification of CRISPR-Cas systems. *Nat Rev Microbiol* **13:** 722-736

Muntoni F, Fletcher S, Wilton S (2017) Response to "Railroading at the FDA". *Nature biotechnology* **35:** 207-209

Nance ME, Duan D (2015) Perspective on adeno-associated virus (AAV) capsid modification for Duchenne muscular dystrophy gene therapy. *Hum Gene Ther* **26:** 786-800

Nance ME, Hakim CH, Yang NN, Duan D (2017) Nanotherapy for Duchenne muscular dystrophy. *Wiley Interdiscip Rev Nanomed Nanobiotechnol*

Nelson CE, Hakim CH, Ousterout DG, Thakore PI, Moreb EA, Rivera RM, Madhavan S, Pan X, Ran FA, Yan WX, Asokan A, Zhang F, Duan D, Gersbach CA (2016) In vivo genome editing improves muscle function in a mouse model of Duchenne muscular dystrophy. *Science* **351:** 403-407

Nicholson LV (1993) The "rescue" of dystrophin synthesis in boys with Duchenne muscular dystrophy. *Neuromuscul Disord* **3:** 525-531.

Nicholson LV, Johnson MA, Bushby KM, Gardner-Medwin D, Curtis A, Ginjaar IB, den Dunnen JT, Welch JL, Butler TJ, Bakker E, et al. (1993) Integrated study of 100 patients with Xp21 linked muscular dystrophy using clinical, genetic, immunochemical, and histopathological data. Part 3. Differential diagnosis and prognosis. *Journal of medical genetics* **30:** 745-751.

Nigro G, Comi LI, Politano L (1984) Electrocardiographic evaluation of the P-type stage of dystrophic cardiomyopathy. *Cardiomyology* **3:** 45-58

Platt RJ, Chen S, Zhou Y, Yim MJ, Swiech L, Kempton HR, Dahlman JE, Parnas O, Eisenhaure TM, Jovanovic M, Graham DB, Jhunjhunwala S, Heidenreich M, Xavier RJ, Langer R, Anderson DG, Hacohen N, Regev A, Feng G, Sharp PA, Zhang F (2014) CRISPR-Cas9 knockin mice for genome editing and cancer modeling. *Cell* **159:** 440-455

Shin JH, Bostick B, Yue Y, Hajjar R, Duan D (2011) SERCA2a gene transfer improves electrocardiographic performance in aged mdx mice. *J Transl Med* **9:** 132

Tabebordbar M, Zhu K, Cheng JK, Chew WL, Widrick JJ, Yan WX, Maesner C, Wu EY, Xiao R, Ran FA, Cong L, Zhang F, Vandenberghe LH, Church GM, Wagers AJ (2016) In vivo gene editing in dystrophic mouse muscle and muscle stem cells. *Science* **351:** 407-411

Unger EF, Califf RM (2017) Regarding "Eteplirsen for the treatment of Duchenne muscular dystrophy". *Annals of Neurology* **81:** 162-164

van den Bergen JC, Wokke BH, Janson AA, van Duinen SG, Hulsker MA, Ginjaar HB, van Deutekom JC, Aartsma-Rus A, Kan HE, Verschuuren JJ (2014) Dystrophin levels and clinical severity in Becker muscular dystrophy patients. *Journal of neurology, neurosurgery, and psychiatry* **85:** 747-753

van Putten M, Hulsker M, Young C, Nadarajah VD, Heemskerk H, van der Weerd L, t Hoen PA, van Ommen GJ, Aartsma-Rus AM (2013) Low dystrophin levels increase survival and improve muscle pathology and function in dystrophin/utrophin double-knockout mice. *FASEB J* **27:** 2484-2495

Wang Y, Ravanfar M, Zhang K, Duan D, Yao G (2016) Mapping 3D fiber orientation in tissue using dual-angle optical polarization tractography. *Biomedical optics express* **7:** 3855-3870

Wang Y, Zhang K, Duan D, Yao G (2017) Heart structural remodeling in a mouse model of Duchenne cardiomyopathy revealed using optical polarization tractography [Invited]. *Biomedical optics express* **8:** 1271-1276

Wasala NB, Bostick B, Yue Y, Duan D (2013) Exclusive skeletal muscle correction does not modulate dystrophic heart disease in the aged mdx model of Duchenne cardiomyopathy. *Hum Mol Genet* **22:** 2634-2641

Wasala NB, Lai Y, Shin JH, Zhao J, Yue Y, Duan D (2016) Genomic removal of a therapeutic mini-dystrophin gene from adult mice elicits a Duchenne muscular dystrophy-like phenotype. *Hum Mol Genet***:** In-press. Online publiation 04/22/16

Wasala NB, Yue Y, Vance J, Duan D (2017) Uniform low-level dystrophin expression in the heart partially preserved cardiac function in an aged mouse model of Duchenne cardiomyopathy. *J Mol Cell Cardiol* **102:** 45-52

Xu L, Zhao L, Gao Y, Xu J, Han R (2016) Empower multiplex cell and tissue-specific CRISPR-mediated gene manipulation with self-cleaving ribozymes and tRNA. *Nucleic acids research*

Xu X, Duan D, Chen SJ (2017) CRISPR-Cas9 cleavage efficiency correlates strongly with target-sgRNA folding stability: from physical mechanism to off-target assessment. *Scientific reports* **7:** 143

Zhang Y, Long C, Li H, McAnally JR, Baskin KK, Shelton JM, Bassel-Duby R, Olson EN (2017) CRISPR-Cpf1 correction of muscular dystrophy mutations in human cardiomyocytes and mice. *Sci Adv* **3:** e1602814

Zhang Y, Yue Y, Li L, Hakim CH, Zhang K, Thomas GD, Duan D (2013) Dual AAV therapy ameliorates exercise-induced muscle injury and functional ischemia in murine models of Duchenne muscular dystrophy. *Hum Mol Genet* **22:** 3720-3729

4. Impact. Nothing to report.

5. Changes/Problems.

Changes in approach and reasons for change.

We have originally proposed to evaluate the therapeutic effect of AAV CRISPR delivery to treat DMD cardiomyopathy in the mouse model using the protocol we have published (Nelson et al, 2016). Specifically, we will delivery two AAV vectors, one encoding the Cas9 gene and the other encoding two gRNAs to remove the mutated exon 23 in the mdx model of DMD. In our preliminary study submitted during grant application, we showed that our approach reduced skeletal muscle pathology and improved skeletal muscle contractility following local injection. We also showed that systemic delivery resulted in dystrophin restoration in the heart on immunofluorescence staining. **When we started the project as we originally planned, we encountered several unexpected surprises**. First, we detected very low-level dystrophin restoration in the heart on the western blot. Second, this level of expression is insufficient to correct histological lesions in the heart. Heart function was also minimally improved at this level of expression. Third, in young adult mdx mice treated with CRISPR, we found a significant reduction in the body weight in treated mice.

In light of the above results, we now request the approval from DoD on a significantly change in the study plan. Specifically, we propose to stop pursuing the original Aims 1 and 3. Based on the new data we presented in this report, we expect to see negative results (i.e. a lack of significant improvement following AAV CRISPR therapy) from the original Aims 1 and 3. Since we have now identified the major hurdles for AAV CRISPR therapy for DMD cardiomyopathy, we would like to shift our focus to address these hurdles. Specifically, we would like to revise the Aims to following:

Revised Aim 1. Evaluation on the body weight reduction in young adult mdx mice following systemic AAV CRISPR delivery. Specifically, we will deliver AAV vectors to 6-week-old mdx mice and follow the mice till they reach 18 months of age. We will carefully monitor the body weight change in treated mice. We will include both male and female mdx mice (female mice have more severer cardiomyopathy) to see if our initial observation can be reproduced. If this is confirmed, then it will be a very important warning to the entire field. In this case, we will (1) test to see reducing AAV.Cas9 dose can minimize the side effect, (2) whether using different gRNA design and/or different Cas9 enzyme can prevent this side-effect, and (3) whether this is specific to the mdx strain only. We will test AAV CRISPR in other strains such as mdx4cv or some newly generated exon-deletion mdx models. A negative result will suggest that this is unique to the mdx strain (may be due to the location of the mutation, the gRNA design or the Cas9 used in the study).

Revised Aim 2. Exploration of novel strategies to improve the level of dystrophin restoration with AAV CRSIPR therapy. Specifically, we will test the following approaches. (1) Alteration of the ratio of AAV.Cas9 and AAV.gRNA vectors. All the published studies have used the 1:1 ratio. A recent study from the Gungping Gao lab at the University of Massachusetts (personal communication. Dr. Gao shared this result when he gave a seminar to our Department recently) suggests that the hairpin-like structure in the gRNA construct may influence the vector genome stability. Our results also support this. Specifically, we found that the gRNA AAV vector genome copy number was

significantly lower than that of the Cas9 AAV vector genome copy number in tissues we harvested (please compare **Figure 5E** and **Figure 9**). Modulating the vector ratio (in particular, increasing the dose of the gRNA vector) may enhance the CRISPR editing efficiency and improve dystrophin restoration. (2) Exploration of different Cas9 enzyme. A recent study from the Eric Olson lab suggests that the use of the Cpf endonuclease, instead of the SaCas9 we used in our study, may lead to higher dystrophin yield (Duan, 2017). (3) Exploration of single gRNA approach. At the Keynote seminar presented at the 2017 Annual meeting of the American Society of Gene and Cell Therapy, Dr. Olson showed the latest data from his lab. Specifically, his lab designed a single gRNA for SpCas9 that targets the splicing signal in the mutated exon 23. This resulted in a dystrophin restoration at 90% of wild type level on western blot in newborn mdx mice. We would like to test the similar approach in young adult mdx mice to see if the strategy used by the Olson lab can be reproduced in adult mdx mice.

Actual or anticipated problems or delays and actions or plans to resolve them.

We do not anticipate significant technical hurdles.

Changes that had a significant impact on expenditures.

Nothing to report.

Significant changes in use or care of human subjects, vertebrate animal, biohazards and/or selected agents.

Nothing to report.

6. Products

6.1. Peer-reviewed publications (a total of 7)

1) **Duan D.** *Systemic delivery of adeno-associated viral vectors.* **Current Opinion in Virology** 21:16-25, **2016**.

2) Wasala NB, Lai Y, Shin J-H, Zhao J, Yue Y, **Duan D.** *Genomic removal of a therapeutic mini-dystrophin gene from adult mice elicits a Duchenne muscular dystrophy-like phenotype.* **Human Molecular Genetics** 25(13):2633-2644**, 2016**.

3) Wasala NB, Yue Y, Jenna Vance, **Duan D.** *Uniform low-level dystrophin expression in the heart partially preserved cardiac function in an aged mouse model of Duchenne cardiomyopathy.* **Journal of Molecular and Cellular Cardiology** 102:45-52, **2017**.

4) Nance ME, Hakim CH, Yang NN and **Duan D.** *Nanotherapy for Duchenne muscular dystrophy.* **WIREs Nanomedicine and Nanobiotechnology** e1472**, 2017**.

5) Xu X, **Duan D**, Chen S. *CRISPR-Cas9 cleavage efficiency correlates strongly with target-sgRNA folding stability: from physical mechanism to off-target assessment*. **Scientific Reports** 7:143, **2017**.

6) Wang Y, Zhang K, **Duan D**, Yao G. *Heart structure remodeling in the mdx4cv mouse model of Duchenne cardiomyopathy revealed using optical polarization tractography.* **Biomedical Optics Express** 8(3):1271-1276**, 2017**.

7) **Duan D.** *A new kid in the playground of CRISPR DMD therapy.* **Human Gene Therapy Clinical Development** 28(2):62-64**, 2017**.

6.3. Conference presentations

1) **Duan D.** Large mammal translation in the canine model for DMD gene therapy. Dec 13, 2016 *Developing Gene Editing as a Therapeutic Strategy* (Banbury meeting). Cold Spring Harbor, NY. (Oral Presentation, no abstract available)
2) **Duan D.** AAV microgene therapy and CRISPR therapy for DMD. May 6, 2017 *Jett Foundation St Louise Education Roundtable.* St Louis, MO. (Oral Presentation, no abstract available)
3) We plan to present the results shown in this report in 2017 September at the 4th Ottawa International Conference on Neuromuscular Disease and Biology. Ottawa, Ontario, Canada.

7. Participants/collaborating organizations:

What individuals have worked on the project?

Name: Dongsheng Duan
Project Role: PI
Research Identifier: ORCID#: 0000-0003-4109-1132
Nearest person month worked: 1
Contribution to project: Dr. Duan has overseen all aspects of the project.

Name: Nalinda Wasala
Project Role: Postdoc
Research Identifier: N/A
Nearest person month worked: 5
Contribution to project: Dr. Wasala will be responsible for function assays, histopathology assays and biochemical analysis and assist with AAV preparation and purification.

Christopher Nelson, Ph.D.
Project Role: Postdoc
Researcher Identifier: N/A
Nearest person month worked: 2 months
Contribution to project: Dr. Nelson led the completion of experiments at Duke, including design of gRNAs, AAV constructs, and analysis of gene editing and off-target effects by next generation sequencing.

Matthew Gemberling, Ph.D.
Project Role: Postdoc
Researcher Identifier: N/A
Nearest person month worked: 1 month
Contribution to project: Dr. Gemberling assisted Dr. Nelson with design and completion of off-target analysis.

Adrianne Pittman, B.S.
Project Role: Postdoc
Researcher Identifier: N/A
Nearest person month worked: 1 month
Contribution to project: Ms. Pittman assisted Dr. Nelson with preparation of sequencing libraries for off-target analysis.

Changes in the active other support of the PI and key personnel since the last reporting period.

Dongsheng Duan, PI

Previous Active Grants That Have Closed

A canine tissue bank for Duchenne muscular dystrophy study
3% effort, PI
Muscular Dystrophy Association
Haley McCombs; Muscular Dystrophy Association, Inc.; 3300 E. Sunrise Drive; Tucson, AZ 85718
05/01/2014-04/30/2016
$76,909 (direct costs/year)
This infrastructural grant is to establish a tissue bank from normal and dystrophic dogs for the entire DMD community to share.
The specific aims are (1) collect tissues and cells from normal, carrier and three different strains of dystrophic dogs, (2) generate a detailed archive for every specimen in the tissue bank, (3) develop and maintain a web site for public access, management and tissue distribution.
(There is no scientific/budget overlap with the current proposal.)

A pilot study on systemic delivery of an AAV-9 five-repeat micro-dystrophin vector in juvenile DMD dogs
10% effort, PI
Solid Ventures
Joel Schneider, Ph.D.; 101 Main Street; Cambridge, MA 02142
06/01/2015-08/31/2016
$250,000 (15 month duration, total direct costs)
A pilot study on systemic delivery of an AAV-9 Five-repeat micro-dystrophin vector in juvenile DMD dogs.
The aim is to establish the proof-of-principle for systemic gene therapy of Duchenne muscular dystrophy using an AAV-9 5-repeat micro-dystrophin vector in the canine model.
(There is no scientific/budget overlap with the current proposal.)

A pilot study to evaluate dual AAV mini dystrophin vectors in DMD dogs
3% effort, PI
Hope for Javier
Jennifer Portnoy, P.O. Box 251, East Setauket, NY 11733-0251
06/01/2015-05/31/2016
$50,000 (direct costs)
We propose to engineer the third-generation dual AAV minigene vectors to express a larger mini-dystrophin protein. We further propose to test the third-generation vectors by local injection in one infected dog to generate preliminary data for future NIH application.
Specific aims are (1) to design and engineer dual AAV vectors to express a 7-kb canine mini-dystrophin gene and (2) to test the canine minigene dual AAV vectors in the extensor carpi ularis (ECU) muscle in adult dystrophic dogs.

(There is no scientific/budget overlap with the current proposal.)

AAV gene therapy for Krabbe disease
3% effort, Co-I (Steve LeVine, PI)
KCALSI
Kansas City Area Life Sciences Institute; 30 W. Pershing Road, Suite 210; Kansas City, MO 64108
08/01/2015-07/31/2016
$27,273 (direct costs)
As Co-I of this grant, I will construct, produce and purify high quality AAV.galactosylceramidase vector for Dr. LeVine, PI to test in cellular and animal models of Krabbe disease.
(There is no scientific/budget overlap with the current proposal.)

Design low-immunogenic Cas9 for gene repair in the mdx model of DMD
1% effort, PI
Hope for Javier
Jennifer Portnoy, P.O. Box 251, East Setauket, NY 11733-0251
10/01/2015-09/30/2016
$25,000 (direct costs)
The goal of this project is to design and evaluate a low-immunogenic Cas9 AAV vector in the hope of applying it for CRISPR/Cas9-mediated gene repair therapy for DMD.
The specific aims are (1) to design and engineer a low immunogenic AAV Cas9 vector and (2) to test the low immunogenic AAV Cas9 vector.
(There is no scientific/budget overlap with the current proposal).

Maximum feasible dose study in a canine model of Duchenne muscular dystrophy
10% effort, PI
Solid Biosciences
Joel Schneider, Ph.D.; 101 Main Street; Cambridge, MA 02142
07/01/2016-04/30/2017
$80,000 (direct costs)
This study will assess the expression, localization and bio-distribution of canine SGT-001.
(There is no scientific/budget overlap with the current proposal).

Current Research Support

A translational pathway towards a clinical trial using the second-generation AAV micro-dystrophin vector
10% effort, (5% effort during ncte), PI
Department of Defense (MD130014)
Wendy A. Baker, Grants Officer; USA Medical Research ACQ Activity; 820 Chandler Street; Fort Detrick, MD 21702
09/01/2014-12/31/2017 (extension)
$175,000 (direct costs/year)

The goal of this grant will explore an AAV-8 human micro-dystrophin gene vector in adult dystrophic dogs.
The specific aims are (1) to validate therapeutic efficacy of the human version of the ΔR2-15/ΔR18-19/ΔR20-23/ΔC microgene AAV-8 vector in adult dystrophic dogs by local injection and (2) to explore bodywide AAV-8 gene therapy in young adult dystrophic dogs using the human version of the ΔR2-15/ΔR18-19/ΔR20-23/ΔC microgene vector.
(There is no scientific/budget overlap with the current proposal.)

Evaluation of the human version second-generation AAV micro-dystrophin vector in adult dystrophic dogs
5% effort, PI
Jesse's Journey; The Foundation for Gene & Cell Therapy
Rick Moss; Managing Director; 195 Dufferin Avenue; Suite #605; London, ON N6A 1K7 CANADA
7/1/14-12/31/2017
$100,000 CAN (direct costs/year)
Goal: We propose to generate the human version microgene vector and confirm its function in adult DMD dogs.
The specific aims are: (1) to engineer a codon-optimized second-generation human dystrophin microgene in a customer-optimized expression cassette and package it in an AAV-8 vector; (2) to validate the efficacy of the human version vector in dystrophin deficient mdx mice by systemic gene transfer; (3) to validate the efficacy of the human version vector in adult dystrophic dogs by local gene transfer; (4) to explore systemic gene therapy in young adult dystrophic dogs.
(This is a supplementary grant to the DOD grant awarded September 2014 that has been approved for extension to 12/31/2017).
(There is no scientific/budget overlap with the current proposal.)

Whole body single AAV microgene therapy in canine DMD
17% effort, PI
NIH, NINDS R01 NS090634
National Institutes of Health; 6701 Rockledge Drive; Suite 1040, MSC 7710; Bethesda, MD 20817
09/01/2015-07/31/2020
$406,687 (direct costs/current year)
In this study, we will test whether a newly developed canine Y731F AAV-9 micro-dystrophin vector gene therapy can lead to clinically meaningful improvement in dystrophic dogs.
Specific aim 1 is to test regional therapy in the hope of applying it to improve life quality in late-stage patients and aim 2 is to test systemic therapy in the hope of achieving bodywide improvement in young patients.
(There is no scientific/budget overlap with the current proposal).

R16/17-independent nNOS anchoring mechanism
8% effort, PI
NIH/NIAMS (R21 AR067985-01A1)

National Institutes of Health; 6701 Rockledge Drive, Suite 1040, MSC 7710; Bethesda, MD 20817
O4/01/2016-03/31/2018
$110,000 (direct costs/current year)
The goal is to identify the dog nNOS-binding domain and develop relevant gene delivery vectors.
The specific aims are (1) to identify the canine specific nNOS-binding domain in dog dystrophin and (2) to develop the nNOS-binding canine dystrophin adeno-associated virus (AAV) vector.
(There is no scientific/budget overlap with the current proposal.)

CRISPR/Cas9-based gene editing for the correction of Duchenne muscular dystrophy
8% effort, Co-PI (PI: Charles Gersbach)
Duke University, NIH (R01 AR069085-01A1)
Charles Gersbach, Ph.D.; Duke University, 2353C CIEMAS Box 90281; Durham, NC 27708-0281
04/01/2016-03/31/2021
$63,754 (total direct costs/current year)
The Duan lab will perform in vivo gene delivery and functional outcome measurements in mice treated by AAV-CRISPR gene repair vectors and if needed will also assist with the production of recombinant AAV vectors.
Specific aim: To test CRSPR/Cas9 gene therapy to treat muscle disease in mdx mice and hDMD mice.

(There is no scientific/budget overlap with the current proposal)

New Active Grants

Treatment of Duchenne muscular dystrophy with the muscle calcium pump
17% effort, PI
NIH/NIAMS (R01 AR070517-01)
National Institutes of Health; 6701 Rockledge Drive, Suite 1040, MSC 7710; Bethesda, MD 20817
07/01/2016-08/31/2021
$406,296 (direct costs/current year)
Goal: Elevation of cytosolic calcium is a pivotal pathogenic event in Duchenne muscular dystrophy (DMD). We found that sarco/endoplasmic reticulum calcium ATPase 2a (SERCA2a) therapy can reduce muscle disease and improve muscle function in the mouse DMD model. In the proposed study, we will test whether this therapy can treat symptomatic DMD dogs and our results will lay the foundation for a future clinical trial.
The specific aims are: (1) to test whether regional AAV SERCA2a therapy can ameliorate limb muscle disease and improve function and (2) to test whether systemic AAV SERCA2a therapy can lead to bodywide improvement in affected dogs.
(There is no scientific/budget overlap with the current proposal.)

A pilot study to evaluate long-term safety and efficacy of AAV-9 5Rc micro-dystrophin therapy
5% effort, PI
Solid Biosciences

Joel Schneider, Ph.D.; 101 Main Street; Cambridge, MA 02142
06/01/2016-05/31/2019
$100,000 (direct costs/current year)
The overarching goal of this project is to determine whether systemic AAV-9 5Rc micro-dystrophin gene therapy can yield long-term (up to 4 years after injection) microgene expression without causing serious adverse events (SAEs).
(There is no scientific/budget overlap with the current proposal.)

Fine-needle microscopic tractography for in vivo high-resolution imaging of muscle damage
2% effort, Co-PI (PI: Gang Yao)
University of Missouri, Interdisciplinary Pilot Studies in Translational Science and Biomedical Innovations
Debbie Taylor, MA204 Medical Sciences Building, University of Missouri
07/01/2017 to 06/30/2018
$50,000 (direct costs/current year)
The goal and aim of this project is to develop a new microscopic imaging method for minimal invasive imaging of muscle damage.
(There is no scientific/budget overlap with the current proposal.)

Evaluation of Montelukast as a potential therapy for Duchenne muscular dystrophy in the murine model
3% effort, PI
Duchenne UK
Fiona Lawrence; 11 Bedford Road; London, W4 1 JD; GBR United Kingdom
03/01/2017-02/28/2020
$60,000 (direct costs/current year)
We propose to evaluate safety and therapeutic efficacy of Montelukast in mdx mice, the most commonly used mouse model for DMD.
(There is no scientific/budget overlap with the current proposal)

Evaluation of Montelukast as a potential therapy for Duchenne muscular dystrophy in the murine model
0% effort, PI
Michael's Cause
Robert Capolongo; PO Box 120323; Staten Island, NY 10312
03/01/2017-02/28/2020
$16,666 (direct costs/current year)
We propose to evaluate safety and therapeutic efficacy of Montelukast in mdx mice, the most commonly used mouse model for DMD. This is a supplementary grant to the Duchenne UK grant.
(There is no scientific/budget overlap with the current proposal)

Evaluation of Montelukast as a potential therapy for Duchenne muscular dystrophy in the murine model
0% effort, PI
Ryan's Quest

David Shultz; PO Box 2544; Hamilton, NJ 08690
03/01/2017-02/28/2020
$16,666 (direct costs/current year)
We propose to evaluate safety and therapeutic efficacy of Montelukast in mdx mice, the most commonly used mouse model for DMD. This is a supplementary grant to the Duchenne UK grant.
(There is no scientific/budget overlap with the current proposal)

Evaluation of Montelukast as a potential therapy for Duchenne muscular dystrophy in the murine model
0% effort, PI
Rally for Ryan
Marty Karlin; 2623 Evercrest Court; Naperville, IL 60564
03/01/2017-02/28/2020
$16,666 (direct costs/current year)
We propose to evaluate safety and therapeutic efficacy of Montelukast in mdx mice, the most commonly used mouse model for DMD. This is a supplementary grant to the Duchenne UK grant.
(There is no scientific/budget overlap with the current proposal)

DMD gene therapy in the canine model by intramuscular sarcolipin knockdown
5% effort, PI
Jesse's Journey: The Foundation for Gene & Cell Therapy
Lisa Hoffman; PO Box 51 Station B; London, ON NGA 4V3; CANADA
08/01/2017-07/31/2020
$131,515 CAN
The major goal of this study is to demonstrate that sarcolipin (SLN) knockdown improves the carco/endoplasmic reticulum calcium ATPase (SERCA) function and ameliorate the muscle disease in a dog model of Duchenne muscular dystrophy.
(There is no scientific/budget overlap with the current proposal)

Other Support – Progress Report YR 1
Gersbach, Charles A.

Previous Active Grants That Have Closed

Title: Engineering Morphogenetic Factors for Enhanced Genetic Reprogramming
Time commitments: 2 academic/0.25 summer months (18.7% calendar)
Supporting Agency: National Institutes of Health, 1DP2-OD008586 (Gersbach, PI)
Point of Contact:
Program Official (PO)
Basavappa, Ravi
301-435-7204
basavapr@mail.nih.gov
Performance Period: 9/30/11-6/30/16

Level of Funding: $300,000
Goals/Aims: To use protein engineering of transcription factors to increase the efficacy of genetic reprogramming of mammalian cells for regenerative medicine.
Overlap: None

Title: Photoregulated Gene Expression for Spatiotemporal Control of Morphogenesis
Time Commitments: 0
Supporting Agency: NSF Career Award, CBET-1151035 (Gersbach, PI)
Point of Contact:
Friedrich Srienc
Program Director
703.292.7029
fsrienc@nsf.gov
Performance Period: 4/1/12-3/31/17
Level of Funding: $62,052
Goals/Aims: To use light-inducible gene expression to spatially control the development of muscle and bone tissue in vitro.
Overlap: None

Title: Circulatory System and Integrated Muscle Tissue for Drug and Tissue Toxicity
Time Commitments: 0.5 academic months (or 4.1% calendar)
Supporting Agency: National Institutes of Health, 4UH3-TR000505-03 (Truskey, PI)
Point of Contact:
Long Nguyen
Grants Management Specialist
NIH-NCATS
nguyen1@mail.nih.gov
Performance Period: 7/24/12-6/30/17
Level of Funding: $724,754
Goals/Aims: To develop a circulatory system that consists of a high-pressure arterial system interfaced with various tissue microcirculatory test beds. A computer controlled pump will produce flow that mimics arterial flow.
Overlap: None

Title: Genetic Correction of Duchenne Muscular Dystrophy by Engineered Nucleases
Time Commitments: 0.25 academic/0.25 summer months (or 4.1% calendar)
Supporting Agency: Muscular Dystrophy Association, (Gersbach, PI)
Point of Contact:
Karen Smith
Grants Manager
520-529-2000
ksmith@mdausa.org
Performance Period: 8/1/13-7/31/16
Level of Funding: $90,909
Goals/Aims: To evaluate gene correction by artificial zinc finger nucleases and TALENs in cultured cells as a therapeutic approach to muscular dystrophy.

Overlap: None

Title: Genome Editing of Stem Cells for Analysis of Osteoarthritis Causal Variants
Time Commitments: 0.96 academic months (or 8% calendar)
Supporting Agency: NIH, 1R21AR065956 (Guilak and Gersbach, co-PI)
Point of Contact:
Program Official(PO)
Tyree, Bernadette
301-594-5032
tyreeb@mail.nih.gov
Performance Period: 4/1/14-3/31/16
Level of Funding: $132,000
Goals/Aims: To examine how genetic variation is linked to osteoarthritis by generating cartilage tissue from stem cells that have been modified to contain the gene variant of interest.
Overlap: None

Title: Targeted Gene Editing of Skeletal Muscle Progenitor Cells
Time Commitments: 0
Supporting Agency: Duke Coulter Translational Partnership, (Gersbach and Smith, Co-PIs)
Point of Contact:
Kristi D. Viles
Project Leader
919-668-8154
k.viles@duke.edu
Performance Period: 9/1/15-8/31/16
Level of Funding: $105,312
Goals/Aims: To evaluate gene delivery to muscle stem cells with widely-used vectors based on adeno-associated virus (AAV) and use molecular evolution strategies to develop novel AAV vectors with improved transduction of muscle stem cells.
Overlap: None

Title: Cell and Gene Modification Core
Time Commitments: 0.46 academic months (or 3.8% calendar)
Supporting Agency: NIH, 1P30AR066527(Li, PI)
Point of Contact:
Program Official(PO)
TSENG, HUNG H
tsengh@mail.nih.gov
Performance Period: 8/1/14-7/31/16
Level of Funding: $88,635
Goals/Aims: The main goal of the Cell and Gene Modification Core is to make available state-of-the-art gene and cellular modification techniques to the Duke SDRC membership.
Overlap: None

Title: Scaffold-Mediated Gene Delivery for Engineering of Osteochondral Tissues
Time Commitments: 0.74 academic/0.22 summer months (or 8% calendar)
Supporting Agency: NIH, 1R21AR067467 (Gersbach and Guilak, co-PIs)
Point of Contact:
Program Official(PO)
Wang, Fei
301-594-5055
wangf@mail.nih.gov
Performance Period: 7/1/15-6/30/17
Level of Funding: $110,000
Goals/Aims: To functionalize scaffolds with viral gene carriers in a spatially controlled manner for enhancing healing of osteochondral defects.

Title: Multiplex CRISPR/Cas9-Based Genome Engineering for the Genetic Correction of Duchenne Muscular Dystrophy
Time Commitments: 0.50 summer effort (or 4.1% calendar)
Supporting Agency: W81XWH-15-1-0469, USAMRMC MD140071 (Gersbach)
Point of Contact:
Marielena McGuire, PhD
Program Manager
301-619-8969
Marlena.v.mcguire.civ@mail.mil
Performance Period: 9/1/15-8/31/17
Level of Funding: $150,000
This proposal will focus on the correction of a mouse model of DMD (Duchenne Muscular Dystrophy with custom-engineered nucleases that treat this disease.

Current Research Support

Title: Engineering Targeted Epigenetic Modifiers for Precise Control of Gene Regulation
Time Commitments: 1.28 academic/0.22 summer effort (or 12.5% calendar)
Supporting Agency: NIH, 1R01DA036865 (Gersbach and Crawford, co-PI)
Point of Contact:
Program Official(PO)
Satterlee, John S
satterleej@mail.nih.gov
410-360-4734
Performance Period: 9/15/13-5/31/18
Level of Funding: $304,021 direct costs for current year
Goals/Aims: In this proposal we will develop tools for precisely modifying genome structure that will catalyze innovative advances in gene and cell therapy, drug development, and basic science.
Overlap: None

Title: Decoding and Reprogramming the Corticosteroid Transcriptional Regulatory Network
Time Commitments: 1.44 academic/0 summer months (or 17% calendar)*
Supporting Agency: NIH, 1U01-HG007900-01 (Reddy)

Point of Contact:
Program Official (PO)
PAZIN, MICHAEL J
pazinm@mail.nih.gov
Performance Period: 7/1/14-11/30/17
Level of Funding: $1,255,905 direct costs for current budget year
Goals/Aims: To comprehensively map the genomic effects of treatment with common anti-inflammatory drugs.
Overlap: Effort Note—actual summer effort for this project for the period of 12/1/16-11/30/17 is 0.6 summer months for calendar year 2017, however this has been removed to avoid the appearance of overlap as this effort has already been taken and this project will end 11/30/17. The 17% calendar reflects actual effort and calendar effort does not exceed 100%.

Title: Human EGFRvIII-specific BiTE for the treatment of Glioblastoma
Time Commitments: 0.9 academic months/0.3 summer months (or 10% calendar); Effort ended on project
Supporting Agency: NIH, 1U01NS090284 (Sampson)
Point of Contact:
Jane W. Fountain
Program Officer
Phone: 301-496-1431
Email: fountai@ninds.nih.gov
Performance Period: 7/1/15-6/30/20
Level of Funding: $361,911
Goals/Aims: To perform Investigational New Drug (IND) application required toxicity, stability and pharmacokinetic analysis of human EGFRvIII-specific BiTE for the treatment of glioblastoma.
Overlap: None

Title: Investigating Autophagy in GSD-1a
Time Commitments: 0.3 summer months (or 2.5% calendar)
Supporting Agency: NIH, 1R01DK105434 (Koeberl)
Point of Contact:
Grants and Contracts Specialist
Ellen W. Leschek
lescheke@extra.niddk.nih.gov
301-402-8291
Performance Period: 12/15/15-11/30/19
Level of Funding: $229,500 direct costs for current budget year
Goals/Aims: The goal of this project is to develop a gene therapy for glycogen storage disorder type 1a
Overlap: None

Title: In Vivo Epigenome Editing with CRISPR-Based Histone Acetyltransferase Transgenic Mice
Time Commitments: 0.6 academic/0 summer months (or 5% calendar)

Supporting Agency: NIH, 1R21DA041878 (West and Gersbach)
Point of Contact:
Grants and Contracts Specialist
Cheryl A. Nathaniel
nathanic@mail.nih.gov
202-526-0108
Performance Period: 4/1/16-3/31/18
Level of Funding: $121,452 direct costs for current budget year
Goals/Aims: We will generate novel Cre/loxP-conditional CRISPR/Cas9-based transgenic mouse strains in order to use epigenome editing to test the functional consequences of chromatin modifications for the long-lasting behavioral plasticities induced by psychostimulant drugs of abuse.
Overlap: None

Title: CRISPR/Cas9-Based Gene Editing for the Correction of Duchenne Muscular Dystrophy
Time Commitments: 0.58 academic/0.57 summer months (or 9.5% calendar)
Supporting Agency: NIH, R01AR069085 (Gersbach, PI)
Point of Contact:
Grants Management Specialist
Steve Austin
austins2@mail.nih.gov
301-594-3504
Performance Period: 4/1/16-3/31/21
Level of Funding: $274,560 direct costs for current budget year
Goals/Aims: The overall objective of this research proposal is to develop methods to restore dystrophin expression via targeted genome editing in vivo.
Overlap: None, although there is some conceptual overlap between R01AR06985 and the University of Missouri (USAMRMC) funded work, the proposed experiments are distinct. In particular, the USAMRMC W81XWH-15-1-0469 funded work is supporting the proof-of-principle studies used in the R01AR069085 proposal as preliminary data.

New Active Grants

Title: A Platform Technology for High-Thoroughput Screening of Gene Regulatory Elements
Time Commitments: 0.38 academic month (or 3.1% calendar)
Supporting Agency: Element Genomics, Inc (Gersbach, PI)
Point of Contact:
John Oxaal, CEO
300 West Duke Street
Durham, NC 27701
Performance Period: 11/15/16-11/14/17
Level of Funding: $52,415 direct costs for current budget year
Goals/Aims: The goal of this project is to develop a platform technology to assign function to putative regulatory elements in high-throughput to identify the gene regulatory mechanisms responsible for cell phenotype and disease states.
Overlap: None

Title: Engineering Novel Genome Engineering Systems

Time Commitments: 0.05 academic (or 0.4% calendar) *minimum effort covered by Duke

Supporting Agency: Locus Biosciences (Gersbach, PI)

Point of Contact:

Dave Ousterout, PhD
6845 Piershill Lane
Cary, NC 27519

Performance Period: 7/1/16-6/30/18

Level of Funding: $78,616 direct costs for current budget year

The purpose of this sponsored research agreement is to develop novel technologies for genome editing of mammalian cells.

Overlap—None

Title: Treating Duchenne Cardiomyopathy in the Mouse Model by Gene Repair

Time Commitments: 0.05 academic (or 0.4% calendar)*minimum effort covered by Duke

Supporting Agency: University of Missouri (Prime award USAMRMC W81XWH1610221)

Point of Contact:

Craig David, Director, OSPA
115 Business Loop 70W
Mizzou North Room 501
Columbia, MO 65211

Performance Period: 9/1/16-8/31/19

Level of Funding: $60,000 direct costs for current budget year

Overlap: None, although there is some conceptual overlap between R01AR06985 and the University of Missouri (USAMRMC) funded work, the proposed experiments are distinct. In particular, the USAMRMC W81XWH-15-1-0469 funded work is supporting the proof-of-principle studies used in the R01AR069085 proposal as preliminary data.

Title: Defining the Mechanisms of Gene Regulation and Drug Resistance in Cancer

Time Commitments: 0.05 academic (or 0.4% calendar)*minimum effort covered by Duke

Supporting Agency: Thorek Memorial Foundation (Gersbach)

Point of Contact:

Timothy Maeder, Executive Director
850 West Irving Park Road
Chicago, IL 60613
tmaeder@thorekfoundation.org

Performance Period: 2/1/17-1/31/19

Level of Funding: $250,000 direct costs for current budget period

In this project, we will use our new technology to complete the first genome-wide screen of endogenous regulatory contributions to cancer drug. We will use imatinib resistance in K562 cells as a model system. Imatinib is a tyrosine kinase inhibitor and first line treatment for chronic myologenous leukemia

Overlap—None

Title: Epigenome Editing Technologies to Control Diverse Biological Functions

Time Commitments: 1.6 academic and 0.8 summer months (or 20% calendar)

Supporting Agency: Allen Frontiers Group (Gersbach)

Point of Contact:

Kathy Richmond, Program Officer
kathrynr@alleninstitute.org
206-548-8491

Performance Period: 8/1/17-7/31/20

Level of Funding: $486,609 direct costs for current budget period

The objective of this proposal is to optimize and apply epigenome editing tools to probing mechanisms of neuronal differentiation and neurological behaviors including learning and memory.

Overlap—None

Title: Systemic Inflammation in Microphysiological Models of Muscle and Vascular Disease

Time Commitments: 0.75 summer months (or 6.2% calendar)

Supporting Agency: 1UG3-TR002142-01- NIH (Truskey)

Point of Contact:

Danilo A. Tagle, Program Officer
tagled@ninds.nih.gov
301-496-5745

Performance Period: 8/1/17-6/30/19

Level of Funding: $750,000 direct costs for current budget period

Our goal in this project is to develop clinically relevant hMPS disease models to examine rheumatoid arthritis (RA) risk for muscle dysfunction and atherosclerosis and the role of exercise in attenuating disease-associated inflammation.

Overlap—None

Title: Collaborative Research: Adapting Cas9 Protein from CRISPR as a Structural Unit for Molecular Assembly

Time Commitments: 0.25 summer effort (or 2.1% calendar)

Supporting Agency: 1709527 – NSF (LaBean and Gersbach) Dates or calendar does not match

Point of Contact:

Aleksandr Simonian, Program Official
703-292-2191

Performance Period: 7/1/17-6/30/20

Level of Funding $45,845 direct costs

Design, clone, express, and purify dCas9 fusion proteins bearing binding domains for various materials including gold nanoparticles and carbon nanotubes for testing (at the LaBean lab) the assembly of functional electronic and photonic nano-devices. Design, clone, express, and purify dCas9 fusion proteins bearing functional enzymatic domains for testing (at the LaBean lab) the assembly of multienzyme cascades.

Overlap--None

Other Support – Progress Report YR 1
Gang Yao, Co-I

Previous/active grants that have closed

Title: A pilot study on systemic delivery of an AAV-9 five-repeat micro-dystrophin vector in juvenile DMD dogs
Level of Effort: 4% effort, Co-I
Funding Agency: Solid Ventures
Project Goals and Specific Aims: This project is to evaluate the effectiveness of a new treatment for Duchenne muscular dystrophy in a dog model of the disease. My specific responsibility as a Co-I is to help apply an imaging system for the assessment of the animals' whole body overnight activity.
Performance Period: 06/01/2015 to 08/31/2016
Level of Funding: $100,000
Point of contact at the agency: Joel Schneider, Ph.D.; 101 Main Street; Cambridge, MA 02142
Overlap/complement with the current proposal: None

Title: Evaluation of pupillary light reflex as a biomarker of neurodevelopmental disorder
Level of Effort: 11% effort, PI
Funding Agency: National Institutes of Health
Project Goals and Specific Aims: The goal of this project is to evaluate pupillary light reflex as a biomarker for autism in young 2-6 years old children.
Performance Period: 07/08/2013 to 04/30/2015 (no-cost extension to 04/30/16)
Level of Funding: $405,000
Point of contact at the agency: George Giacoia, 9000 Rockville Pike. Bethesda, Maryland 20892
Overlap/complement with the current proposal: None

Current Research Support

Title: Developing Pupillary Light Reflex Technologies for Early Screening of Neurodevelopmental Disorders
Level of Effort: 10% effort, PI
Funding Agency: National Science Foundation
Project Goals and Specific Aims: The goal of this project is to develop a new imaging system and data analysis methodology for investigating pupillary light reflex in infants and extracting neurological information specific to autonomic nervous system.
Performance Period: 07/15/2015 to 06/30/2018
Level of Funding: $203,688 total direct costs
Point of contact at the agency: Alexander Leonessa, 201 Wilson Boulevard, Arlington, Virginia 22230, USA
Overlap/complement with the current proposal: None

New Active Grants

Title: Fine-needle microscopic tractography for in vivo high-resolution imaging of muscle damage
Level of Effort: 5% effort, PI
Funding Agency: University of Missouri, Interdisciplinary Pilot Studies in Translational Science and Biomedical Innovations
Debbie Taylor, MA204 Medical Sciences Building, University of Missouri
Performance Period: 07/01/2017 to 06/30/2018
Level of Funding: $50,000
Project Goals and Specific Aims: The goal of this project is to develop a new microscopic imaging method for minimal invasive imaging of muscle damage.
Overlap/complement with the current proposal: None

Title: Optical polarization tractography for cervical lesion detection
Level of Effort: 5% effort, Co-PI
Funding Agency: University of Missouri, MU Coulter Partnership
Project Goals and Specific Aims: The goal of this project is to investigate the potential of using optical polarization tractography to detect and differentiate cervical lesions.
Performance Period: 07/01/2017 to 12/31/2017
Level of Funding: $22,000
Point of contact at the agency: Cynthia Helphingstine, 235 Agricultural Engineering Building, University of Missouri
Overlap/complement with the current proposal: None

Title: A pilot study to evaluate long-term safety and efficacy of AAV-9 5Rc micro-dystrophin therapy
Level of Effort: 4% effort, Co-I
Funding Agency: Solid Biosciences
Project Goals and Specific Aims: The overarching goal of this project is to determine whether systemic AAV-9 5Rc micro-dystrophin gene therapy can yield long-term (up to 4 years after injection) microgene expression without causing serious adverse events (SAEs).
Performance Period: 06/01/2016-05/31/2019
Level of Funding: $100,000
Point of contact at the agency: Joel Schneider, Ph.D.; 101 Main Street; Cambridge, MA 02142
Overlap/complement with the current proposal: None

Organizations that have involved as partners.

Organization Name: Duke University
Location of Organization: Durham, NC
Partner's contribution to the project: Dr. Gersbach's lab will perform droplet PCR to quantify genome editing and RNA correction and in vivo quantification of off-target effect in the study of Duchenne cardiomyopathy gene editing therapy in the mouse model for DMD.

Dr. Gersbach's lab has quantified on-target and off-target genome editing in the study in the current funding period. The results of these collaborative efforts are combined in the accomplishments section.

8. Special reporting requirements: N/A

9. Appendices:

Peer-reviewed publications

Available online at www.sciencedirect.com

ScienceDirect

Current Opinion in Virology

Systemic delivery of adeno-associated viral vectors

Dongsheng Duan[1,2,3,4]

For diseases like muscular dystrophy, an effective gene therapy requires bodywide correction. Systemic viral vector delivery has been attempted since early 1990s. Yet a true success was not achieved until mid-2000 when adeno-associated virus (AAV) serotype-6, 8 and 9 were found to result in global muscle transduction in rodents following intravenous injection. The simplicity of the technique immediately attracts attention. Marvelous whole body amelioration has been achieved in rodent models of many diseases. Scale-up in large mammals also shows promising results. Importantly, the first systemic AAV-9 therapy was initiated in patients in April 2014. Recent studies have now begun to reveal molecular underpinnings of systemic AAV delivery and to engineer new AAV capsids with superior properties for systemic gene therapy.

Addresses
[1] Department of Molecular Microbiology and Immunology, School of Medicine, The University of Missouri, Columbia, MO 65212, USA
[2] Department of Neurology, School of Medicine, The University of Missouri, Columbia, MO 65212, USA
[3] Department of Bioengineering, The University of Missouri, Columbia, MO 65212, USA
[4] Department of Biomedical Sciences, College of Veterinary Medicine, The University of Missouri, Columbia, MO 65212, USA

Corresponding author: Duan, Dongsheng (duand@missouri.edu)

Current Opinion in Virology 2016, **21**:16–25

This review comes from a themed issue on **Viral gene therapy vector–host interactions**

Edited by **David Markusic** and **Roland Herzog**

http://dx.doi.org/10.1016/j.coviro.2016.07.006

Introduction

Many life-threatening diseases affect a number of organs or affect tissues that are widely distributed. A successful gene therapy for these diseases requires a viral vector that can effectively reach all target cells throughout the body. Since our vessels are a built-in and ready-to-use system for bodywide transportation, a convenient strategy to achieve systemic delivery would be infusion of a therapeutic viral vector into the circulation. For this seeming straightforward method to work, a viral vector has to reach the target area, get out from the vasculature and infect the diseased cells.

A report in 1992 claimed to have achieved 'widespread long-term gene transfer' to striated muscles in newborn mice using recombinant adenovirus [1]. The authors delivered adenovirus intravenously to 2–5-day-old mice and detected some expression in the liver, lung, heart and skeletal muscle. While the adenoviral vector had indeed spread to various tissues and organs, there were only sporadic transduction in skeletal muscle and ~0.2% transduction in the heart. This is far from 20 to 50% gene transfer efficiency required to treat skeletal muscle disease and cardiomyopathy in diseases like Duchenne muscular dystrophy (DMD) [2,3]. Several strategies were developed to overcome the endothelial barrier for systemic adenovirus delivery. These include the application of the vessel dilator and permeabilizer, hydrodynamic injection and viral capsid modification [4–6]. Despite improved intravascular transduction of a single limb with pressurized infusion and endothelial permeabilization, adenoviral vectors eventually lose the favor for systemic delivery due to severe immune responses and fatal complications [7].

Over the last two decades, adeno-associated virus (AAV) has emerged and now become the most preferred vector for gene therapy [8•,9•,10•,11]. AAV is a single stranded DNA virus discovered in 1965 [12]. It persists mainly as episomal molecules in infected tissues [13–15]. More than 12 different serotypes and hundreds of capsid variants have been isolated from adenoviral stocks and animal tissues or engineered in laboratories. In contrast to adenovirus, intramuscular injection of recombinant AAV serotype-2 (AAV-2) resulted in yearlong robust transduction with nominal cellular immune responses [16,17]. Strategies that have been shown to enhance adenoviral intravascular delivery (such as pharmacological vessel permeabilization and forced extravasation) also resulted in uniform whole limb muscle transduction by AAV-2 [4,18]. However, there remains a significant gap to achieve whole body gene transfer from peripheral vessels. A bona fide breakthrough in systemic gene delivery has to wait until new AAV serotypes are isolated.

Systemic gene delivery with AAV in rodents

In early days of AAV vector development, most studies are focused on AAV-2. Isolation of new serotypes has greatly expanded the repertoire [19–21]. Rutledge *et al.* isolated AAV-6 from an adenovirus stock [22]. Gao *et al.* isolated AAV-8 and AAV-9 from tissues of rhesus monkey and human, respectively [23••,24]. These three serotypes open the door to a successful systemic delivery. Gregorevic *et al.* showed efficient whole body striated muscle transduction in mice after tail vein

Figure 1

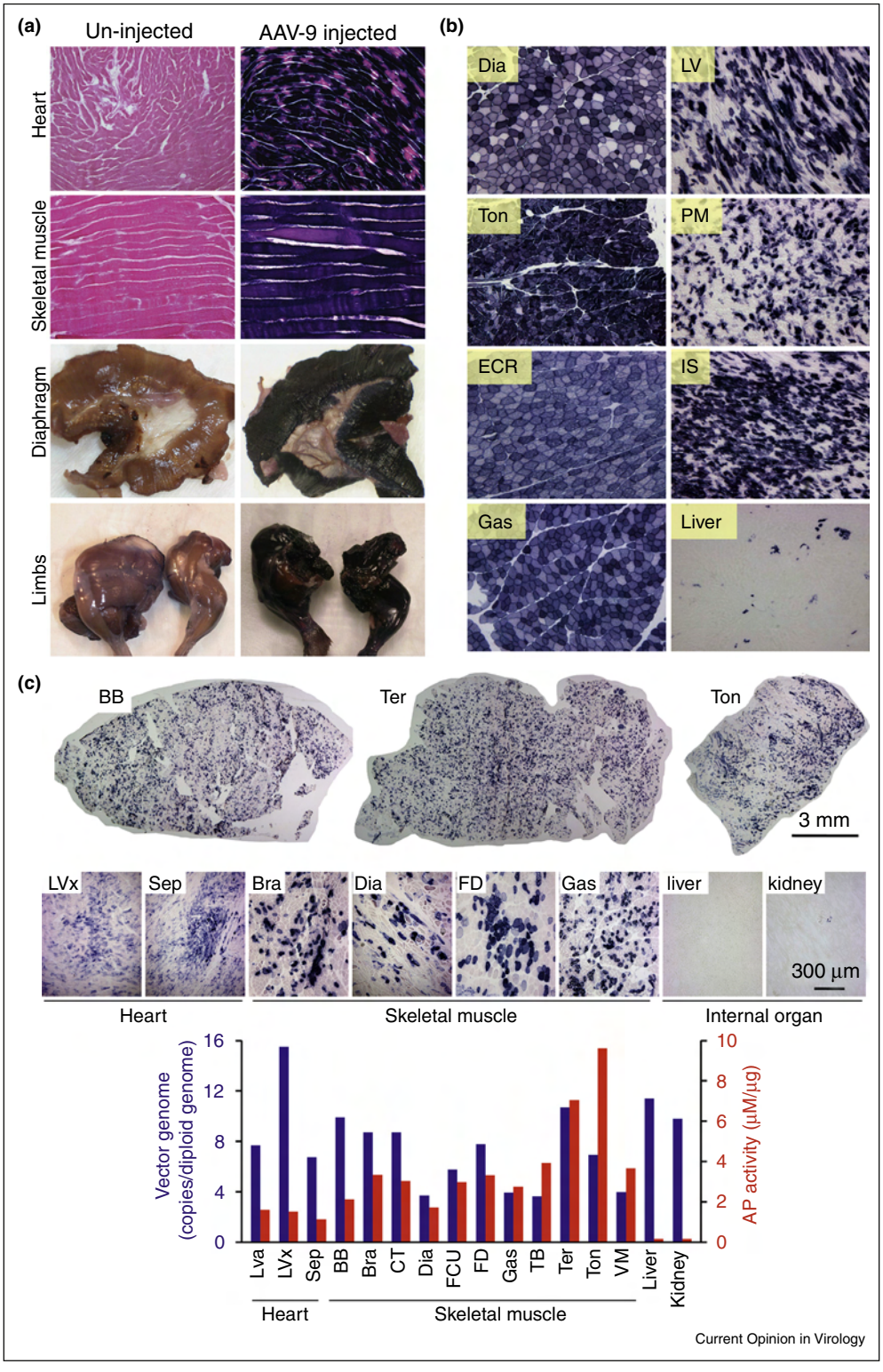

Systemic AAV delivery results in bodywide gene transfer in rodents and large mammals. Peripheral vascular delivery provides a method that allows an AAV vector to reach most, if not every, part of the body. **(a)** Bodywide muscle transduction in mice following tail vein delivery of an alkaline phosphatase (AP) reporter gene AAV-9 vector. **(b)** Robust and persistent (up to one year) skeletal muscle and myocardial transduction after jugular vein injection of an AAV-8 AP vector in a neonatal dog. **(c)** Tyrosine mutant AAV-9 results in whole body striated muscle transduction in young adult dystrophic dogs. Top panel, representative full-view images from selected skeletal muscles; middle panel, representative

Table 1

Comparison of AAV-2 with AAV-1, 6, 7, 8 and 9 for systemic delivery

	AAV-1	AAV-2	AAV-6	AAV-7	AAV-8	AAV-9	References
In vitro capsid stability	Moderate	Low	?	?	Moderate	?	[140]
Blood clearance	Fast	Fast	Fast	Fast	Fast	Slow	[31•,94]
Transcytosis	?	Poor	Poor	?	High	High	[99,100•,101]
Direct muscle transduction efficiency	High	Moderate	Very high	High	Moderate	High–very high	[23••,129]
Systemic transduction efficiency	High	Low	High	High	High–very high	Very high	[26••,30,31•,32]
Unique features		Very efficient in cultured cells			Low immunity[a]	Cardiotropic in rodents[b]; Cross BBB[c]	

[a] See Refs. [40,82•] and [79,141–146].
[b] See Refs. [27•,28•,29•, 30,31•, 32].
[c] See Refs. [85••,86–89]. BBB, blood–brain-barrier.

injection of AAV-6 and the vascular endothelium growth factor for transient microvasculature permeabilization [25••]. Wang *et al.* achieved widespread saturated transduction of the heart as well as axial and appendicular muscles in mice and hamsters via systemic delivery of AAV-8 [26••]. Shortly after, successful bodywide systemic gene transfer was established for AAV-9 (Figure 1) [27•,28•,29•]. Interestingly, peripheral delivery of AAV-9 resulted in superior myocardial and central nervous system transduction. It is now clear that other AAV serotypes (such as AAV-1 and AAV-7) can also lead to systemic transduction (Table 1) [26••,30,31•]. Nevertheless, AAV-9 remains the most potent serotype for systemic delivery in rodents [30,31•,32].

The establishment of systemic AAV delivery technique immediately raises the possibility for bodywide correction in rodent models of human diseases. Today, impressive results have been reported in neonatal, adult and even aged animals. Some of these examples include AAV-1 mediated gene therapy for Pompe disease, limb-girdle muscular dystrophy (LGMD) and myotonic dystrophy [33–35], AAV-6 mediated gene therapy for DMD and facioscapulohumeral muscular dystrophy [25••,36•,37,38], AAV-8-mediated gene therapy for DMD, LGMD and atherosclerosis [26••,39–41], and AAV-9 mediated gene therapy for cardiomyopathy, lysosomal storage disorders and neuronal diseases [42,43,44•,45–51].

The maximal packaging capacity of an AAV vector is ~5-kb [52–55]. This limits the use of AAV for a number of diseases including DMD and dysferlin-deficient myopathy. Various dual AAV strategies have been developed to overcome this hurdle (reviewed in [56–58]). Optimized dual AAV vectors have reach transduction efficiency of the single AAV vector [59,60]. Ghosh *et al.* provided the first proof-of-principle evidence for efficient systemic dual AAV delivery in normal and diseased mice [61•,62]. Subsequent studies from several laboratories showed unequivocal evidence that systemic dual AAV therapy is a viable option for bodywide alleviation for DMD and dysferlin-deficient myopathy [63–65].

Scale-up systemic AAV delivery in large mammals

The remarkable success in rodents and the convenience of the technique have stimulated tremendous interests in adopting systemic AAV delivery to large mammals. The first successful systemic AAV delivery to a large mammal was achieved with AAV-9 in newborn canines (Figure 1) [66•]. Surprisingly, despite spectacular bodywide skeletal muscle transduction, few cardiomyocytes were transduced [66•]. In sharp contrast, AAV-8 yielded robust transduction of both skeletal and cardiac muscles in dog puppies (Figure 1) [67,68]. AAV-1 and AAV-6 are two other serotypes that have shown good systemic transduction in rodents [26••,30,31•]. Recent studies suggest that mutating surface-exposed tyrosine can significantly enhance AAV transduction [69,70]. Hakim *et al.* tested tyrosine modified AAV-1 and AAV-6 in neonatal dogs [71]. Interestingly, AAV-1 showed high efficient whole body striated muscle transduction but AAV-6 resulted in little muscle transduction (Figure 1). Two groups explored systemic AAV-9 delivery in newborn DMD puppies [72,73•]. Gene transfer was observed in multiple muscles up to 4 months of age. However, Kornegay *et al.* encountered a catastrophic inflammatory response potentially linked to the transgene product [73•]. Contrary to Kornegay *et al.*, Hinderer *et al.* reasoned that neonatal period could be a window to induce immune tolerance to the transgene product [74].

(Figure 1 Legend Continued) high-power images from selected skeletal muscles, heart and internal organs; bottom panel, quantification of the AAV genome and AP expression in selective tissues. BB, biceps brachii; Bra, brachialis; Dia, diaphragm; CT, cranial tibialis; ECR, extensor carpi radialis; FCU, flexor carpi ulnaris; FD, flexor digitorum; Gas, gastrocnemius; IS, interstitial septum; LV, left ventricle; LVa, left ventricle anterior portion; LVx, left ventricle apex; PM, papillary muscle; Sep, septum; TB, triceps brachii; Ter, teres; Ton, tongue; VM, vastus medialis.

Indeed, they were able to achieve this goal by systemic delivery of low-dose AAV-8 (30-fold lower than used by Kornegay *et al.*) in rhesus monkeys and type I mucopolysaccharidosis dogs [74].

Very few studies have evaluated systemic AAV delivery to adult large mammals. An early work in cynomologus monkeys suggests that even very low-dose AAV ($\leq 5 \times 10^{10}$ particles/kg) can result in vector genome accumulation in the spleen and expression in the lympho nodes [75]. Intriguingly, regional intravascular delivery of AAV to nonhuman primates is devoid of cellular immunotoxicity [76–78]. Several groups have shown successful regional limb perfusion with AAV-1 and 8 in normal and diseased dogs [79–81,82•]. A breakthrough of systemic AAV transfer in a diseased adult large mammal has not been achieved until recently. Yue *et al.* injected tyrosine mutant AAV-9 to young adult DMD dogs from a peripheral vein and observed efficient global skeletal and cardiac muscle transduction without serious complications (Figure 1) [83••]. Hakim *et al.* further extended this result demonstrating systemic delivery of an AAV-9 micro-dystrophin vector can lead to near saturated expression for at least 12 months without any toxicity in adult affected dogs [84].

The most exciting progress is the ongoing clinical trial in neonatal spinal muscular atrophy (SMA) patients using AAV-9 by Drs. Mendel, Kaspar and colleagues (clinical trial ID: NCT02122952) [85••]. SMA is caused by mutations in the survival motor neuron 1 (SMN1) gene. Earlier studies from several groups have revealed remarkable therapeutic benefits in newborn SMA mice with AAV-9 mediated systemic SMN1 gene therapy [86–89]. In this game-changing clinical trial, fifteen 1 to 8-m-old patients received intravenous injection of up to 2×10^{14} particles/kg of the AAV-9 SMN1 vector. Some patients have been treated for almost two years. There was no major safety concerns. Importantly, high-dose group patients showed clinical improvement [85••].

Mechanistic insights of systemic AAV delivery

A better understanding on the mechanisms of systemic AAV transduction is essential to further improve this important gene therapy technology. The major rate-limiting steps may include interaction with serum proteins, blood clearance, vessel escape, attachment, endocytosis, intracellular processing, nuclear entry and vector genome conversion (Figure 2, Table 1). The last five steps have been extensively reviewed elsewhere and will not be discussed here [90,91].

Figure 2

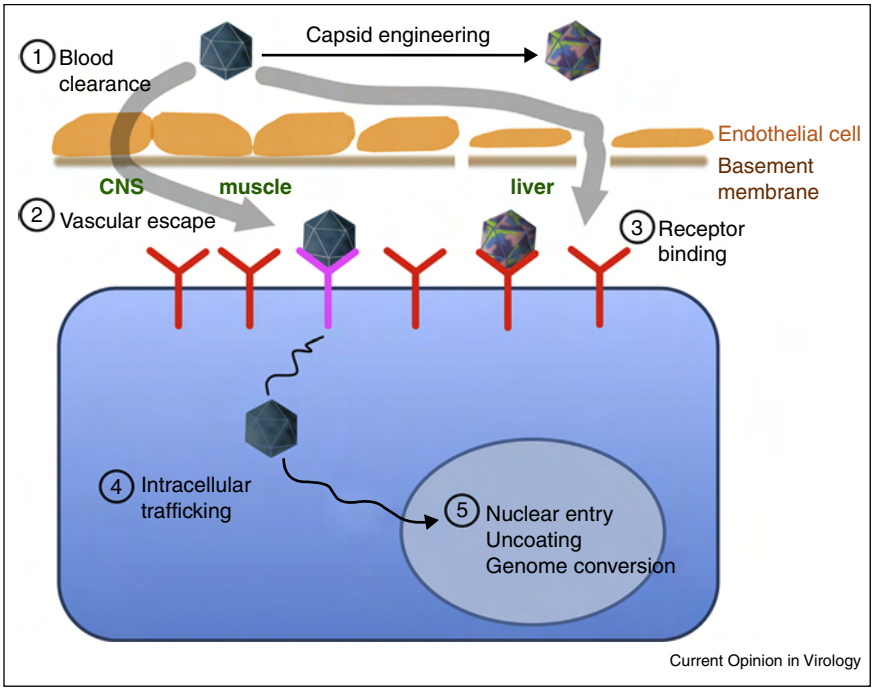

Rate-limiting steps in systemic AAV delivery. The major rate-limiting steps include interaction with serum proteins (such as neutralizing antibodies), blood clearance, vessel escape, attachment, endocytosis, intracellular processing, nuclear entry and vector genome conversion. Capsid engineering can yield new AAV variants with enhanced systemic delivery properties. Numerical numbers highlight five rate-limiting barriers. Capillaries in the central nerve system (CNS) are sealed by the blood–brain barrier. Transcytosis is the only way for AAV to exit the vasculature in CNS. Capillaries in the liver and spleen are fenestrated and discontinuous. This allows for efficient paracellular diffusion of AAV into the parenchyma. Capillaries in muscles may allow for limited paracellular transport of AAV. However, transcytosis may likely be the primary pathway for AAV to get to muscle.

Interaction of AAV with circulating proteins greatly influences the outcome of systemic delivery. Inactivation by pre-existing neutralizing antibodies has been well documented. Recently, Denard *et al.* found that some blood proteins bind to certain AAV serotypes in a species-specific manner [92,93]. In particular, AAV-6 interacts with the galectin 3 binding protein in human and dog sera but not macaque and mouse sera. This interaction aggregates AAV particles and hampers systemic delivery [92]. On the other side, AAV-6 interacts with the C-reactive protein in mouse but not human sera. Instead of inhibition, this interaction boosts systemic delivery [93].

Blood clearance varies dramatically among AAV serotypes [31•,94]. While rapid clearance may not necessarily abort systemic delivery, prolongation of the circulation time certainly enhances it [31•,94,95,96•]. In this regard, delayed clearance has been suggested as a primary reason underlying pronounced systemic delivery of AAV-9 [94]. Shen *et al.* investigated the underlying mechanisms for extended persistence of AAV-9 in blood and found that it is due to the low abundance of the AAV-9 receptor, hence reduced tissue binding [95]. It is very likely that the blood clearance of AAV is regulated by many factors. Additional studies may reveal these yet unknown factors. On the other side, future studies are also needed to explain why fast blood clearance of some AAV serotypes (such as AAV-8) has minimal impact on systemic delivery (Table 1).

Depending on the architecture of capillary, AAV may get out from blood via two different pathways, paracellular or transcellular (Figure 2). Paracellular transport refers to the escape of a virus from the circulation through the space between adjacent endothelial cells. Capillaries in the liver and spleen are fenestrated and discontinuous (Figure 2). In these tissues, AAV can readily diffuse out through large gaps between endothelial cells. This paracellular mechanism contributes to the accumulation of the AAV genome in the liver following systemic delivery [25••,27•,30,31•,83••,97].

In the central nerve system, the tight junctions between neighboring endothelial cells form the highly selective blood-brain barrier (Figure 2). In this case, the only way to escape from the circulation is transcellular transcytosis (Figure 2). In this process, AAV is taken into endothelial cells in specialized vesicles [98]. These vesicles traffic to the other side of the cell and release the virus into the interstitium. AAV transcytosis has been documented *in vitro* [99,100•,101]. Interestingly, AAV-8 and 9 show efficient transcytosis but AAV-6 dose not [100•,101,102]. Recent studies have revealed two distinctive mechanisms of transcytosis, dependent or independent of caveolae [103]. Kotchey *et al.* found that systemic AAV-9 transduction is not compromised in cavelin-1 knockout mice. Since AAV-9 displays unparalleled superior neuronal tissue transduction when delivered through the peripheral vein [104], it is very likely that transvascular transport of AAV-9 is through caveolae-independent transcytosis [94].

Re-engineering AAV for improved systemic delivery

Despite the great promise of systemic delivery, the current technology remains limited. For example, a large proportion of humans are seropositive for known AAV serotypes [105,106]. Further, systemic delivery often leads to gene transfer in non-target tissues and organs. AAV transduction is largely determined by the viral capsid, especially variable loops on the surface [107,108•,109]. Several strategies have been used to develop novel capsids for improved systemic delivery. These include (1) isolation and reconstruction from existing or ancestral species [110,111], and (2) modification by rational design and directed evolution [112•,113].

Many new AAV isolates have been tested for systemic delivery recently. These studies have revealed some unique organism, organ, tissue, or cell-type specific transduction patterns after intravascular delivery. For example, AAV-3B showed superior hepatotropism in the primate but not rodent liver [114–116]. AAV-4 showed selective cardiopulmonary tropism [117]. AAV-rh8 and rh10 are as efficient as AAV-9 in crossing the blood–brain barrier [118].

A hurdle to systemic AAV delivery is the high prevalence (40–80%) of pre-existing immunity in human populations (reviewed in [119]). While some successes have been achieved with the application of immune suppressive drugs (such as anti-CD20 antibody rituximab) and plasmapheresis [120–122], modification of the antigenic epitope on the capsid may yield neutralizing-resistant 'designer' AAV variants. Several approaches have been used to map the neutralizing antibody binding epitopes for different AAV serotypes (reviewed in [123]). These studies suggest that protrusions around the 3-fold axis and 2/5-fold wall participate in interactions with neutralizing antibodies [123]. Targeted mutagenesis of these residues may circumvent preexisting immunity [124,125]. An alternative and highly effective method to targeted mutagenesis is forced evolution in the presence of high amounts of neutralizing antibodies (such as pooled immunoglobulins from human donors) (reviewed in [112•,126]). This approach has allowed isolation of neutralizing antibody escaping AAV variants AAV-r2.15 by Maheshri *et al.* and AAV-DJ by Grimm *et al.* [127•,128]. More recently, Li *et al.* found that capsid variants isolated following *in vitro* selection in human serum had poor *in vivo* transduction strength although they were able to escape neutralization [129]. *In vivo* selection in the presence of the patient serum may yield escaping-capsids with better *in vivo* performance [129].

Blood clearance is a rate-limiting barrier in systemic delivery. The determinants for AAV-9 blood clearance were reported recently [94,95,130]. These mainly consist of surface-exposed amino acids and overlap with the receptor footprint. Mutations in these residues substantially shorten the circulation half-life and reduce systemic transduction [94,95,130].

Delivery of a viral vector through the bloodstream will likely spread the virus to untoward tissues/organs. This raises safety concerns. Sequestration of AAV in these non-target locations also reduces the amount of vectors that can be delivered to the targets and hence has significant implications on the effective vector dose needed for systemic therapy. Tissue/cell-specific AAV will help resolve this problem. A series of tropism-modified AAV capsid variants have been developed using either *in vivo* evolution or educated engineering. These capsid chimeras are highly desirable for systemic gene therapy of various diseases, for example, liver-detargeted vectors for muscular dystrophy [96•,130–132], liver-enhanced vectors for hemophilia [128,133•], myocardium tropic vectors for cardiomyopathy [134], central nerve system-enhanced vectors for neurodegenerative diseases [135].

AAV uses cell surface carbohydrates as its binding receptors [136]. The nature and abundance of these extracellular glycans vary dramatically between different species and at different developmental stages. Since AAV attachment is a determining factor in systemic delivery, cautions should be taken to extrapolate re-engineered capsids for different applications [102,115,116,137].

Conclusion

The non-invasive nature and the convenience of peripheral vascular delivery promise a straightforward approach to treating a number of diseases. Many barriers have been overcome. However, there remain significant hurdles to translate the promise of systemic delivery into clinical benefits in human patients. Further, new challenges will surface as we learn more about AAV (such as the discovery of the universal AAV receptor) and begin to apply systemic delivery to new technologies (such as gene editing with the CRISPR technology) [138•,139]. The study on systemic viral vector delivery has just reached its prime time and the best is yet to come.

Acknowledgements

The research in the Duan lab is supported by the National Institutes of Health (NS-90634, AR-69085, AR-67985 and AR-70517), Department of Defense (MD130014 and MD150133), Muscular Dystrophy Association, Jesse's Journey-The Foundation for Gene and Cell Therapy, Parent Project Muscular Dystrophy, Hope for Javier, Solid GT LLC and the University of Missouri.

Disclosure: D.D. is a member of the scientific advisory board for Solid GT, LLC and an equity holder of Solid GT, LLC. The Duan lab has received research supports from Solid GT, LLC.

References and recommended reading

Papers of particular interest, published within the period of review, have been highlighted as:

- • of special interest
- •• of outstanding interest

1. Stratford-Perricaudet LD, Makeh I, Perricaudet M, Briand P: **Widespread long-term gene transfer to mouse skeletal muscles and heart**. *J Clin Invest* 1992, **90**:626-630.

2. Chamberlain JS: **Gene therapy of muscular dystrophy**. *Hum Mol Genet* 2002, **11**:2355-2362.

3. Duan D: **Challenges and opportunities in dystrophin-deficient cardiomyopathy gene therapy**. *Hum Mol Genet* 2006, **15(Spec No 2)**:R253-R261.

4. Greelish JP, Su LT, Lankford EB, Burkman JM, Chen H, Konig SK, Mercier IM, Desjardins PR, Mitchell MA, Zheng XG *et al.*: **Stable restoration of the sarcoglycan complex in dystrophic muscle perfused with histamine and a recombinant adeno-associated viral vector**. *Nat Med* 1999, **5**:439-443.

5. Douglas JT, Curiel DT: **Strategies to accomplish targeted gene delivery to muscle cells employing tropism-modified adenoviral vectors**. *Neuromuscul Disord* 1997, **7**:284-298.

6. Cho WK, Ebihara S, Nalbantoglu J, Gilbert R, Massie B, Holland P, Karpati G, Petrof BJ: **Modulation of Starling forces and muscle fiber maturity permits adenovirus-mediated gene transfer to adult dystrophic (mdx) mice by the intravascular route**. *Hum Gene Ther* 2000, **11**:701-714.

7. Wilson JM: **Lessons learned from the gene therapy trial for ornithine transcarbamylase deficiency**. *Mol Genet Metab* 2009, **96**:151-157.

8. • Muzyczka N: **Use of adeno-associated virus as a general transduction vector for mammalian cells**. *Curr Top Microbiol Immunol* 1992, **158**:97-129.
This review article summarizes the very early stage of AAV vector development.

9. • Carter BJ: **Adeno-associated virus and the development of adeno-associated virus vectors: a historical perspective**. *Mol Ther* 2004, **10**:981-989.
This is a comprehensive review of the history of AAV vector development.

10. • Samulski RJ, Muzyczka N: **AAV-mediated gene therapy for research and therapeutic purposes**. *Annu Rev Virol* 2014, **1**:427-451.
This is a comprehensive review of AAV transduction biology.

11. Muzyczka N, Berns KI: **AAV's golden jubilee**. *Mol Ther* 2015, **23**:807-808.

12. Atchison RW, Casto BC, Hammon WM: **Adenovirus-associated defective virus particles**. *Science* 1965, **149**:754-756.

13. Duan D, Sharma P, Yang J, Yue Y, Dudus L, Zhang Y, Fisher KJ, Engelhardt JF: **Circular intermediates of recombinant adeno-associated virus have defined structural characteristics responsible for long term episomal persistence in muscle**. *J Virol* 1998, **72**:8568-8577.

14. Schnepp BC, Jensen RL, Chen CL, Johnson PR, Clark KR: **Characterization of adeno-associated virus genomes isolated from human tissues**. *J Virol* 2005, **79**:14793-14803.

15. Penaud-Budloo M, Le Guiner C, Nowrouzi A, Toromanoff A, Cherel Y, Chenuaud P, Schmidt M, von Kalle C, Rolling F, Moullier P *et al.*: **Adeno-associated virus vector genomes persist as episomal chromatin in primate muscle**. *J Virol* 2008, **82**:7875-7885.

16. Xiao X, Li J, Samulski RJ: **Efficient long-term gene transfer into muscle tissue of immunocompetent mice by adeno-associated virus vector**. *J Virol* 1996, **70**:8098-8108.

17. Kessler PD, Podsakoff GM, Chen X, McQuiston SA, Colosi PC, Matelis LA, Kurtzman GJ, Byrne BJ: **Gene delivery to skeletal muscle results in sustained expression and systemic delivery of a therapeutic protein**. *Proc Natl Acad Sci U S A* 1996, **93**:14082-14087.

18. Su LT, Gopal K, Wang Z, Yin X, Nelson A, Kozyak BW, Burkman JM, Mitchell MA, Low DW, Bridges CR *et al.*: **Uniform scale-independent gene transfer to striated muscle after transvenular extravasation of vector**. *Circulation* 2005, **112**:1780-1788.

19. Wu Z, Asokan A, Samulski RJ: **Adeno-associated virus serotypes: vector toolkit for human gene therapy**. *Mol Ther* 2006, **14**:316-327.

20. Gao G, Vandenberghe LH, Wilson JM: **New recombinant serotypes of AAV vectors**. *Curr Gene Ther* 2005, **5**:285-297.

21. Vandenberghe LH, Wilson JM, Gao G: **Tailoring the AAV vector capsid for gene therapy**. *Gene Ther* 2009, **16**:311-319.

22. Rutledge EA, Halbert CL, Russell DW: **Infectious clones and vectors derived from adeno-associated virus (AAV) serotypes other than AAV type 2**. *J Virol* 1998, **72**:309-319.

23. •• Gao GP, Alvira MR, Wang L, Calcedo R, Johnston J, Wilson JM: **Novel adeno-associated viruses from rhesus monkeys as vectors for human gene therapy**. *Proc Natl Acad Sci U S A* 2002, **99**:11854-11859.
This study opens the door of isolating new AAV variants from mammalian tissues. Several AAV serotypes discovered in this study (such as AAV-8 and AAV-9) show excellent systemic delivery property and are currently in human trials.

24. Gao G, Vandenberghe LH, Alvira MR, Lu Y, Calcedo R, Zhou X, Wilson JM: **Clades of adeno-associated viruses are widely disseminated in human tissues**. *J Virol* 2004, **78**:6381-6388.

25. •• Gregorevic P, Blankinship MJ, Allen JM, Crawford RW, Meuse L, Miller DG, Russell DW, Chamberlain JS: **Systemic delivery of genes to striated muscles using adeno-associated viral vectors**. *Nat Med* 2004, **10**:828-834.
This is the first report of successful systemic AAV delivery in mice. The authors utilized AAV-6. In order to achieve high efficient bodywide delivery, the authors co-administrated VEGF, a transient vessel permeabilizer.

26. •• Wang Z, Zhu T, Qiao C, Zhou L, Wang B, Zhang J, Chen C, Li J, Xiao X: **Adeno-associated virus serotype 8 efficiently delivers genes to muscle and heart**. *Nat Biotechnol* 2005, **23**:321-328.
This is the first report demonstrating whole body systemic delivery of an AAV vector in rodents in the absence of pharmacological vessel permeabilization.

27. • Inagaki K, Fuess S, Storm TA, Gibson GA, McTiernan CF, Kay MA, Nakai H: **Robust systemic transduction with AAV9 vectors in mice: efficient global cardiac gene transfer superior to that of AAV8**. *Mol Ther* 2006, **14**:45-53.
The study shows robust myocardial transduction of AAV-9 suggesting AAV-9 is cardiotropic in rodent heart.

28. • Pacak CA, Mah CS, Thattaliyath BD, Conlon TJ, Lewis MA, Cloutier DE, Zolotukhin I, Tarantal AF, Byrne BJ: **Recombinant adeno-associated virus serotype 9 leads to preferential cardiac transduction in vivo**. *Circ Res* 2006, **99**:e3-e9.
See annotation to Ref. [27•].

29. • Bostick B, Ghosh A, Yue Y, Long C, Duan D: **Systemic AAV-9 transduction in mice is influenced by animal age but not by the route of administration**. *Gene Ther* 2007, **14**:1605-1609.
See annotation to Ref. [27•].

30. Bish LT, Morine K, Sleeper MM, Sanmiguel J, Wu D, Gao G, Wilson JM, Sweeney HL: **Adeno-associated virus (AAV) serotype 9 provides global cardiac gene transfer superior to AAV1, AAV6, AAV7, and AAV8 in the mouse and rat**. *Hum Gene Ther* 2008, **19**:1359-1368.

31. • Zincarelli C, Soltys S, Rengo G, Rabinowitz JE: **Analysis of AAV serotypes 1–9 mediated gene expression and tropism in mice after systemic injection**. *Mol Ther* 2008, **16**:1073-1080.
This study reports side-by-side comparison of systemic delivery efficiency of AAV-1 to AAV-9. This study suggests that AAV-9 is suprior to other serotypes.

32. Prasad KM, Xu Y, Yang Z, Acton ST, French BA: **Robust cardiomyocyte-specific gene expression following systemic injection of AAV: in vivo gene delivery follows a Poisson distribution**. *Gene Ther* 2011, **18**:43-52.

33. Bisset DR, Stepniak-Konieczna EA, Zavaljevski M, Wei J, Carter GT, Weiss MD, Chamberlain JR: **Therapeutic impact of systemic AAV-mediated RNA interference in a mouse model of myotonic dystrophy**. *Hum Mol Genet* 2015, **24**:4971-4983.

34. Mah C, Pacak CA, Cresawn KO, Deruisseau LR, Germain S, Lewis MA, Cloutier DA, Fuller DD, Byrne BJ: **Physiological correction of Pompe disease by systemic delivery of adeno-associated virus serotype 1 vectors**. *Mol Ther* 2007, **15**:501-507.

35. Fougerousse F, Bartoli M, Poupiot J, Arandel L, Durand M, Guerchet N, Gicquel E, Danos O, Richard I: **Phenotypic correction of alpha-sarcoglycan deficiency by intra-arterial injection of a muscle-specific serotype 1 rAAV vector**. *Mol Ther* 2007, **15**:53-61.

36. • Gregorevic P, Allen JM, Minami E, Blankinship MJ, Haraguchi M, Meuse L, Finn E, Adams ME, Froehner SC, Murry CE *et al.*: **rAAV6-microdystrophin preserves muscle function and extends lifespan in severely dystrophic mice**. *Nat Med* 2006, **12**:787-789.
This study shows systemic AAV-6 therapy ameliroated dystrophic phenotype in dystrophin/utrophin double knockout mice.

37. Gregorevic P, Blankinship MJ, Allen JM, Chamberlain JS: **Systemic microdystrophin gene delivery improves skeletal muscle structure and function in old dystrophic mdx mice**. *Mol Ther* 2008, **16**:657-664.

38. Bortolanza S, Nonis A, Sanvito F, Maciotta S, Sitia G, Wei J, Torrente Y, Di Serio C, Chamberlain JR, Gabellini D: **AAV6-mediated systemic shRNA delivery reverses disease in a mouse model of facioscapulohumeral muscular dystrophy**. *Mol Ther* 2011, **19**:2055-2064.

39. Nishiyama A, Ampong BN, Ohshima S, Shin JH, Nakai H, Imamura M, Miyagoe-Suzuki Y, Okada T, Takeda S: **Recombinant adeno-associated virus type 8-mediated extensive therapeutic gene delivery into skeletal muscle of alpha-sarcoglycan-deficient mice**. *Hum Gene Ther* 2008, **19**:719-730.

40. Qiao C, Li J, Jiang J, Zhu X, Wang B, Xiao X: **Myostatin propeptide gene delivery by adeno-associated virus serotype 8 vectors enhances muscle growth and ameliorates dystrophic phenotypes in mdx mice**. *Hum Gene Ther* 2008, **19**:241-254.

41. Khan JA, Cao M, Kang BY, Liu Y, Mehta JL, Hermonat PL: **Systemic human Netrin-1 gene delivery by adeno-associated virus type 8 alters leukocyte accumulation and atherogenesis in vivo**. *Gene Ther* 2011, **18**:437-444.

42. Goehringer C, Rutschow D, Bauer R, Schinkel S, Weichenhan D, Bekeredjian R, Straub V, Kleinschmidt JA, Katus HA, Muller OJ: **Prevention of cardiomyopathy in delta-sarcoglycan knockout mice after systemic transfer of targeted adeno-associated viral vectors**. *Cardiovasc Res* 2009, **82**:404-410.

43. Bostick B, Yue Y, Long C, Duan D: **Prevention of dystrophin-deficient cardiomyopathy in twenty-one-month-old carrier mice by mosaic dystrophin expression or complementary dystrophin/utrophin expression**. *Circ Res* 2008, **102**:121-130.

44. • Bostick B, Shin J-H, Yue Y, Duan D: **AAV-microdystrophin therapy improves cardiac performance in aged female mdx mice**. *Mol Ther* 2011, **19**:1826-1832.
This study demonstrates systemic AAV-9 delivery can treat severe dystrophic cardiomyopathy in a phenotypic model.

45. Shin JH, Nitahara-Kasahara Y, Hayashita-Kinoh H, Ohshima-Hosoyama S, Kinoshita K, Chiyo T, Okada H, Okada T, Takeda S: **Improvement of cardiac fibrosis in dystrophic mice by rAAV9-mediated microdystrophin transduction**. *Gene Ther* 2011, **18**:910-919.

46. Bostick B, Shin JH, Yue Y, Wasala NB, Lai Y, Duan D: **AAV micro-dystrophin gene therapy alleviates stress-induced cardiac death but not myocardial fibrosis in >21-m-old mdx mice, an end-stage model of Duchenne muscular dystrophy cardiomyopathy**. *J Mol Cell Cardiol* 2012, **53**:217-222.

47. Shin JH, Bostick B, Yue Y, Hajjar R, Duan D: **SERCA2a gene transfer improves electrocardiographic performance in aged mdx mice**. *J Transl Med* 2011, **9**:132.

48. Spampanato C, De Leonibus E, Dama P, Gargiulo A, Fraldi A, Sorrentino NC, Russo F, Nusco E, Auricchio A, Surace EM *et al.*:

Efficacy of a combined intracerebral and systemic gene delivery approach for the treatment of a severe lysosomal storage disorder. *Mol Ther* 2011, **19**:860-869.

49. Fu H, Dirosario J, Killedar S, Zaraspe K, McCarty DM: **Correction of neurological disease of mucopolysaccharidosis IIIB in adult mice by rAAV9 trans-blood–brain barrier gene delivery**. *Mol Ther* 2011, **19**:1025-1033.

50. Katare R, Caporali A, Zentilin L, Avolio E, Sala-Newby G, Oikawa A, Cesselli D, Beltrami AP, Giacca M, Emanueli C *et al.*: **Intravenous gene therapy with PIM-1 via a cardiotropic viral vector halts the progression of diabetic cardiomyopathy through promotion of prosurvival signaling**. *Circ Res* 2011, **108**:1238-1251.

51. Dufour BD, Smith CA, Clark RL, Walker TR, McBride JL: **Intrajugular vein delivery of AAV9-RNAi prevents neuropathological changes and weight loss in Huntington's disease mice**. *Mol Ther* 2014, **22**:797-810.

52. Dong JY, Fan PD, Frizzell RA: **Quantitative analysis of the packaging capacity of recombinant adeno-associated virus**. *Hum Gene Ther* 1996, **7**:2101-2112.

53. Dong B, Nakai H, Xiao W: **Characterization of genome integrity for oversized recombinant AAV vector**. *Mol Ther* 2010, **18**:87-92.

54. Lai Y, Yue Y, Duan D: **Evidence for the failure of adeno-associated virus serotype 5 to package a viral genome > or = 8.2 kb**. *Mol Ther* 2010, **18**:75-79.

55. Wu Z, Yang H, Colosi P: **Effect of genome size on AAV vector packaging**. *Mol Ther* 2010, **18**:80-86.

56. Chamberlain K, Riyad JM, Weber T: **Expressing transgenes that exceed the packaging capacity of adeno-associated virus capsids**. *Hum Gene Ther Methods* 2016, **27**:1-12.

57. Hirsch ML, Wolf SJ, Samulski RJ: **Delivering transgenic DNA exceeding the carrying capacity of AAV vectors**. *Methods Mol Biol* 2016, **1382**:21-39.

58. Ghosh A, Duan D: **Expending adeno-associated viral vector capacity: a tale of two vectors**. *Biotechnol Genetic Eng Rev* 2007, **24**:165-177.

59. Lai Y, Yue Y, Liu M, Ghosh A, Engelhardt JF, Chamberlain JS, Duan D: **Efficient in vivo gene expression by trans-splicing adeno-associated viral vectors**. *Nat Biotechnol* 2005, **23**:1435-1439.

60. Trapani I, Colella P, Sommella A, Iodice C, Cesi G, de Simone S, Marrocco E, Rossi S, Giunti M, Palfi A *et al.*: **Effective delivery of large genes to the retina by dual AAV vectors**. *EMBO Mol Med* 2014, **6**:194-211.

61. • Ghosh A, Yue Y, Long C, Bostick B, Duan D: **Efficient whole-body transduction with trans-splicing adeno-associated viral vectors**. *Mol Ther* 2007, **15**:750-755.
This study demonstrates the feasiblity of systemic delivery with the dual AAV vectors.

62. Ghosh A, Yue Y, Shin J-H, Duan D: **Systemic trans-splicing AAV delivery efficiently transduces the heart of adult mdx mouse, a model for Duchenne muscular dystrophy**. *Hum Gene Ther* 2009, **20**:1319-1328.

63. Zhang Y, Yue Y, Li L, Hakim CH, Zhang K, Thomas GD, Duan D: **Dual AAV therapy ameliorates exercise-induced muscle injury and functional ischemia in murine models of Duchenne muscular dystrophy**. *Hum Mol Genet* 2013, **22**:3720-3729.

64. Odom GL, Gregorevic P, Allen JM, Chamberlain JS: **Gene therapy of mdx mice with large truncated dystrophins generated by recombination using rAAV6**. *Mol Ther* 2011, **19**:36-45.

65. Lostal W, Bartoli M, Bourg N, Roudaut C, Bentaib A, Miyake K, Guerchet N, Fougerousse F, McNeil P, Richard I: **Efficient recovery of dysferlin deficiency by dual adeno-associated vector-mediated gene transfer**. *Hum Mol Genet* 2010, **19**:1897-1907.

66. • Yue Y, Ghosh A, Long C, Bostick B, Smith BF, Kornegay JN, Duan D: **A single intravenous injection of adeno-associated virus serotype-9 leads to whole body skeletal muscle transduction in dogs**. *Mol Ther* 2008, **16**:1944-1952.
This is the first study demonstrating efficient systemic AAV delivery in a large mammalian species.

67. Pan X, Yue Y, Zhang K, Lostal W, Shin JH, Duan D: **Long-term robust myocardial transduction of the dog heart from a peripheral vein by adeno-associated virus serotype-8**. *Hum Gene Ther* 2013, **24**:584-594.

68. Pan X, Yue Y, Zhang K, Hakim CH, Kodippili K, McDonald T, Duan D: **AAV-8 is more efficient than AAV-9 in transducing neonatal dog heart**. *Hum Gene Ther Methods* 2015, **26**:54-61.

69. Zhong L, Li B, Mah CS, Govindasamy L, Agbandje-McKenna M, Cooper M, Herzog RW, Zolotukhin I, Warrington KH Jr, Weigel-Van Aken KA *et al.*: **Next generation of adeno-associated virus 2 vectors: point mutations in tyrosines lead to high-efficiency transduction at lower doses**. *Proc Natl Acad Sci U S A* 2008, **105**:7827-7832.

70. Qiao C, Zhang W, Yuan Z, Shin JH, Li J, Jayandharan GR, Zhong L, Srivastava A, Xiao X, Duan D: **AAV6 capsid tyrosine to phenylalanine mutations improve gene transfer to skeletal muscle**. *Hum Gene Ther* 2010, **21**:1343-1348.

71. Hakim CH, Yue Y, Shin JH, Williams RR, Zhang K, Smith BF, Duan D: **Systemic gene transfer reveals distinctive muscle transduction profile of tyrosine mutant AAV-1, -6, and -9 in neonatal dogs**. *Mol Ther Methods Clin Dev* 2014, **1**:14002.

72. Duan D: **Duchenne muscular dystrophy gene therapy in the canine model**. *Hum Gene Ther Clin Dev* 2015, **26**:57-69.

73. • Kornegay JN, Li J, Bogan JR, Bogan DJ, Chen C, Zheng H, Wang B, Qiao C, Howard JF Jr, Xiao X: **Widespread muscle expression of an AAV9 human mini-dystrophin vector after intravenous injection in neonatal dystrophin-deficient dogs**. *Mol Ther* 2010, **18**:1501-1508.
This study suggests that systemic delivery may induce catastrophic inflammatory response in a diseased large mammal.

74. Hinderer C, Bell P, Louboutin JP, Zhu Y, Yu H, Lin G, Choa R, Gurda BL, Bagel J, O'Donnell P *et al.*: **Neonatal systemic AAV induces tolerance to CNS gene therapy in MPS I dogs and nonhuman primates**. *Mol Ther* 2015, **23**:1298-1307.

75. Mori S, Takeuchi T, Enomoto Y, Kondo K, Sato K, Ono F, Iwata N, Sata T, Kanda T: **Biodistribution of a low dose of intravenously administered AAV-2, 10, and 11 vectors to cynomolgus monkeys**. *Jpn J Infect Dis* 2006, **59**:285-293.

76. Rodino-Klapac LR, Montgomery CL, Bremer WG, Shontz KM, Malik V, Davis N, Sprinkle S, Campbell KJ, Sahenk Z, Clark KR *et al.*: **Persistent expression of FLAG-tagged micro dystrophin in nonhuman primates following intramuscular and vascular delivery**. *Mol Ther* 2010, **18**:109-117.

77. Toromanoff A, Adjali O, Larcher T, Hill M, Guigand L, Chenuaud P, Deschamps JY, Gauthier O, Blancho G, Vanhove B *et al.*: **Lack of immunotoxicity after regional intravenous (RI) delivery of rAAV to nonhuman primate skeletal muscle**. *Mol Ther* 2010, **18**:151-160.

78. Toromanoff A, Cherel Y, Guilbaud M, Penaud-Budloo M, Snyder RO, Haskins ME, Deschamps JY, Guigand L, Podevin G, Arruda VR *et al.*: **Safety and efficacy of regional intravenous (r.i.) versus intramuscular (i.m.) delivery of rAAV1 and rAAV8 to nonhuman primate skeletal muscle**. *Mol Ther* 2008, **16**:1291-1299.

79. Qiao C, Li J, Zheng H, Bogan J, Yuan Z, Zhang C, Bogan D, Kornegay J, Xiao X: **Hydrodynamic limb vein injection of AAV8 canine myostatin propeptide gene in normal dogs enhances muscle growth**. *Hum Gene Ther* 2009, **20**:1-10.

80. Vulin A, Barthelemy I, Goyenvalle A, Thibaud JL, Beley C, Griffith G, Benchaouir R, le Hir M, Unterfinger Y, Lorain S *et al.*: **Muscle function recovery in golden retriever muscular dystrophy after AAV1-U7 exon skipping**. *Mol Ther* 2012, **20**:2120-2133.

81. Le Guiner C, Montus M, Servais L, Cherel Y, Francois V, Thibaud JL, Wary C, Matot B, Larcher T, Guigand L *et al.*: **Forelimb treatment in a large cohort of dystrophic dogs supports delivery of a recombinant AAV for exon skipping in Duchenne patients**. *Mol Ther* 2014, **22**:1923-1935.

82. • Childers MK, Joubert R, Poulard K, Moal C, Grange RW, Doering JA, Lawlor MW, Rider BE, Jamet T, Daniele N *et al.*: **Gene**

therapy prolongs survival and restores function in murine and canine models of myotubular myopathy. *Sci Transl Med* 2014, **6**:220ra210.
This study suggests that isolated limb perfusion can result in bodywide improvement if the therapeutic product is an enzyme. The authors also showed that intravenous delivery of AAV-8 did not induce any immune response in the canine model of myotubular myopathy.

83. •• Yue Y, Pan X, Hakim CH, Kodippili K, Zhang K, Shin JH, Yang HT, McDonald T, Duan D: **Safe and bodywide muscle transduction in young adult Duchenne muscular dystrophy dogs with adeno-associated virus**. *Hum Mol Genet* 2015, **24**:5880-5890.
This is the first study demonstraing successful systemic AAV delivery in young adult subjects in a large animal model of human diseases. This study sets the foundation for conducting systemic AAV therapy in boys afflicted by Duchenne muscular dystrophy.

84. Hakim CH, Pan X, Kodippili K, Blessa T, Yang HT, Yao G, Leach S, Emter C, Yue Y, Zhang K *et al.*: **Intravenous delivery of a novel micro-dystrophin vector prevented muscle deterioration in young adult canine Duchenne muscular dystrophy dogs**. *Mol Ther* 2016, **24**:S198-S199.

85. •• Mendell JR, Al-Zaidy S, Shell R, Arnold WD, Rodino-Klapac L, Kissel JT, Prior TW, Miranda C, Lowes L, Alfano L *et al.*: **Gene therapy for spinal muscular atrophy type 1 shows potential to improve survival and motor functional outcomes**. *Mol Ther* 2016, **24**:S190.
In this meeting report, Dr. Mendell presented results of the first-in-human study on systemic AAV gene therapy in severelly affected newborn spinal muscular dystrophy patients. A total of 15 patients have been treated with an AAV-9 vector at the dose of 6.7×10^{13} to 2×10^{14} for 4 months to 2 years. The results of this ongoing study suggest that systemic AAV gene therapy is safe and may dramatically change the disease course. This study opens the door for systemic AAV gene therapy for other diseases in human patients.

86. Valori CF, Ning K, Wyles M, Mead RJ, Grierson AJ, Shaw PJ, Azzouz M: **Systemic delivery of scAAV9 expressing SMN prolongs survival in a model of spinal muscular atrophy**. *Sci Transl Med* 2010, **2**:35ra42.

87. Bevan AK, Hutchinson KR, Foust KD, Braun L, McGovern VL, Schmelzer L, Ward JG, Petruska JC, Lucchesi PA, Burghes AH *et al.*: **Early heart failure in the SMNDelta7 model of spinal muscular atrophy and correction by postnatal scAAV9-SMN delivery**. *Hum Mol Genet* 2010, **19**:3895-3905.

88. Foust KD, Wang X, McGovern VL, Braun L, Bevan AK, Haidet AM, Le TT, Morales PR, Rich MM, Burghes AH *et al.*: **Rescue of the spinal muscular atrophy phenotype in a mouse model by early postnatal delivery of SMN**. *Nat Biotechnol* 2010, **28**:271-274.

89. Dominguez E, Marais T, Chatauret N, Benkhelifa-Ziyyat S, Duque S, Ravassard P, Carcenac R, Astord S, Pereira de Moura A, Voit T *et al.*: **Intravenous scAAV9 delivery of a codon-optimized SMN1 sequence rescues SMA mice**. *Hum Mol Genet* 2011, **20**:681-693.

90. Ding W, Zhang L, Yan Z, Engelhardt JF: **Intracellular trafficking of adeno-associated viral vectors**. *Gene Ther* 2005, **12**:873-880.

91. Nonnenmacher M, Weber T: **Intracellular transport of recombinant adeno-associated virus vectors**. *Gene Ther* 2012, **19**:649-658.

92. Denard J, Beley C, Kotin R, Lai-Kuen R, Blot S, Leh H, Asokan A, Samulski RJ, Moullier P, Voit T *et al.*: **Human galectin 3 binding protein interacts with recombinant adeno-associated virus type 6**. *J Virol* 2012, **86**:6620-6631.

93. Denard J, Marolleau B, Jenny C, Rao TN, Fehling HJ, Voit T, Svinartchouk F: **C-reactive protein (CRP) is essential for efficient systemic transduction of recombinant adeno-associated virus vector 1 (rAAV-1) and rAAV-6 in mice**. *J Virol* 2013, **87**:10784-10791.

94. Kotchey NM, Adachi K, Zahid M, Inagaki K, Charan R, Parker RS, Nakai H: **A potential role of distinctively delayed blood clearance of recombinant adeno-associated virus serotype 9 in robust cardiac transduction**. *Mol Ther* 2011, **19**:1079-1089.

95. Shen S, Bryant KD, Sun J, Brown SM, Troupes A, Pulicherla N, Asokan A: **Glycan binding avidity determines the systemic fate of adeno-associated virus type 9**. *J Virol* 2012, **86**:10408-10417.

96. • Asokan A, Conway JC, Phillips JL, Li C, Hegge J, Sinnott R, Yadav S, DiPrimio N, Nam HJ, Agbandje-McKenna M *et al.*: **Reengineering a receptor footprint of adeno-associated virus enables selective and systemic gene transfer to muscle**. *Nat Biotechnol* 2010, **28**:79-82.
This study provides the proof-of-principle to engineer AAV capsid for improved systemic delivery.

97. Gray SJ, Matagne V, Bachaboina L, Yadav S, Ojeda SR, Samulski RJ: **Preclinical differences of intravascular AAV9 delivery to neurons and glia: a comparative study of adult mice and nonhuman primates**. *Mol Ther* 2011, **19**:1058-1069.

98. Tuma P, Hubbard AL: **Transcytosis: crossing cellular barriers**. *Physiol Rev* 2003, **83**:871-932.

99. Di Pasquale G, Ostedgaard L, Vermeer D, Swaim WD, Karp P, Chiorini JA: **Bovine AAV transcytosis inhibition by tannic acid results in functional expression of CFTR in vitro and altered biodistribution in vivo**. *Gene Ther* 2012, **19**:576-581.

100. • Di Pasquale G, Chiorini JA: **AAV transcytosis through barrier epithelia and endothelium**. *Mol Ther* 2006, **13**:506-516.
This study provides *in vitro* evidence of AAV transcytosis.

101. He B, Yuan Z, Qiao C, Madden V, Thakker D, Li J, Xiao X: **Transcytosis of AAV8 and AAV9 across endothelial Barrier**. *Mol Ther* 2009, **17**:S175.

102. Byrne LC, Lin YJ, Lee T, Schaffer DV, Flannery JG: **The expression pattern of systemically injected AAV9 in the developing mouse retina is determined by age**. *Mol Ther* 2015, **23**:290-296.

103. Cheng JP, Nichols BJ: **Caveolae: one function or many?** *Trends Cell Biol* 2016, **26**:177-189.

104. Foust KD, Nurre E, Montgomery CL, Hernandez A, Chan CM, Kaspar BK: **Intravascular AAV9 preferentially targets neonatal neurons and adult astrocytes**. *Nat Biotechnol* 2009, **27**:59-65.

105. Calcedo R, Vandenberghe LH, Gao G, Lin J, Wilson JM: **Worldwide epidemiology of neutralizing antibodies to adeno-associated viruses**. *J Infect Dis* 2009, **199**:381-390.

106. Boutin S, Monteilhet V, Veron P, Leborgne C, Benveniste O, Montus MF, Masurier C: **Prevalence of serum IgG and neutralizing factors against adeno-associated virus (AAV) types 1, 2, 5, 6, 8, and 9 in the healthy population: implications for gene therapy using AAV vectors**. *Hum Gene Ther* 2010, **21**:704-712.

107. Van Vliet KM, Blouin V, Brument N, Agbandje-McKenna M, Snyder RO: **The role of the adeno-associated virus capsid in gene transfer**. *Methods Mol Biol* 2008, **437**:51-91.

108. • Drouin LM, Agbandje-McKenna M: **Adeno-associated virus structural biology as a tool in vector development**. *Future Virol* 2013, **8**:1183-1199.
This is an excellent review article on AAV capsid structure.

109. Agbandje-McKenna M, Kleinschmidt J: **AAV capsid structure and cell interactions**. *Methods Mol Biol* 2011, **807**:47-92.

110. Santiago-Ortiz J, Ojala DS, Westesson O, Weinstein JR, Wong SY, Steinsapir A, Kumar S, Holmes I, Schaffer DV: **AAV ancestral reconstruction library enables selection of broadly infectious viral variants**. *Gene Ther* 2015, **22**:934-946.

111. Zinn E, Pacouret S, Khaychuk V, Turunen HT, Carvalho LS, Andres-Mateos E, Shah S, Shelke R, Maurer AC, Plovie E *et al.*: **In silico reconstruction of the viral evolutionary lineage yields a potent gene therapy vector**. *Cell Rep* 2015, **12**:1056-1068.

112. • Kotterman MA, Schaffer DV: **Engineering adeno-associated viruses for clinical gene therapy**. *Nat Rev Genet* 2014, **15**:445-451.
This is a comprehensive review on the current status of AAV capsid engineering and clinical application of synthetic AAV variants.

113. Nance ME, Duan D: **Perspective on adeno-associated virus (AAV) capsid modification for Duchenne muscular dystrophy gene therapy**. *Hum Gene Ther* 2015, **26**:786-800.

114. Ling C, Lu Y, Kelsi JK, Jayandharan GR, Li B, Ma W, Cheng B, Gee SW, McGoogan KE, Govindasamy L *et al.*: **Human**

hepatocyte growth factor receptor is a cellular co-receptor for AAV3. *Hum Gene Ther* 2010, **21**:1741-1747.

115. Li S, Ling C, Zhong L, Li M, Su Q, He R, Tang Q, Greiner DL, Shultz LD, Brehm MA *et al.*: **Efficient and targeted transduction of nonhuman primate liver with systemically delivered optimized AAV3B vectors**. *Mol Ther* 2015, **23**:1867-1876.

116. Wang L, Bell P, Somanathan S, Wang Q, He Z, Yu H, McMenamin D, Goode T, Calcedo R, Wilson JM: **Comparative study of liver gene transfer with AAV vectors based on natural and engineered AAV capsids**. *Mol Ther* 2015, **23**:1877-1887.

117. Shen S, Troupes AN, Pulicherla N, Asokan A: **Multiple roles for sialylated glycans in determining the cardiopulmonary tropism of adeno-associated virus 4**. *J Virol* 2013, **87**:13206-13213.

118. Yang B, Li S, Wang H, Guo Y, Gessler DJ, Cao C, Su Q, Kramer J, Zhong L, Ahmed SS *et al.*: **Global CNS transduction of adult mice by intravenously delivered rAAVrh.8 and rAAVrh.10 and nonhuman primates by rAAVrh.10**. *Mol Ther* 2014, **22**:1299-1309.

119. Louis Jeune V, Joergensen JA, Hajjar RJ, Weber T: **Pre-existing anti-adeno-associated virus antibodies as a challenge in AAV gene therapy**. *Hum Gene Ther Methods* 2013, **24**:59-67.

120. Mingozzi F, Chen Y, Edmonson SC, Zhou S, Thurlings RM, Tak PP, High KA, Vervoordeldonk MJ: **Prevalence and pharmacological modulation of humoral immunity to AAV vectors in gene transfer to synovial tissue**. *Gene Ther* 2013, **20**:417-424.

121. Mingozzi F, Chen Y, Murphy SL, Edmonson SC, Tai A, Price SD, Metzger ME, Zhou S, Wright JF, Donahue RE *et al.*: **Pharmacological modulation of humoral immunity in a nonhuman primate model of AAV gene transfer for hemophilia B**. *Mol Ther* 2012, **20**:1410-1416.

122. Monteilhet V, Saheb S, Boutin S, Leborgne C, Veron P, Montus MF, Moullier P, Benveniste O, Masurier C: **A 10 patient case report on the impact of plasmapheresis upon neutralizing factors against adeno-associated virus (AAV) types 1, 2, 6, and 8**. *Mol Ther* 2011, **19**:2084-2091.

123. Tseng YS, Agbandje-McKenna M: **Mapping the AAV capsid host antibody response toward the development of second generation gene delivery vectors**. *Front Immunol* 2014, **5**:9.

124. Lochrie MA, Tatsuno GP, Christie B, McDonnell JW, Zhou S, Surosky R, Pierce GF, Colosi P: **Mutations on the external surfaces of adeno-associated virus type 2 capsids that affect transduction and neutralization**. *J Virol* 2006, **80**:821-834.

125. Maersch S, Huber A, Buning H, Hallek M, Perabo L: **Optimization of stealth adeno-associated virus vectors by randomization of immunogenic epitopes**. *Virology* 2010, **397**:167-175.

126. Bartel M, Schaffer D, Buning H: **Enhancing the clinical potential of AAV vectors by capsid engineering to evade pre-existing immunity**. *Front Microbiol* 2011, **2**:204.

127. • Maheshri N, Koerber JT, Kaspar BK, Schaffer DV: **Directed evolution of adeno-associated virus yields enhanced gene delivery vectors**. *Nat Biotechnol* 2006, **24**:198-204.
This paper describes the first application of directed evolution to generate novel AAV capsids. This library-based approach allows investigators to obtain functionally superior AAV mutants without prior knowledge of the capsid structure.

128. Grimm D, Lee JS, Wang L, Desai T, Akache B, Storm TA, Kay MA: **In vitro and in vivo gene therapy vector evolution via multispecies interbreeding and retargeting of adeno-associated viruses**. *J Virol* 2008, **82**:5887-5911.

129. Li C, Wu S, Albright B, Hirsch M, Li W, Tseng YS, Agbandje-McKenna M, McPhee S, Asokan A, Samulski RJ: **Development of patient-specific AAV vectors after neutralizing antibody selection for enhanced muscle gene transfer**. *Mol Ther* 2016, **24**:53-65.

130. Adachi K, Enoki T, Kawano Y, Veraz M, Nakai H: **Drawing a high-resolution functional map of adeno-associated virus capsid by massively parallel sequencing**. *Nat Commun* 2014, **5**:3075.

131. Pulicherla N, Shen S, Yadav S, Debbink K, Govindasamy L, Agbandje-McKenna M, Asokan A: **Engineering liver-detargeted AAV9 vectors for cardiac and musculoskeletal gene transfer**. *Mol Ther* 2011, **19**:1070-1078.

132. Shen S, Horowitz ED, Troupes AN, Brown SM, Pulicherla N, Samulski RJ, Agbandje-McKenna M, Asokan A: **Engraftment of a galactose receptor footprint onto adeno-associated viral capsids improves transduction efficiency**. *J Biol Chem* 2013, **288**:28814-28823.

133. • Lisowski L, Dane AP, Chu K, Zhang Y, Cunningham SC, Wilson EM, Nygaard S, Grompe M, Alexander IE, Kay MA: **Selection and evaluation of clinically relevant AAV variants in a xenograft liver model**. *Nature* 2014, **506**:382-386.
This study decribes a unique *in vivo* evolution approach in human tissue xenograft. The resulting AAV variants hold great promise for human application.

134. Yang L, Jiang J, Drouin LM, Agbandje-McKenna M, Chen C, Qiao C, Pu D, Hu X, Wang DZ, Li J *et al.*: **A myocardium tropic adeno-associated virus (AAV) evolved by DNA shuffling and in vivo selection**. *Proc Natl Acad Sci U S A* 2009, **106**:3946-3951.

135. Choudhury SR, Harris AF, Cabral DJ, Keeler AM, Sapp E, Ferreira JS, Gray-Edwards HL, Johnson JA, Johnson AK, Su Q *et al.*: **Widespread central nervous system gene transfer and silencing after systemic delivery of novel AAV-AS vector**. *Mol Ther* 2016, **24**:726-735.

136. Huang LY, Halder S, Agbandje-McKenna M: **Parvovirus glycan interactions**. *Curr Opin Virol* 2014, **7**:108-118.

137. Murlidharan G, Corriher T, Ghashghaei HT, Asokan A: **Unique glycan signatures regulate adeno-associated virus tropism in the developing brain**. *J Virol* 2015, **89**:3976-3987.

138. • Pillay S, Meyer NL, Puschnik AS, Davulcu O, Diep J, Ishikawa Y, Jae LT, Wosen JE, Nagamine CM, Chapman MS *et al.*: **An essential receptor for adeno-associated virus infection**. *Nature* 2016, **530**:108-112.
This paper describes the identification of a poorly characterized transmembrane protein KIAA0319L as a ubiquitous AAV receptor for multiple serotypes.

139. Nelson CE, Hakim CH, Ousterout DG, Thakore PI, Moreb EA, Rivera RM, Madhavan S, Pan X, Ran FA, Yan WX *et al.*: **In vivo genome editing improves muscle function in a mouse model of Duchenne muscular dystrophy**. *Science* 2016, **351**:403-407.

140. Rayaprolu V, Kruse S, Kant R, Venkatakrishnan B, Movahed N, Brooke D, Lins B, Bennett A, Potter T, McKenna R *et al.*: **Comparative analysis of adeno-associated virus capsid stability and dynamics**. *J Virol* 2013, **87**:13150-13160.

141. Vandenberghe LH, Wang L, Somanathan S, Zhi Y, Figueredo J, Calcedo R, Sanmiguel J, Desai RA, Chen CS, Johnston J *et al.*: **Heparin binding directs activation of T cells against adeno-associated virus serotype 2 capsid**. *Nat Med* 2006, **12**:967-971.

142. Lu Y, Song S: **Distinct immune responses to transgene products from rAAV1 and rAAV8 vectors**. *Proc Natl Acad Sci U S A* 2009, **106**:17158-17162.

143. Wang L, Figueredo J, Calcedo R, Lin J, Wilson JM: **Cross-presentation of adeno-associated virus serotype 2 capsids activates cytotoxic T cells but does not render hepatocytes effective cytolytic targets**. *Hum Gene Ther* 2007, **18**:185-194.

144. Ohshima S, Shin JH, Yuasa K, Nishiyama A, Kira J, Okada T, Takeda S: **Transduction efficiency and immune response associated with the administration of AAV8 vector into dog skeletal muscle**. *Mol Ther* 2009, **17**:73-80.

145. Mays LE, Wang L, Lin J, Bell P, Crawford A, Wherry EJ, Wilson JM: **AAV8 induces tolerance in murine muscle as a result of poor APC transduction, T cell exhaustion and minimal MHCI upregulation on target cells**. *Mol Ther* 2014, **22**:28-41.

146. Koo T, Okada T, Athanasopoulos T, Foster H, Takeda S, Dickson G: **Long-term functional adeno-associated virus-microdystrophin expression in the dystrophic CXMDj dog**. *J Gene Med* 2011, **13**:497-506.

Human Molecular Genetics, 2016, Vol. 25, No. 13 2633–2644

doi: 10.1093/hmg/ddw123
Advance Access Publication Date: 22 April 2016
Original Article

ORIGINAL ARTICLE

Genomic removal of a therapeutic mini-dystrophin gene from adult mice elicits a Duchenne muscular dystrophy-like phenotype

Nalinda B. Wasala[1], Yi Lai[1], Jin-Hong Shin[1,†], Junling Zhao[1], Yongping Yue[1] and Dongsheng Duan[1,2,3,*]

[1]Department of Molecular Microbiology and Immunology, School of Medicine, [2]Department of Neurology, School of Medicine and [3]Department of Bioengineering, The University of Missouri, Columbia, MO 65212, USA

*To whom correspondence should be addressed at: Department of Molecular Microbiology and Immunology, One Hospital Dr, Columbia, MO 65212, USA. Tel: +1-573 884 9584; Fax: +1-573 882 4287; Email: duand@missouri.edu

Abstract

Duchenne muscular dystrophy (DMD) is caused by dystrophin deficiency. A fundamental question in DMD pathogenesis and dystrophin gene therapy is whether muscle health depends on continuous dystrophin expression throughout the life. Published data suggest that transient dystrophin expression in early life might offer permanent protection. To study the consequences of adulthood dystrophin loss, we generated two strains of floxed mini-dystrophin transgenic mice on the dystrophin-null background. Muscle diseases were prevented in skeletal muscle of the YL238 strain and the heart of the SJ13 strain by selective expression of a therapeutic mini-dystrophin gene in skeletal muscle and heart, respectively. The mini-dystrophin gene was removed from the tibialis anterior (TA) muscle of 8-month-old YL238 mice and the heart of 7-month-old SJ13 mice using an adeno-associated virus serotype-9 Cre recombinase vector (AAV.CBA.Cre). At 12 and 15 months after AAV.CBA.Cre injection, mini-dystrophin expression was reduced by ∼87% in the TA muscle of YL238 mice and ∼64% in the heart of SJ13 mice. Mini-dystrophin reduction caused muscle atrophy, degeneration and force loss in the TA muscle of YL238 mice and significantly compromised left ventricular hemodynamics in SJ13 mice. Our results suggest that persistent dystrophin expression is essential for continuous muscle and heart protection.

Introduction

Duchenne muscular dystrophy (DMD) is an X-linked life limiting genetic disease resulted from the loss of dystrophin (1). It affects ∼1 in 5000 newborn boys (2). Patients often fail to meet their motor development milestones at 3–5 years of age and lose their mobility in early teenage. They die either from respiratory muscle failure and/or heart failure in the second and third decade of the life. Currently there is no cure. Restoration of dystrophin expression holds a great promise to treat DMD at the molecular level (3–6).

A fundamental question in DMD pathogenesis and dystrophin gene replacement therapy is whether muscle health depends on continuous dystrophin expression. If dystrophin is required for muscle health throughout the lifespan of the patient, then an effective therapy will have to depend on persistent dystrophin expression. On the other hand, if dystrophin is only required during certain developmental/growth stages, then transient expression at these stages may meet the therapeutic need. Although it is generally believed that DMD therapy

†Present address: Pusan National University Yangsan Hospital, Yangsan, Republic of Korea.
Received: January 4, 2016. **Revised:** March 29, 2016. **Accepted:** April 18, 2016

requires continuous dystrophin expression, experimental support for this notion is lacking. In contrast, existing evidence seems to suggest that the opposite might be true. In particular, Ghahramani Seno *et al.* (7) found that knockdown of dystrophin expression in skeletal muscle of adult normal mice did not cause overt dystrophic pathology. Hence, dystrophin might be more important in the early developmental stage and could become dispensable once this stage is over (8). Consistently, Ahmad *et al.* (9) demonstrated that sustained dystrophin production was more critical in younger growing muscle than in older muscle. Collectively, these studies suggest that dystrophin is less essential in fully developed muscle. In other words, transient restoration of dystrophin during muscle maturation (such as in young adolescent patients) might grant long-lasting protection, or even lifelong therapy. If this theory is confirmed, it will have tremendous implications on our understanding of DMD pathogenesis and the development of dystrophin replacement gene therapy.

To address this critical question, we generated floxed ΔH2-R15 mini-dystrophin transgenic mice in the background of dystrophin-null FVB/mdx mice (10). The ΔH2-R15 mini-dystrophin gene is a fully characterized and highly functional synthetic dystrophin gene. Transgenic expression of this minigene completely prevented dystrophic muscle pathology, restored sarcolemmal neuronal nitric oxide synthase (nNOS), normalized muscle force and improved exercise performance in mdx mice (11). Systemic gene therapy with this minigene significantly improved muscle morphology, prevented functional ischemia and enhanced muscle force in mdx mice (12). Since both skeletal muscle and the heart are compromised in DMD, we generated two independent strains of transgenic mice. In strain YL238, we selectively expressed the loxP-flanked ΔH2-R15 mini-dystrophin gene in skeletal muscle using the human skeletal α-actin (HSA) promoter (Table 1). In strain SJ13, we achieved heart-specific expression of the loxP-flanked ΔH2-R15 mini-dystrophin gene with the α-myosin heavy chain (α-MHC) promoter (Table 1). As expected, expression of the ΔH2-R15 minigene prevented skeletal muscle disease in YL238 mice and cardiomyopathy in SJ13 mice. To test whether persistent dystrophin expression is absolutely required for continuous skeletal muscle and heart protection, we removed the mini-dystrophin gene in adult transgenic mice using Cre recombinase expressed from an adeno-associated virus serotype-9 vector (AAV.CBA.Cre). We then examined dystrophin expression, muscle and heart histology and function. At 12 and 15 months after injection of the AAV.CBA.Cre vector, mini-dystrophin expression was reduced by ∼87% in the skeletal muscle of YL238 mice and by ∼64% in the heart of SJ13 mice, respectively. Reduction of mini-dystrophin in skeletal muscle resulted in significant degeneration, atrophy and force reduction in YL238 mice. Partial removal of mini-dystrophin from the myocardium also significantly compromised left ventricular (LV) hemodynamics in SJ13 mice. Our results suggest that an effective gene therapy for DMD requires persistent dystrophin expression in both skeletal muscle and the heart.

Table 1. Comparison of two strains of floxed mini-dystrophin transgenic mice

	YL238	SJ13
Promoter	HSA	α-MHC
Transgene	ΔH2-R15	ΔH2-R15
Mini-dystrophin expression	Skeletal muscle only	Heart only
Skeletal muscle protection	Yes	No
Heart protection	No	Yes
Acute cardiac death from systemic AAV.CBA.Cre injection	Yes	No

Results

Generation of floxed skeletal muscle-specific mini-dystrophin transgenic mice

Full-length dystrophin has four functional domains including the N-terminal, rod, cysteine-rich and C-terminal domain. The rod domain can be further divided into four hinges and 24 spectrin-like repeats (Fig. 1A). Due to the limitation of viral vector packaging, the vast majority of dystrophin replacement therapies are based on abbreviated mini- or micro-dystrophins. In this study, we opt to use ΔH2-R15 mini-dystrophin. This mini-dystrophin has a smaller rod domain due to a deletion from hinge 2 to spectrin-like repeat 15 (Fig. 1A). We have previously shown that the ΔH2-R15 minigene can prevent muscle pathology, normalize muscle force and restore sarcolemmal nNOS in mdx and mdx4cv mice (11–13).

To generate floxed skeletal muscle-specific ΔH2-R15 mini-dystrophin transgenic mice, we cloned two loxP sites (one before the HSA promoter and the other before the polyadenylation site) into our previously published HSA.ΔH2-R15 mini-dystrophin construct (Fig. 1B, Supplementary Material, Fig. S1A and Table S1) (11). *In vitro* test in 293 cells showed effective excision of the floxed mini-dystrophin gene from the transgenic construct by Cre recombinase (Supplementary Material, Fig. S1B). The floxed HSA.ΔH2-R15 minigene construct was microinjected to the zygotes of FVB mice. The founder mouse was identified by polymerase chain reaction and crossed to the background of dystrophin-null FVB/mdx mice (10). The resulting mice were called YL238 mice. These mice selectively expressed a floxed ΔH2-R15 mini-dystrophin gene in skeletal muscle but not the heart (Fig. 1D, Supplementary Material, Fig. S2A). As expected, we did not see any signs of skeletal muscle pathology by hematoxylin and eosin (HE) staining (Fig. 2A). Neither was inflammation detected in skeletal muscle of YL238 mice by macrophage and neutrophil immunohistochemical staining (Fig. 2A).

Genomic elimination of minigene significantly reduced mini-dystrophin expression in skeletal muscle but had minimal impact on the dystrophin-associated glycoprotein complex in adult YL238 mice

To study the consequences of dystrophin loss in adult skeletal muscle, we used the AAV.CBA.Cre vector. In this vector, the Cre recombinase is expressed from the ubiquitous cytomegalovirus enhancer-chicken β-actin promoter (CBA). 2.7×10^{12} viral genome (vg) particles of AAV.CBA.Cre were administrated to the tibialis anterior (TA) muscle of 8-month-old male YL238 transgenic mice (Fig. 1C). We first evaluated the kinetics of the loss of mini-dystrophin by western blot (Supplementary Material, Fig. S3A). We observed a time-dependent reduction of mini-dystrophin. However, by 16 weeks after AAV.CBA.Cre injection, we still detected a substantial amount of residual mini-dystrophin (Supplementary Material, Fig. S3A). To this end, we decided to not perform terminal studies until injected mice reached 20-month-old.

Mice were euthanized at the age of 20 months. On immunostaining, AAV.CBA.Cre injected muscles showed reduced dystrophin staining intensity (Fig. 1D). On western blot, mini-dystrophin expression was also greatly decreased in

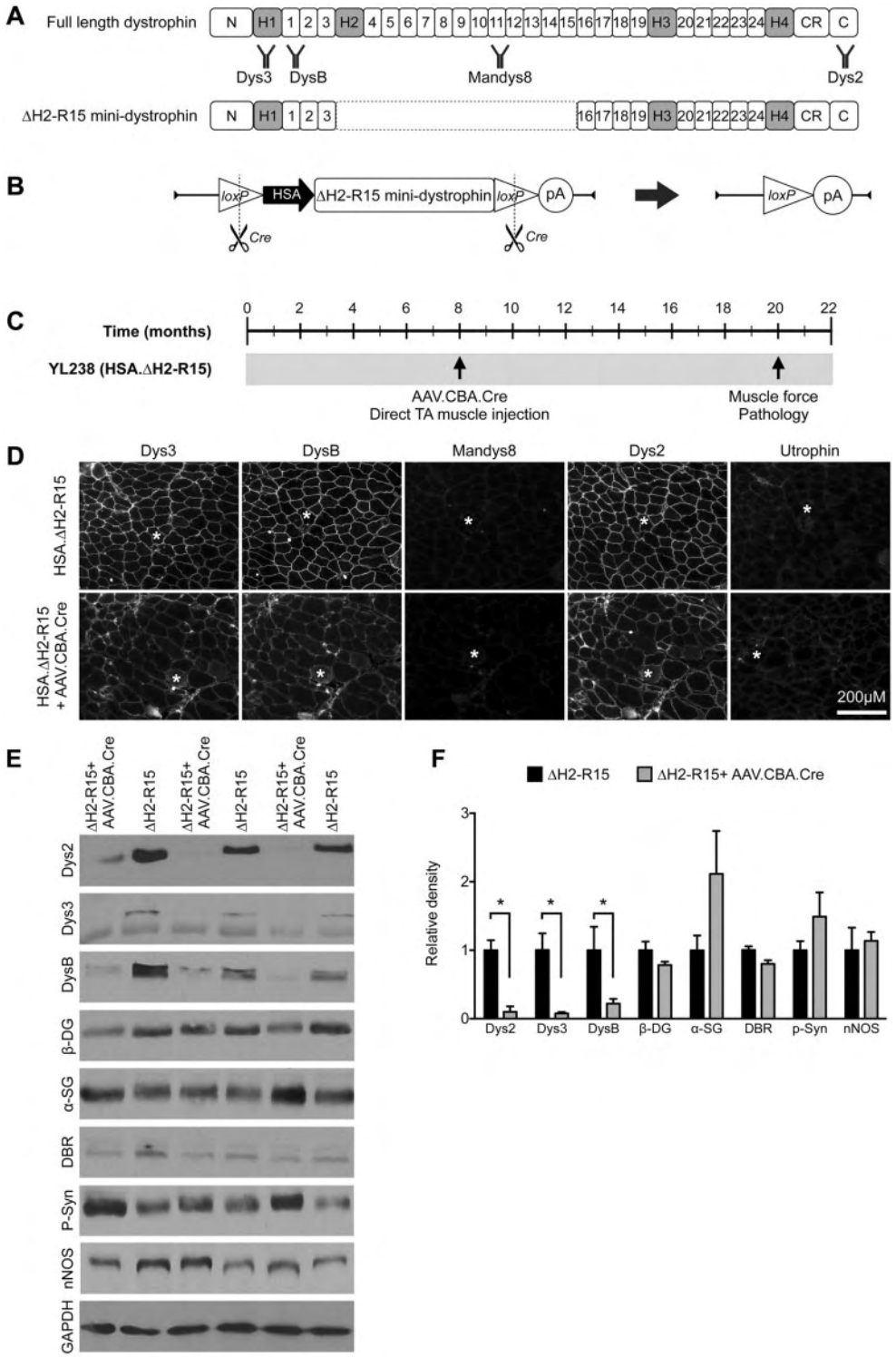

Figure 1. Genomic excision of the floxed HSA.ΔH2-R15 transgeneic cassette leads to significant reduction of mini-dystrophin expression in skeletal muscle. **(A)** Schematic outline of the structure of full-length dystrophin and ΔH2-R15 mini-dystrophin. Dys3, DysB, Mandys8 and Dys2 are four different dystrophin monoclonal antibodies used in the study. Dys2 recognizes an epitope in the dystrophin C-terminal domain. Dys3 recognizes an epitope in dystrophin hinge 1. DysB recognizes an epitope that is located between hinge 1 and dystrophin spectrin-like repeat 2. Mandys8 recognizes an epitope in dystrophin spectrin-like repeat 11, which is absent in ΔH2-R15 mini-dystrophin. **(B)** Graphical representation of the floxed HSA.ΔH2-R15 transgenic cassette and Cre recombinase-mediated excision of the cassette. In YL238 transgenic mice, the expression of the ΔH2-R15 minigene is under the control of the skeletal muscle-specific human α-skeletal actin promoter (HSA). **(C)** Experimental outline. AAV.CBA.Cre was injected to one side of the TA muscle in 8-month-old YL238 transgenic mice. The contralateral side was mock injected and served as the untreated control. Dystrophin expression and muscle force were assessed when mice reached 20 months of age. **(D)** Representative photomicrographs of dystrophin and utrophin immunofluorescence staining in the TA muscles of 20-month-old YL238 mice. Asterisk, the same myofiber in serial muscle sections. **(E)** Representative western blots of dystrophin and components of DGC (β-DG, β-dystroglycan; α-SG, α-sarcoglycan; DBR, dystrobrevin; P-Syn, pan-syntrophin; nNOS, neuronal nitric oxide synthase) from the TA muscles of 20-month-old YL238 mice. **(F)** Densitometry quantification of western blots. N = 3. Asterisk, significantly different.

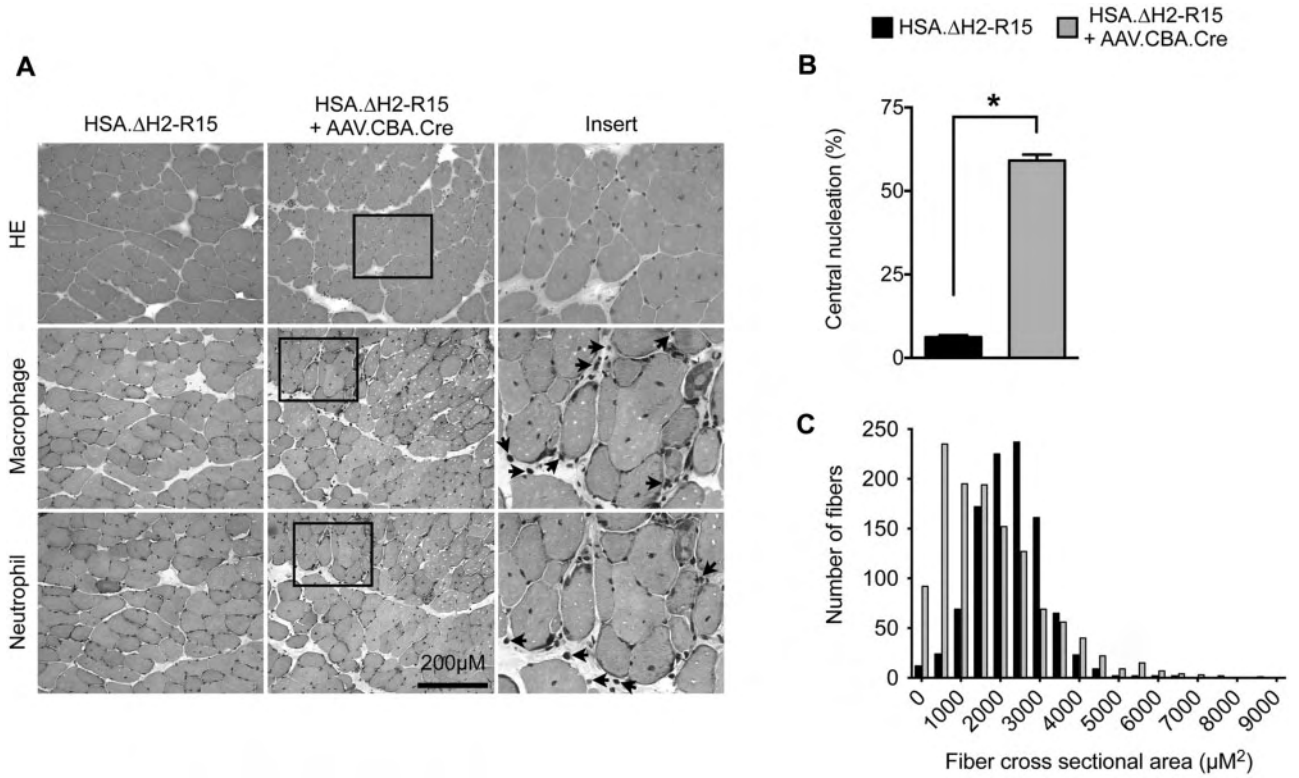

Figure 2. Adulthood loss of dystrophin alters skeletal muscle histology. (**A**) Representative photomicrographs of hematoxylin and eosin (HE) staining, and macrophage and neutrophil immunohistochemical staining from the tibialis anterior muscles of 20-m-old YL238 mice. One side of the tibialis anterior muscle received AAV.CBA.Cre. The contralateral side served as the untreated control. Dark spots on HE and immunohistochemical staining are myonuclei and infiltrating immune cells. Left panels are the enlarged view of the boxed area in the corresponding middle panels. Arrows indicate macrophages and neutrophils in respective images. (**B**) Quantification of centrally located myonuclei. Asterisk, significantly different. (**C**) Myofiber size distribution. N = 1223 myofibers for AAV. CBA.Cre injected muscle. N = 1005 myofibers for contralateral mock injected control.

AAV.CBA.Cre injected muscles (Fig. 1E). Consistent results were obtained with three independent antibodies (Dys2, Dys3 and DysB) that recognize different regions of mini-dystrophin (Fig. 1A, D and E). Quantitative densitometry analysis of western blots showed statistically significant reduction (Fig. 1F, Supplementary Material, Table S1). Compared with that of contralateral untreated muscle, AAV.CBA.Cre injection resulted in a loss of 86.7 ± 3.4% of mini-dystrophin (the average from results of western blot using three independent antibodies).

We next examined expression of the dystrophin-associated glycoprotein complex (DGC) components and utrophin. In sharp contrast to the dramatic reduction of mini-dystrophin, there were nominal changes in the expression of β-dystroglycan, β-sarcoglycan, dystrobrevin and syntrophin (Fig. 1F, Supplementary Material, Fig. S4). On immunostaining, we did not see substantial changes in utrophin expression (Fig. 1D).

Adulthood loss of mini-dystrophin resulted in skeletal muscle myopathy

After confirming effective mini-dystrophin removal, we examined muscle histology and function. On HE staining, we observed clear signs of myopathy in AAV.CBA.Cre injected muscles (such as great variations in the myofiber size and abundant centrally nucleated myofibers) (Fig. 2A). Immunohistochemical staining revealed macrophage, neutrophil and T cell infiltration in muscles treated with AAV.CBA.Cre (Fig. 2A, Supplementary Material, Fig. S5A). On Masson trichrome staining, we did not detect obvious fibrosis (Supplementary Material, Fig. S5B). Quantification showed a central nucleation of 59.1 ± 0.6% in AAV.CBA.Cre injected muscle while it was only 6.2 ± 0.2% in contralateral untreated muscle (Fig. 2B). Removal of mini-dystrophin also skewed the distribution of the myofiber size (Fig. 2C). There was an apparent shift of the peak toward smaller size myofibers although the number of super-large myofibers was also increased in AAV.CBA.Cre injected muscles (Fig. 2C). Consistent with myofiber size quantification, the weight and cross-sectional area (CSA) of AAV.CBA.Cre injected muscles were significantly reduced (Table 2).

To evaluate physiological consequences of adulthood dystrophin removal, we measured the contractile properties of the TA muscle *in situ*. On single twitch, force-frequency and eccentric contraction studies, AAV.CBA.Cre injected muscles generated significantly much lower absolute force though CSA normalized specific forces were not altered (Fig. 3).

Intravenous delivery of AAV.CBA.Cre to adult YL238 mice elicited acute cardiac death

Next, we delivered 8×10^{12} vg particles of AAV.CBA.Cre through the tail vein to 3-month-old YL238 mice. Our goal was to study the consequences of the loss of the therapeutic mini-dystrophin gene in all skeletal muscles in the body. To our surprise none of the injected mice survived beyond 20 days

postinjection. The majority of the injected mice (>75%) died around 13–15 days after AAV.CBA.Cre administration (Fig. 4A). Necropsy revealed severe heart damage. On HE staining, we found extensive myocardial inflammation in atrial and ventricular walls consistent with the diagnosis of acute cardiac death (Fig. 4B and C, Supplementary Material, Fig. S2A and Table S1).

Removal of cardiac ΔH2-R15 mini-dystrophin from adult SJ13 mice by AAV.CBA.Cre recombinase altered LV hemodynamics

To study the impact of adulthood loss of the therapeutic mini-dystrophin gene in the heart, we generated SJ13 mice. We used the same approach as described for the generation of YL238 mice except that a floxed cardiac-specific mini-dystrophin transgenic construct was used. Specifically, expression of the ΔH2-R15 mini-dystrophin was confined to the heart by the α-MHC promoter and the entire expression cassette was flanked by the loxP sites (Fig. 5A, Supplementary Material, Fig. S1A).

Table 2. Anatomic properties of the TA muscle of 20-month-old YL238 mice

	HSA.ΔH2-R15	HSA.ΔH2R15 +AAV.CBA.Cre
Sample size (*n*)	11	10
TA weight (mg)	48.17 ± 2.32	40.13 ± 1.39[a]
CSA (mm^2)	5.41 ± 0.28	4.53 ± 0.18[a]
L_0 (mm)	14.02 ± 0.12	13.95 ± 0.12

TA, anterior tibialis muscle; CSA, cross-sectional area; L_0, optimal muscle length.

[a]Significantly different.

Cardiac-specific ΔH2-R15 mini-dystrophin expression prevented myocardial inflammation and fibrosis (Fig. 5D, Supplementary Material, Fig. S6D).

To remove the ΔH2-R15 mini-dystrophin gene, we administered 8×10^{12} vg particles of AAV.CBA.Cre to 7-month-old SJ13 mice via the tail vein. Early time points (up to 20 weeks post AAV.CBA.Cre injection) showed limited reduction of mini-dystrophin in the heart of SJ13 mice (Supplementary Material, Fig. S3B). To achieve the maximal level of mini-dystrophin removal from the heart, we evaluated cardiac dystrophin/DGC/utrophin expression, histology, electrocardiogram (ECG) and LV hemodynamics when mice reached 22 months of age (15 months after injection) (Fig. 5, Supplementary Material, Figs. S6 and S7 and Tables S2 and S5). On western blot, the mini-dystrophin level in the heart was reduced by 64.32 ± 5.32% in AAV.CBA.Cre injected SJ13 mice (Fig. 5C, Supplementary Material, Table S2). Interestingly, immunostaining showed a non-homogeneous loss of mini-dystrophin expression in the heart (Fig. 5D). Although mini-dystrophin expression was greatly reduced in some cardiomyocytes, patches of mini-dystrophin positive cardiomyocytes were readily visible (Fig. 5D). Additional studies showed that AAV.CBA.Cre-mediated removal of mini-dystrophin did not change DGC expression neither did it induced utrophin upregulation in the heart (Supplementary Material, Fig. S6).

On histology examination, we did not see obvious abnormalities in the heart of AAV.CBA.Cre injected SJ13 mice (Fig. 5D, Supplementary Material, Figs S2B and S6D). There was neither inflammatory cell infiltration nor myocardial fibrosis (Fig. 5D and Supplementary Material, Fig. S6D). The body weight (BW), TA muscle weight (TW), heart weight (HW) and ventricular weight (VW) of AAV.CBA.Cre injected mice were not altered

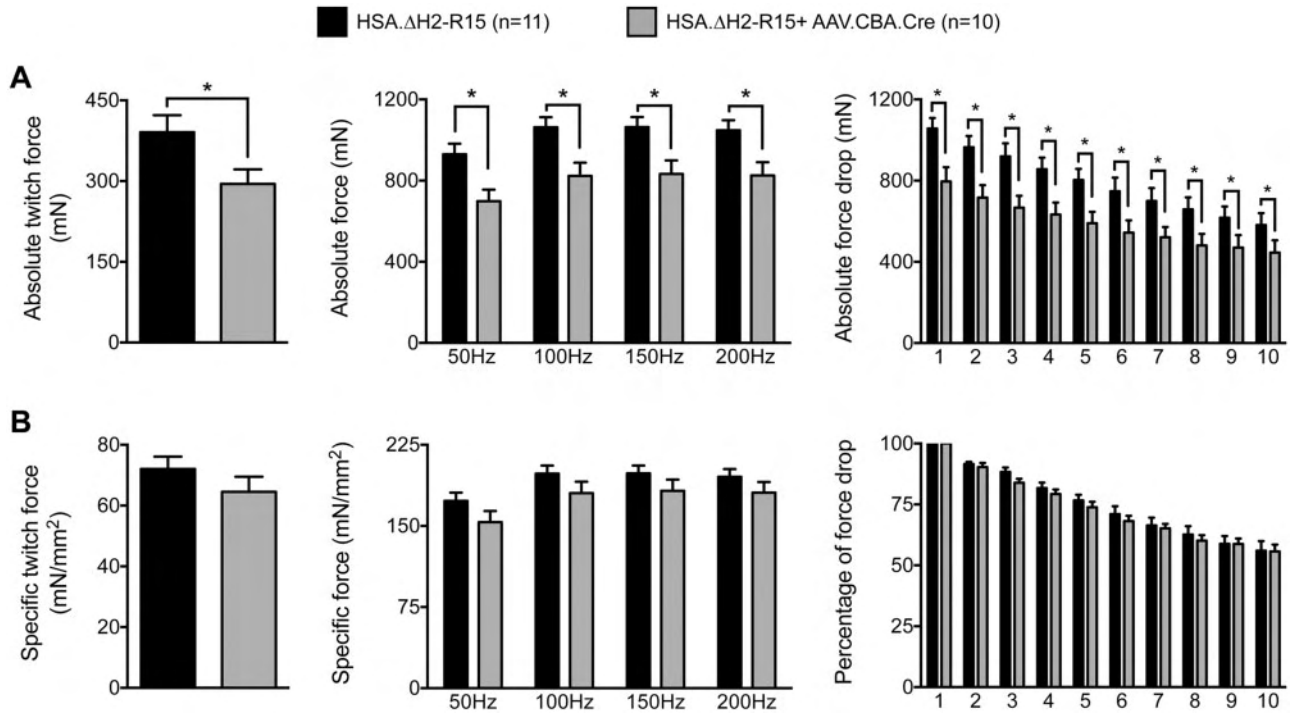

Figure 3. Removal of dystrophin in adult mice significantly reduces absolute muscle force. **(A)** Absolute muscle force. Left panel, twitch force; Middle panel, tetanic forces at different stimulation frequencies; Right panel, force drop during 10 cycles of eccentric contractions. **(B)** Specific muscle force. Left panel, twitch force; Middle panel, tetanic forces at different stimulation frequencies; Right panel, percentage of force drop from the baseline during 10 cycles of eccentric contractions. Asterisk, significantly different.

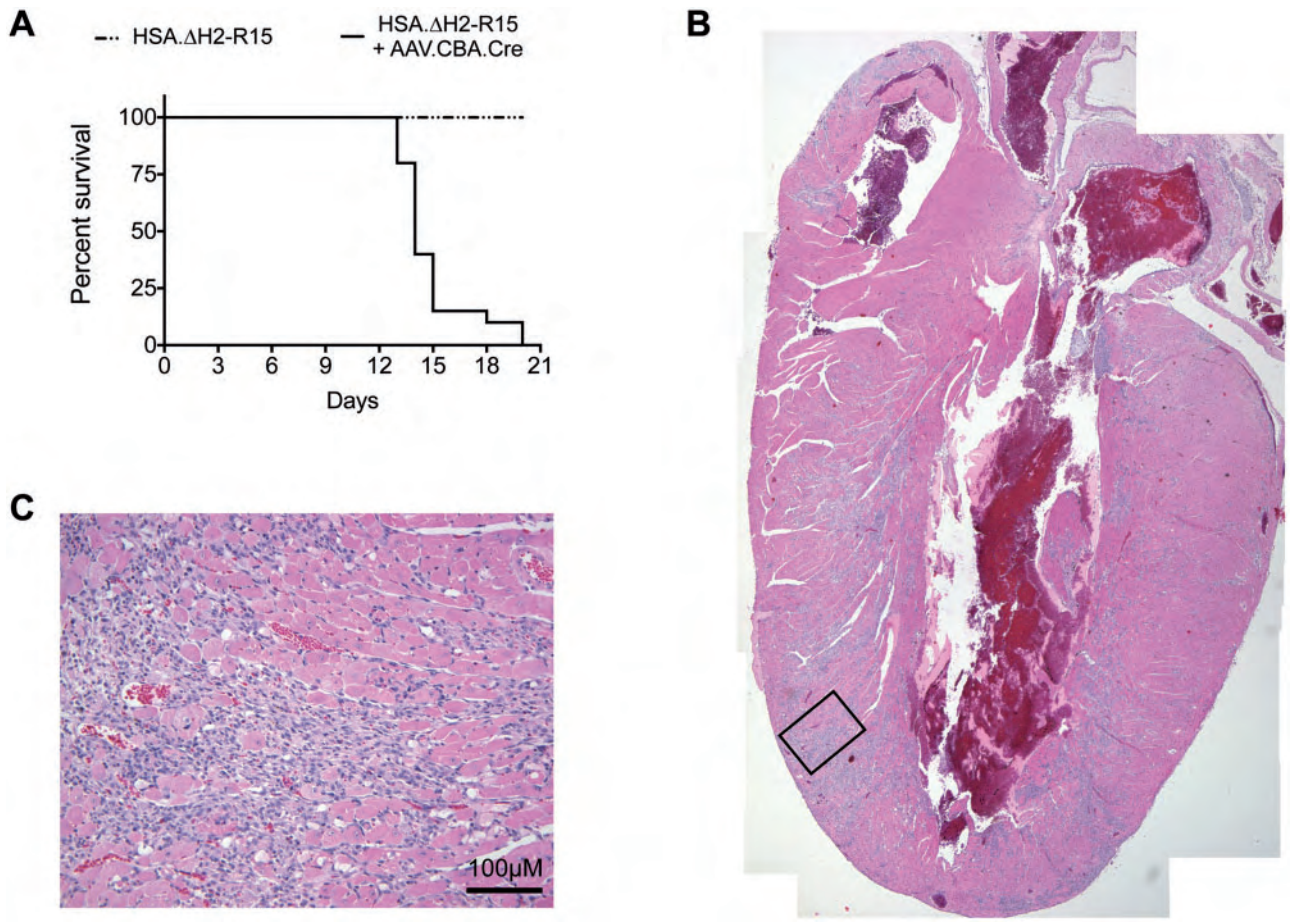

Figure 4. Intravenous injection of AAV.CBA.Cre results in lethal myocarditis in skeletal muscle mini-dystrophin transgenic FVB/mdx (YL238) mice. AAV.CBA.Cre was injected to adult YL238 mice at the dose of 8×10^{12} vg/mouse via the tail vein. Survival was monitored until all injected mice died. **(A)** Kaplan-Meier survival curve. N = 20 mice for each group. **(B)** Representative HE staining photomicrographs of whole heart section from a mouse died at day 15 after AAV.CBA.Cre injection. **(C)** Higher magnification photomicrograph of the boxed area in panel B. Abundant inflammatory cells were seen in myocardia.

(Table 3). However, the ratios of HW/BW, HW/TW and VW/TW showed a trend of increase. Importantly, the VW/BW ratio was significantly higher in SJ13 mice that received AAV.CBA.Cre injection (Table 3). On ECG examination, we clearly detected significant differences in many parameters between FVB and FVB/mdx mice (Supplementary Material, Table S3). However, no difference was observed in ECG tracing between SJ13 mice and AAV.CBA.Cre injected SJ13 mice (Supplementary Material, Fig. S7). Irrespective of AAV.CBA.Cre injection, all experimental mice showed the similar heart rate, PR interval, QRS duration, QT interval, Q amplitude and cardiomyopathy index (Supplementary Material, Fig. S7). Left ventricle catheterization was used to evaluate hemodynamic function of the heart. Compared with FVB mice, FVB/mdx mice had a significantly enlarge volume at the ends of systole and diastole (Supplementary Material, Table S4). FVB/mdx mice also showed reduced maximum pressure and ejection fraction (Supplementary Material, Table S4). All these parameters were normalized in SJ13 mice (Fig. 5E). However, the chamber size was clearly enlarged in AAV.CBA.Cre injected SJ13 mice as demonstrated by the significant increase in both end systolic and end diastolic volumes (Fig. 5E). Significant reduction in the maximum pressure and ejection fraction of AAV.CBA.Cre injected SJ13 mice suggested that the pump function of the heart was compromised in these mice (Fig. 5E). Nevertheless, there was no significant difference in other hemodynamic parameters (such as stroke volume, cardiac output, dP/dt max, dP/dt min and Tau) between SJ13 mice and AAV.CBA.Cre injected SJ13 mice (Supplementary Material, Table S5).

Discussion

In this study, we examined the consequences of adulthood loss of dystrophin in skeletal muscle and the heart in ΔH2-R15 mini-dystrophin transgenic FVB/mdx mice. We found that a partial loss of therapeutic mini-dystrophin is associated with significant detrimental changes in muscle structure and function. Our results suggest that dystrophin reduction alone is sufficient to induce DMD-like myopathy in adult muscle and persistent dystrophin expression is essential for long-term protection. Our results also bring in new perspective on the therapeutic significance of low-level dystrophin expression.

It is well established that the absence of dystrophin causes DMD (14,15). However, it is not clear whether myopathy seen in patients originates from congenital dystrophin deficiency during embryogenesis (16). In other words, it is not clear whether the loss of dystrophin from mature muscle alone is sufficient to cause dystrophic changes. Discrepancy between dystrophin deficiency and muscular dystrophy has been documented in the literature. At least three patients who had nonsense mutation

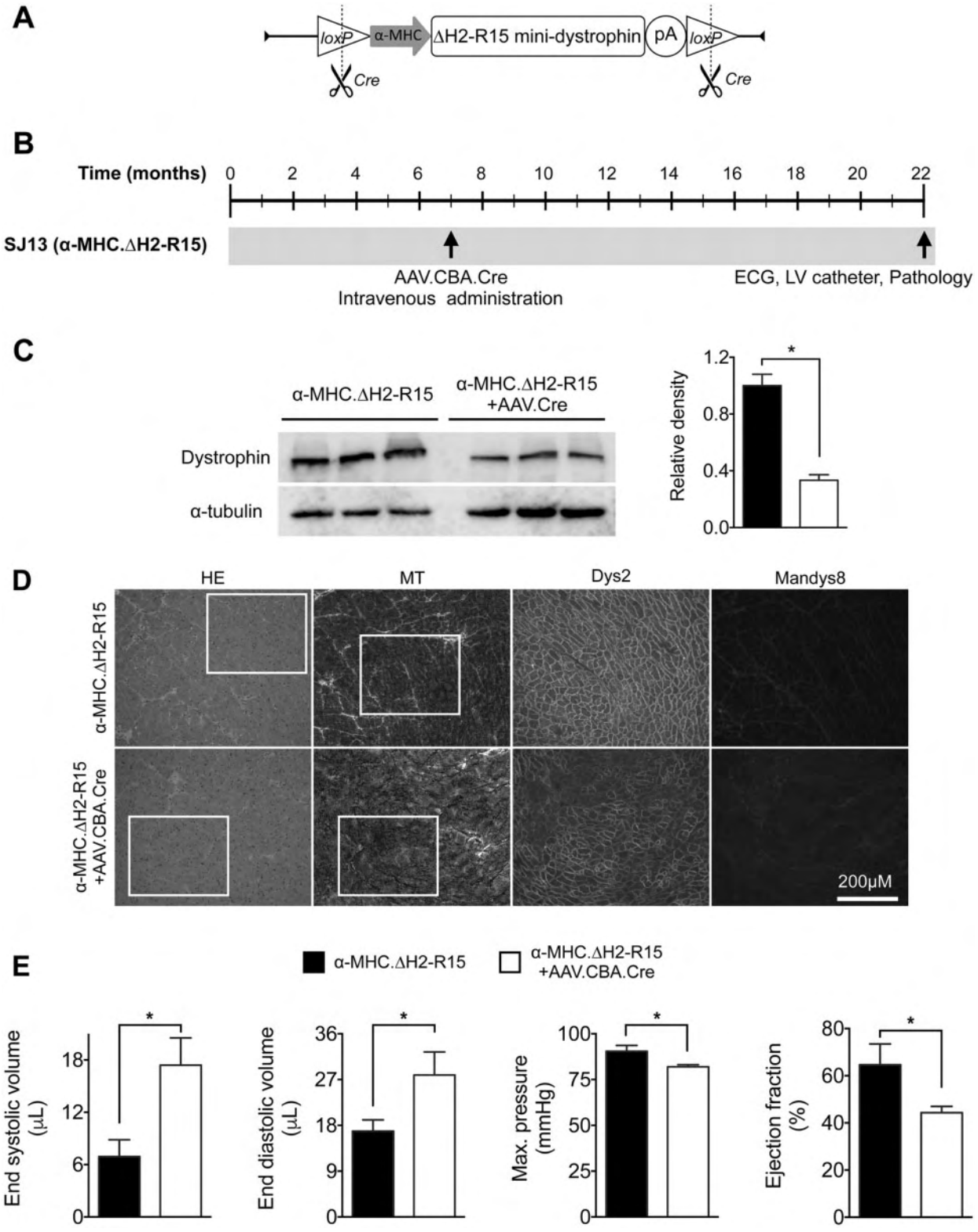

Figure 5. Loss of dystrophin in the heart of adult mice compromises LV hemodynamics. To evaluate the effects of loss of dystrophin in the heart of adult mice, we generated SJ13 mice. These mice selectively expressed ΔH2-R15 mini-dystrophin in the heart from a floxed α-MHC.ΔH2-R15 expression cassette. **(A)** Graphical representation of the floxed α-MHC.ΔH2-R15 transgenic cassette. Vertical dotted lines mark Cre recombinase-mediated excision of the cassette. **(B)** Experimental outline. AAV.CBA.Cre was injected to 7-month-old SJ13 mice via the tail vein. Dystrophin expression and heart function were assessed when mice reached 22 months of age. **(C)** Representative dystrophin western blots and densitometry quantification. **(D)** Representative photomicrographs of HE staining, Masson trichrome staining and dystrophin immunostaining with Dys2 and Mandys8 monoclonal antibodies. Boxed areas in HE and Masson trichrome staining are enlarged in Supplementary Material, Figure S6D. In AAV.CBA.Cre injected SJ13 mice, Dys2 immunostaining revealed patchy mini-dystrophin expression. **(E)** Selective LV hemodynamic parameters measured by cardiac catheterization in AAV.CBA.Cre injected ($N = 5$) and un-injected ($N = 6$) SJ13 mice. Asterisk, significantly different.

Table 3. Weights and weight ratios of 22-month-old SJ13 mice

	α-MHC.ΔH2-R15	α-MHC.ΔH2-R15 +AAV.CBA.Cre
Sample size (*n*)	9	6
Age (m)	22.91 ± 0.05	22.25 ± 0.65
BW (g)	30.68 ± 2.03	26.93 ± 1.85
TW (mg)	34.26 ± 1.46	33.46 ± 2.2
HW (mg)	143.64 ± 6.63	149.17 ± 8.06
VW (mg)	132.90 ± 5.83	139.38 ± 8.39
TW/BW (mg/g)	1.14 ± 0.06	1.26 ± 0.07
HW/BW (mg/g)	4.79 ± 0.25	5.61 ± 0.26
HW/TW (mg/g)	4.30 ± 0.26	4.51 ± 0.22
VW/BW (mg/g)	4.43 ± 0.23	5.24 ± 0.26[a]
VW/TW (mg/g)	3.98 ± 0.23	4.21 ± 0.21

BW, body weight; TW, anterior tibialis muscle weight; HW, heart weight; VW, ventricle weight.
[a]Significantly different.

in the dystrophin gene and no detectable dystrophin in their muscle were clinically asymptomatic and/or mildly affected (17,18). Lack of histological and physiological defects in ≤14-day-old mdx mice is another example where the absence of dystrophin is not accompanied with muscle disease (19–22). To determine whether dystrophin deficiency alone can elicit myopathy in adult muscle, Ghahramani Seno *et al.* (7) applied AAV-mediated dystrophin RNA interference (RNAi) in adult normal mice. Although they successfully reduced dystrophin expression, no overt dystrophic pathology was observed (7). Collectively, these observations appear to support the notion that dystrophin deficiency by itself may, at least in some cases, not lead to overt muscular dystrophy. Dystrophin replacement gene therapy has the potential to bring back the missing dystrophin protein in large mammals (23,24). However, current approaches may not lead to lifelong dystrophin restoration due to the cellular immune response and muscle cell turnover. Patients may end up lose their restored dystrophin again. Hence, there is a strong need to understand what will happen after therapeutic dystrophin is lost.

We designed this study to investigate whether the adulthood loss of dystrophin is associated with deleterious consequences. In Ghahramani Seno *et al.* (7) study, RNAi cannot completely eliminate dystrophin because muscle still carries a transcriptionally competent dystrophin gene in the genome. The residual dystrophin expression may at least partially account for the lack of muscle disease seen by the authors. To avoid this caveat, we decided to use the gene elimination approach in our study. Specifically, we engineered floxed mini-dystrophin transgenic FVB/mdx mice. We hypothesized that excision by Cre recombinase will eliminate the minigene from the genome and consequently completely remove mini-dystrophin from muscle. Because AAV is the most robust muscle gene transfer vector and intramuscular AAV injection is not associated with any toxicity (25), we opted to use AAV to deliver the Cre recombinase gene. In the Ghahramani Seno *et al.* (7) study, dystrophin knockdown was only performed in skeletal muscle. Considering cardiomyopathy is a leading cause of morbidity and mortality in DMD patients, we made two independent strains of floxed transgenic mdx mice (Table 1). Strain YL238 only had functional mini-dystrophin expression in skeletal muscle while strain SJ13 only had functional mini-dystrophin expression in the heart (Supplementary Material, Fig. S2). Characterization of the transgenic constructs in 293 cells confirmed digestion of the minigene by AAV.CBA.Cre (Supplementary Material, Fig. S1). To determine how long it would take to remove dystrophin expression from muscle in transgenic mice, we performed a time course study (Supplementary Material, Fig. S3). In strain YL238, reduction in mini-dystrophin expression became apparent at 8 weeks after local AAV.CBA.Cre injection. However, mini-dystrophin remained readily detectable at the 16-week time point (Supplementary Material, Fig. S3A). Systemic AAV.CBA.Cre injection was performed in strain SJ13 to knockdown myocardial mini-dystrophin expression. Surprisingly, at 20 weeks after injection we still observed substantial amount of mini-dystrophin in the heart on western blot (Supplementary Material, Fig. S3B). It has been shown that full-length dystrophin is extremely stable (7,9). Our results suggest that ΔH2-R15 mini-dystrophin may also have a fairly long half-life. Alternatively, our results may also suggest that Cre recombinase digestion was incomplete (either not enough Cre recombinase due to poor AAV transduction or not enough digestion time). Since the dosages used in our studies are known to cause saturated gene transfer (26), we decided to extend the experiment duration until these mice reached the terminal age of their life (20–22 months) (Figs 1C and 5B).

To study dystrophin loss in skeletal muscle, we delivered AAV.CBA.Cre to 8-month-old YL238 mice and examined muscle histology and force when they reached 20 months of age. On western blot, mini-dystrophin level was reduced by ∼87% (Fig. 1E and 1F, Supplementary Material, Table S1). In contrast to the results of AAV-mediated dystrophin knockdown by RNAi (7), we observed significant muscle atrophy, myofiber size change, degeneration/regeneration, inflammation and significant loss of absolute muscle force (Figs 2 and 3, Supplementary Material, Fig. S5 and Table S2). Our data suggest that dystrophin deficiency alone can cause skeletal muscle myopathy in an adult mammal. Loss of therapeutic dystrophin will lead to the relapse of myopathy. An effective therapy for DMD requires persistent expression.

Most of DMD patients die from respiratory muscle failure. However, these muscles (including the diaphragm, intercostal muscle, abdominal muscle and chest muscle) cannot be easily reached by direct muscle injection. To study the consequences of bodywide loss of mini-dystrophin in skeletal muscle of adult mice, we delivered AAV.CBA.Cre intravenously to YL238 mice. Unexpectedly, all injected mice died between 13 and 20 days after injection. Autopsy suggests that the death was due to acute myocarditis (Fig. 4, Supplementary Material, Fig. S2A). Chronic overexpression of Cre recombinase in cardiac Cre transgenic mice has been shown to cause cardiomyopathy at the age of 8–12 months (27). However, AAV-mediated Cre expression in the heart has not been associated with any toxicity (28,29). To troubleshoot our study, we injected the same batch of the AAV.CBA.Cre vector to SJ13 mice at the same dose. None of the injected SJ13 mice died (Supplementary Material, Fig. S2B). This new piece of data suggests that the death seen in YL238 mice was not due to AAV vector contamination, but rather, caused by the lack of dystrophin in the heart of YL238 mice. We have previously successfully delivered several different AAV vectors (such as alkaline phosphatase reporter vector and micro-dystrophin vector) to the heart of adult (and even aged) mdx mice without seeing any toxicity (30–32). Hence, we don't believe that the delivery of AAV to the heart of mdx mice *per se* is the cause of cardiac death. We suspect that, very likely, the observed cardiac death in YL238 mice is due to a combined effect of Cre toxicity and dystrophin deficiency. Future studies are needed to clarify this issue.

In our preliminary study, we found that SJ13 mice were more resistant to the genetic removal of mini-dystrophin from the heart (Supplementary Material, Fig. S3B). In the hope of achieving better dystrophin removal, we injected AAV.CBA.Cre to 7-month-old SJ13 mice and waited until they were 22-month-old (Fig. 5B). On western blot, mini-dystrophin expression in the heart was significantly reduced in mice that received AAV.CBA.Cre injection. On average, the mini-dystrophin level was reduced by ~64% (Fig. 5C, Supplementary Material, Table S2). On immunostaining, homogenous cardiac mini-dystrophin expression became patchy in AAV.CBA.Cre injected SJ13 mice (Fig. 5D). Similar to what we seen in YL238 mice, expression of the DGC components and utrophin was not altered (Figs 1C–E, Supplementary Material, Fig. S4). However, in contrast to the histological signs of myopathy seen in YL238 mice, we did not detect any overt pathological lesions in the heart of SJ13 mice following AAV.CBA.Cre injection (Fig. 5D, Supplementary Material, Fig. S6D). On ECG examination, no difference was detected either (Supplementary Material, Fig. S7). Nevertheless, signs of dilated cardiomyopathy were clearly noted (Fig. 5E, Table 3). Specifically, the VW to BW ratio (VW/BW) was significantly increased (Table 3). On hemodynamic assays, end systolic/diastolic volumes were significantly increased, and the maximum pressure and ejection fraction were significantly reduced (Fig. 5E). Collectively, our data suggest that the reduction of dystrophin alone is sufficient to induce Duchenne cardiomyopathy-like functional changes in adult mice. If we extrapolate these findings to gene therapy, it will suggest that a loss of therapeutic dystrophin after it has been expressed for a while may lead to the deterioration of an already improved heart. Continuous cardiac dystrophin expression is absolutely required to reduce cardiac morbidity and mortality in DMD.

An important goal of DMD gene therapy studies is to determine how much dystrophin is enough for muscle and heart protection. Homogenous expression of marginal level (4–5%) dystrophin starting from *in utero* has been shown to partially preserve muscle function in mdx mice and increase survival of severely affected utrophin/dystrophin double knockout mice (33–36). More recently, the Wells laboratory showed that exon-skipping restoration of 15% homogenous dystrophin expression significantly improved the eccentric contraction profile in adult mdx mice (37). In our study, we originally hoped to completely eliminate transgenic ΔH2-R15 mini-dystrophin expression. However, this did not happen. We still got ~13 and 36% mini-dystrophin expression in skeletal muscle and heart, respectively. In skeletal muscle, we observed clear morphological evidence of myopathy but the specific muscle force and eccentric contraction profile were preserved (Figs 2 and 3B). Our results suggest that the amount of dystrophin needed for preserving muscle histology is different from that needed for preserving specific force. More dystrophin is required to preserve muscle histology (36).

For reasons yet unclear, we obtained patchy mini-dystrophin elimination in the heart on immunostaining in SJ13 mice (Fig. 5D). We have previously shown that 50% mosaic dystrophin expression and complementary utrophin upregulation are sufficient to completely prevent dilated cardiomyopathy in mdx mice (38,39). In the heart of SJ13 mice, AAV.CBA.Cre injection resulted in a loss of ~64% mini-dystrophin (Fig. 5C, Supplementary Material, Table S2). However, we did not detect evident histological change in the myocardium (Fig. 5D and Supplementary Material, Fig. S6D). The ECG profile was not altered either (Supplementary Material, Fig. S7). Nevertheless, the hemodynamic function of the left ventricle was significantly compromised. These data have further lowed the therapeutic threshold for the protection of heart morphology and electrophysiology (from 50 to ~36%). On the other side, the rescue of the heart hemodynamics may require complementary utrophin upregulation in dystrophin-negative cardiomyocytes and/or ≥50% dystrophin expression in the heart.

In summary, our results have provided clear evidence that an effective gene therapy for DMD depends on persistent expression of a therapeutic dystrophin gene.

Materials and Methods

Experimental animals

All animal experiments were approved by the institutional animal care and use committee and were in accordance with National Institutes of Health guidelines. Two FVB background founders of human ΔH2-R15 mini-dystrophin transgenic mice were generated at the University of Missouri transgenic core. In one founder, the ΔH2-R15 mini-dystrophin gene was driven by the skeletal muscle-specific HSA promoter. The promoter and the minigene were flanked by two unidirectional loxP repeats (Fig. 1B, Supplementary Material, Fig. S1A). This founder was subsequently crossed with dystrophin-null FVB/mdx mice (10). The resulting skeletal muscle-specific mini-dystrophin transgenic mdx mice were termed YL238 mice. In the other founder, the ΔH2-R15 mini-dystrophin gene was driven by the cardiac-specific α-MHC promoter. The entire expression cassette (promoter, minigene and pA) was flanked by two unidirectional loxP repeats (Fig. 5A, Supplementary Material, Fig. S1A). Following crossing with dystrophin-null FVB/mdx mice (10), we obtained cardiac-specific mini-dystrophin transgenic mdx mice and named these mice SJ13 mice. All mice were maintained in a specific-pathogen free animal care facility on a 12-h light (25 lux):12-h dark cycle with access to food and water *ad libitum*. In light of the gender bias in mdx skeletal muscle disease and cardiomyopathy, male mice were used in the YL238 mouse study and female mice were used in the SJ13 mouse study (40,41). Mice were euthanized following the functional assays and tissues were harvested.

AAV.CBA.Cre production and *in vivo* delivery

The *cis*-plasmid for AAV.CBA.Cre production was a generous gift of Dr Weidong Xiao (Temple University, Philadelphia, PA) (42). The AAV-9 packaging plasmid was a generous gift of Dr James Wilson (University of Pennsylvania, Philadelphia, PA) (43). The AAV.CBA.Cre was packaged in AAV-9 according to our published protocol (44). For intramuscular delivery, 2.7×10^{12} vg (50 μl) particles of AAV.CBA.Cre were injected into one side TA muscle using a 32G Hamilton syringe (Reno, NV). The contralateral TA muscle received saline as the untreated control. For systemic delivery, 8×10^{12} vg (500 μl) particles of AAV.CBA.Cre were administered in a single bolus via the tail vein.

Morphological studies

Dystrophin expression was evaluated by immunofluorescence staining using four independent dystrophin monoclonal antibodies including Dys2 (1:30; Vector Laboratories, Burlingame, CA), Dys3 (1:20; Leica Biosystems, Buffalo Grove, IL), DysB (1:80, clone 34C5, IgG1; Novocastra, Newcastle, UK) and Mandys8 (1:200; Sigma Aldrich, St Louis, MO). Dys2 recognizes an epitope in the dystrophin C-terminal domain. Dys3 recognizes an epitope in dystrophin

hinge 1. DysB recognizes an epitope that is located between hinge 1 and dystrophin spectrin-like repeat 2. Dys2, Dys3 and DysB react with ΔH2-R15 mini-dystrophin (Fig. 1A). Mandys8 recognizes an epitope in dystrophin spectrin-like repeat 11, which is absent in ΔH2-R15 mini-dystrophin (38,45). General histology was examined by HE staining. Central nucleation was quantified on six random 20× field images for each muscle. Fiber size was quantified on digitized images using the Adobe Photoshop software (San Jose, CA). Briefly, the micrometer scale was defined with the set measurement scale option in the software. The perimeter of each individual fiber was marked using the quick selection tool. The CSA was then calculated by the software. Approximately 400 myofibers were quantified in each TA muscle. Fibrosis was examined by Masson trichrome staining as we described before (46). Macrophages (1:200; Caltag Laboratories, Burlingame, CA), neutrophils (1:80; BD Pharmingen, San Jose, CA), CD^{4+} T cells (1:800; Affinity Bioreagent, Golden, CO) and CD^{8+} T cells (1:800; BD Pharmingen) were examined by immunoshistochemistry staining. Slides were viewed at the identical exposure setting using a Nikon E800 fluorescence microscope. Photomicrographs were taken with a Qimage Retiga 1300 camera (46).

Western blot

TA muscles and hearts lysates were prepared as described before (47). Briefly, the tissues were snap frozen in liquid nitrogen. The frozen tissue samples were ground to fine powder in liquid nitrogen followed by homogenization in a buffer containing 10% sodium dodecyl sulfate, 5 mM Ethylenediaminetetraacetic acid, 62.5 mM Tris–HCl at pH6.8 and the protease inhibitor cocktail (Roche, Indianapolis, IN). The crude lysate were heated at 95°C for 3 min, chilled on ice for 2 min and then centrifuged at 14 000*g* for 2 min. Supernatant was collected as the whole muscle lysate. Protein concentration was measured using the DC protein assay kit (Bio-Rad, Hercules, CA) and 50 μg of protein was used to load per lane for the western blot. Dystrophin was detected with Dys3 (1:50 Leica Biosystems), DysB (1:100, clone 34C5, IgG1; Novocastra) and Dys2 (1:100 Vector Laboratories) antibodies (Fig. 1A). β-Dystroglycan was detected with a mouse monoclonal antibody against the β-dystroglycan C-terminus (NCL-b-DG, 1:100; clone 43DAG1/8D5, IgG2a; Novocastra). α-Sarcoglycan was detected with a mouse monoclonal antibody against α-sarcoglycan amino acid residues 217–289 (VP-A105; 1:1000; clone Ad1/20A6, IgG1; Vector Laboratories). Syntrophin was detected with a pan-syntrophin mouse monoclonal antibody that recognized the syntrophin PSD-95/Dlg/ZO-1 domain (ab11425, 1:2000; clone 1351, IgG1; Abcam, Cambridge, MA). Dystrobrevin was detected with a mouse monoclonal antibody against dystrobrevin amino acid residues 249–403 (#610766, 1:000; clone 23, IgG1; BD Biosciences, San Diego, CA). nNOS was detected with a rabbit polyclonal antibody (N7280, 1:2000; Sigma Aldrich). For the loading control, we used the glyceraldehyde 3-phosphate dehydrogenase antibody (1:3000; Millipore, Billerica, MA) and α-tubulin antibody (1:3000; clone B-5-1-2; Sigma) for TA muscle and heart western blot, respectively. Western blot quantification was performed using the ImageJ (http://rsbweb.nih.gov/ij/; last accessed January 05, 2016) or LI-COR Image Studio Version 5.0.21 software (https://www.licor.com; last accessed January 05, 2016). The relative intensity of the respective protein band was normalized to the corresponding loading control in the same blot. The relative band intensity in AAV.CBA.Cre treated muscles was normalized to that of untreated controls.

TA muscle function evaluation

The TA muscle force was measured *in situ* according to our published protocol (48,49). Briefly, mice were anesthetized via intraperitoneal injection of a cocktail containing 25 mg/ml ketamine, 2.5 mg/ml xylazine and 0.5 mg/ml acepromazine at 2.5 μl/g BW. The TA muscle and the sciatic nerve were exposed. The mouse was transferred to a custom-designed thermo-controlled platform of the footplate apparatus (48,49). After 5 min equilibration, the sciatic nerve was stimulated at the frequency of 1 Hz (20 V, 1000 mA) to elicit twitch muscle contraction using a custom-made 25G platinum electrode at 2.0–6.0 g resting tensions. The muscle length (L_m) of the TA muscle was measured with an electronic digital caliper (Fisher Scientific, Waltham, MA, USA) at the resting tension that generated the maximal twitch force. This length was defined as the optimal muscle length (L_0). The twitch force was measured at 1 Hz frequency followed by the force frequency assay at 50, 100, 150 and 200 Hz with 1 min resting between each contraction. Specific muscle force was determined by dividing the maximum isometric tetanic force with the muscle CSA. The CSA was calculated according to the following equation, CSA = (muscle mass, in gram)/[(optimal fiber length, in cm) × (muscle density, in g/cm^3)]. A muscle density of 1.06 g/cm^3 was used in calculation. Optimal fiber length was calculated as 0.60 × L_0. In total, 0.60 represents the ratio of the fiber length to the L_0 of the TA muscle. After tetanic force measurement, the muscle was rested for 5 min and then subjected to 10 rounds of eccentric contraction according to our previously published protocol (48,49). Briefly, following a tetanic contraction the TA muscle was stretched by 10% L_0 at a rate 0.5 L_0/s. The muscle was allowed to rest 1 min between each eccentric contraction cycle. The percentage of force drop following each round of eccentric contraction was recorded. Muscle twitch and tetanic forces and the eccentric contraction profile were measured with a 305C-LR dual-mode servomotor transducer (Aurora Scientific, Inc.). Data were processed using the Laboratory View-based DMC and DMA programs (Version 3.12, Aurora Scientific, Inc.).

ECG and LV hemodynamic assay

A 12-lead ECG assay was performed using a commercial system from AD Instruments (Colorado Springs, CO) according to our previously published protocol (50). The Q wave amplitude was determined using the lead I tracing. Other ECG parameters were analyzed using the lead II tracing. The QTc interval was determined by correcting the QT interval with the heart rate as described by Mitchell *et al.* (51). The cardiomyopathy index was calculated by dividing the QT interval by the PQ segment (52). LV hemodynamics was evaluated using a closed chest approach as we previously described (50). The resulting pressure-volume (PV) loops were analyzed with the PVAN software (Millar Instruments, Houston, TX). Detailed protocols for ECG and hemodynamic assays are available at the Parent Project Muscular Dystrophy standard operating protocol web site (http://www.parentprojectmd.org/site/PageServer?pagename=Advance_researchers_sops; last accessed January 05, 2016).

Statistical analysis

Data are presented as mean ± standard error of mean (s.e.m.). Statistical significance between un-injected controls and AAV.CBA.Cre injected samples were determined by the Student *t*-test. For data that were non-parametric, statistical analysis was performed with the Wilcoxon Rank Sum test. Difference was considered statistically significant when $P < 0.05$.

Supplementary Material

Supplementary Material is available at *HMG* online.

Acknowledgements

The authors thank Dr Weidong Xiao for providing the *cis*-plasmid used for AAV.CBA.Cre production and Dr Jim Wilson for providing AAV-9 packaging plasmid.

Conlict of Interest statement. D.D. is a member of the scientific advisory board for and an equity holder of Solid GT, a subsidiary of Solid Biosciences.

Funding

This work was supported by grants from the National Institutes of Health (HL-91883, NS-90634); Department of Defense (MD130014, MD150133); Jesse's Journey-The Foundation for Gene and Cell Therapy. N.W. was partially supported by the life science fellowship, University of Missouri.

Disclosure

D.D. is a member of the scientific advisory board for and an equity holder of Solid GT, a subsidiary of Solid Biosciences.

References

1. Kunkel, L.M. (2005) 2004 William Allan Award address. Cloning of the DMD gene. *Am. J. Hum. Genet.*, **76**, 205–214.
2. Mendell, J.R. and Lloyd-Puryear, M. (2013) Report of MDA muscle disease symposium on newborn screening for Duchenne muscular dystrophy. *Muscle Nerve*, **48**, 21–26.
3. Bengtsson, N.E., Seto, J.T., Hall, J.K., Chamberlain, J.S. and Odom, G.L. (2016) Progress and prospects of gene therapy clinical trials for the muscular dystrophies. *Hum. Mol. Genet.*, **25**, R9–R17.
4. Duan, D. (2015) Duchenne muscular dystrophy gene therapy in the canine model. *Hum. Gene Ther. Clin. Dev.*, **26**, 57–69.
5. Al-Zaidy, S., Rodino-Klapac, L. and Mendell, J.R. (2014) Gene therapy for muscular dystrophy: moving the field forward. *Pediatr. Neurol.*, **51**, 607–618.
6. Kawecka, K., Theodoulides, M., Hasoglu, Y., Jarmin, S., Kymalainen, H., Le-Heron, A., Popplewell, L., Malerba, A., Dickson, G. and Athanasopoulos, T. (2015) Adeno-associated virus (AAV) mediated dystrophin gene transfer studies and exon skipping strategies for Duchenne muscular dystrophy (DMD). *Curr. Gene Ther.*, **15**, 395–415.
7. Ghahramani Seno, M.M., Graham, I.R., Athanasopoulos, T., Trollet, C., Pohlschmidt, M., Crompton, M.R. and Dickson, G. (2008) RNAi-mediated knockdown of dystrophin expression in adult mice does not lead to overt muscular dystrophy pathology. *Hum. Mol. Genet.*, **17**, 2622–2632.
8. Duan, D. (2008) Dystrophin knockdown mice suggest that early, transient dystrophin expression might be enough to prevent later pathology. *Neuromuscul. Disord.*, **18**, 904–905.
9. Ahmad, A., Brinson, M., Hodges, B.L., Chamberlain, J.S. and Amalfitano, A. (2000) Mdx mice inducibly expressing dystrophin provide insights into the potential of gene therapy for duchenne muscular dystrophy. *Hum. Mol. Genet.*, **9**, 2507–2515.
10. Wasala, N.B., Zhang, K., Wasala, L.P., Hakim, C.H. and Duan, D. (2015) The FVB background does not dramatically alter the dystrophic phenotype of mdx mice. *PLoS Curr.*, **7**, pii:e-currents.md.28266819ca28266810ec28266815fefcac28266767ea28266819a28263461c.
11. Lai, Y., Thomas, G.D., Yue, Y., Yang, H.T., Li, D., Long, C., Judge, L., Bostick, B., Chamberlain, J.S., Terjung, R.L. *et al.* (2009) Dystrophins carrying spectrin-like repeats 16 and 17 anchor nNOS to the sarcolemma and enhance exercise performance in a mouse model of muscular dystrophy. *J. Clin. Invest.*, **119**, 624–635.
12. Zhang, Y., Yue, Y., Li, L., Hakim, C.H., Zhang, K., Thomas, G.D. and Duan, D. (2013) Dual AAV therapy ameliorates exercise-induced muscle injury and functional ischemia in murine models of Duchenne muscular dystrophy. *Hum. Mol. Genet.*, **22**, 3720–3729.
13. Zhang, Y. and Duan, D. (2012) Novel mini-dystrophin gene dual adeno-associated virus vectors restore neuronal nitric oxide synthase expression at the sarcolemma. *Hum. Gene Ther.*, **23**, 98–103.
14. Hoffman, E.P., Brown, R.H., Jr and Kunkel, L.M. (1987) Dystrophin: the protein product of the Duchenne muscular dystrophy locus. *Cell*, **51**, 919–928.
15. Bonilla, E., Samitt, C.E., Miranda, A.F., Hays, A.P., Salviati, G., DiMauro, S., Kunkel, L.M., Hoffman, E.P. and Rowland, L.P. (1988) Duchenne muscular dystrophy: deficiency of dystrophin at the muscle cell surface. *Cell*, **54**, 447–452.
16. Merrick, D., Stadler, L.K., Larner, D. and Smith, J. (2009) Muscular dystrophy begins early in embryonic development deriving from stem cell loss and disrupted skeletal muscle formation. *Dis. Model. Mech.*, **2**, 374–388.
17. Castro-Gago, M. (2014) Milder course in Duchenne patients with nonsense mutations and no muscle dystrophin. *Neuromuscul. Disord.*, **25**, 443.
18. Zatz, M., Pavanello, R.C., Lazar, M., Yamamoto, G.L., Lourenco, N.C., Cerqueira, A., Nogueira, L. and Vainzof, M. (2014) Milder course in Duchenne patients with nonsense mutations and no muscle dystrophin. *Neuromuscul. Disord.*, **24**, 986–989.
19. Grange, R.W., Gainer, T.G., Marschner, K.M., Talmadge, R.J. and Stull, J.T. (2002) Fast-twitch skeletal muscles of dystrophic mouse pups are resistant to injury from acute mechanical stress. *Am. J. Physiol. Cell Physiol.*, **283**, C1090–C1101.
20. Reed, P. and Bloch, R.J. (2005) Postnatal changes in sarcolemmal organization in the mdx mouse. *Neuromuscul. Disord.*, **15**, 552–561.
21. Grady, R.M., Teng, H., Nichol, M.C., Cunningham, J.C., Wilkinson, R.S. and Sanes, J.R. (1997) Skeletal and cardiac myopathies in mice lacking utrophin and dystrophin: a model for Duchenne muscular dystrophy. *Cell*, **90**, 729–738.
22. Deconinck, A.E., Rafael, J.A., Skinner, J.A., Brown, S.C., Potter, A.C., Metzinger, L., Watt, D.J., Dickson, J.G., Tinsley, J.M. and Davies, K.E. (1997) Utrophin-dystrophin-deficient mice as a model for Duchenne muscular dystrophy. *Cell*, **90**, 717–727.
23. Shin, J.H., Pan, X., Hakim, C.H., Yang, H.T., Yue, Y., Zhang, K., Terjung, R.L. and Duan, D. (2013) Microdystrophin ameliorates muscular dystrophy in the canine model of Duchenne muscular dystrophy. *Mol. Ther.*, **21**, 750–757.
24. Yue, Y., Pan, X., Hakim, C.H., Kodippili, K., Zhang, K., Shin, J.H., Yang, H.T., McDonald, T. and Duan, D. (2015) Safe and bodywide muscle transduction in young adult Duchenne muscular dystrophy dogs with adeno-associated virus. *Hum. Mol. Genet.*, **24**, 5880–5890.
25. Liu, M., Yue, Y., Harper, S.Q., Grange, R.W., Chamberlain, J.S. and Duan, D. (2005) Adeno-associated virus-mediated microdystrophin expression protects young mdx muscle from contraction-induced injury. *Mol. Ther.*, **11**, 245–256.
26. Bostick, B., Ghosh, A., Yue, Y., Long, C. and Duan, D. (2007) Systemic AAV-9 transduction in mice is influenced by

animal age but not by the route of administration. *Gene Ther.*, **14**, 1605–1609.
27. Davis, J., Maillet, M., Miano, J.M. and Molkentin, J.D. (2012) Lost in transgenesis: a user's guide for genetically manipulating the mouse in cardiac research. *Circ. Res.*, **111**, 761–777.
28. Iwatate, M., Gu, Y., Dieterle, T., Iwanaga, Y., Peterson, K.L., Hoshijima, M., Chien, K.R. and Ross, J. (2003) In vivo high-efficiency transcoronary gene delivery and Cre-LoxP gene switching in the adult mouse heart. *Gene Ther.*, **10**, 1814–1820.
29. Werfel, S., Jungmann, A., Lehmann, L., Ksienzyk, J., Bekeredjian, R., Kaya, Z., Leuchs, B., Nordheim, A., Backs, J., Engelhardt, S. *et al.* (2014) Rapid and highly efficient inducible cardiac gene knockout in adult mice using AAV-mediated expression of Cre recombinase. *Cardiovasc. Res.*, **104**, 15–23.
30. Bostick, B., Shin, J.H., Yue, Y., Wasala, N.B., Lai, Y. and Duan, D. (2012) AAV micro-dystrophin gene therapy alleviates stress-induced cardiac death but not myocardial fibrosis in > 21-m-old mdx mice, an end-stage model of Duchenne muscular dystrophy cardiomyopathy. *J. Mol. Cell. Cardiol.*, **53**, 217–222.
31. Bostick, B., Shin, J.H., Yue, Y. and Duan, D. (2011) AAV-micro-dystrophin therapy improves cardiac performance in aged female mdx mice. *Mol. Ther.*, **19**, 1826–1832.
32. Ghosh, A., Yue, Y., Shin, J.H. and Duan, D. (2009) Systemic trans-splicing AAV delivery efficiently transduces the heart of adult mdx mouse, a model for Duchenne muscular dystrophy. *Hum. Gene. Ther.*, **20**, 1319–1328.
33. van Putten, M., Hulsker, M., Nadarajah, V.D., van Heiningen, S.H., van Huizen, E., van Iterson, M., Admiraal, P., Messemaker, T., den Dunnen, J.T., t Hoen, P.A. *et al.* (2012) The effects of low levels of dystrophin on mouse muscle function and pathology. *PLoS One*, **7**, e31937.
34. van Putten, M., Hulsker, M., Young, C., Nadarajah, V.D., Heemskerk, H., van der Weerd, L., t Hoen, P.A., van Ommen, G.J. and Aartsma-Rus, A.M. (2013) Low dystrophin levels increase survival and improve muscle pathology and function in dystrophin/utrophin double-knockout mice. *FASEB J.*, **27**, 2484–2495.
35. Li, D., Yue, Y. and Duan, D. (2010) Marginal level dystrophin expression improves clinical outcome in a strain of dystrophin/utrophin double knockout mice. *PLoS One*, **5**, e15286.
36. Li, D., Yue, Y. and Duan, D. (2008) Preservation of muscle force in mdx3cv mice correlates with low-level expression of a near full-length dystrophin protein. *Am. J. Pathol.*, **172**, 1332–1341.
37. Godfrey, C., Muses, S., McClorey, G., Wells, K.E., Coursindel, T., Terry, R.L., Betts, C., Hammond, S., O'Donovan, L., Hildyard, J. *et al.* (2015) How much dystrophin is enough: the physiological consequences of different levels of dystrophin in the mdx mouse. *Hum. Mol. Genet.*, **24**, 4225–4237.
38. Yue, Y., Skimming, J.W., Liu, M., Strawn, T. and Duan, D. (2004) Full-length dystrophin expression in half of the heart cells ameliorates beta-isoproterenol-induced cardiomyopathy in mdx mice. *Hum. Mol. Genet.*, **13**, 1669–1675.
39. Bostick, B., Yue, Y., Long, C. and Duan, D. (2008) Prevention of dystrophin-deficient cardiomyopathy in twenty-one-month-old carrier mice by mosaic dystrophin expression or complementary dystrophin/utrophin expression. *Circ. Res.*, **102**, 121–130.
40. Bostick, B., Yue, Y. and Duan, D. (2010) Gender influences cardiac function in the mdx model of Duchenne cardiomyopathy. *Muscle Nerve*, **42**, 600–603.
41. Hakim, C.H. and Duan, D. (2012) Gender differences in contractile and passive properties of mdx extensor digitorum longus muscle. *Muscle Nerve*, **45**, 250–256.
42. Wang, J., Xie, J., Lu, H., Chen, L., Hauck, B., Samulski, R.J. and Xiao, W. (2007) Existence of transient functional double-stranded DNA intermediates during recombinant AAV transduction. *Proc. Natl. Acad. Sci. U. S. A.*, **104**, 13104–13109.
43. Gao, G., Vandenberghe, L.H., Alvira, M.R., Lu, Y., Calcedo, R., Zhou, X. and Wilson, J.M. (2004) Clades of Adeno-associated viruses are widely disseminated in human tissues. *J. Virol.*, **78**, 6381–6388.
44. Shin, J.H., Yue, Y. and Duan, D. (2012) Recombinant adeno-associated viral vector production and purification. *Methods Mol. Biol.*, **798**, 267–284.
45. Kodippili, K., Vince, L., Shin, J.H., Yue, Y., Morris, G.E., McIntosh, M.A. and Duan, D. (2014) Characterization of 65 epitope-specific dystrophin monoclonal antibodies in canine and murine models of duchenne muscular dystrophy by immunostaining and western blot. *PLoS One*, **9**, e88280.
46. Wasala, N.B., Bostick, B., Yue, Y. and Duan, D. (2013) Exclusive skeletal muscle correction does not modulate dystrophic heart disease in the aged mdx model of Duchenne cardiomyopathy. *Hum. Mol. Genet.*, **22**, 2634–2641.
47. Li, D., Long, C., Yue, Y. and Duan, D. (2009) Sub-physiological sarcoglycan expression contributes to compensatory muscle protection in mdx mice. *Hum. Mol. Genet.*, **18**, 1209–1220.
48. Hakim, C.H., Li, D. and Duan, D. (2011) Monitoring murine skeletal muscle function for muscle gene therapy. *Methods Mol. Biol.*, **709**, 75–89.
49. Hakim, C.H., Wasala, N.B. and Duan, D. (2013) Evaluation of muscle function of the extensor digitorum longus muscle ex vivo and tibialis anterior muscle in situ in mice. *J. Vis. Exp.*, **72**, e50183.
50. Bostick, B., Yue, Y. and Duan, D. (2011) Phenotyping cardiac gene therapy in mice. *Methods Mol. Biol.*, **709**, 91–104.
51. Mitchell, G.F., Jeron, A. and Koren, G. (1998) Measurement of heart rate and Q-T interval in the conscious mouse. *Am. J. Physiol.*, **274**, H747–H751.
52. Nigro, G., Comi, L.I., Politano, L. and Nigro, G. (2004) Cardiomyopathies associated with muscular dystrophies. In Engel, A. and Franzini-Armstrong, C. (eds), *Myology: Basic and Clinical*. McGraw-Hill, Medical Pub. Division, New York, Vol. **2**, pp. 1239–1256.

Journal of Molecular and Cellular Cardiology 102 (2017) 45–52

Contents lists available at ScienceDirect

Journal of Molecular and Cellular Cardiology

journal homepage: www.elsevier.com/locate/yjmcc

Uniform low-level dystrophin expression in the heart partially preserved cardiac function in an aged mouse model of Duchenne cardiomyopathy

Nalinda B. Wasala [a], Yongping Yue [a], Jenna Vance [a], Dongsheng Duan [a,b,c,d,*]

[a] Department of Molecular Microbiology and Immunology, School of Medicine, The University of Missouri, Columbia, MO 65212, USA
[b] Department of Neurology, School of Medicine, The University of Missouri, Columbia, MO 65212, USA
[c] Department of Bioengineering, The University of Missouri, Columbia, MO 65212, USA
[d] Department of Biomedical Sciences, College of Veterinary Medicine, The University of Missouri, Columbia, MO 65212, USA

ARTICLE INFO

Article history:
Received 4 July 2016
Received in revised form 17 November 2016
Accepted 23 November 2016
Available online 29 November 2016

Keywords:
Duchenne muscular dystrophy
DMD
Duchenne cardiomyopathy
Dystrophin
Gene therapy
Heart
Low-level expression
Dilated cardiomyopathy
Adeno-associated virus
AAV
ECG
Hemodynamics

ABSTRACT

Dystrophin deficiency results in Duchenne cardiomyopathy, a primary cause of death in Duchenne muscular dystrophy (DMD). Gene therapy has shown great promise in ameliorating the cardiac phenotype in mouse models of DMD. However, it is not completely clear how much dystrophin is required to treat dystrophic heart disease. We and others have shown that mosaic dystrophin expression at the wild-type level, depending on the percentage of dystrophin positive cardiomyocytes, can either delay the onset of or fully prevent cardiomyopathy in dystrophin-null mdx mice. Many gene therapy strategies will unlikely restore dystrophin to the wild-type level in a cardiomyocyte. To determine whether low-level dystrophin expression can reduce the cardiac manifestations in DMD, we examined heart histology, ECG and hemodynamics in 21-m-old normal BL6 and two strains of BL6-background dystrophin-deficient mice. Mdx3cv mice show uniform low-level expression of a near full-length dystrophin protein in every myofiber while mdx4cv mice have no dystrophin expression. Immunostaining and western blot confirmed marginal level dystrophin expression in the heart of mdx3cv mice. Although low-level expression did not reduce myocardial histopathology, it significantly ameliorated QRS prolongation and normalized diastolic hemodynamic deficiencies. Our study demonstrates for the first time that low-level dystrophin can partially preserve heart function.

1. Introduction

Deficiency of cytoskeletal protein dystrophin leads to Duchenne muscular dystrophy (DMD) [1,2]. Skeletal muscle related symptoms (such as limited ambulation and respiratory restriction) are observed early on in young DMD patients [3]. While cardiac involvement appears at the later stage of the disease, all patients eventually develop cardiac dysfunction and heart failure causes up to 40% of death [4–6]. Currently, only palliative treatments are available for symptom management. Restoration of dystrophin expression using adeno-associated virus (AAV)-mediated micro/mini-dystrophin gene transfer, exon-skipping and genome editing are promising new approaches to treat DMD [7,8]. However, these therapies may not restore dystrophin expression to the normal level in patients. An important issue is whether low-level dystrophin expression is therapeutically relevant.

Numerous studies have investigated the amount of dystrophin required for treating skeletal muscle disease in mouse models of DMD and in human patients. These studies suggest that homogenous dystrophin expression at 20–30% of the wild-type level in every myofiber can significantly enhance muscle function and reduce muscle pathology [9–13]. Recent studies further suggest that uniform low-level dystrophin expression at even 5% of the normal level can still improve clinical outcome in dystrophic mice [14–17]. In the case of mosaic expression, approximately 50% myofibers have to express dystrophin in order to achieve a mild phenotype in skeletal muscle [18–20].

In contrast to the abundant information on low-level dystrophin expression in skeletal muscle, little is known about the dystrophin level needed for correcting heart disease in DMD. A study in genetically modified mice suggests that expression in 3 to 5% of cardiomyocytes at the wild-type level (in every dystrophin positive cell) may delay the onset of heart disease [21]. In a different study, Wu et al. found that 5% dystrophin positive cells in the heart of adult mdx mice did not improve cardiac histology/baseline function although mice tolerated dobutamine stress better [22]. We examined female carrier mice and found that normal level dystrophin expression in half of heart cells is sufficient to completely prevent dystrophic cardiomyopathy [23,24]. While these results have provided critical insight on the percentage of dystrophin positive cells needed for treating cardiac manifestations, it should be noted

* Corresponding author at: Department of Molecular Microbiology and Immunology, One Hospital Dr., Columbia, MO 65212, USA.
E-mail address: duand@missouri.edu (D. Duan).

http://dx.doi.org/10.1016/j.yjmcc.2016.11.011
0022-2828/

that in all these studies dystrophin is expressed at the wild-type level in every positive cardiomyocyte. It remains unclear whether sub-physiological expression in a cardiomyocyte can benefit the heart.

We and others have previously shown that mdx3cv mice express marginal level dystrophin in skeletal muscle [14,15,25]. This residual level expression significantly enhanced skeletal muscle function although it did not improve histopathology [14,26]. Mdx3cv mice were generated by Chapmen et al. using N-ethyl-N-nitrosourea mutagenesis [27]. A point mutation in intron 65 aborts full-length dystrophin expression. However, a slightly truncated Δ65/66 transcript is generated (Supplementary Fig. 1). This results in the production of a near full-length dystrophin protein at ~5% of the wild-type level [15,25].

To study the impact of low-level uniform dystrophin expression in the heart, we compared the cardiac phenotype among C57Bl/6 (BL6), mdx3cv and mdx4cv mice. All three strains are on the BL6 background. BL6 and mdx4cv mice are normal and dystrophin-null controls, respectively. The characteristic heart presentation in DMD is dilated cardiomyopathy. We have previously shown that dystrophin-deficient mice do not develop dilated cardiomyopathy until they reach 21 months of age [24,28]. For this reason, we intentionally conducted our study in aged

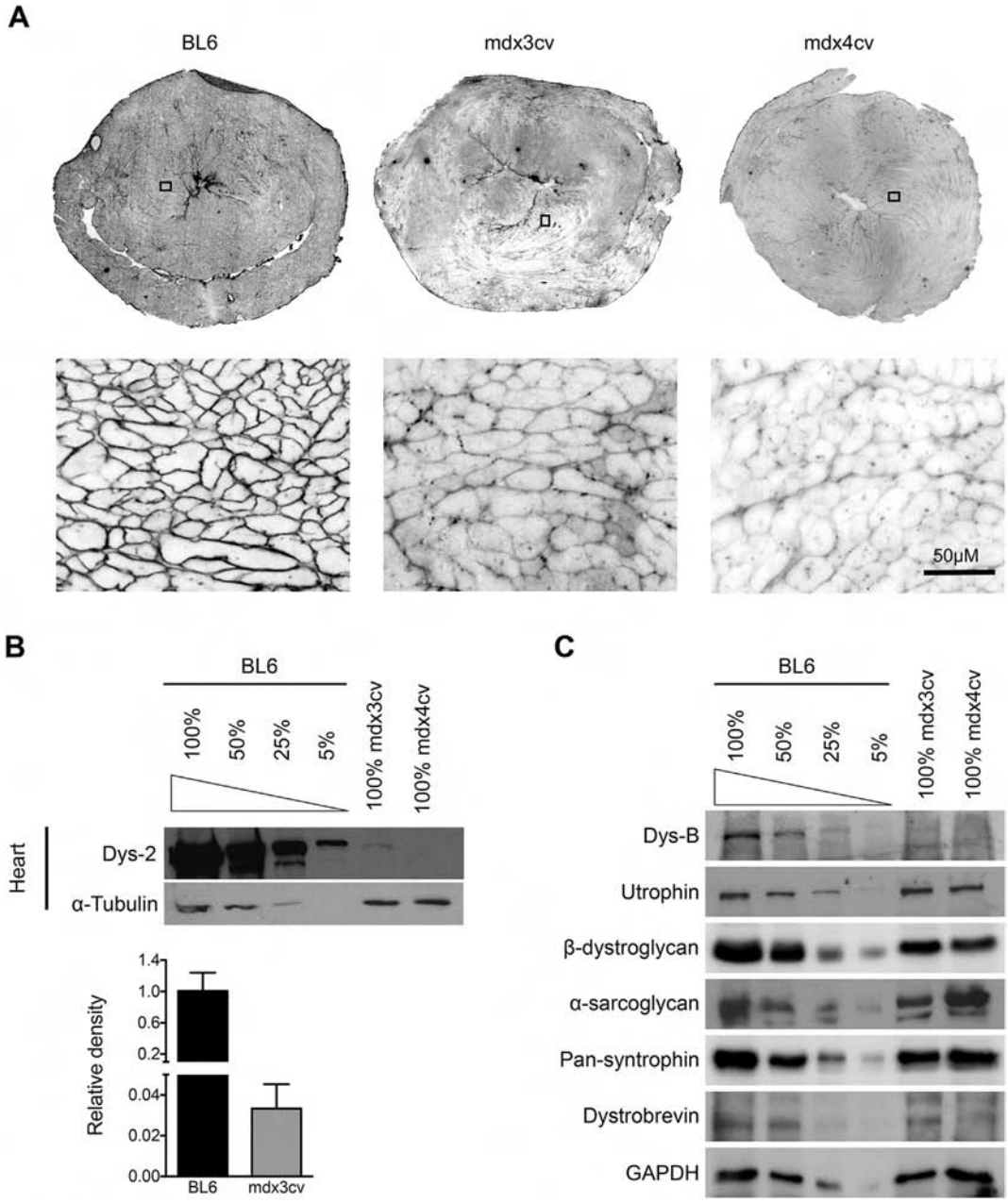

Fig. 1. Mdx3cv mouse heart expressed low-level dystrophin. A, Representative photomicrographs of dystrophin immunofluorescence staining in BL6, mdx3cv and mdx4cv heart. Upper panel shows the whole heart view and the lower panel shows a higher magnification of the corresponding boxed region in the whole heart view. B, Top panel, Representative heart western blot from BL6, mdx3cv and mdx4cv mice. The BL6 heart lysate was loaded at 100%, 50%, 25% and 5%. The mdx3cv and mdx4cv heart lysate was loaded at 100%; Bottom panel, Densitometry quantification of cardiac dystrophin expression ($N = 3$ for each group). Dys-2, a monoclonal antibody against the dystrophin C-terminal domain. The heart of mdx3cv mice showed uniform dystrophin expression at approximately 3.3% of the wild-type level. C, Representative cardiac western blots for utrophin and selected components of dystrophin-associated glycoprotein complex (β-dystroglycan, α-sarcoglycan, syntrophin and dystrobrevin). DysB, a monoclonal antibody against the dystrophin exons 10–12; GAPDH, glyceraldehyde 3-phosphate dehydrogenase.

mice. We detected uniform dystrophin expression at ~3.3% of the wild-type level in the heart of 21-m-old mdx3cv mice. Importantly, we observed significant improvement in some ECG and hemodynamic parameters suggesting low-level dystrophin expression can benefit the heart.

2. Results

2.1. The heart of aged mdx3cv mice expressed low-level dystrophin

We first performed dystrophin immunostaining in the heart (Fig. 1A). We observed robust, no and very low expression in the heart of BL6, mdx4cv and mdx3cv mice, respectively. To quantify dystrophin expression, we performed whole heart lysate western blot (Fig. 1B). Serially diluted BL6 heart lysate was used to show band intensity at 5, 25, 50 and 100% of the wild-type levels (Fig. 1B). As expected, no dystrophin was detected in mdx4cv. Mdx3cv showed a faint band. On quantification, it reached approximately 3.3% of the wild-type level (Fig. 1B).

2.2. Low dystrophin expression in the mdx3cv heart had minimal impact on the expression of utrophin and components of the dystrophin-associated glycoprotein (DGC) complex

We have previously found that the hearts of 21-m-old normal BL10 mice and BL10-background dystrophin-null mdx mice had similar levels of utrophin expression on western blot [29]. Consistently, there was not much difference in the cardiac utrophin level among aged BL6, mdx3cv and mdx4cv mice (Fig. 1C). We also compared the expression level of representative DGC components including β-dystroglycan, α-sarcoglycan, syntrophin and dystrobrevin. Compared to that of the BL6 mouse heart, there appeared a slight reduction of the DGC components in the heart of mdx3cv and mdx4cv mice (Fig. 1C).

2.3. Low-level dystrophin expression did not improve cardiac histopathology

On HE staining, BL6 mouse heart showed normal morphology (Fig. 2A). Some myocardial distortion and mononuclear cell infiltration were noted in both mdx3cv and mdx4cv heart. But there was no apparent difference between these two strains (Fig. 2A). Cardiac fibrosis was examined using Masson trichrome staining (Fig. 2B). The BL6 heart had no fibrosis. The hearts of mdx3cv and mdx4cv mice showed similar patchy myocardial fibrosis (Fig. 2B). Cardiac inflammation was examined by immunohistochemical staining (Fig. 2C). Abundant macrophages and neutrophils were detected in the heart of mdx3cv and mdx4cv mice but not BL6 mice (Fig. 2C).

2.4. The anatomic properties of the heart were similar between mdx3cv and mdx4cv mice

The absolute heart weight (HW) and ventricular weight (VW) were similar between mdx3cv and mdx4cv mice (Table 1). Both were significantly lower than those of BL6 mice. For the tibial length (TL) and anterior tibialis muscle weight (TW) normalized heart weight and ventricular weight (HW/TL, HW/TW, VW/TL and VW/TW), we did not see a difference between mdx3cv and mdx4cv mice. These ratios were all significantly lower than those of BL6 mice (Table 1). The body weight (BW) of BL6 and mdx3cv mice was comparable. However, the BW of mdx4cv mice was significantly reduced (Table 1). Hypertrophy of anterior tibialis muscle was obvious in mdx3cv and mdx4cv mice. Interestingly, the TW of mdx3cv mice was significantly higher than that of mdx4cv mice (Table 1).

2.5. Mdx3cv mice showed improved QRS duration

To study cardiac electrophysiology, we performed 12-lead ECG recordings using our published protocol [30,31]. Compared with BL6, mdx4cv showed characteristic dystrophic ECG changes such as tachycardia, PR-interval reduction, QRS duration and QT interval prolongation, and a significant increase in the cardiomyopathy index (Fig. 3) [24,28,32,33]. Surprisingly, we did not detect a significant change in the amplitude of Q wave among three strains (Fig. 3). Compared to those of mdx4cv, several ECG parameters (the heart rate, QT interval and cardiomyopathy index) showed a trend of improvement in mdx3cv mice but did not reach statistical significance. The only ECG parameter that was significantly improved in mdx3cv mice was the QRS duration. It was significantly reduced compared to that of mdx4cv mice (Fig. 3).

2.6. Low-level dystrophin in the heart normalized diastolic function in mdx3cv mice

We next examined the pump function of the heart using an ultra-miniature Millar ventricular catheter [30,31]. Compared with BL6, mdx4cv showed the characteristic profile of dilated cardiomyopathy (Fig. 4). Specifically, the end-systolic volume was significantly increased (Fig. 4A). The end-diastolic volume also showed an apparent increase though not statistically significant (Fig. 4B). Cardiac contractility (as reflexed by the maximum pressure, absolute values of dP/dt max and dP/dt min) was significantly reduced. The isovolumic relaxation time constant during diastole (tau) was prolonged (Fig. 4B). As a result, the stroke volume, ejection fraction and cardiac output were all significantly decreased in mdx4cv mice (Fig. 4C).

Low-level dystrophin expression in mdx3cv mice completely normalized diastolic parameters including the end diastolic volume, tau and dP/dt min (Fig. 4B). The end systolic volume showed a trend of reduction (Fig. 4A). However, overall heart performance (stroke volume, ejection fraction and cardiac output) was not significantly improved in mdx3cv mice.

2.7. Expression of sarcoplasmic/endoplasmic reticulum calcium ATPase 2a (SERCA2a), phospholamban and calsequesterin in aged BL6, mdx3cv and mdx4cv hearts

To gain molecular insight on how low-level dystrophin controls heart function, we performed quantitative western blot on the expression of three major calcium handling proteins in the heart including SERCA2a, phospholamban and calsequesterin. No statistically significant difference was detected among BL6, mdx3cv and mdx4cv mice (Fig. 5). Unfortunately, our western blot for the phosphorylated form of phospholamban did not work.

3. Discussion

In this study, we tested the hypothesis that a uniform low-level dystrophin expression can benefit the heart in the mouse model of Duchenne cardiomyopathy. We found marginal level (approximately 3.3% of the wild-type level) homogenous dystrophin expression in the myocardium of aged mdx3cv mice (Fig. 1). This residual level expression did not change the anatomic properties of the heart (Table 1). Neither did it reduce histological lesions in the heart (Fig. 2). However, some aspects of heart function measures were significantly improved (Figs. 3 and 4). Specifically, the abnormally elongated QRS duration was shortened and deficiencies in diastolic hemodynamics were completely prevented (Figs. 3 and 4). Interestingly, there was no difference in the expression level of SERCA2a, phospholamban and calsequesterin (Fig. 5). Our results suggest that low-level dystrophin is far from sufficient to cure Duchenne cardiomyopathy. However, it can still offer some protection to the heart.

Recent progress in genetic engineering and molecular medicine is making gene therapy for DMD a reality [7,8]. Large scale clinical trials have been conducted to test therapeutic benefits of exon-skipping [34,35]. Systemic AAV micro-dystrophin therapy is slotted to start in the

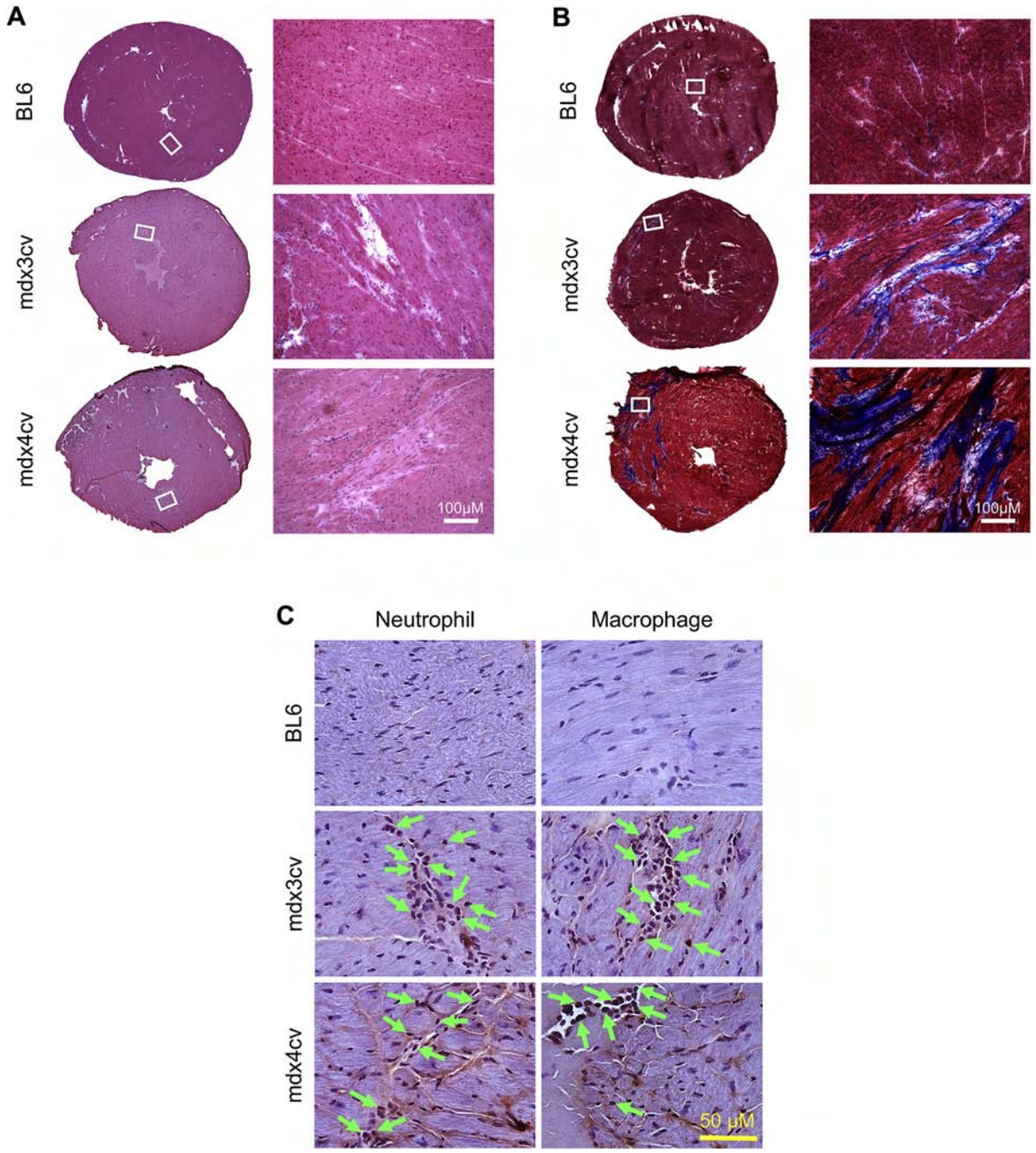

Fig. 2. Low-level dystrophin expression did not ameliorate myocardial inflammation and fibrosis in mdx3cv mice. A, Representative heart HE staining photomicrographs from BL6, mdx3cv and mdx4cv mice. Left panel, whole heart cross-sectional images; right panel, high-power images of the respective boxed areas in the whole heart view. B, Representative Masson trichrome staining photomicrographs of the BL6, mdx3cv and mdx4cv heart. Left panel, whole heart cross-sectional images; right panel, high-power images of the respective boxed areas in the whole heart view. The blue color in Masson trichrome staining marks myocardial fibrosis. C, Representative macrophage and neutrophil immunohistochemical staining photomicrographs of the BL6, mdx3cv and mdx4cv heart. Arrow, dark brown stained macrophages and neutrophils.

next couple of years [7,8]. Most recently, investigators have achieved remarkable proof-of-concept evidence in repairing the mutated dystrophin gene in mdx mice [36]. Despite these successes, it is still not completely clear whether sub-physiological level dystrophin expression can help mitigating dystrophic manifestations. A comprehensive understanding of the dystrophin expression level in striated muscle requires information on (a) the percentage of dystrophin positive myofibers and (b) the amount of dystrophin protein in these positive myofibers. The former is obtained by quantifying dystrophin immunostaining and the latter by western blot. Accordingly, for DMD gene therapy we need to know what percentage of muscle cells should express dystrophin and what are the dystrophin levels in these cells.

Therapeutic relevance of mosaic dystrophin expression has been extensively examined [18–20,23,24]. These studies have documented remarkable disease amelioration and function preservation in both skeletal and cardiac muscles when half myofibers show positive dystrophin staining. Homogenous sub-physiological dystrophin expression has been shown to protect skeletal muscle by a number of laboratories [9–17]. However, it is not clear whether a low-level uniform dystrophin expression in the heart can reduce cardiomyopathy.

Table 1
Anatomical measurements and ratios.

	BL6	mdx3cv	mdx4cv
Sample size (N)	11	28	19
Age (m)	21.67 ± 0.54	21.85 ± 0.33	20.76 ± 0.19
BW (g)	26.78 ± 0.79	27.60 ± 0.37	23.59 ± 0.91[a]
HW (mg)	117.80 ± 3.42	101.99 ± 2.73[b]	101.58 ± 3.22[b]
VW (mg)	111.49 ± 3.25	89.91 ± 2.52[b]	94.32 ± 3.10[b]
TL (mm)	18.51 ± 0.09	18.42 ± 0.08	18.94 ± 0.09[a]
TW (mg)	36.75 ± 1.14[a]	63.14 ± 2.02[a]	55.42 ± 2.32[a]
HW/BW (mg/g)	4.41 ± 0.11	3.71 ± 0.11[a]	4.38 ± 0.16
HW/TL (mg/mm)	6.36 ± 0.17	5.21 ± 0.10[b]	5.17 ± 0.16[b]
HW/TW (mg/g)	3.25 ± 0.16	1.81 ± 0.25[b]	1.89 ± 0.10[b]
VW/TL (mg/mm)	6.02 ± 0.16	4.81 ± 0.11[b]	4.78 ± 0.15[b]
VW/TW (mg/g)	3.08 ± 0.15	1.60 ± 0.23[b]	1.76 ± 0.09[b]

Abbreviations: BW, body weight; HW, heart weight; VW, ventricle weight; TL, tibia length; TW, anterior tibialis muscle weight.
[a] Significantly different from other two groups.
[b] Significantly different from BL6 mice.

Townsend et al. compared dystrophin expression in the heart of young adult (4-m-old) and aged (23-m-old) BL10 mice [37]. The authors observed a ubiquitous reduction of dystrophin content in every cardiomyocyte in aged mice. On average, the dystrophin level was reduced by 57% in the aged BL10 heart. Loss of dystrophin resulted in a decline of cardiac function in aged BL10 mice [37]. Our recent studies also suggest that removal of existing dystrophin from the myocardium can compromise the pump function of the heart [38]. These two studies suggest that sub-physiological level dystrophin is insufficient to maintain normal heart function. While this is an important conclusion, it does not tell us whether a heart with low-level dystrophin expression is structurally and/or functionally superior to a heart that has no dystrophin expression. Our study in aged mdx3cv mice is aimed to address this knowledge gap. Consistent with our previous studies on the mdx3cv mouse skeletal muscle [14,15], we demonstrated a partial function preservation but not histopathology amelioration in the mdx3cv heart.

Little is known about the molecular mechanisms underlying electrophysiological defects and hemodynamic deficiencies in Duchenne cardiomyopathy. A number of hypotheses have been suggested such as myocardial necrosis and inflammation, cardiac fibrosis, vacuolar degeneration in the conduction system, perturbation of calcium homeostasis, oxidative stress, sarcolemma tearing, mitochondrial dysfunction and aberrant signaling [39–42]. We have previously demonstrated characteristic ECG changes in young adult (4-m-old) mdx mice in the absence of apparent histological lesions in the heart [43]. We have also shown significant ECG improvement but not histology amelioration in terminally aged (21 to 23-m-old) mdx mice by AAV micro-dystrophin gene therapy [32]. These data challenge a direct causal relationship between myocardial structural damage and ECG abnormality. In mdx3cv mice, residual level dystrophin expression did not reduce myocardial inflammation and fibrosis. Yet the extended QRS complex was significantly shortened. The QRS complex reflects depolarization of ventricular cells. In the absence of dystrophin, the time of ventricular depolarization was increased by 30% (Fig. 3). With merely ~3.3% dystrophin, the speed of ventricular depolarization was significantly increased. As a result, the QRS duration was reduced in mdx3cv mice compared to that of dystrophin-null mdx4cv mice (Fig. 3). Cardiomyocyte depolarization and repolarization is tightly controlled by various ion channels on the sarcolemma. Interestingly, dystrophin and some DGC components (such as syntrophin and nNOS) have been shown to regulate these ion channels [44–47]. Our results suggest that low-level dystrophin may partially restore dystrophin/DGC-mediated regulation on ion channels.

An unexpected finding of our study is the full normalization of diastolic hemodynamic parameters in mdx3cv mice. This suggests that low-level dystrophin may meet the need of myocardial relaxation during the cardiac cycle. However, a much higher level of dystrophin

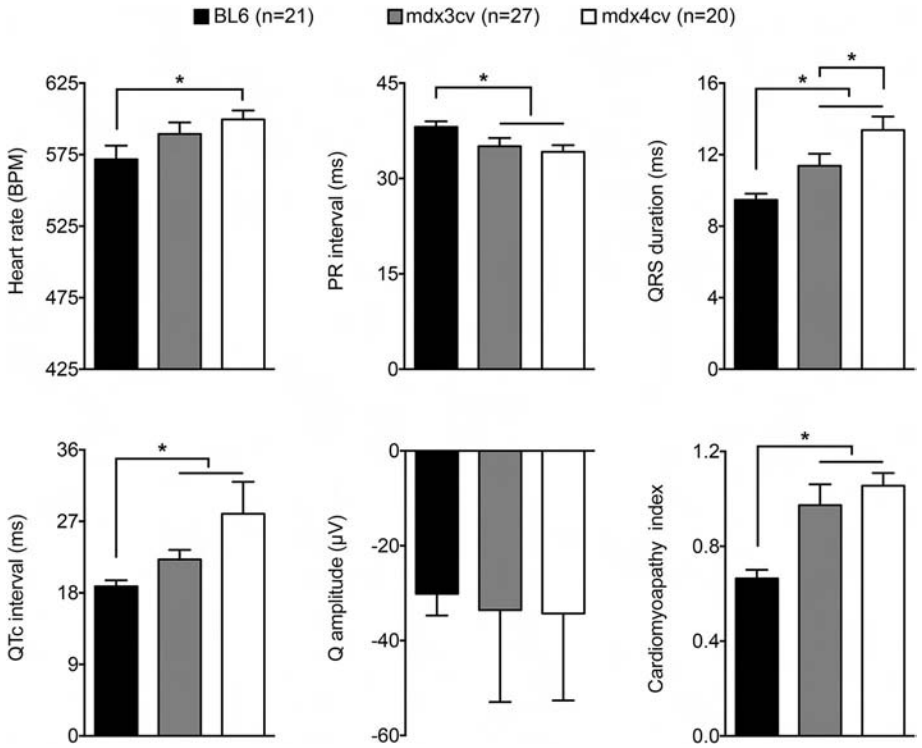

Fig. 3. Low-level dystrophin expression improved QRS duration but not other ECG parameters in mdx3cv mice. Quantitative evaluation of the heart rate, PR interval, QRS duration, Mitchell corrected QT interval (QTc), cardiomyopathy index and the Q wave amplitude. The QTc interval was determined by correcting the QT interval with the heart rate as described by Mitchell et al. [49]. Asterisk, statistically significant ($p < 0.05$).

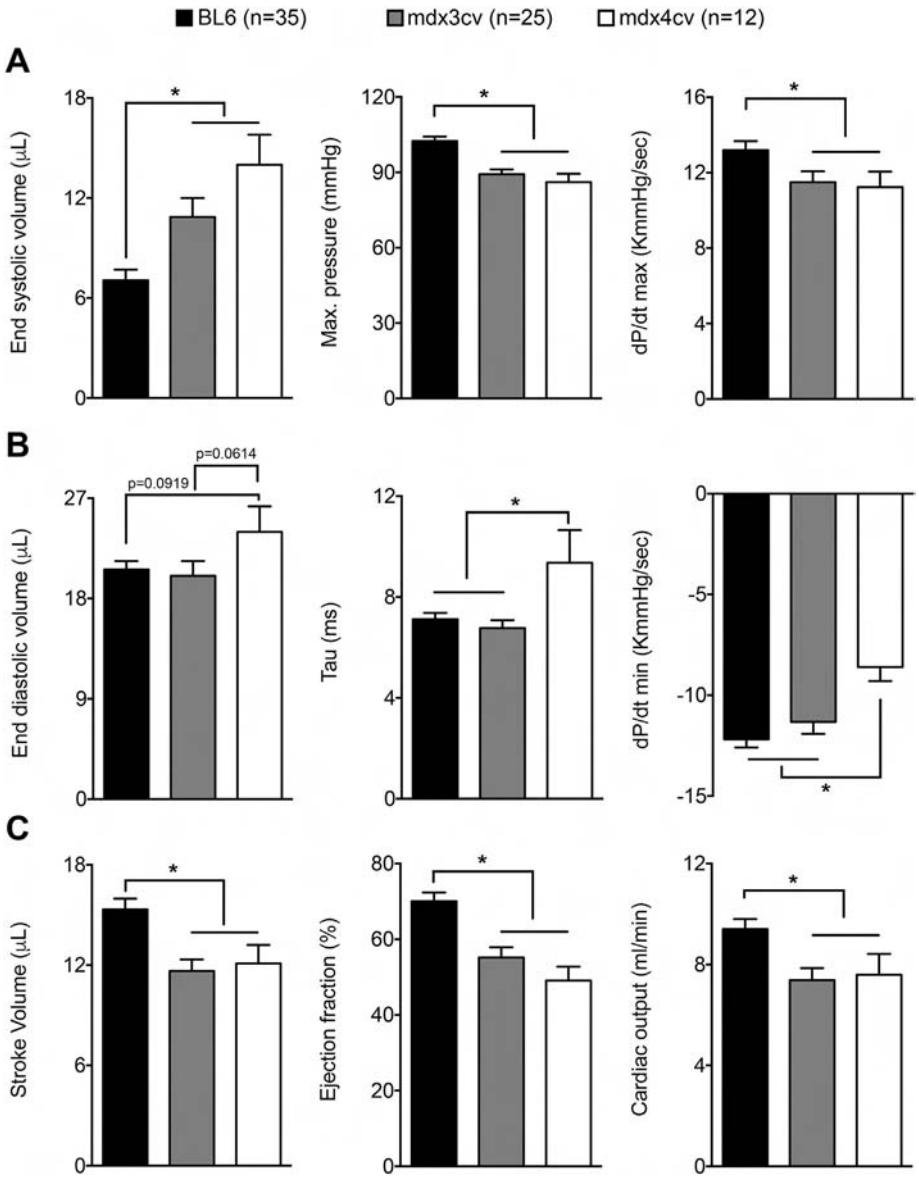

Fig. 4. Low-level dystrophin expression partially improved hemodynamics in mdx3cv mice. A, Quantitative evaluation of systolic hemodynamic parameters. B, Quantitative evaluation of diastolic hemodynamic parameters. End-diastolic volume, tau and dP/dt min were all normalized in mdx3cv mice. C, Quantitative evaluation of overall heart function. Asterisk, statistically significant ($p < 0.05$). The heart rate at the hemodynamic assay was 616.9 ± 9.10 bpm, 619.9 ± 25.5 bpm and 629.3 ± 8.3 bpm for BL6, mdx3cv and mdx4cv, respectively. There is no statistically significance difference.

expression is needed to enhance ventricular muscle contraction in order to improve the blood pumping function of the heart. We would like to point out that it is not unusual that different levels of dystrophin expression are needed for the correction of different aspects of disease. For example, a recent study in skeletal muscle by Godfrey et al. suggests that protection against eccentric contraction-induced injury requires homogenous dystrophin expression at the 15% of wild-type level. However, reduction of skeletal muscle histopathology requires much more dystrophin [11].

While the ultimate goal of the study is to translate our findings into human patients, it is important to remember that scaling up to a large dystrophic mammal is much more complex than we can model in mice. Whether marginal level expression can result in clinically appreciable improvement in human patients will depend on a number of factors, such as the configuration of the therapeutic dystrophin protein (full-length, moderately truncated mini-dystrophin, or highly abbreviated micro-dystrophin), treatment regime (the age at the start of the therapy, the duration of the therapy and the gene therapy vector dose etc.), and the abundance of dystrophin (percentage of dystrophin expressing cells and dystrophin level in these cells). Our data suggest that uniform low-level dystrophin expression may have therapeutic implications for treating Duchenne cardiomyopathy. Future studies in large animal models of DMD (such as dystrophic dogs) may testify whether this observation can be translated to large mammals.

4. Materials and methods

4.1. Experimental animals

All animal experiments were approved by the institutional animal care and use committee and were in accordance with NIH guidelines. Experimental mice were generated in a barrier facility using founders from The Jackson Laboratory (Bar Harbor, ME). Female mice were used in the study because we have previously shown that female mice are better than male mice in modeling Duchenne cardiomyopathy seen in human patients [28]. All mice were maintained in a specific-pathogen free animal care facility on a 12-h light (25 lx):12-h dark

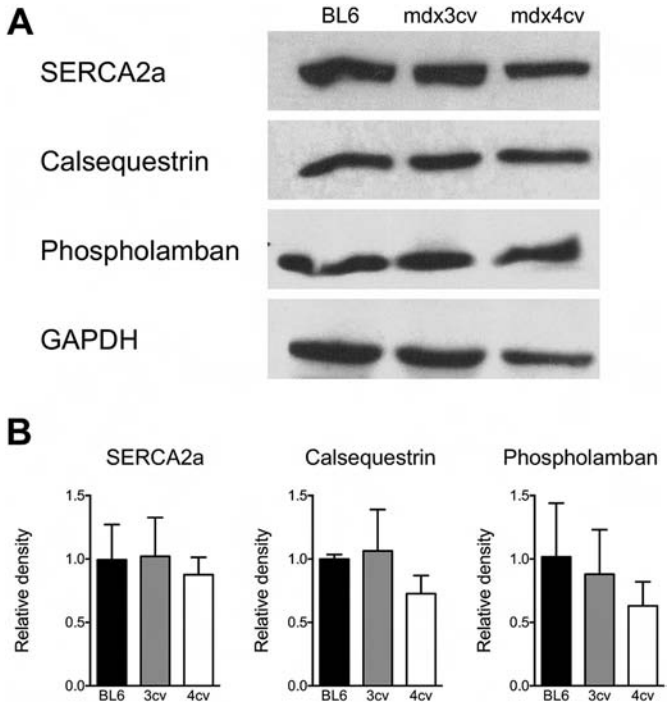

Fig. 5. Western blot evaluation of SERCA2a, calsequestrin and phospholamban in the heart. A, Representative western blot results from BL6, mdx3cv and mdx4cv mice. B, Densitometry quantification of calcium handling proteins shown in panel A ($N = 3$ for each group).

cycle with access to food and water ad libitum. Mice were euthanized following functional assays for tissue collection.

4.2. Morphological studies

Dystrophin expression was evaluated by immunofluorescence staining using the Dys2 monoclonal antibody (1:30; Vector Laboratories, Burlingame, CA). General histology was examined by hematoxylin and eosin (HE) staining. Fibrosis was examined by Masson trichrome staining. Inflammation was studied with immunohistochemistry staining using antibodies specific to mouse neutrophils (Ly-6G, 1:8,00, BD Pharmingen, San Diego, CA) and macrophages (F4/80, 1:200, Caltag Laboratories, Burlingame, CA) according to our published protocol [29]. Slides were viewed at the identical exposure setting using a Nikon E800 fluorescence microscope. Photomicrographs were taken with a QImage Retiga 1300 camera [31].

4.3. Western blot

Whole heart lysate was prepared as we described before [48]. Briefly, the freshly isolated heart was snap frozen in liquid nitrogen. The frozen heart sample was ground to fine powder in liquid nitrogen followed by homogenization in a buffer containing 10% sodium dodecyl sulfate, 5 mM ethylenediaminetetraacetic acid, 62.5 mM Tris at pH 6.8 and the protease inhibitor cocktail (Roche, Indianapolis, IN). The crude lysate was heated at 95 °C for 3 min, chilled on ice for 2 min and then centrifuged at 14,000 rpm for 2 min (Eppendorf 5418, Hauppauge, NY). Supernatant was collected as the whole muscle lysate. Protein concentration was measured using the DC protein assay kit (Bio-Rad, Hercules, CA). For western blot, we loaded 5 to 100 μg of protein per lane as indicated in the figures. Dystrophin was detected with Dys2 (1:100 Vector Laboratories, Burlingame, CA) and DysB (1:100, clone 34C5, IgG1; Novocastra, Newcastle, United Kingdom) antibodies. Utrophin was detected with a mouse monoclonal antibody against utrophin amino acid residues 768–874 (1:200; clone 55, IgG1; BD Biosciences, San Diego, CA). β-Dystroglycan was detected with a mouse monoclonal antibody against the β-dystroglycan C-terminus (NCL-b-DG, 1:100; clone 43DAG1/8D5, IgG2a; Novocastra, Newcastle, United Kingdom). α-Sarcoglycan was detected with a mouse monoclonal antibody against α-sarcoglycan amino acid residues 217–289 (VP-A105; 1:1000; clone Ad1/20A6, IgG1; Vector Laboratories, Burlingame, CA). Syntrophin was detected with a pan-syntrophin mouse monoclonal antibody that recognizes the syntrophin PDZ domain (ab11425, 1:2000; clone 1351, IgG1; Abcam, Cambridge, MA). Dystrobrevin was detected with a mouse monoclonal antibody against dystrobrevin amino acid residues 249 to 403 (#610766, 1:1000; clone 23, IgG1; BD Biosciences, San Diego, CA). The calcium handling proteins were detected using sarcoplasmic/endoplasmic reticulum calcium ATPase 2a (SERCA2a, 1:2500 Badrilla, Leeds UK), calsequestrin (1:2500, Thermo Scientific, Grand Island NY) and phospholamban (1:2500 Badrilla, Leeds UK) antibodies. For the loading control, we used an antibody against glyceraldehyde 3-phosphate dehydrogenase (1:3000; Millipore, Billerica, MA) and the α-tubulin antibody (1:3000; clone B-5-1-2; Sigma, St Louis, MO). Western blot quantification was performed using the ImageJ software (http://rsbweb.nih.gov/ij/) and LI-COR Image Studio Version 5.0.21 (https://www.licor.com) software. The intensity of the respective protein band was normalized to the corresponding loading control in the same blot. The relative band intensity in mdx3cv and mdx4cv mice was normalized to that of BL6 mice.

4.4. ECG and hemodynamic assay

A 12-lead ECG assay was performed using a commercial system from AD Instruments (Colorado Springs, CO) according to our previously published protocol [30,31]. The Q wave amplitude was determined using the lead I tracing. Other ECG parameters were analyzed using the lead II tracing. The QTc interval was determined by correcting the QT interval with the heart rate as described by Mitchell et al. [49]. The cardiomyopathy index was calculated by dividing the QT interval by the PQ segment [50]. Left ventricular hemodynamics was evaluated using a Millar ultra-miniature pressure–volume (PV) catheter SPR 839. The catheter was placed in the left ventricle using a closed chest approach as we have previously described [30,31]. The resulting PV loops were analyzed with the PVAN software (Millar Instruments, Houston, TX). Detailed protocols for ECG and hemodynamic assays are available at the Parent Project Muscular Dystrophy standard operating protocol web site (http://www.parentprojectmd.org/site/PageServer?pagename=Advance_researchers_sops) [51].

4.5. Statistical analysis

Data are presented as mean ± stand error of mean. One-way ANOVA with Bonferroni's multiple comparison analysis was performed using the GraphPad PRISM software version 6.0 for Mac OSX (GraphPad Software, La Jolla, CA, www.graphpad.com). A $P < 0.05$ was considered statistically significant.

Supplementary data to this article can be found online at http://dx.doi.org/10.1016/j.yjmcc.2016.11.011.

Disclosures/conflict of interests

DD is a member of the scientific advisory board for Solid GT, LLC and equity holders of Solid GT, LLC. DD and YY are inventors on patents that were licensed to Solid GT, LLC. The Duan lab has received research supports from Solid GT, LLC.

Acknowledgments

This work was supported by grants from the National Institutes of Health (HL-91883, NS-90634, AR-69085), Department of Defense (MD130014, MD150133), Jesse's Journey-The Foundation for Gene and Cell

Therapy. N.W. was partially supported by the life science fellowship, University of Missouri. We thank Dr. Brian Bostick for helpful discussion.

References

[1] L.M. Kunkel, 2004 William Allan award address. Cloning of the DMD gene, Am. J. Hum. Genet. 76 (2005) 205–214.
[2] E.P. Hoffman, R.H. Brown Jr., L.M. Kunkel, Dystrophin: the protein product of the duchenne muscular dystrophy locus, Cell 51 (1987) 919–928.
[3] A.E.H. Emery, F. Muntoni, Duchenne Muscular Dystrophy, 3rd ed. Oxford Oxford University Press, New York, 2003.
[4] F. Muntoni, Cardiomyopathy in muscular dystrophies, Curr. Opin. Neurol. 16 (2003) 577–583.
[5] J. Finsterer, C. Stollberger, The heart in human dystrophinopathies, Cardiology 99 (2003) 1–19.
[6] G.F. Cox, L.M. Kunkel, Dystrophies and heart disease, Curr. Opin. Cardiol. 12 (1997) 329–343.
[7] D. Duan, Dystrophin gene replacement and gene repair therapy for Duchenne muscular dystrophy in 2016, Hum. Gene Ther. Clin. Dev. 27 (2016) 9–18.
[8] N.E. Bengtsson, J.T. Seto, J.K. Hall, J.S. Chamberlain, G.L. Odom, Progress and prospects of gene therapy clinical trials for the muscular dystrophies, Hum. Mol. Genet. 25 (R1) (2016) R9–17.
[9] S.F. Phelps, M.A. Hauser, N.M. Cole, J.A. Rafael, R.T. Hinkle, J.A. Faulkner, et al., Expression of full-length and truncated dystrophin mini-genes in transgenic mdx mice, Hum. Mol. Genet. 4 (1995) 1251–1258.
[10] D.J. Wells, K.E. Wells, E.A. Asante, G. Turner, Y. Sunada, K.P. Campbell, et al., Expression of human full-length and minidystrophin in transgenic mdx mice: implications for gene therapy of Duchenne muscular dystrophy, Hum. Mol. Genet. 4 (1995) 1245–1250.
[11] C. Godfrey, S. Muses, G. McClorey, K.E. Wells, T. Coursindel, R.L. Terry, et al., How much dystrophin is enough: the physiological consequences of different levels of dystrophin in the mdx mouse, Hum. Mol. Genet. 24 (2015) 4225–4237.
[12] P.S. Sharp, H. Bye-a-Jee, D.J. Wells, Physiological characterization of muscle strength with variable levels of dystrophin restoration in mdx mice following local antisense therapy, Mol. Ther. 19 (2011) 165–171.
[13] M. Neri, S. Torelli, S. Brown, I. Ugo, P. Sabatelli, L. Merlini, et al., Dystrophin levels as low as 30% are sufficient to avoid muscular dystrophy in the human, Neuromuscul. Disord. 17 (2007) 913–918.
[14] D. Li, Y. Yue, D. Duan, Preservation of muscle force in mdx3cv mice correlates with low-level expression of a near full-length dystrophin protein, Am. J. Pathol. 172 (2008) 1332–1341.
[15] D. Li, Y. Yue, D. Duan, Marginal level dystrophin expression improves clinical outcome in a strain of dystrophin/utrophin double knockout mice, PLoS One 5 (2010), e15286. .
[16] M. van Putten, M. Hulsker, V.D. Nadarajah, S.H. van Heiningen, E. van Huizen, M. van Iterson, et al., The effects of low levels of dystrophin on mouse muscle function and pathology, PLoS One 7 (2012), e31937. .
[17] M. van Putten, M. Hulsker, C. Young, V.D. Nadarajah, H. Heemskerk, L. van der Weerd, et al., Low dystrophin levels increase survival and improve muscle pathology and function in dystrophin/utrophin double-knockout mice, FASEB J. 27 (2013) 2484–2495.
[18] J.S. Chamberlain, Dystrophin levels required for correction of Duchenne muscular dystrophy, Basic Appl. Myol. 7 (1997) 251–255.
[19] E.P. Hoffman, K. Arahata, C. Minetti, E. Bonilla, L.P. Rowland, Dystrophinopathy in isolated cases of myopathy in females, Neurology 42 (1992) 967–975.
[20] R.W. Arpke, R. Darabi, T.L. Mader, Y. Zhang, A. Toyama, C.L. Lonetree, et al., A new immuno-, dystrophin-deficient model, the NSG-mdx4cv mouse, provides evidence for functional improvement following allogeneic satellite cell transplantation, Stem Cells 31 (2013) 1611–1620.
[21] M. van Putten, E.M. van der Pijl, M. Hulsker, I.E. Verhaart, V.D. Nadarajah, L. van der Weerd, et al., Low dystrophin levels in heart can delay heart failure in mdx mice, J. Mol. Cell. Cardiol. 69 (2014) 17–23.
[22] B. Wu, B. Xiao, C. Cloer, M. Shaban, A. Sali, P. Lu, et al., One-year treatment of morpholino antisense oligomer improves skeletal and cardiac muscle functions in dystrophic mdx mice, Mol. Ther. 19 (2011) 576–583.
[23] Y. Yue, J.W. Skimming, M. Liu, T. Strawn, D. Duan, Full-length dystrophin expression in half of the heart cells ameliorates beta-isoproterenol-induced cardiomyopathy in mdx mice, Hum. Mol. Genet. 13 (2004) 1669–1675.
[24] B. Bostick, Y. Yue, C. Long, D. Duan, Prevention of dystrophin-deficient cardiomyopathy in twenty-one-month-old carrier mice by mosaic dystrophin expression or complementary dystrophin/utrophin expression, Circ. Res. 102 (2008) 121–130.
[25] G.A. Cox, S.F. Phelps, V.M. Chapman, J.S. Chamberlain, New mdx mutation disrupts expression of muscle and nonmuscle isoforms of dystrophin, Nat. Genet. 4 (1993) 87–93.
[26] J.A. Rafael, Y. Nitta, J. Peters, K.E. Davies, Testing of SHIRPA, a mouse phenotypic assessment protocol, on Dmd(mdx) and Dmd(mdx3cv) dystrophin-deficient mice, Mamm. Genome 11 (2000) 725–728.
[27] V.M. Chapman, D.R. Miller, D. Armstrong, C.T. Caskey, Recovery of induced mutations for X chromosome-linked muscular dystrophy in mice, Proc. Natl. Acad. Sci. 86 (1989) 1292–1296.
[28] B. Bostick, Y. Yue, D. Duan, Gender influences cardiac function in the mdx model of Duchenne cardiomyopathy, Muscle Nerve 42 (2010) 600–603.
[29] Y. Lai, J. Zhao, Y. Yue, N.B. Wasala, D. Duan, Partial restoration of cardiac function with ΔPDZ nNOS in aged mdx model of Duchenne cardiomyopathy, Hum. Mol. Genet. 23 (2014) 3189–3199.
[30] B. Bostick, Y. Yue, D. Duan, Phenotyping cardiac gene therapy in mice, Methods Mol. Biol. 709 (2011) 91–104 (Clifton, NJ).
[31] N.B. Wasala, B. Bostick, Y. Yue, D. Duan, Exclusive skeletal muscle correction does not modulate dystrophic heart disease in the aged mdx model of Duchenne cardiomyopathy, Hum. Mol. Genet. 22 (2013) 2634–2641.
[32] B. Bostick, J.H. Shin, Y. Yue, N.B. Wasala, Y. Lai, D. Duan, AAV micro-dystrophin gene therapy alleviates stress-induced cardiac death but not myocardial fibrosis in >21-m-old mdx mice, an end-stage model of Duchenne muscular dystrophy cardiomyopathy, J. Mol. Cell. Cardiol. 53 (2012) 217–222.
[33] B. Bostick, J.H. Shin, Y. Yue, D. Duan, AAV-microdystrophin therapy improves cardiac performance in aged female mdx mice, Mol. Ther. 19 (2011) 1826–1832.
[34] A. Aartsma-Rus, A. Ferlini, N. Goemans, A.M. Pasmooij, D.J. Wells, K. Bushby, et al., Translational and regulatory challenges for exon skipping therapies, Hum. Gene Ther. 25 (2014) 885–892.
[35] T. Koo, M.J. Wood, Clinical trials using antisense oligonucleotides in Duchenne muscular dystrophy, Hum. Gene Ther. 24 (2013) 479–488.
[36] C.E. Nelson, C.H. Hakim, D.G. Ousterout, P.I. Thakore, E.A. Moreb, R.M. Rivera, et al., In vivo genome editing improves muscle function in a mouse model of Duchenne muscular dystrophy, Science 351 (2016) 403–407.
[37] D. Townsend, M. Daly, J.S. Chamberlain, J.M. Metzger, Age-dependent dystrophin loss and genetic reconstitution establish a molecular link between dystrophin and heart performance during aging, Mol. Ther. 19 (2011) 1821–1825.
[38] N.B. Wasala, Y. Lai, J.H. Shin, J. Zhao, Y. Yue, D. Duan, Genomic removal of a therapeutic mini-dystrophin gene from adult mice elicits a Duchenne muscular dystrophy-like phenotype, Hum. Mol. Genet. 25 (2016) 2633–2644.
[39] S. Guiraud, A. Aartsma-Rus, N.M. Vieira, K.E. Davies, G.J. van Ommen, L.M. Kunkel, The pathogenesis and therapy of muscular dystrophies, Annu. Rev. Genomics Hum. Genet. 16 (2015) 281–308.
[40] N. Shirokova, E. Niggli, Cardiac phenotype of duchenne muscular dystrophy: insights from cellular studies, J. Mol. Cell. Cardiol. 58 (2013) 217–224.
[41] F. Kamdar, D.J. Garry, Dystrophin-deficient cardiomyopathy, J. Am. Coll. Cardiol. 67 (2016) 2533–2546.
[42] T.L. van Westering, C.A. Betts, M.J. Wood, Current understanding of molecular pathology and treatment of cardiomyopathy in duchenne muscular dystrophy, Molecules 20 (2015) 8823–8855.
[43] B. Bostick, Y. Yue, Y. Lai, C. Long, D. Li, D. Duan, Adeno-associated virus serotype-9 microdystrophin gene therapy ameliorates electrocardiographic abnormalities in mdx mice, Hum. Gene Ther. 19 (2008) 851–856.
[44] B. Gavillet, J.S. Rougier, A.A. Domenighetti, R. Behar, C. Boixel, P. Ruchat, et al., Cardiac sodium channel Nav1.5 is regulated by a multiprotein complex composed of syntrophins and dystrophin, Circ. Res. 99 (2006) 407–414.
[45] B.C. Willis, D. Ponce-Balbuena, J. Jalife, Protein assemblies of sodium and inward rectifier potassium channels control cardiac excitability and arrhythmogenesis, Am. J. Physiol. Heart Circ. Physiol. 308 (2015) H1463–H1473.
[46] L.A. Barouch, R.W. Harrison, M.W. Skaf, G.O. Rosas, T.P. Cappola, Z.A. Kobeissi, et al., Nitric oxide regulates the heart by spatial confinement of nitric oxide synthase isoforms, Nature 416 (2002) 337–339.
[47] G.P. Ahern, S.F. Hsu, V.A. Klyachko, M.B. Jackson, Induction of persistent sodium current by exogenous and endogenous nitric oxide, J. Biol. Chem. 275 (2000) 28810–28815.
[48] D. Li, Y. Yue, Y. Lai, C.H. Hakim, D. Duan, Nitrosative stress elicited by nNOSμ delocalization inhibits muscle force in dystrophin-null mice, J. Pathol. 223 (2011) 88–98.
[49] G.F. Mitchell, A. Jeron, G. Koren, Measurement of heart rate and Q-T interval in the conscious mouse, Am. J. Phys. 274 (1998) H747–H751.
[50] G. Nigro, L.I. Comi, L. Politano, G. Nigro, Cardiomyopathies associated with muscular dystrophies, in: A. Engel, C. Franzini-Armstrong (Eds.), Myology: Basic and Clinical, third ed.McGraw-Hill, Medical Pub. Division, New York 2004, pp. 1239–1256.
[51] D. Duan, J.A. Rafael-Fortney, A. Blain, D.A. Kass, E.M. McNally, J.M. Metzger, et al., Standard operating procedures (SOPs) for evaluating the heart in preclinical studies of Duchenne muscular dystrophy, J. Cardiovasc. Transl. Res. 9 (2016) 85–86.

Uniform low-level dystrophin expression in the heart partially preserved cardiac function in an aged mouse model of Duchenne cardiomyopathy

Nalinda B. Wasala[1], Yongping Yue[1], Jenna Vance[1], Dongsheng Duan [1-4, *]

1, Department of Molecular Microbiology and Immunology, School of Medicine, The University of Missouri, Columbia, MO 65212, USA

2, Department of Neurology, School of Medicine, The University of Missouri, Columbia, MO 65212, USA

3, Department of Bioengineering, The University of Missouri, Columbia, MO 65212, USA

4, Department of Biomedical Sciences, College of Veterinary Medicine, The University of Missouri, Columbia, MO 65212, USA

*Corresponding Address:

Dongsheng Duan Ph.D.
Professor
Department of Molecular Microbiology and Immunology
One Hospital Dr.
Columbia, MO 65212
Phone: 573-884-9584
Fax: 573-882-4287
Email: duand@missouri.edu

Supplementary Figure legend

Supplementary Figure 1. Mdx3cv mouse produces low levels of dystrophin due to an aberrant splicing event. A, A carton showing in-frame splicing events (occurring in exon 63-67) in wildtype mice to produce full length dystrophin. **B,** In mdx3cv mice, a mutation (marked in red) results in out-of-frame transcript. **C,** The transcript generated by skipping exons 65 and 66 (Δ65/66) generates an in-frame transcript that produces low levels of dystrophin in mdx3cv mice.

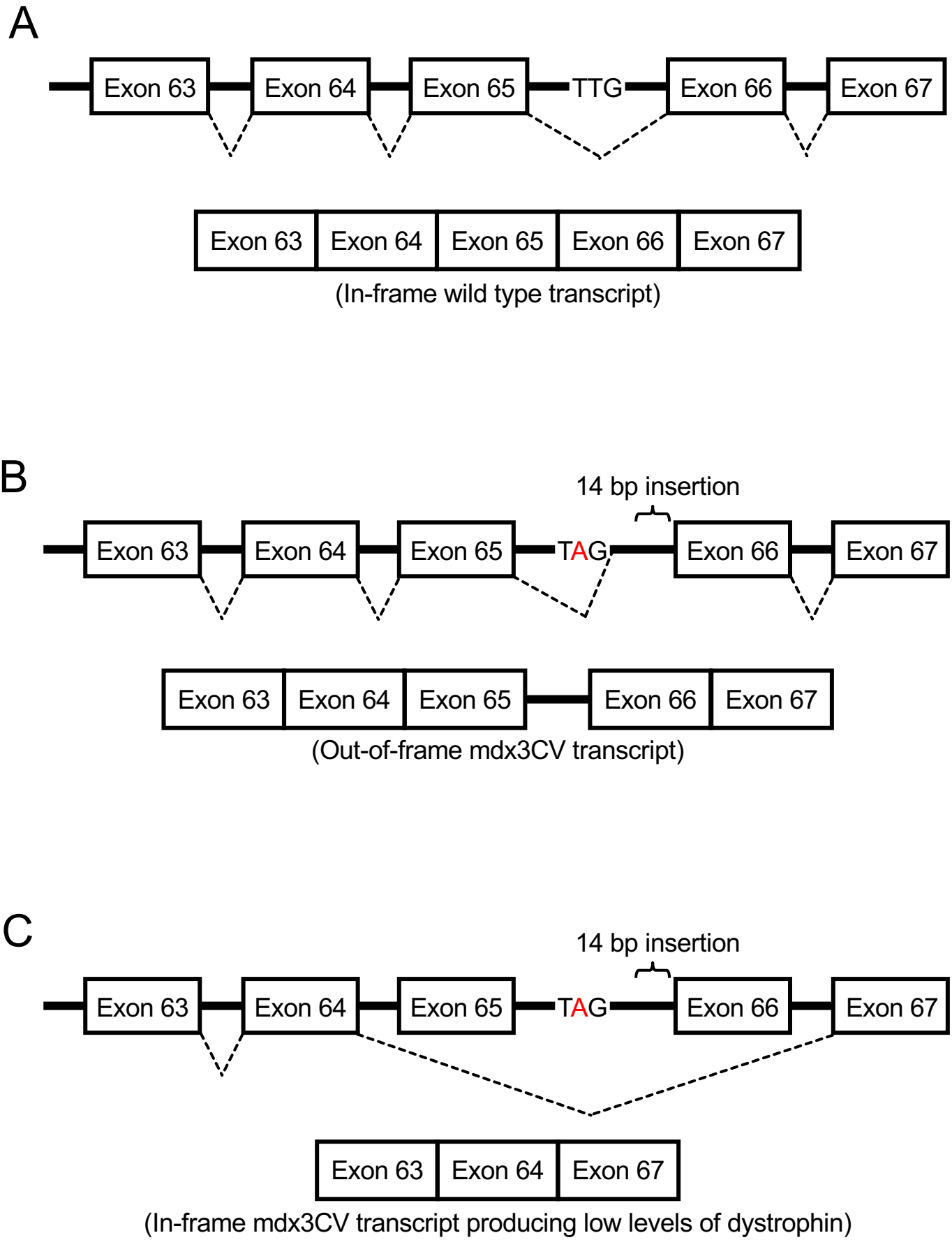
A
Exon 63
Exon 64
Exon 65
TTG
Exon 66
Exon 67
Exon 63
Exon 64
Exon 65
Exon 66
Exon 67
(In-frame wild type transcript)
B
14 bp insertion
Exon 63
Exon 64
Exon 65
TAG
Exon 66
Exon 67
Exon 63
Exon 64
Exon 65
Exon 66
Exon 67
(Out-of-frame mdx3CV transcript)
C
14 bp insertion
Exon 63
Exon 64
Exon 65
TAG
Exon 66
Exon 67
Exon 63
Exon 64
Exon 67
(In-frame mdx3CV transcript producing low levels of dystrophin)

Focus Article

Nanotherapy for Duchenne muscular dystrophy

Michael E. Nance,[1] Chady H. Hakim,[1,2] N. Nora Yang[2] and Dongsheng Duan[1,3,4,5]*

Duchenne muscular dystrophy (DMD) is a lethal X-linked childhood muscle wasting disease caused by mutations in the dystrophin gene. Nanobiotechnology-based therapies (such as synthetic nanoparticles and naturally existing viral and nonviral nanoparticles) hold great promise to replace and repair the mutated dystrophin gene and significantly change the disease course. While a majority of DMD nanotherapies are still in early preclinical development, several [such as adeno-associated virus (AAV)-mediated systemic micro-dystrophin gene therapy] are advancing for phase I clinical trials. Recent regulatory approval of Ataluren (a nonsense mutation read-through chemical) in Europe and Exondys51 (an exon-skipping antisense oligonucleotide drug) in the United States shall offer critical insight in how to move DMD nanotherapy to human patients. Progress in novel, optimized nano-delivery systems may further improve emerging molecular therapeutic modalities for DMD. Despite these progresses, DMD nanotherapy faces a number of unique challenges. Specifically, the dystrophin gene is one of the largest genes in the genome while nanoparticles have an inherent size limitation per definition. Furthermore, muscle is the largest tissue in the body and accounts for 40% of the body mass. How to achieve efficient bodywide muscle targeting in human patients with nanomedication remains a significant translational hurdle. New creative approaches in the design of the miniature micro-dystrophin gene, engineering of muscle-specific synthetic AAV capsids, and novel nanoparticle-mediated exon-skipping are likely to result in major breakthroughs in DMD therapy.

How to cite this article:
WIREs Nanomed Nanobiotechnol 2017, e1472. doi: 10.1002/wnan.1472

INTRODUCTION

Duchenne muscular dystrophy (DMD) is a progressive, eventually fatal muscle wasting disease in male children resulting from the functional loss of the dystrophin protein. The estimated disease occurrence is 1:5000 male births.[1–3] Affected children are typically diagnosed between the ages of 2 and 5 due to delayed motor skills, cognitive delay, and elevated creatine kinase. Without intervention, patients are unable to walk and require a wheelchair by the ages of 10–12 and have a mean survival of 19 years due to cardiopulmonary complications (http://www.cdc.gov/ncbddd/musculardystrophy/data.html#ref).[4] Microscopically, affected muscles show an absence of dystrophin at the sarcolemma by immunostaining and a variety of histological features of muscle degeneration, regeneration, inflammation, and fatty fibrosis (Figure 1). In

*Correspondence to: duand@missouri.edu

[1]Department of Microbiology and Immunology, University of Missouri School of Medicine, Columbia, MO, USA

[2]National Center for Advancing Translational Sciences, NIH, Rockville, MD, USA

[3]Department of Neurology, University of Missouri, Columbia, MO, USA

[4]Department of Bioengineering, University of Missouri, Columbia, MO, USA

[5]Department of Biomedical Sciences, University of Missouri, Columbia, MO, USA

Conflict of interest: The authors ME Nance, CH Hakim and NN Yang have declared no conflicts of interest for this article whereas author whereas author D Duan has the following conflict of interest. D Duan is a member of the scientific advisory board for Solid GT, LLC and an equity holder of Solid GT, LLC. D Duan is an inventor on a patent licensed to Solid GT, LLC. The Duan lab has received research supports from Solid GT, LLC.

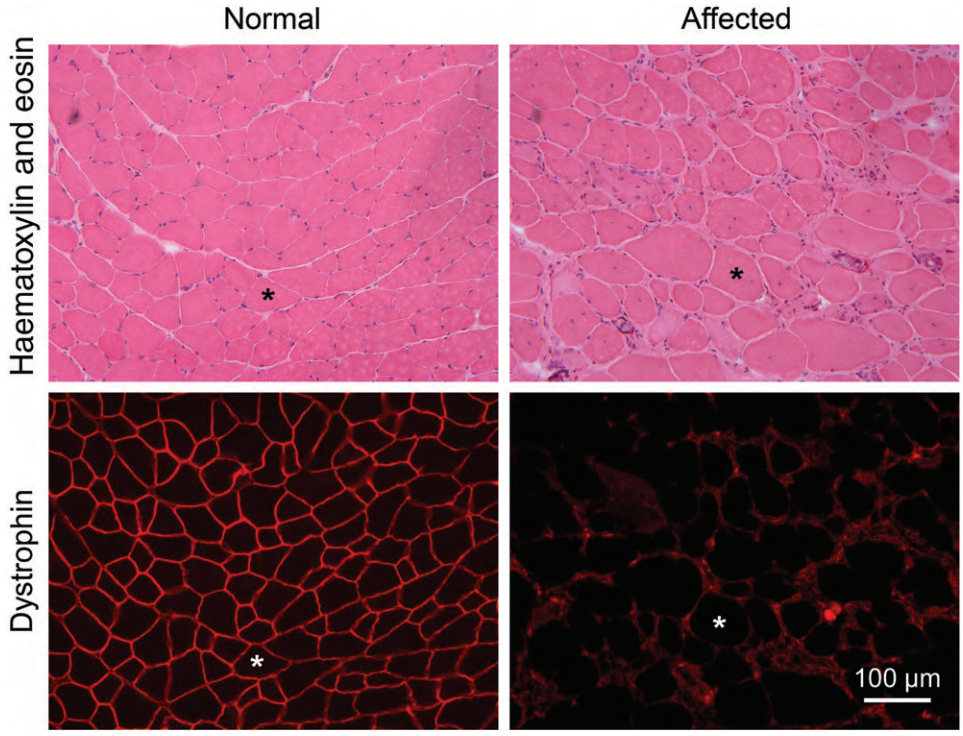

FIGURE 1 | Histopathology and dystrophin immunostaining. Top panels show representative photomicrographs of hematoxylin–eosin (HE)-stained skeletal muscle cross-sections from a normal and an affected mouse. Bottom panels are serial sections immunostained with a monoclonal antibody that recognizes dystrophin. In normal muscle, dystrophin is localized at the muscle cell membrane. Lack of dystrophin leads to muscle degeneration/regeneration, necrosis, inflammatory cell infiltration, and replacement of deceased muscle by fat and fibrotic tissues. The presence of centrally located nuclei in dystrophic muscle fibers indicates recent fiber regeneration. Asterisks represent the same myofiber in serial muscle sections. The interstitial fluorescence signals seen in the immunostaining image of the affected mouse muscle is due to cross-reaction of the secondary antibody (Alex 594-conjugated anti-mouse antibody) to the inflamed mouse muscle.

the heart, dystrophin-deficient cardiomyocytes are vulnerable to mechanical stress resulting in cardiac injury and the development of dilated cardiomyopathy and arrhythmias (see Box 1).[5,6] Currently, glucocorticoids are the most widely used medication for DMD. Although it has been shown that glucocorticoids can expand the lifespan by approximately 3 years, reduce scoliosis, and delay cardiomyopathy,[7–9] long-term use of steroid is notoriously associated with a constellation of side effects including Cushingoid features, adverse behavioral events, hypertension, vertebral fracture, cataracts, excessive weight gain, and growth retardation.[10,11] These untoward reactions reduce the life quality and health span of patients. A definitive therapy for DMD will require restoration of a functional dystrophin protein to the muscle sarcolemma. This can be achieved by replacing, repairing, or bypassing the mutated dystrophin gene. The emergence of several viable options for DMD gene therapy has turned the focus to drug delivery systems. Indeed, the pharmacokinetic challenges involved in the delivery of therapeutic molecules is one of the foremost obstacles in the gene therapy field. Selectivity is a key concern especially when considering gene supplementation, replacement, integration, or genome editing. Herein lies a great opportunity for nanomedicine and, in particular, nanometer scale drug delivery systems. In this review, we discuss the current and emerging nanomedications and nanotechnologies that can restore dystrophin expression. We divide DMD nanotherapy into nonviral and viral approaches. We begin with a historical discussion on strategies that are highly relevant but often not considered as nanotherapy. These include read-through molecules, naked plasmid DNA, and antisense oligonucleotides (AONs). Next, we discuss nonviral nanotechnology including lipid- and polymer-based nanoparticles, chemically modified nanoparticles, and exosome therapies. Finally, we consider viral approaches with a special focus on the progress with adeno-associated virus (AAV)-mediated micro-dystrophin gene therapy (Table 1).

BOX 1

CLINICAL AND PATHOLOGICAL ASPECTS OF DILATED CARDIOMYOPATHY IN DMD

Cardiac manifestations are present in around 25% of patients by age 6, 59% by age 10, and >90% by age 18 years or older.[31] Primary clinical findings include fatigue, shortness of breath, and palpitations related to a decline in the systolic ejection fraction, autonomic dysfunction, and increased occurrence of arrhythmias. On electrocardiogram, DMD patients show tachycardia and have a shortened PR interval, tall R wave, and deep Q wave in the left precordial leads.[32] Echocardiography typically shows decreased wall motion in the left postero-basal ventricle, ventricular wall dilation, and thinning with a reduced ejection fraction. Histologically, the progression of dystrophic cardiomyopathy is characterized by interstitial fibrosis, myocardial inflammation, and loss of cardiomyocytes.[32]

A HISTORICAL PERSPECTIVE ON DMD GENE THERAPY

Great successes have been achieved over the last four decades in the development of a genetic therapy for DMD. These include reading through of nonsense mutations using chemicals, modulation of the splicing machinery to skip mutated exons using AONs, and introduction of a functional dystrophin gene. Advances in these fronts have set the stage for nanoparticle-mediated DMD gene therapy. To frame DMD nanotherapy in the right context, next we briefly review the current status of nonnanotherapies.

Small Molecules Targeting Nonsense Mutations

About 10% of DMD cases results from nonsense mutation (a mutation that coverts an amino acid coding codon into one of the three stop codons including TAG, TGA, or TAA). Premature stop codons result in various truncated, nonfunctional dystrophin proteins that are often degraded. For these mutations, small molecules targeting ribosomal recognition of stop codons may be used to continue translation through the premature stop codon. Initially, this phenomenon was appreciated with the aminoglycoside antibiotic gentamicin. However, gentamicin is poorly tolerated in humans and has a low potency.[33] In 2007, Welch and colleagues identified PTC124 through high-throughput screening of over 800,000 small molecules followed by chemical modification and optimization.[34] PTC124, now known as Ataluren, is thought to cause translation read through; however, this mechanism has been debated. Several studies have raised questions about the assay used in the molecule's discovery.[35,36] Although contested, a subset of patients treated with low-dose (40 mg/kg/day) Ataluren showed improvement in the 6-min walk test (6MWT).[37] Interestingly, these benefits were not seen with the high dose (80 mg/kg/day). Based on the results of the clinical trials, Ataluren may be well suited for patients that meet a certain set of criteria. In July 2014, Ataluren received approval in the European Union for treatment of ambulant DMD patients who are older than 5 years and carry a nonsense mutation.[38] Additional high-throughput screenings are ongoing in several places. It is very likely that new compounds with better pharmacokinetic and pharmacodynamic profiles will be identified to suppress nonsense mutations in DMD.[39]

Naked Plasmid DNA Delivery of the Dystrophin Gene

In the early 1990s, it was recognized that naked plasmid DNA containing the dystrophin cDNA could be delivered to muscle via direct injection.[40,41] Naked plasmid DNA has the advantage of delivering a full-length dystrophin coding sequence and may likely be minimally immunogenic. However, low transduction efficiency has limited its use. A number of strategies have been developed to enhance plasmid DNA delivery by electroporation, ultrasound, or pretreatment with hyaluronidase.[42,43] Yet, it is not clear whether these strategies can be translated to human patients. Furthermore, even with these strategies, dystrophin expression remains moderate from naked plasmid delivery. Some groups have shown that dystrophin plasmid can be delivered to dystrophic dog muscle.[44] A human trial by direct muscle injection showed some limited dystrophin expression with no evidence of an immune response.[45] Limiting factors for direct plasmid DNA delivery may include, but not limited to, promoter inactivation, plasmid loss, and inefficient trafficking to the nucleus.

Exon-Skipping with AONs

More than 90% mutations in DMD disrupt the reading frame. AONs-mediated exon-skipping is developed to modulate the cellular splicing machinery, so that the targeted exon(s) can be deleted in the RNA transcript. Exon-skipping could, in theory, address a large percentage of frame-shift mutations by intentionally skipping one or multiple exons to restore the normal

TABLE 1 | Overview of DMD Nanotherapy

	Comments	Reference
Nonviral nanotherapy		
Polymersomes	Amphiphilic block copolymers encapsidating AON, siRNA, or viral nucleic acids. Improved exon-skipping in mdx mice	Kim et al.[12]
Liposomes and lipid-nucleic acid complexes	Liposomes, thermoplastic nanoparticles with cationic lipids and bubble liposomes. Tested in mice	Afzal et al.[13]; Negishi et al.[14]
Cell-penetrating peptides and peptide–nucleic acid complexes	Peptide–AONs. Very promising for improved exon-skipping; studies mainly in mice	Ezzat et al.[15]; Gao et al.[16]; Lehto et al.[17]; Shabanpoor et al.[18]
PMMA nanoparticles	T1 and ZM2 nanoparticles are highly promising for bodywide muscle delivery. Greatly enhances exon-skipping in mice	Rimessi et al.[19]; Ferlini et al.[20]; Bassi et al.[21]; Falzarano et al.[22]
Exosomes	A very promising new gene delivery approach not explored for DMD therapy yet	
Viral nanotherapy		
AAV	20–25 nm. Persists as episome. AAV micro-dystrophin has been tested in human patients. Systemic AAV microgene therapy is at the forefront for DMD therapy. AAV-mediated CRISPR genome editing also holds great promise.	Mendell et al.[23]; Yue et al.[24]; Nelson et al.[25]
Adenovirus	100 nm. Tested in animals extensively in 1990s. Unlikely to be used due to toxicity and immunogenicity	DelloRusso et al.[26]; Deol et al.[27]; Maggio et al.[28]
Lentivirus	80–120 nm. Chromosomally integrated. Lentiviral micro-dystrophin tested in mice. Transduces satellite cells	Muir et al.[29]; Naldini et al.[30]

reading frame. This results in the production of internally truncated but likely functional dystrophin proteins. Uncharged phosphorodiamidate morpholino oligonucleotides (PMOs) are among the most commonly used AONs. PMOs have phosphorodiamidate linkages and a morpholine ring instead of ribose sugar. These modifications confer nuclease resistance, enhance binding to mRNA, and prevent RNaseH activity that would degrade the mRNA. The most widely known PMO for DMD exon-skipping is Exondys51 (also known as AVI-4658 and Eteplirsen). Exondys51 specifically targets exon 51, which could theoretically treat 13% of DMD patients. Exondys51 has been tested in several clinical trials.[46] These studies suggest that Exondys51 is safe and can restore dystrophin expression on immunofluorescence staining. Compared with historic data, Exondys51 appears to have improved ambulation. On September 19, 2016, the U.S. Food and Drug Administration (FDA) granted accelerated approval to Exondys51 as an injection drug for treating DMD patients who have a confirmed mutation amenable to exon 51 skipping (http://www.fda.gov/NewsEvents/Newsroom/PressAnnouncements/ucm521263.htm).

One of the most exciting new developments in exon-skipping is the engineering of tri-cycloDNA AONs (tcDNA-AONs) by Goyenvalle et al.[47] TcDNA spontaneously forms nanoparticles ranging in size from 40 to 100 nm. Systemic administration of tcDNA-AONs resulted in phenomenal uptake in many tissues including skeletal muscle, heart, and brain. Importantly, tcDNA exon-skipping significantly attenuated dystrophic phenotypes in mdx mice and the much severer utrophin–dystrophin double knockout mice. Skeletal muscle, cardiac, respiratory, and behavior functions were all significantly improved and were not associated with overt toxicity.[47] In addition to tcDNA-AONs, another recently developed octaguanidine dendrimer-conjugated AONs (called vivomorpholinos) may also greatly enhance exon-skipping efficiency (reviewed in Ref 48). Studies from several groups suggest that vivo morpholinos are highly powerful for long-term systemic exon-skipping therapy in both rodent and canine models of DMD.[49–52]

NONVIRAL-BASED NANOPARTICLES FOR DMD THERAPY

The delivery of nucleic acids can be significantly enhanced by the modification of nucleotide chemistry and/or complexing with polymers, lipids, and

peptides. In essence, these changes result in the formation of chemically and/or biologically engineered nanoparticles. Such nanoparticles can improve tissue targeting/penetration, protect nucleic acids from degradation, and help evade untoward immune reactions. A number of conjugated AONs have been tested in animal models of DMD.[48] Next, we discuss the current and emerging nonviral nano delivery strategies focusing on advances in AON exon skipping.

Polymersomes

Originally described in 1995, polymersomes are biocompatible nanoparticles composed of amphiphilic block copolymers (e.g., polyethylene glycol and polylactic acid mixtures).[53,54] In the years following their discovery, polymersomes were shown to have enhanced physical properties in comparison to liposomes such as increased water resistance and enormous flexibility in composition.[55] Recent studies have further expanded our knowledge of polymersome formulation. Polymersomes are highly variable in terms of their properties. Depending on the polymers used in formulation and methods used in production, polymersomes can be generated to display a variety of different chemical, physical, and biological features.[56] Polymersomes may also be functionalized by the inclusion of integral membrane proteins such as channels and tailored to specific sizes. The ideal size of polymersomes is in the range of approximately 90 to ≤120 nm. This size allows efficiently entry into the cells while at the same time not be removed from the blood by the mononuclear phagocyte system.[57] Importantly, polymersomes may be loaded with DNA molecules either through encapsidation during formulation or by using virus to inject DNA through integral proteins.[57,58] As a tool for DMD therapy, Discher's group recently developed a polycaprolactone-formulated, degradable polymersome for AON delivery. Compared to naked AON, polymersome delivery significantly enhanced exon-skipping efficiency in mdx mice.[12] Recent data from the Lu laboratory suggest that polyethylenimine-conjugated pluronic polycarbamates represent yet another type of chemically complexed nanoparticles very promising for enhancing dystrophin exon-skipping.[59–62]

Lipid Nanoparticles

The concept of lipid enclosed drug delivery systems emerged over 40 years ago (reviewed in Ref 63). The initial observations in the early 1980s that lipid formulations could enhance the delivery of nucleic acids opened an entire field of nanomedicines.[64,65] Over the years, our understanding of lipid–nucleic acid complexes has greatly increased. In addition to extending the circulation time and reducing toxicity, lipid-based nanoparticles also enhance the potency of the nucleic acid cargo by protecting it from degradation.[66]

Lipid nanoparticles and liposomes have been used to deliver exon-skipping AONs for DMD gene therapy. In the former, cationic lipids are used to coat chemically engineered dendrimeric AON nanoparticles such as poly-methyl methacrylate (PMMA) nanoparticles.[67] In the later, AONs are encapsidated inside hallow lipid nanospheres. Dendritic nanoparticles can also be incorporated into liposomes and form nanolipodendrosome for improved delivery.[13] Recently, investigators have begun to explore bubble liposomes for AON delivery. Bubble liposomes contain an ultrasound-responsive imaging gas such as perfluoropropane that may be triggered to burst with ultrasound cavitation.[68] This novel strategy has greatly improved localized exon-skipping following direct muscle injection.[14] Lastly, as liposomes mimic the cellular membrane, it is possible to functionalize liposomes with various cell targeting peptides.

PMMA Nanoparticles

Dendrimeric PMMA nanoparticles are a highly promising group of drug carriers developed by the Ferlini laboratory (reviewed in Ref 67). Based on the size, PMMA nanoparticles are divided into two categories, approximately 420 nm T1 PMMA nanoparticles and approximately 130 nm ZM2 PMMA nanoparticles. T1 nanoparticles have greatly improved the pharmacokinetics of AONs delivery. In one study, T1 nanoparticles at a 50-fold lower dose (~3 mg/kg) yielded the similar levels of exon-skipping in comparison to that of naked AONs (~150 mg/kg).[19] The major limitation of T1 nanoparticles is the poor transduction efficiency in the heart. Furthermore, accumulation of T1 nanoparticles in circulating macrophages and endothelial cells may represent an important immunological concern. ZM2 nanoparticles are developed as an alternative to T1 nanoparticles. They consist of a PMMA core and an *N*-isopropyl-acrylamide shell. In contrast to T1 nanoparticles, ZM2 nanoparticle delivery resulted in efficient myocardial exon-skipping. Recent studies suggest that PMMA nanoparticles can greatly improve bodywide delivery of AONs and dystrophin restoration by exon-skipping in striated muscles.[19–22,67] Further development of this delivery strategy is warranted.

Cell-Penetrating Peptides

Peptide conjugation significantly enhances biological activities of AON nanoparticles (reviewed in Refs 69–71). Two types of peptides are used including (1) - cell-penetrating peptides which contain peptide transduction domains for efficient delivery into cells, and (2) homing peptides for targeting specific cells and/or tissues. In this regard, muscle- and heart-specific peptides are especially critical for DMD gene therapy.[72] Peptide can be conjugated to the cargo either covalently or indirectly via a linker. Failure to reach the heart is a major hurdle in early DMD exon-skipping studies. The development of peptide-conjugated AON nanoparticles has successfully overcome this obstacle.[61,73–83] Recent studies have further illustrated therapeutic potential of peptide-AON nanoparticles for DMD therapy.[15–18]

Exosomes, Naturally Occurring Biological Nanoparticles for DMD Therapy

Exosomes are 30–100 nm extracellular vesicles released by many cell types throughout the body. Naturally, exosomes may be found in the blood and are known to transport mRNA, small noncoding RNAs, and proteins. Exosomes originate from endosomal-derived multivesicular bodies, which give rise to intraluminal vesicles.[84] Exosomes are nonimmunogenic and tend to share characteristics with the host cell from which they are derived. Exosomes have been explored to treat ischemia/reperfusion in the myocardial infarction model in animals.[85,86] Recent studies suggest that exosomes may also be responsible for conveying the cardioprotective effects of cardiosphere-derived cells.[87] Importantly, exosomes have been used to package therapeutically relevant nucleic acids (such as short-interfering silencing RNAs) for *in vivo* gene therapy in muscle.[88] Furthermore, cell/tissue-targeting peptides can be fused to the selected exosomal membrane proteins to achieve targeted delivery.[88] While direct evidence for exosome-mediated DMD nanotherapy is currently lacking, it is expected that engineered exosomes will be a highly attractive future avenue for delivering muscle/heart-specific noncoding RNAs (such as microRNAs, silencing RNAs, and long noncoding RNAs) to modulate DMD pathogenesis.[89–92] Perhaps, the most appealing application of exosomes is to use these nanoparticles to deliver dystrophin mRNA (either full-length or abbreviated) for DMD gene replacement therapy and/or to deliver the CRISPR-Cas9 system for DMD gene-editing therapy.

VIRAL VECTORS AS BIOLOGICAL NANOPARTICLES

Viral particles have a long history as gene therapy tools but the utility and modularity of viral particles is only being realized in more recent years. Compared to nonviral nanoparticles, viral vectors have inherent advantages. Viruses are versatile, nano-scale biological carriers that have been evolved over millions of years to target, enter, and alter cellular behaviors through the expression of viral-coded genes. Several viruses also establish latent infection which leads to prolonged gene expression. This is highly beneficial for DMD where long-term expression is required. Furthermore, the atomic structures of many viruses have been solved and structure–function correlation studies have started to reveal critical structural domains involved in targeting, stability, and immune evasion.[72]

In the context of this review article, it is worth pointing out that the distinction between viral and nonviral nanoparticles is increasingly becoming blurred from the standpoint of gene delivery vehicles. On one hand, viral proteins have been incorporated in nanoparticles for effective cellular and nuclear entry (such as the Tat protein from human immunodeficiency virus). On the other hand, numerous fully striped or gutted viral vectors have emerged over the last two decades. These gutless viral vectors contain minimal viral sequences and do not express any viral replication or capsid proteins. The development of custom-designed viral capsids by forced evolution and/or educated engineering has created huge potentials in manufacturing virus-like capsids. These custom-designed capsid proteins bear nominal amino acid similarity to wild-type viral capsid proteins. In other words, such engineered virus-like particles have no naturally existing counterpart.

Due to space limitations, we only discuss vectors based on lentivirus, adenovirus, and AAV.

Lentivirus

Lentivirus is a genus of retroviridae family virus. Lentivirus is enveloped and has a size of 80–120 nm. Lentivirus carries two copies of the positive single-stranded RNA genome. Lentivirus can infect quiescent cells and induces long-term expression by integrating into the host genome.[30,93] While it has been shown that lentivirus can target satellite cells *in vivo* in neonatal and young dystrophic mice,[94,95] most applications have focused on *ex vivo* cell therapy. In brief, stem cells (including myogenic progenitor cells, mesenchymal stem cells, and dermal fibroblasts) are

infected with a lentivirus carrying either a full-length or an abbreviated dystrophin gene. Subsequent engraftment in dystrophic muscle results in dystrophin expression in regenerated muscle.[29,96–100] Alternatively, stem cells can also be isolated from human patients and transplanted back to dystrophic muscle after correction with lentivirus-mediated delivery of various dystrophin repair mechanisms.[99,101,102]

Adenovirus

Adenoviruses are 90–100 nm nonenveloped icosahedral double-stranded DNA viruses. Several generations of adenovirus vectors have been developed including E1/E3-deleted first-generation (can package ~8 kb), E1/E2/E3 and E4-deletec second-generation (can package ~14 kb), and the entire genome-deleted gutted adenovirus (can package ~38 kb). Adenovirus has been used to deliver the 6- to 8-kb mini-dystrophin gene, the full-length dystrophin coding sequence, the dystrophin homologue utrophin gene, and the CRISPR-Cas9 system.[26–28,103–105] However, because adenovirus infection induces prominent cellular immune responses and adenovirus cannot efficiently infect mature muscle, it is generally agreed that adenoviral vector is not an ideal vector system for DMD gene therapy.

Adeno-Associated Virus

Basic Biology of AAV

AAV is the premier gene delivery vector for DMD.[106,107] It belongs to the parvovirus family and is dependent on a helper virus (such as adenovirus) for productive infection.[108–111] The nonenveloped, icosahedral AAV capsid is approximately 20 nm.[112] Wild-type AAV is considered nonpathogenic. Recombinant AAV vectors are in general devoid of all viral genes. AAV can persist episomally allowing long-term gene expression.[113] Most importantly, AAV is the only virus that can effectively transduce all striated muscles in the body.[114]

Twelve AAV serotypes and several hundreds of AAV variants have been published.[72,115–121] While they all share significant sequence homology, the differences in regions primarily localized to the surface exposed loops yield a variety of unique tropisms and immunogenicity.[122–125]

Overcoming the Packaging Size Restrain

AAV-mediated DMD gene therapy faces several unique challenges. The most obvious one is the limited packaging capacity of AAV. The wild-type AAV genome is approximately 4.6 to 4.8 kb. The maximal size of a recombinant AAV genome is 5 kb.[126] The size of the dystrophin gene, mRNA, and coding sequence is 2.4 mb, 14 kb, and 11.2 kb, respectively. This creates a compatibility dilemma. Several distinctive approaches have been investigated to overcome this hurdle. These include the development of highly truncated micro-dystrophins, invention of high-capacity dual and tri-AAV vectors, and AAV-mediated exon-skipping.

The micro-dystrophin genes are less than 4 kb in size.[106] The first series of microgenes were published in 1998.[127] Unfortunately, they were minimally protective. In early 2000s, the C-terminal deleted second-generation microgenes were developed in the Xiao lab and Chamberlain lab.[128,129] These microgenes effectively ameliorated skeletal muscle disease, improved muscle function, and reduced Duchenne cardiomyopathy in various mouse models of DMD.[128–145] Recent optimization (such as codon usage optimization, removal/replacement of rigid hinge 2, and inclusion of the syntrophin/dystrobrevin-binding site) has further enhanced therapeutic potency.[146–148]

To validate the therapeutic effect of micro-dystrophin in a large mammal, many studies have been performed in the canine model of DMD.[149,150] While AAV administration induces minimal cellular immune reaction in rodents, it turns out that the T-cell response is a major hurdle for AAV gene therapy in dystrophic large mammals.[23,151,152] Application of transient immune suppression greatly attenuates the immune response and results in robust and persistent expression following local gene transfer in the canine model of DMD.[153,154] Importantly, direct injection of the AAV micro-dystrophin vector to affected dog muscle has ameliorated muscle pathology and enhanced muscle function.[155]

A major deficiency of these early microgenes is their failure to restore neuronal nitric oxide synthase (nNOS) to the sarcolemma. Membrane localization of nNOS is crucial for muscle physiology.[156] Loss of sarcolemmal nNOS leads to functional ischemia, a significant insult to muscle health and function.[157,158] Delocalized nNOS causes nitrosative stress, which directly inhibits muscle contractility.[159] Collectively, disruption of normal nNOS homeostasis is undoubtedly an important factor of DMD pathogenesis.[160–162] Through a comprehensive structure–function analysis, we recently identified spectrin-like repeats 16 and 17 (R16/17) as the dystrophin nNOS-binding domain.[135,163,164] With this new information, we developed R16/17-based third-generation micro-dystrophins.[135] Inclusion of R16/17

in synthetic dystrophin genes significantly enhanced recovery in dystrophic mice.[135,165] As commented by Harper, 'the structural elements (R16/17) required for proper nNOS localization should be included in any DMD therapy for which dystrophin restoration is the goal.'[166]

An alternative to the gene shrink strategy is to expand the carrying capacity of the AAV vector. This is achieved with dual and tri-AAV vectors.[167,168] Basically, a large expression cassette is split into two or three parts and delivered into the cell by independent AAV vectors. Reconstitution is achieved by concatamerization between AAV-inverted terminal repeats and/or via homologous recombination. Following initial proof-of-principle studies with various reporter genes,[169–175] we demonstrated the feasibility of delivering a 6- to 8-kb mini-dystrophin gene with a set of dual AAV vectors.[176–178] Importantly, optimized mini-dystrophin dual AAV vectors resulted in a transduction efficiency comparable to that of a single AAV vector, significantly reduced muscle degeneration and inflammation, and increased muscle force.[176] Most recently, our group and Dickson's lab independently demonstrated feasibility of delivering the full-length dystrophin coding sequence using the tri-AAV system.[179,180] The transduction efficiency of the tri-AAV vectors remains low. Significant amount of work is needed before we can achieve therapeutically meaningful level of expression from tri-AAV full-length dystrophin vectors.

DMD is caused by out-of-frame mutations. Many of these mutations can be converted to an in-frame coding transcript by removing the mutated exon(s) and/or the neighboring exons using AONs.[181] While many exon-skipping therapeutics have focused on the chemical modification and optimization of AONs (see *Nonviral-Based Nanoparticles for DMD Therapy* section), investigators have begun to take the advantage of the powerful gene transfer capability of AAV to deliver AONs.[182–184] In AAV-mediated AON exon skipping, AONs are embedded in a U7 snRNA expression cassette for delivery to muscle nuclei. In the nucleus, AAV directs long-term expression of the AON and the U7 snRNA directs the AON to the complementary sequences in the dystrophin pre-mRNA. By binding to splicing enhancers/silencers and splicing donor and acceptor signals, AONs may alter the inclusion and/or exclusion of one or more exons allowing the targeted 'skipping' of out-of-frame mutations.[183,184] The removal of out-of-frame mutations restores the reading frame and results in the production of a functional, albeit, truncated dystrophin. As AAV directs long-term gene expression, packaging AON in AAV allows for persistent AON expression and obviates the need for weekly or biweekly injections.[185] Unlike AAV-mediated dystrophin gene replacement therapy, exon-skipping has to be tailored to the specific mutations. Nevertheless, recent successes in the canine model suggest that AAV exon-skipping has reached its prime time for a clinical trial.[185–188]

Bodywide Gene Therapy

Muscle is one of the largest tissues in the body. An effective gene therapy for DMD requires efficient delivery of the therapeutic gene to muscles all over the body including limb, respiratory, and cardiac muscles.[114] While there are some preclinical evidence suggesting that drug-mediated endothelial permeabilization can lead to multiple muscle transduction through a regional vessel,[189] bodywide treatment has been considered a mission impossible for many years. The situation changed in 2004 when several newly identified AAV serotypes were tested for intravenous delivery.[190–192] A flow of studies from different laboratories showed that AAV-6, -8, and -9 can effectively reach to all body muscles through the circulation.[138,193–196] Subsequent studies indicate that many other AAV serotypes are also capable of systemic delivery with different levels of efficiency (reviewed in Ref 114). Unprecedented results from reporter gene vectors stimulated immediate application of this novel gene delivery technology to animal models of muscular dystrophies including DMD (Figure 2).[134,138,193] Of particular interest are the studies performed in severely affected mouse models including utrophin/dystrophin double knockout mice and aged mdx mice.[136,137,139,143] These models are thought to better model dystrophic changes than young adult mdx mice. Surprisingly, severe muscle pathology, especially extensive fibrosis, did not limit AAV transduction. Systemic injection significantly improved overall condition of these mice, increased lifespan, and mitigated dystrophic cardiomyopathy.[136,137,139,143]

Following the success of systemic delivery of a single AAV vector, we explored systemic delivery of the dual AAV vectors.[197,198] Consistent with the results of the single AAV vector, we found that intravenous injection of the dual AAV vectors also results in fairly efficient transduction of skeletal muscle and the heart in normal and mdx mice.[197,198] Subsequent tests with therapeutic mini-dystrophin dual AAV vectors have provided unequivocal evidence that AAV therapy with a larger, 6- to 8-kb mini-dystrophin gene can offer whole body benefits in mouse models of DMD.[165,199]

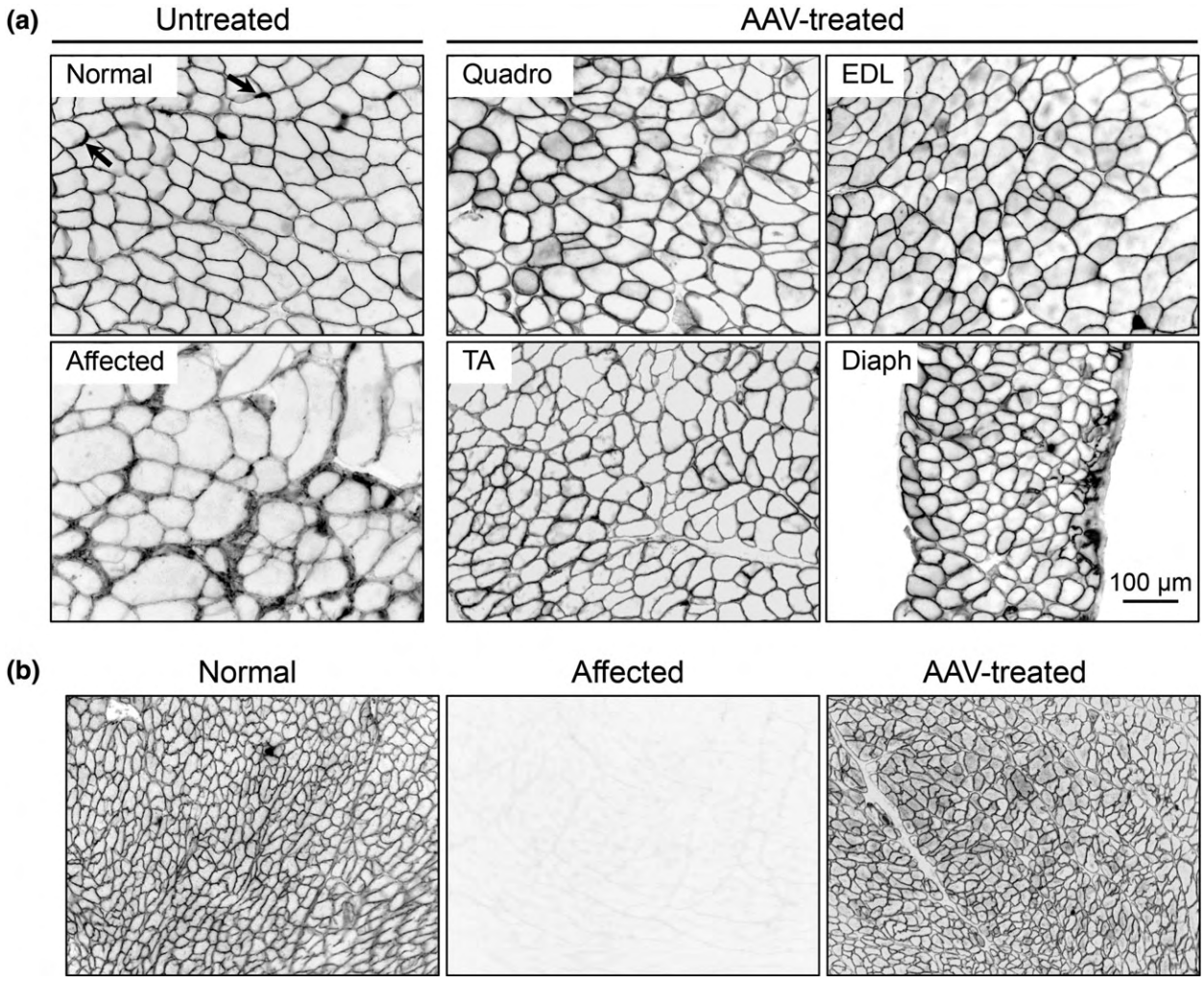

FIGURE 2 | Systemic AAV-9 micro-dystrophin gene transfer results in bodywide dystrophin restoration in striated muscles in the mouse model of Duchenne muscular dystrophy. (a) Representative dystrophin immunostaining photomicrographs from skeletal muscles of normal, untreated, and adeno-associated virus (AAV)-treated mdx mice. Normal muscle shows sarcolemmal expression of dystrophin, which is enriched at the neuromuscular junction (arrows). Dystrophic muscle has no dystrophin expression at the sarcolemma. Cross-reaction of the immunostaining antibody with inflamed/fibrotic interstitial tissues illustrates an irregular pattern of dystrophic muscle with extremely large and small myofibers. Systemic AAV-9 micro-dystrophin therapy restores dystrophin expression in the quadriceps (Quadro), extensor digitorum longus (EDL), tibialis anterior (TA), and diaphragm (Diaph). (b) Representative dystrophin immunostaining photomicrographs from the heart of normal, affected, and AAV micro-dystrophin-treated mice. Scale bar in panel (a) applies to all images.

The body weight of a 20-g young adult mouse is 750-fold lower than that of a 15-kg boy. To minimize the risks of scaling up from mice to humans, we have tested systemic AAV gene delivery in dogs. The body weight difference between a 20-g mouse and a 5-kg dog is 250-fold while going from a dog to a boy is only threefold. Initial studies in neonatal dogs have revealed several species-specific differences in AAV transduction biology between mice and dogs. First, cardiotropic AAV-9 fails to transduce the newborn dog heart.[152,200] Screening of alternative AAV serotypes identifies AAV-8 and Y445F/Y731F AAV-1 as the preferred vectors for effective heart and skeletal muscle gene transfer in newborn puppies.[201–203] Second, unlike mice, dogs carry high titers of AAV-6 neutralization antibody, which blocks systemic delivery with AAV-6.[201,204–206] Third, intravenous delivery by AAV-8 and -9 leads to high-level expression in the liver in mice.[194] However, there is minimal expression in the liver of dogs (even with a ubiquitous promoter and a reporter gene) although a significant amount of the AAV genome is detected in the liver.[152,201–203] Finally, a study from the Xiao lab suggests that systemic injection of AAV-9 may result

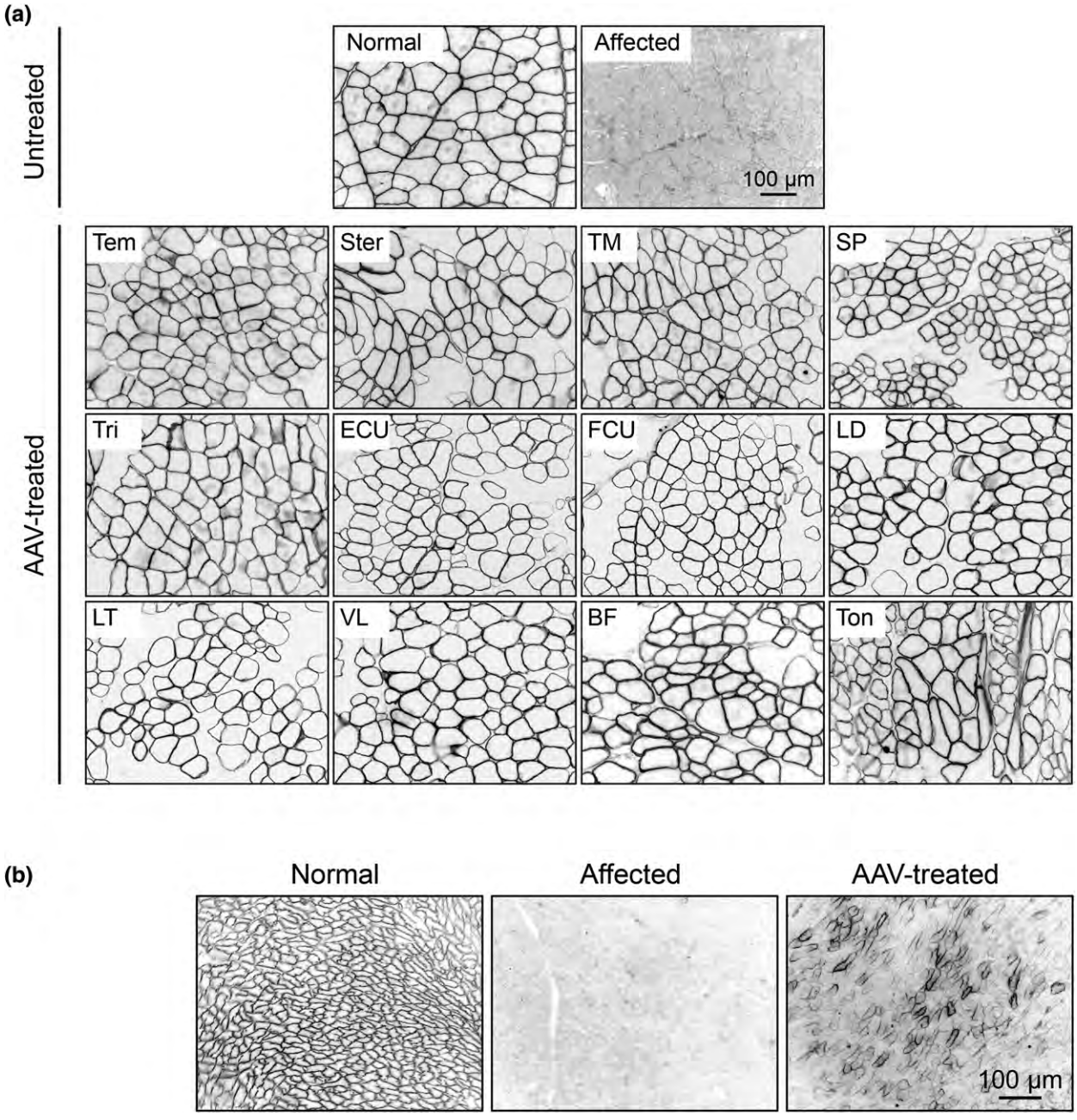

FIGURE 3 | A single intravenous injection of the adeno-associated virus (AAV)-9 micro-dystrophin vector leads to bodywide muscle transduction in the canine model of Duchenne muscular dystrophy. (a) Top panels: representative dystrophin immunostaining photomicrographs from skeletal muscles of normal and affected dogs. Bottom panels: representative dystrophin immunostaining photomicrographs from different skeletal muscle of an AAV-treated dog. Tem, temporalis; Ster, sternohyoid; TM, teres major; SP, superficial pectoral; Tri, triceps; ECU, extensor carpi ulnaris; FCU, flexor carpi ulnaris; LD, latissimus dorsi; LT, longissimus thoracis; VL, vastus lateralis; BF, biceps femoris; Ton, tongue. (b) Representative dystrophin immunostaining photomicrographs from the heart of normal, affected, and AAV mciro-dystrophin-treated dogs.

in a massive inflammatory response under certain condition (the ubiquitous promoter, human transgene, dystrophic puppy, or vector stock impurity).[207]

As our ultimate goal is to treat DMD boys with systemic gene therapy, we recently explored AAV-9-mediated micro-dystrophin therapy in young adult affected dogs.[24,208] After a single dose injection, we observed widespread bodywide micro-dystrophin expression in skeletal muscle and the heart (Figure 3). No adverse reactions were detected.

AAV-9 micro-dystrophin therapy greatly reduced dystrophic histopathology, improved the growth, and enhanced function.[24,155] Our data suggest that systemic AAV micro-dystrophin therapy is safe and efficient in young adult dystrophic large mammals. A similar approach may translate to DMD boys in the near future (https://solidbio.com/content/steps-forward-duchenne-muscular-dystrophy).[106]

New Developments in AAV-Mediated DMD Gene Therapy

Dystrophin-independent DMD gene therapy has emerged as a highly promising new direction. These therapeutic candidates can be divided into two categories including (1) structure and/or functional homologues of dystrophin such as utrophin and integrin,[209,210] and (2) alternative targets that are involved in different aspects of disease mechanisms such as follistatin, nNOS, cytotoxic T-cell GalNAc transferase (Galgt2), sarcospan, and sarcoplasmic reticulum calcium ATPase (SERCA).[211–215] In these approaches, the therapeutic candidate genes are already expressed in DMD patients. Hence, they are unlikely to induce the transgene product-associated immune response.

The biological properties of AAV (such as tissue tropism and intracellular processing) are largely dependent on the viral capsids. A number of highly creative strategies have been used to engineer novel AAV capsids with superior properties for different applications. In the forced evolution approach, an AAV capsid library is subject to a variety of *in vitro* and *in vivo* selection pressures. The best-fit capsids can then be used for gene therapy.[119] The resolution of the high-definition AAV capsid structure and the discovery of AAV receptors and coreceptors in recent years have opened the door for educated engineering of AAV capsids to meet the needs of gene therapy applications.[123–125,216] It is expected that an integrated approach combining various rational design and direct evolution methods will yield one or several super-AAV capsids for DMD gene therapy in the near future.[72]

There is no doubt that the CRISPR technology is the most exciting advance in the entire field of biology in recent years.[217,218] While it is still at an early stage of development, AAV-mediated genome editing with the CRISPR technology has yielded very promising results in mdx mice.[25,219,220] Further improvement in this technology, especially in terms of increasing editing specificity and minimizing potential immunogenicity of bacterial derived Cas9 protein, may one day bring this revolutionary technology to DMD patients.

NANOTHERAPY AGAINST PATHOGENIC MECHANISMS OF DMD

While most of the above-described DMD nanotherapies focus on restoration of dystrophin in diseased muscle, many investigators have also begun to apply nanotechnology to address the downstream pathogenic events in DMD. For example, it has been recognized that loss of dystrophin influences muscle autophagy.[221,222] Hence, modulating or enhancing autophagy could theoretically improve DMD pathogenesis. Several studies show that upregulation of autophagy by rapamycin can significantly ameliorate muscle pathology.[222,223] However, improvement on muscle function was moderate.[222] By delivering rapamycin in nanoparticles, Bibee et al. showed a much better enhancement of muscle function.[222] These findings suggest that nanoparticle delivery may also greatly improve the therapeutic outcomes of drugs targeting dystrophic mechanisms such as fibrosis and inflammation.

CONCLUSION

The small size and modular flexibility of the nanotechnology provides an excellent platform for the development of drug and gene therapies that target the etiology of DMD. Improvements in analytical chemistry, instrumentation, structural biology, protein and nucleic acid engineering, and the availability of nanomaterials have fostered an explosion in nanotechnology for DMD in the last decade. The regulatory approval of the read-through drug Ataluren and exon-skipping drug Exondys51 has set good examples on the path forward for DMD nanotherapy. Rapid advance in the nanotechnology offers an expanding repertoire of candidate therapies for DMD. Preclinical studies in small and large animals as well as early phase human trials have been instrumental in the development of nanotherapy for DMD. It is clear from these studies that some of the strategies (such as naked plasmid injection and adenovirus gene therapy) will not be appropriate for DMD therapy. However, some of the emerging new technologies (such as nanoparticle-AONs and AAV micro-dystrophin vectors) are likely going to change the landscape of DMD nanotherapy in next few years. With the extensive possibilities of nanotechnology, the future of etiology-based DMD therapies should be very exciting in the coming years.

ACKNOWLEDGMENTS

The Duchenne muscular dystrophy gene therapy research in the Duan lab is currently supported by the National Institutes of Health (NS-90634, AR-69085, AR-67985 and AR-70517), Department of Defense (MD130014 and MD150133), Jesse's Journey-The Foundation for Gene and Cell Therapy, Jackson Freel DMD Research Fund, Solid GT LLC and the University of Missouri.

REFERENCES

1. Mendell JR, Lloyd-Puryear M. Report of MDA muscle disease symposium on newborn screening for Duchenne muscular dystrophy. *Muscle Nerve* 2013, 48:21–26.
2. Romitti PA, Zhu Y, Puzhankara S, James KA, Nabukera SK, Zamba GK, Ciafaloni E, Cunniff C, Druschel CM, Mathews KD, et al. Prevalence of Duchenne and Becker muscular dystrophies in the United States. *Pediatrics* 2015, 135:513–521. (Epub ahead of print; February 16, 2015).
3. Mah JK, Korngut L, Dykeman J, Day L, Pringsheim T, Jette N. A systematic review and meta-analysis on the epidemiology of Duchenne and Becker muscular dystrophy. *Neuromuscul Disord* 2014, 24:482–491.
4. Bushby K, Finkel R, Birnkrant DJ, Case LE, Clemens PR, Cripe L, Kaul A, Kinnett K, McDonald C, Pandya S, et al. Diagnosis and management of Duchenne muscular dystrophy, part 1: diagnosis, and pharmacological and psychosocial management. *Lancet Neurol* 2010, 9:77–93.
5. Danialou G, Comtois AS, Dudley R, Karpati G, Vincent G, Des Rosiers C, Petrof BJ. Dystrophin-deficient cardiomyocytes are abnormally vulnerable to mechanical stress-induced contractile failure and injury. *FASEB J* 2001, 15:1655–1657.
6. McNally EM, Kaltman JR, Benson DW, Canter CE, Cripe LH, Duan D, Finder JD, Groh WJ, Hoffman EP, Judge DP, et al. Contemporary cardiac issues in Duchenne muscular dystrophy. Working Group of the National Heart, Lung, and Blood Institute in collaboration with Parent Project Muscular Dystrophy. *Circulation* 2015, 131:1590–1598.
7. Bello L, Gordish-Dressman H, Morgenroth LP, Henricson EK, Duong T, Hoffman EP, Cnaan A, McDonald CM, CINRG Investigators. Prednisone/prednisolone and deflazacort regimens in the CINRG Duchenne Natural History Study. *Neurology* 2015, 85:1048–1055.
8. Pane M, Fanelli L, Mazzone ES, Olivieri G, D'Amico A, Messina S, Scutifero M, Battini R, Petillo R, Frosini S, et al. Benefits of glucocorticoids in non-ambulant boys/men with Duchenne muscular dystrophy: a multicentric longitudinal study using the Performance of Upper Limb test. *Neuromuscul Disord* 2015, 25:749–753.
9. Tandon A, Villa CR, Hor KN, Jefferies JL, Gao Z, Towbin JA, Wong BL, Mazur W, Fleck RJ, Sticka JJ, et al. Myocardial fibrosis burden predicts left ventricular ejection fraction and is associated with age and steroid treatment duration in Duchenne muscular dystrophy. *J Am Heart Assoc* 2015, 4:e001338.
10. Ricotti V, Ridout DA, Muntoni F. Steroids in Duchenne muscular dystrophy. *Neuromuscul Disord* 2013, 23:696–697.
11. Ricotti V, Ridout DA, Scott E, Quinlivan R, Robb SA, Manzur AY, Muntoni F, NorthStar CN. Long-term benefits and adverse effects of intermittent versus daily glucocorticoids in boys with Duchenne muscular dystrophy. *J Neurol Neurosurg Psychiatry* 2013, 84:698–705.
12. Kim Y, Tewari M, Pajerowski JD, Cai S, Sen S, Williams JH, Sirsi SR, Lutz GJ, Discher DE. Polymersome delivery of siRNA and antisense oligonucleotides. *J Control Release* 2009, 134:132–140.
13. Afzal E, Zakeri S, Keyhanvar P, Bagheri M, Mahjoubi P, Asadian M, Omoomi N, Dehqanian M, Ghalandarlaki N, Darvishmohammadi T, et al. Nanolipodendrosome-loaded glatiramer acetate and myogenic differentiation 1 as augmentation therapeutic strategy approaches in muscular dystrophy. *Int J Nanomed* 2013, 8:2943–2960.
14. Negishi Y, Ishii Y, Shiono H, Akiyama S, Sekine S, Kojima T, Mayama S, Kikuchi T, Hamano N, Endo-Takahashi Y, et al. Bubble liposomes and ultrasound exposure improve localized morpholino oligomer delivery into the skeletal muscles of dystrophic mdx mice. *Mol Pharm* 2014, 11:1053–1061.
15. Ezzat K, Aoki Y, Koo T, McClorey G, Benner L, Coenen-Stass A, O'Donovan L, Lehto T, Garcia-Guerra A, Nordin J, et al. Self-assembly into nanoparticles is essential for receptor mediated uptake of therapeutic antisense oligonucleotides. *Nano Lett* 2015, 15:4364–4373.
16. Gao X, Shen X, Dong X, Ran N, Han G, Cao L, Gu B, Yin H. Peptide nucleic acid promotes systemic dystrophin expression and functional rescue in dystrophin-deficient mdx mice. *Mol Ther Nucleic Acids* 2015, 4:e255.

17. Lehto T, Castillo Alvarez A, Gauck S, Gait MJ, Coursindel T, Wood MJ, Lebleu B, Boisguerin P. Cellular trafficking determines the exon skipping activity of Pip6a-PMO in mdx skeletal and cardiac muscle cells. *Nucleic Acids Res* 2014, 42:3207–3217.
18. Shabanpoor F, McClorey G, Saleh AF, Jarver P, Wood MJ, Gait MJ. Bi-specific splice-switching PMO oligonucleotides conjugated via a single peptide active in a mouse model of Duchenne muscular dystrophy. *Nucleic Acids Res* 2015, 43:29–39.
19. Rimessi P, Sabatelli P, Fabris M, Braghetta P, Bassi E, Spitali P, Vattemi G, Tomelleri G, Mari L, Perrone D, et al. Cationic PMMA nanoparticles bind and deliver antisense oligoribonucleotides allowing restoration of dystrophin expression in the mdx mouse. *Mol Ther* 2009, 17:820–827.
20. Ferlini A, Sabatelli P, Fabris M, Bassi E, Falzarano S, Vattemi G, Perrone D, Gualandi F, Maraldi NM, Merlini L, et al. Dystrophin restoration in skeletal, heart and skin arrector pili smooth muscle of mdx mice by ZM2 NP-AON complexes. *Gene Ther* 2010, 17:432–438.
21. Bassi E, Falzarano S, Fabris M, Gualandi F, Merlini L, Vattemi G, Perrone D, Marchesi E, Sabatelli P, Sparnacci K, et al. Persistent dystrophin protein restoration 90 days after a course of intraperitoneally administered naked 2′OMePS AON and ZM2 NP-AON complexes in mdx mice. *J Biomed Biotechnol* 2012, 2012:897076.
22. Falzarano MS, Passarelli C, Bassi E, Fabris M, Perrone D, Sabatelli P, Maraldi NM, Dona S, Selvatici R, Bonaldo P, et al. Biodistribution and molecular studies on orally administered nanoparticle-AON complexes encapsulated with alginate aiming at inducing dystrophin rescue in mdx mice. *Biomed Res Int* 2013, 2013:527418.
23. Mendell JR, Campbell K, Rodino-Klapac L, Sahenk Z, Shilling C, Lewis S, Bowles D, Gray S, Li C, Galloway G, et al. Dystrophin immunity in Duchenne's muscular dystrophy. *N Engl J Med* 2010, 363:1429–1437.
24. Yue Y, Pan X, Hakim CH, Kodippili K, Zhang K, Shin JH, Yang HT, McDonald T, Duan D. Safe and bodywide muscle transduction in young adult Duchenne muscular dystrophy dogs with adeno-associated virus. *Hum Mol Genet* 2015, 24:5880–5890.
25. Nelson CE, Hakim CH, Ousterout DG, Thakore PI, Moreb EA, Castellanos Rivera RM, Madhavan S, Pan X, Ran FA, Yan WX, et al. In vivo genome editing improves muscle function in a mouse model of Duchenne muscular dystrophy. *Science* 2016, 351:403–407.
26. DelloRusso C, Scott JM, Hartigan-O'Connor D, Salvatori G, Barjot C, Robinson AS, Crawford RW, Brooks SV, Chamberlain JS. Functional correction of adult mdx mouse muscle using gutted adenoviral vectors expressing full-length dystrophin. *Proc Natl Acad Sci USA* 2002, 99:12979–12984.
27. Deol JR, Danialou G, Larochelle N, Bourget M, Moon JS, Liu AB, Gilbert R, Petrof BJ, Nalbantoglu J, Karpati G. Successful compensation for dystrophin deficiency by a helper-dependent adenovirus expressing full-length utrophin. *Mol Ther* 2007, 15:1767–1774.
28. Maggio I, Stefanucci L, Janssen JM, Liu J, Chen X, Mouly V, Goncalves MA. Selection-free gene repair after adenoviral vector transduction of designer nucleases: rescue of dystrophin synthesis in DMD muscle cell populations. *Nucleic Acids Res* 2016, 44:1449–1470.
29. Muir LA, Nguyen QG, Hauschka SD, Chamberlain JS. Engraftment potential of dermal fibroblasts following in vivo myogenic conversion in immunocompetent dystrophic skeletal muscle. *Mol Ther Methods Clin Dev* 2014, 1:14025.
30. Naldini L, Trono D, Verma IM. Lentiviral vectors, two decades later. *Science* 2016, 353:1101–1102.
31. Nigro G, Comi LI, Politano L, Bain RJ. The incidence and evolution of cardiomyopathy in Duchenne muscular dystrophy. *Int J Cardiol* 1990, 26:271–277.
32. Kamdar F, Garry DJ. Dystrophin-deficient cardiomyopathy. *J Am Coll Cardiol* 2016, 67:2533–2546.
33. Malik V, Rodino-Klapac LR, Viollet L, Wall C, King W, Al-Dahhak R, Lewis S, Shilling CJ, Kota J, Serrano-Munuera C, et al. Gentamicin-induced readthrough of stop codons in Duchenne muscular dystrophy. *Ann Neurol* 2010, 67:771–780.
34. Welch EM, Barton ER, Zhuo J, Tomizawa Y, Friesen WJ, Trifillis P, Paushkin S, Patel M, Trotta CR, Hwang S, et al. PTC124 targets genetic disorders caused by nonsense mutations. *Nature* 2007, 447:87–91.
35. Auld DS, Thorne N, Maguire WF, Inglese J. Mechanism of PTC124 activity in cell-based luciferase assays of nonsense codon suppression. *Proc Natl Acad Sci USA* 2009, 106:3585–3590.
36. McElroy SP, Nomura T, Torrie LS, Warbrick E, Gartner U, Wood G, McLean WH. A lack of premature termination codon read-through efficacy of PTC124 (Ataluren) in a diverse array of reporter assays. *PLoS Biol* 2013, 11:e1001593.
37. Bushby K, Finkel R, Wong B, Barohn R, Campbell C, Comi GP, Connolly AM, Day JW, Flanigan KM, Goemans N, et al. Ataluren treatment of patients with nonsense mutation dystrophinopathy. *Muscle Nerve* 2014, 50:477–487.
38. Haas M, Vlcek V, Balabanov P, Salmonson T, Bakchine S, Markey G, Weise M, Schlosser-Weber G, Brohmann H, Yerro CP, et al. European Medicines Agency review of ataluren for the treatment of ambulant patients aged 5 years and older with Duchenne muscular dystrophy resulting from a nonsense

mutation in the dystrophin gene. *Neuromuscul Disord* 2015, 25:5–13.

39. Gintjee TJ, Magh AS, Bertoni C. High throughput screening in Duchenne muscular dystrophy: from drug discovery to functional genomics. *Biology (Basel)* 2014, 3:752–780.
40. Wolff JA, Malone RW, Williams P, Chong W, Acsadi G, Jani A, Felgner PL. Direct gene transfer into mouse muscle in vivo. *Science* 1990, 247:1465–1468.
41. Acsadi G, Dickson G, Love DR, Jani A, Walsh FS, Gurusinghe A, Wolff JA, Davies KE. Human dystrophin expression in mdx mice after intramuscular injection of DNA constructs. *Nature* 1991, 352:815–818.
42. Danialou G, Comtois AS, Dudley RW, Nalbantoglu J, Gilbert R, Karpati G, Jones DH, Petrof BJ. Ultrasound increases plasmid-mediated gene transfer to dystrophic muscles without collateral damage. *Mol Ther* 2002, 6:687–693.
43. Pichavant C, Chapdelaine P, Cerri DG, Bizario JC, Tremblay JP. Electrotransfer of the full-length dog dystrophin into mouse and dystrophic dog muscles. *Hum Gene Ther* 2010, 21:1591–1601.
44. Romero NB, Benveniste O, Payan C, Braun S, Squiban P, Herson S, Fardeau M. Current protocol of a research phase I clinical trial of full-length dystrophin plasmid DNA in Duchenne/Becker muscular dystrophies. Part II: clinical protocol. *Neuromuscul Disord* 2002, 12(suppl 1):S45–48.
45. Duan D. Myodys, a full-length dystrophin plasmid vector for Duchenne and Becker muscular dystrophy gene therapy. *Curr Opin Mol Ther* 2008, 10:86–94.
46. Kinali M, Arechavala-Gomeza V, Feng L, Cirak S, Hunt D, Adkin C, Guglieri M, Ashton E, Abbs S, Nihoyannopoulos P, et al. Local restoration of dystrophin expression with the morpholino oligomer AVI-4658 in Duchenne muscular dystrophy: a single-blind, placebo-controlled, dose-escalation, proof-of-concept study. *Lancet Neurol* 2009, 8:918–928.
47. Goyenvalle A, Griffith G, Babbs A, El Andaloussi S, Ezzat K, Avril A, Dugovic B, Chaussenot R, Ferry A, Voit T, et al. Functional correction in mouse models of muscular dystrophy using exon-skipping tricyclo-DNA oligomers. *Nat Med* 2015, 21:270–275.
48. Moulton HM, Wu B, Jearawiriyapaisarn N, Sazani P, Lu QL, Kole R. Peptide-morpholino conjugate: a promising therapeutic for Duchenne muscular dystrophy. *Ann N Y Acad Sci* 2009, 1175:55–60.
49. Wu B, Li Y, Morcos PA, Doran TJ, Lu P, Lu QL. Octa-guanidine morpholino restores dystrophin expression in cardiac and skeletal muscles and ameliorates pathology in dystrophic mdx mice. *Mol Ther* 2009, 17:864–871.
50. Aoki Y, Yokota T, Nagata T, Nakamura A, Tanihata J, Saito T, Duguez SM, Nagaraju K, Hoffman EP, Partridge T, et al. Bodywide skipping of exons 45–55 in dystrophic mdx52 mice by systemic antisense delivery. *Proc Natl Acad Sci USA* 2012, 109:13763–13768.
51. Yokota T, Nakamura A, Nagata T, Saito T, Kobayashi M, Aoki Y, Echigoya Y, Partridge T, Hoffman EP, Takeda S. Extensive and prolonged restoration of dystrophin expression with vivo-morpholino-mediated multiple exon skipping in dystrophic dogs. *Nucleic Acid Ther* 2012, 22:306–315.
52. Echigoya Y, Aoki Y, Miskew B, Panesar D, Touznik A, Nagata T, Tanihata J, Nakamura A, Nagaraju K, Yokota T. Long-term efficacy of systemic multiexon skipping targeting dystrophin exons 45–55 with a cocktail of vivo-morpholinos in mdx52 mice. *Mol Ther Nucleic Acids* 2015, 4:e225.
53. van Hest JC, Delnoye DA, Baars MW, van Genderen MH, Meijer EW. Polystyrene-dendrimer amphiphilic block copolymers with a generation-dependent aggregation. *Science* 1995, 268:1592–1595.
54. Zhang L, Eisenberg A. Multiple morphologies of "crew-cut" aggregates of polystyrene-b-poly(acrylic acid) block copolymers. *Science* 1995, 268:1728–1731.
55. Discher BM, Won YY, Ege DS, Lee JC, Bates FS, Discher DE, Hammer DA. Polymersomes: tough vesicles made from diblock copolymers. *Science* 1999, 284:1143–1146.
56. Lee JS, Feijen J. Biodegradable polymersomes as carriers and release systems for paclitaxel using Oregon Green(R) 488 labeled paclitaxel as a model compound. *J Control Release* 2012, 158:312–318.
57. Discher DE, Eisenberg A. Polymer vesicles. *Science* 2002, 297:967–973.
58. Graff A, Sauer M, Van Gelder P, Meier W. Virus-assisted loading of polymer nanocontainer. *Proc Natl Acad Sci USA* 2002, 99:5064–5068.
59. Wang M, Wu B, Tucker JD, Bollinger LE, Lu P, Lu Q. Poly(ester amine) composed of polyethylenimine and pluronic enhance delivery of antisense oligonucleotides in vitro and in dystrophic mdx mice. *Mol Ther Nucleic Acids* 2016, 5:e341.
60. Wang M, Wu B, Lu P, Tucker JD, Milazi S, Shah SN, Lu QL. Pluronic-PEI copolymers enhance exon-skipping of 2′-O-methyl phosphorothioate oligonucleotide in cell culture and dystrophic mdx mice. *Gene Ther* 2014, 21:52–59.
61. Wang M, Tucker JD, Lu P, Wu B, Cloer C, Lu Q. Tris[2-(acryloyloxy)ethyl]isocyanurate cross-linked low-molecular-weight polyethylenimine as gene delivery carriers in cell culture and dystrophic mdx mice. *Bioconjug Chem* 2012, 23:837–845.
62. Wang M, Wu B, Tucker JD, Lu P, Lu Q. Tris[2-(acryloyloxy)ethyl]isocyanurate cross-linked polyethylenimine enhanced exon-skipping of antisense 2′-O-

methyl phosphorothioate oligonucleotide in vitro and in vivo. *J Nanomed Nanotechnol* 2015, 6:1000261.

63. Allen TM, Cullis PR. Liposomal drug delivery systems: from concept to clinical applications. *Adv Drug Deliv Rev* 2013, 65:36–48.
64. Fraley R, Straubinger RM, Rule G, Springer EL, Papahadjopoulos D. Liposome-mediated delivery of deoxyribonucleic acid to cells: enhanced efficiency of delivery related to lipid composition and incubation conditions. *Biochemistry* 1981, 20:6978–6987.
65. Fraley R, Subramani S, Berg P, Papahadjopoulos D. Introduction of liposome-encapsulated SV40 DNA into cells. *J Biol Chem* 1980, 255:10431–10435.
66. Prakash TP, Lima WF, Murray HM, Elbashir S, Cantley W, Foster D, Jayaraman M, Chappell AE, Manoharan M, Swayze EE, et al. Lipid nanoparticles improve activity of single-stranded siRNA and gapmer antisense oligonucleotides in animals. *ACS Chem Biol* 2013, 8:1402–1406.
67. Falzarano MS, Passarelli C, Ferlini A. Nanoparticle delivery of antisense oligonucleotides and their application in the exon skipping strategy for Duchenne muscular dystrophy. *Nucleic Acid Ther* 2014, 24:87–100.
68. Negishi Y, Endo Y, Fukuyama T, Suzuki R, Takizawa T, Omata D, Maruyama K, Aramaki Y. Delivery of siRNA into the cytoplasm by liposomal bubbles and ultrasound. *J Control Release* 2008, 132:124–130.
69. Jarver P, Coursindel T, Andaloussi SE, Godfrey C, Wood MJ, Gait MJ. Peptide-mediated cell and in vivo delivery of antisense oligonucleotides and siRNA. *Mol Ther Nucleic Acids* 2012, 1:e27.
70. Betts CA, Wood MJ. Cell penetrating peptide delivery of splice directing oligonucleotides as a treatment for Duchenne muscular dystrophy. *Curr Pharm Des* 2013, 19:2948–2962.
71. Boisguerin P, Deshayes S, Gait MJ, O'Donovan L, Godfrey C, Betts CA, Wood MJ, Lebleu B. Delivery of therapeutic oligonucleotides with cell penetrating peptides. *Adv Drug Deliv Rev* 2015, 87:52–67.
72. Nance ME, Duan D. Perspective on adeno-associated virus capsid modification for Duchenne muscular dystrophy gene therapy. *Hum Gene Ther* 2015, 26:786–800.
73. Wu B, Moulton HM, Iversen PL, Jiang J, Li J, Spurney CF, Sali A, Guerron AD, Nagaraju K, Doran T, et al. Effective rescue of dystrophin improves cardiac function in dystrophin-deficient mice by a modified morpholino oligomer. *Proc Natl Acad Sci USA* 2008, 105:14814–14819.
74. Yin H, Moulton HM, Seow Y, Boyd C, Boutilier J, Iverson P, Wood MJ. Cell-penetrating peptide-conjugated antisense oligonucleotides restore systemic muscle and cardiac dystrophin expression and function. *Hum Mol Genet* 2008, 17:3909–3918.
75. Yin H, Lu Q, Wood M. Effective exon skipping and restoration of dystrophin expression by peptide nucleic acid antisense oligonucleotides in mdx mice. *Mol Ther* 2008, 16:38–45.
76. Jearawiriyapaisarn N, Moulton HM, Buckley B, Roberts J, Sazani P, Fucharoen S, Iversen PL, Kole R. Sustained dystrophin expression induced by peptide-conjugated morpholino oligomers in the muscles of mdx mice. *Mol Ther* 2008, 16:1624–1629.
77. Jearawiriyapaisarn N, Moulton HM, Sazani P, Kole R, Willis MS. Long-term improvement in mdx cardiomyopathy after therapy with peptide-conjugated morpholino oligomers. *Cardiovasc Res* 2010, 85:444–453.
78. Yin H, Moulton HM, Betts C, Seow Y, Boutilier J, Iverson PL, Wood MJ. A fusion peptide directs enhanced systemic dystrophin exon skipping and functional restoration in dystrophin-deficient mdx mice. *Hum Mol Genet* 2009, 18:4405–4414.
79. Yin H, Betts C, Saleh AF, Ivanova GD, Lee H, Seow Y, Kim D, Gait MJ, Wood MJ. Optimization of peptide nucleic acid antisense oligonucleotides for local and systemic dystrophin splice correction in the mdx mouse. *Mol Ther* 2010, 18:819–827.
80. Yin H, Saleh AF, Betts C, Camelliti P, Seow Y, Ashraf S, Arzumanov A, Hammond S, Merritt T, Gait MJ, et al. Pip5 transduction peptides direct high efficiency oligonucleotide-mediated dystrophin exon skipping in heart and phenotypic correction in mdx mice. *Mol Ther* 2011, 19:1295–1303.
81. Jirka SM, Heemskerk H, Tanganyika-de Winter CL, Muilwijk D, Pang KH, de Visser PC, Janson A, Karnaoukh TG, Vermue R, t Hoen PA, et al. Peptide conjugation of 2′-O-methyl phosphorothioate antisense oligonucleotides enhances cardiac uptake and exon skipping in mdx mice. *Nucleic Acid Ther* 2014, 24:25–36.
82. Betts C, Saleh AF, Arzumanov AA, Hammond SM, Godfrey C, Coursindel T, Gait MJ, Wood MJ. Pip6-PMO, a new generation of peptide-oligonucleotide conjugates with improved cardiac exon skipping activity for DMD treatment. *Mol Ther Nucleic Acids* 2012, 1:e38.
83. Betts CA, Saleh AF, Carr CA, Hammond SM, Coenen-Stass AM, Godfrey C, McClorey G, Varela MA, Roberts TC, Clarke K, et al. Prevention of exercised induced cardiomyopathy following Pip-PMO treatment in dystrophic mdx mice. *Sci Rep* 2015, 5:8986.
84. Lee Y, El Andaloussi S, Wood MJ. Exosomes and microvesicles: extracellular vesicles for genetic information transfer and gene therapy. *Hum Mol Genet* 2012, 21:R125–134.
85. Leroyer AS, Ebrahimian TG, Cochain C, Recalde A, Blanc-Brude O, Mees B, Vilar J, Tedgui A, Levy BI, Chimini G, et al. Microparticles from ischemic muscle

promotes postnatal vasculogenesis. *Circulation* 2009, 119:2808–2817.

86. Chen L, Wang Y, Pan Y, Zhang L, Shen C, Qin G, Ashraf M, Weintraub N, Ma G, Tang Y. Cardiac progenitor-derived exosomes protect ischemic myocardium from acute ischemia/reperfusion injury. *Biochem Biophys Res Commun* 2013, 431:566–571.
87. Ibrahim AG, Cheng K, Marban E. Exosomes as critical agents of cardiac regeneration triggered by cell therapy. *Stem Cell Rep* 2014, 2:606–619.
88. Alvarez-Erviti L, Seow Y, Yin H, Betts C, Lakhal S, Wood MJ. Delivery of siRNA to the mouse brain by systemic injection of targeted exosomes. *Nat Biotechnol* 2011, 29:341–345.
89. Fiorillo AA, Heier CR, Novak JS, Tully CB, Brown KJ, Uaesoontrachoon K, Vila MC, Ngheim PP, Bello L, Kornegay JN, et al. TNF-alpha-induced microRNAs control dystrophin expression in Becker muscular dystrophy. *Cell Rep* 2015, 12:1678–1690.
90. Alexander MS, Casar JC, Motohashi N, Vieira NM, Eisenberg I, Marshall JL, Gasperini MJ, Lek A, Myers JA, Estrella EA, et al. MicroRNA-486-dependent modulation of DOCK3/PTEN/AKT signaling pathways improves muscular dystrophy-associated symptoms. *J Clin Invest* 2014, 124:2651–2667.
91. Liu N, Williams AH, Maxeiner JM, Bezprozvannaya S, Shelton JM, Richardson JA, Bassel-Duby R, Olson EN. microRNA-206 promotes skeletal muscle regeneration and delays progression of Duchenne muscular dystrophy in mice. *J Clin Invest* 2012, 122:2054–2065.
92. Perry MM, Muntoni F. Noncoding RNAs and Duchenne muscular dystrophy. *Epigenomics* 2016, 8:1527–1537.
93. Naldini L, Verma IM. Lentiviral vectors. *Adv Virus Res* 2000, 55:599–609.
94. Kobinger GP, Louboutin JP, Barton ER, Sweeney HL, Wilson JM. Correction of the dystrophic phenotype by in vivo targeting of muscle progenitor cells. *Hum Gene Ther* 2003, 14:1441–1449.
95. Kimura E, Li S, Gregorevic P, Fall BM, Chamberlain JS. Dystrophin delivery to muscles of mdx mice using lentiviral vectors leads to myogenic progenitor targeting and stable gene expression. *Mol Ther* 2010, 18:206–213.
96. Li S, Kimura E, Fall BM, Reyes M, Angello JC, Welikson R, Hauschka SD, Chamberlain JS. Stable transduction of myogenic cells with lentiviral vectors expressing a minidystrophin. *Gene Ther* 2005, 12:1099–1108.
97. Bachrach E, Li S, Perez AL, Schienda J, Liadaki K, Volinski J, Flint A, Chamberlain J, Kunkel LM. Systemic delivery of human microdystrophin to regenerating mouse dystrophic muscle by muscle progenitor cells. *Proc Natl Acad Sci USA* 2004, 101:3581–3586.
98. Goncalves MA, de Vries AA, Holkers M, van de Watering MJ, van der Velde I, van Nierop GP, Valerio D, Knaan-Shanzer S. Human mesenchymal stem cells ectopically expressing full-length dystrophin can complement Duchenne muscular dystrophy myotubes by cell fusion. *Hum Mol Genet* 2006, 15:213–221.
99. Quenneville SP, Chapdelaine P, Skuk D, Paradis M, Goulet M, Rousseau J, Xiao X, Garcia L, Tremblay JP. Autologous transplantation of muscle precursor cells modified with a lentivirus for muscular dystrophy: human cells and primate models. *Mol Ther* 2007, 15:431–438.
100. Pichavant C, Chapdelaine P, Cerri DG, Dominique JC, Quenneville SP, Skuk D, Kornegay JN, Bizario JC, Xiao X, Tremblay JP. Expression of dog microdystrophin in mouse and dog muscles by gene therapy. *Mol Ther* 2010, 18:1002–1009.
101. Benchaouir R, Meregalli M, Farini A, D'Antona G, Belicchi M, Goyenvalle A, Battistelli M, Bresolin N, Bottinelli R, Garcia L, et al. Restoration of human dystrophin following transplantation of exon-skipping-engineered DMD patient stem cells into dystrophic mice. *Cell Stem Cell* 2007, 1:646–657.
102. Cazzella V, Martone J, Pinnaro C, Santini T, Twayana SS, Sthandier O, D'Amico A, Ricotti V, Bertini E, Muntoni F, et al. Exon 45 skipping through U1-snRNA antisense molecules recovers the Dys-nNOS pathway and muscle differentiation in human DMD myoblasts. *Mol Ther* 2012, 20:2134–2142.
103. Ragot T, Vincent N, Chafey P, Vigne E, Gilgenkrantz H, Couton D, Cartaud J, Briand P, Kaplan JC, Perricaudet M, et al. Efficient adenovirus-mediated transfer of a human minidystrophin gene to skeletal muscle of mdx mice. *Nature* 1993, 361:647–650.
104. Kochanek S, Clemens PR, Mitani K, Chen HH, Chan S, Caskey CT. A new adenoviral vector: replacement of all viral coding sequences with 28 kb of DNA independently expressing both full-length dystrophin and beta-galactosidase. *Proc Natl Acad Sci USA* 1996, 93:5731–5736.
105. Xu L, Park KH, Zhao L, Xu J, El Refaey M, Gao Y, Zhu H, Ma J, Han R. CRISPR-mediated genome editing restores dystrophin expression and function in mdx mice. *Mol Ther* 2016, 24:564–569.
106. Duan D. Dystrophin gene replacement and gene repair therapy for Duchenne muscular dystrophy in 2016. *Hum Gene Ther Clin Dev* 2016, 27:9–18.
107. Bengtsson NE, Seto JT, Hall JK, Chamberlain JS, Odom GL. Progress and prospects of gene therapy clinical trials for the muscular dystrophies. *Hum Mol Genet* 2015, 25:R9–17. (Epub ahead of print; October 8, 2015).

108. Muzyczka N. Use of adeno-associated virus as a general transduction vector for mammalian cells. *Curr Top Microbiol Immunol* 1992, 158:97–129.

109. Carter BJ. Adeno-associated virus and the development of adeno-associated virus vectors: a historical perspective. *Mol Ther* 2004, 10:981–989.

110. Samulski RJ, Muzyczka N. AAV-mediated gene therapy for research and therapeutic purposes. *Annu Rev Virol* 2014, 1:427–451.

111. Muzyczka N, Berns KI. AAV's golden jubilee. *Mol Ther* 2015, 23:807–808.

112. Atchison RW, Casto BC, Hammon WM. Adenovirus-associated defective virus particles. *Science* 1965, 149:754–756.

113. Duan D, Sharma P, Yang J, Yue Y, Dudus L, Zhang Y, Fisher KJ, Engelhardt JF. Circular intermediates of recombinant adeno-associated virus have defined structural characteristics responsible for long term episomal persistence in muscle. *J Virol* 1998, 72:8568–8577.

114. Duan D. Systemic delivery of adeno-associated viral vectors. *Curr Opin Virol* 2016, 21:16–25.

115. Wu Z, Asokan A, Grieger JC, Govindasamy L, Agbandje-McKenna M, Samulski RJ. Single amino acid changes can influence titer, heparin binding, and tissue tropism in different adeno-associated virus serotypes. *J Virol* 2006, 80:11393–11397.

116. Gao G, Vandenberghe LH, Wilson JM. New recombinant serotypes of AAV vectors. *Curr Gene Ther* 2005, 5:285–297.

117. Vandenberghe LH, Wilson JM, Gao G. Tailoring the AAV vector capsid for gene therapy. *Gene Ther* 2009, 16:311–319.

118. Daya S, Berns KI. Gene therapy using adeno-associated virus vectors. *Clin Microbiol Rev* 2008, 21:583–593.

119. Kotterman MA, Schaffer DV. Engineering adeno-associated viruses for clinical gene therapy. *Nat Rev Genet* 2014, 15:445–451.

120. Santiago-Ortiz J, Ojala DS, Westesson O, Weinstein JR, Wong SY, Steinsapir A, Kumar S, Holmes I, Schaffer DV. AAV ancestral reconstruction library enables selection of broadly infectious viral variants. *Gene Ther* 2015, 22:934–946.

121. Zinn E, Pacouret S, Khaychuk V, Turunen HT, Carvalho LS, Andres-Mateos E, Shah S, Shelke R, Maurer AC, Plovie E, et al. In silico reconstruction of the viral evolutionary lineage yields a potent gene therapy vector. *Cell Rep* 2015, 12:1056–1068.

122. Van Vliet KM, Blouin V, Brument N, Agbandje-McKenna M, Snyder RO. The role of the adeno-associated virus capsid in gene transfer. *Methods Mol Biol* 2008, 437:51–91.

123. Drouin LM, Agbandje-McKenna M. Adeno-associated virus structural biology as a tool in vector development. *Future Virol* 2013, 8:1183–1199.

124. Agbandje-McKenna M, Kleinschmidt J. AAV capsid structure and cell interactions. *Methods Mol Biol* 2011, 807:47–92.

125. Srivastava A. In vivo tissue-tropism of adeno-associated viral vectors. *Curr Opin Virol* 2016, 21:75–80.

126. Lai Y, Yue Y, Bostick B, Duan D. Delivering large therapeutic genes for muscle gene therapy. In: Duan D, ed. *Muscle Gene Therapy*. New York: Springer Science + Business Media, LLC; 2010, 205–218.

127. Yuasa K, Miyagoe Y, Yamamoto K, Nabeshima Y, Dickson G, Takeda S. Effective restoration of dystrophin-associated proteins in vivo by adenovirus-mediated transfer of truncated dystrophin cDNAs. *FEBS Lett* 1998, 425:329–336.

128. Wang B, Li J, Xiao X. Adeno-associated virus vector carrying human minidystrophin genes effectively ameliorates muscular dystrophy in mdx mouse model. *Proc Natl Acad Sci USA* 2000, 97:13714–13719.

129. Harper SQ, Hauser MA, DelloRusso C, Duan D, Crawford RW, Phelps SF, Harper HA, Robinson AS, Engelhardt JF, Brooks SV, et al. Modular flexibility of dystrophin: implications for gene therapy of Duchenne muscular dystrophy. *Nat Med* 2002, 8:253–261.

130. Wang B, Li J, Fu FH, Xiao X. Systemic human minidystrophin gene transfer improves functions and life span of dystrophin and dystrophin/utrophin-deficient mice. *J Orthop Res* 2009, 27:421–426.

131. Yue Y, Li Z, Harper SQ, Davisson RL, Chamberlain JS, Duan D. Microdystrophin gene therapy of cardiomyopathy restores dystrophin-glycoprotein complex and improves sarcolemma integrity in the mdx mouse heart. *Circulation* 2003, 108:1626–1632.

132. Liu M, Yue Y, Harper SQ, Grange RW, Chamberlain JS, Duan D. Adeno-associated virus-mediated microdystrophin expression protects young mdx muscle from contraction-induced injury. *Mol Ther* 2005, 11:245–256.

133. Yue Y, Liu M, Duan D. C-terminal truncated microdystrophin recruits dystrobrevin and syntrophin to the dystrophin-associated glycoprotein complex and reduces muscular dystrophy in symptomatic utrophin/dystrophin double knock-out mice. *Mol Ther* 2006, 14:79–87.

134. Bostick B, Yue Y, Lai Y, Long C, Li D, Duan D. Adeno-associated virus serotype-9 microdystrophin gene therapy ameliorates electrocardiographic abnormalities in mdx mice. *Hum Gene Ther* 2008, 19:851–856.

135. Lai Y, Thomas GD, Yue Y, Yang HT, Li D, Long C, Judge L, Bostick B, Chamberlain JS, Terjung RL, et al. Dystrophins carrying spectrin-like repeats 16 and 17 anchor nNOS to the sarcolemma and enhance exercise performance in a mouse model of muscular dystrophy. *J Clin Invest* 2009, 119:624–635.

136. Bostick B, Shin J-H, Yue Y, Duan D. AAV-microdystrophin therapy improves cardiac performance in aged female mdx mice. *Mol Ther* 2011, 19:1826–1832.

137. Bostick B, Shin JH, Yue Y, Wasala NB, Lai Y, Duan D. AAV micro-dystrophin gene therapy alleviates stress-induced cardiac death but not myocardial fibrosis in >21-m-old mdx mice, an end-stage model of Duchenne muscular dystrophy cardiomyopathy. *J Mol Cell Cardiol* 2012, 53:217–222.

138. Gregorevic P, Blankinship MJ, Allen JM, Crawford RW, Meuse L, Miller DG, Russell DW, Chamberlain JS. Systemic delivery of genes to striated muscles using adeno-associated viral vectors. *Nat Med* 2004, 10:828–834.

139. Gregorevic P, Allen JM, Minami E, Blankinship MJ, Haraguchi M, Meuse L, Finn E, Adams ME, Froehner SC, Murry CE, et al. rAAV6-microdystrophin preserves muscle function and extends lifespan in severely dystrophic mice. *Nat Med* 2006, 12:787–789.

140. Percival JM, Gregorevic P, Odom GL, Banks GB, Chamberlain JS, Froehner SC. rAAV6-microdystrophin rescues aberrant Golgi complex organization in mdx skeletal muscles. *Traffic* 2007, 8:1424–1439.

141. Townsend D, Blankinship MJ, Allen JM, Gregorevic P, Chamberlain JS, Metzger JM. Systemic administration of micro-dystrophin restores cardiac geometry and prevents dobutamine-induced cardiac pump failure. *Mol Ther* 2007, 15:1086–1092.

142. Banks GB, Chamberlain JS, Froehner SC. Truncated dystrophins can influence neuromuscular synapse structure. *Mol Cell Neurosci* 2009, 40:433–441.

143. Gregorevic P, Blankinship MJ, Allen JM, Chamberlain JS. Systemic microdystrophin gene delivery improves skeletal muscle structure and function in old dystrophic mdx mice. *Mol Ther* 2008, 16:657–664.

144. Rodino-Klapac LR, Chicoine LG, Kaspar BK, Mendell JR. Gene therapy for Duchenne muscular dystrophy: expectations and challenges. *Arch Neurol* 2007, 64:1236–1241.

145. Yoshimura M, Sakamoto M, Ikemoto M, Mochizuki Y, Yuasa K, Miyagoe-Suzuki Y, Takeda S. AAV vector-mediated microdystrophin expression in a relatively small percentage of mdx myofibers improved the mdx phenotype. *Mol Ther* 2004, 10:821–828.

146. Banks GB, Judge LM, Allen JM, Chamberlain JS. The polyproline site in hinge 2 influences the functional capacity of truncated dystrophins. *PLoS Genet* 2010, 6:e1000958.

147. Foster H, Sharp PS, Athanasopoulos T, Trollet C, Graham IR, Foster K, Wells DJ, Dickson G. Codon and mRNA sequence optimization of microdystrophin transgenes improves expression and physiological outcome in dystrophic mdx mice following AAV2/8 gene transfer. *Mol Ther* 2008, 16:1825–1832.

148. Koo T, Malerba A, Athanasopoulos T, Trollet C, Boldrin L, Ferry A, Popplewell L, Foster H, Foster K, Dickson G. Delivery of AAV2/9-microdystrophin genes incorporating helix 1 of the coiled-coil motif in the C-terminal domain of dystrophin improves muscle pathology and restores the level of alpha1-syntrophin and alpha-dystrobrevin in skeletal muscles of mdx mice. *Hum Gene Ther* 2011, 22:1379–1388.

149. Duan D. Duchenne muscular dystrophy gene therapy in the canine model. *Hum Gene Ther Clin Dev* 2015, 26:57–69.

150. McGreevy JW, Hakim CH, McIntosh MA, Duan D. Animal models of Duchenne muscular dystrophy: from basic mechanisms to gene therapy. *Dis Model Mech* 2015, 8:195–213.

151. Wang Z, Allen JM, Riddell SR, Gregorevic P, Storb R, Tapscott SJ, Chamberlain JS, Kuhr CS. Immunity to adeno-associated virus-mediated gene transfer in a random-bred canine model of Duchenne muscular dystrophy. *Hum Gene Ther* 2007, 18:18–26.

152. Yue Y, Ghosh A, Long C, Bostick B, Smith BF, Kornegay JN, Duan D. A single intravenous injection of adeno-associated virus serotype-9 leads to whole body skeletal muscle transduction in dogs. *Mol Ther* 2008, 16:1944–1952.

153. Wang Z, Kuhr CS, Allen JM, Blankinship M, Gregorevic P, Chamberlain JS, Tapscott SJ, Storb R. Sustained AAV-mediated dystrophin expression in a canine model of Duchenne muscular dystrophy with a brief course of immunosuppression. *Mol Ther* 2007, 15:1160–1166.

154. Shin JH, Yue Y, Srivastava A, Smith B, Lai Y, Duan D. A simplified immune suppression scheme leads to persistent micro-dystrophin expression in Duchenne muscular dystrophy dogs. *Hum Gene Ther* 2012, 23:202–209.

155. Shin JH, Pan X, Hakim CH, Yang HT, Yue Y, Zhang K, Terjung RL, Duan D. Microdystrophin ameliorates muscular dystrophy in the canine model of Duchenne muscular dystrophy. *Mol Ther* 2013, 21:750–757.

156. Stamler JS, Meissner G. Physiology of nitric oxide in skeletal muscle. *Physiol Rev* 2001, 81:209–237.

157. Thomas GD, Victor RG. Nitric oxide mediates contraction-induced attenuation of sympathetic vasoconstriction in rat skeletal muscle. *J Physiol* 1998, 506:817–826.

158. Sander M, Chavoshan B, Harris SA, Iannaccone ST, Stull JT, Thomas GD, Victor RG. Functional muscle ischemia in neuronal nitric oxide synthase-deficient skeletal muscle of children with Duchenne muscular dystrophy. *Proc Natl Acad Sci USA* 2000, 97:13818–13823.

159. Li D, Yue Y, Lai Y, Hakim CH, Duan D. Nitrosative stress elicited by nNOSmu delocalization inhibits muscle force in dystrophin-null mice. *J Pathol* 2011, 223:88–98.

160. Thomas GD. Functional muscle ischemia in Duchenne and Becker muscular dystrophy. *Front Physiol* 2013, 4:381.

161. Rando TA. Role of nitric oxide in the pathogenesis of muscular dystrophies: a "two hit" hypothesis of the cause of muscle necrosis. *Microsc Res Tech* 2001, 55:223–235.

162. Tidball JG, Wehling-Henricks M. Nitric oxide synthase deficiency and the pathophysiology of muscular dystrophy. *J Physiol* 2014, 592:4627–4638.

163. Lai Y, Zhao J, Yue Y, Duan D. alpha2 and alpha3 helices of dystrophin R16 and R17 frame a microdomain in the alpha1 helix of dystrophin R17 for neuronal NOS binding. *Proc Natl Acad Sci USA* 2013, 110:525–530.

164. Li D, Bareja A, Judge L, Yue Y, Lai Y, Fairclough R, Davies KE, Chamberlain JS, Duan D. Sarcolemmal nNOS anchoring reveals a qualitative difference between dystrophin and utrophin. *J Cell Sci* 2010, 123:2008–2013.

165. Zhang Y, Yue Y, Li L, Hakim CH, Zhang K, Thomas GD, Duan D. Dual AAV therapy ameliorates exercise-induced muscle injury and functional ischemia in murine models of Duchenne muscular dystrophy. *Hum Mol Genet* 2013, 22:3720–3729.

166. Harper SQ. Molecular dissection of dystrophin identifies the docking site for nNOS. *Proc Natl Acad Sci USA* 2013, 110:387–388.

167. Duan D, Yue Y, Yan Z, Engelhardt JF. Trans-splicing vectors expand the packaging limits of adeno-associated virus for gene therapy applications. *Methods Mol Med* 2003, 76:287–307.

168. Ghosh A, Duan D. Expending adeno-associated viral vector capacity: a tale of two vectors. *Biotechnol Gene Eng Rev* 2007, 24:165–177.

169. Duan D, Yue Y, Yan Z, Engelhardt JF. A new dual-vector approach to enhance recombinant adeno-associated virus-mediated gene expression through intermolecular cis activation. *Nat Med* 2000, 6:595–598.

170. Yan Z, Zhang Y, Duan D, Engelhardt JF. Trans-splicing vectors expand the utility of adeno-associated virus for gene therapy. *Proc Natl Acad Sci USA* 2000, 97:6716–6721.

171. Duan D, Yue Y, Engelhardt JF. Expanding AAV packaging capacity with trans-splicing or overlapping vectors: a quantitative comparison. *Mol Ther* 2001, 4:383–391.

172. Sun L, Li J, Xiao X. Overcoming adeno-associated virus vector size limitation through viral DNA heterodimerization. *Nat Med* 2000, 6:599–602.

173. Halbert CL, Allen JM, Miller AD. Efficient mouse airway transduction following recombination between AAV vectors carrying parts of a larger gene. *Nat Biotechnol* 2002, 20:697–701.

174. Hirsch ML, Wolf SJ, Samulski RJ. Delivering transgenic DNA exceeding the carrying capacity of AAV vectors. *Methods Mol Biol* 2016, 1382:21–39.

175. Yan Z, Lei-Butters DC, Zhang Y, Zak R, Engelhardt JF. Hybrid adeno-associated virus bearing nonhomologous inverted terminal repeats enhances dual-vector reconstruction of minigenes in vivo. *Hum Gene Ther* 2007, 18:81–87.

176. Lai Y, Yue Y, Liu M, Ghosh A, Engelhardt JF, Chamberlain JS, Duan D. Efficient in vivo gene expression by trans-splicing adeno-associated viral vectors. *Nat Biotechnol* 2005, 23:1435–1439.

177. Ghosh A, Yue Y, Lai Y, Duan D. A hybrid vector system expands adeno-associated viral vector packaging capacity in a transgene-independent manner. *Mol Ther* 2008, 16:124–130.

178. Zhang Y, Duan D. Novel mini-dystrophin gene dual adeno-associated virus vectors restore neuronal nitric oxide synthase expression at the sarcolemma. *Hum Gene Ther* 2012, 23:98–103.

179. Lostal W, Kodippili K, Yue Y, Duan D. Full-length dystrophin reconstitution with adeno-associated viral vectors. *Hum Gene Ther* 2014, 25:552–562.

180. Koo T, Popplewell L, Athanasopoulos T, Dickson G. Triple trans-splicing adeno-associated virus vectors capable of transferring the coding sequence for full-length dystrophin protein into dystrophic mice. *Hum Gene Ther* 2014, 25:98–108.

181. Spitali P, Aartsma-Rus A. Splice modulating therapies for human disease. *Cell* 2012, 148:1085–1088.

182. Goyenvalle A, Vulin A, Fougerousse F, Leturcq F, Kaplan JC, Garcia L, Danos O. Rescue of dystrophic muscle through U7 snRNA-mediated exon skipping. *Science* 2004, 306:1796–1799.

183. Goyenvalle A, Babbs A, van Ommen GJ, Garcia L, Davies KE. Enhanced exon-skipping induced by U7 snRNA carrying a splicing silencer sequence: Promising tool for DMD therapy. *Mol Ther* 2009, 17:1234–1240.

184. Goyenvalle A, Babbs A, Wright J, Wilkins V, Powell D, Garcia L, Davies KE. Rescue of severely affected dystrophin/utrophin-deficient mice through scAAV-U7snRNA-mediated exon skipping. *Hum Mol Genet* 2012, 21:2559–2571.

185. Bish LT, Sleeper MM, Forbes SC, Wang B, Reynolds C, Singletary GE, Trafny D, Morine KJ, Sanmiguel J, Cecchini S, et al. Long-term restoration of cardiac dystrophin expression in golden retriever muscular dystrophy following rAAV6-mediated exon skipping. *Mol Ther* 2012, 20:580–589.

186. Vulin A, Barthelemy I, Goyenvalle A, Thibaud JL, Beley C, Griffith G, Benchaouir R, le Hir M, Unterfinger Y, Lorain S, et al. Muscle function recovery in golden retriever muscular dystrophy after AAV1-U7 exon skipping. *Mol Ther* 2012, 20:2120–2133.

187. Barbash IM, Cecchini S, Faranesh AZ, Virag T, Li L, Yang Y, Hoyt RF, Kornegay JN, Bogan JR, Garcia L, et al. MRI roadmap-guided transendocardial delivery of exon-skipping recombinant adeno-associated virus restores dystrophin expression in a canine model of Duchenne muscular dystrophy. *Gene Ther* 2013, 20:274–282.

188. Le Guiner C, Montus M, Servais L, Cherel Y, Francois V, Thibaud JL, Wary C, Matot B, Larcher T, Guigand L, et al. Forelimb treatment in a large cohort of dystrophic dogs supports delivery of a recombinant AAV for exon skipping in Duchenne patients. *Mol Ther* 2014, 22:1923–1935.

189. Greelish JP, Su LT, Lankford EB, Burkman JM, Chen H, Konig SK, Mercier IM, Desjardins PR, Mitchell MA, Zheng XG, et al. Stable restoration of the sarcoglycan complex in dystrophic muscle perfused with histamine and a recombinant adeno-associated viral vector. *Nat Med* 1999, 5:439–443.

190. Rutledge EA, Halbert CL, Russell DW. Infectious clones and vectors derived from adeno-associated virus (AAV) serotypes other than AAV type 2. *J Virol* 1998, 72:309–319.

191. Gao GP, Alvira MR, Wang L, Calcedo R, Johnston J, Wilson JM. Novel adeno-associated viruses from rhesus monkeys as vectors for human gene therapy. *Proc Natl Acad Sci USA* 2002, 99:11854–11859.

192. Gao G, Vandenberghe LH, Alvira MR, Lu Y, Calcedo R, Zhou X, Wilson JM. Clades of Adeno-associated viruses are widely disseminated in human tissues. *J Virol* 2004, 78:6381–6388.

193. Wang Z, Zhu T, Qiao C, Zhou L, Wang B, Zhang J, Chen C, Li J, Xiao X. Adeno-associated virus serotype 8 efficiently delivers genes to muscle and heart. *Nat Biotechnol* 2005, 23:321–328.

194. Inagaki K, Fuess S, Storm TA, Gibson GA, McTiernan CF, Kay MA, Nakai H. Robust systemic transduction with AAV9 vectors in mice: efficient global cardiac gene transfer superior to that of AAV8. *Mol Ther* 2006, 14:45–53.

195. Pacak CA, Mah CS, Thattaliyath BD, Conlon TJ, Lewis MA, Cloutier DE, Zolotukhin I, Tarantal AF, Byrne BJ. Recombinant adeno-associated virus serotype 9 leads to preferential cardiac transduction in vivo. *Circ Res* 2006, 99:e3–9.

196. Bostick B, Ghosh A, Yue Y, Long C, Duan D. Systemic AAV-9 transduction in mice is influenced by animal age but not by the route of administration. *Gene Ther* 2007, 14:1605–1609.

197. Ghosh A, Yue Y, Long C, Bostick B, Duan D. Efficient whole-body transduction with trans-splicing adeno-associated viral vectors. *Mol Ther* 2007, 15:750–755.

198. Ghosh A, Yue Y, Shin JH, Duan D. Systemic trans-splicing adeno-associated viral delivery efficiently transduces the heart of adult mdx mouse, a model for Duchenne muscular dystrophy. *Hum Gene Ther* 2009, 20:1319–1328.

199. Odom GL, Gregorevic P, Allen JM, Chamberlain JS. Gene therapy of mdx mice with large truncated dystrophins generated by recombination using rAAV6. *Mol Ther* 2011, 19:36–45.

200. Yue Y, Shin JH, Duan D. Whole body skeletal muscle transduction in neonatal dogs with AAV-9. *Methods Mol Biol* 2011, 709:313–329.

201. Hakim CH, Yue Y, Shin JH, Williams RR, Zhang K, Smith BF, Duan D. Systemic gene transfer reveals distinctive muscle transduction profile of tyrosine mutant AAV-1, -6 and -9 in neonatal dogs. *Mol Ther Methods Clin Dev* 2014, 1:14002.

202. Pan X, Yue Y, Zhang K, Lostal W, Shin JH, Duan D. Long-term robust myocardial transduction of the dog heart from a peripheral vein by adeno-associated virus serotype-8. *Hum Gene Ther* 2013, 24:584–594.

203. Pan X, Yue Y, Zhang K, Hakim CH, Kodippili K, McDonald T, Duan D. AAV-8 is more efficient than AAV-9 in transducing neonatal dog heart. *Hum Gene Ther Methods* 2015, 26:54–61.

204. Shin JH, Yue Y, Smith B, Duan D. Humoral immunity to AAV-6, 8, and 9 in normal and dystrophic dogs. *Hum Gene Ther* 2012, 23:287–294.

205. Rapti K, Louis-Jeune V, Kohlbrenner E, Ishikawa K, Ladage D, Zolotukhin S, Hajjar RJ, Weber T. Neutralizing antibodies against AAV serotypes 1, 2, 6, and 9 in sera of commonly used animal models. *Mol Ther* 2011, 20:73–83.

206. Calcedo R, Franco J, Qin Q, Richardson DW, Mason JB, Boyd S, Wilson JM. Preexisting neutralizing antibodies to adeno-associated virus capsids in large animals other than monkeys may confound in vivo gene therapy studies. *Hum Gene Ther Methods* 2015, 26:103–105.

207. Kornegay JN, Li J, Bogan JR, Bogan DJ, Chen C, Zheng H, Wang B, Qiao C, Howard JF Jr, Xiao X. Widespread muscle expression of an AAV9 human mini-dystrophin vector after intravenous injection in neonatal dystrophin-deficient dogs. *Mol Ther* 2010, 18:1501–1508.

208. Hakim CH, Pan X, Kodippili K, Blessa T, Yang HT, Yao G, Leach S, Emter C, Yue Y, Zhang K, et al. Intravenous delivery of a novel micro-dystrophin vector prevented muscle deterioration in young adult canine Duchenne muscular dystrophy dogs. *Mol Ther* 2016, 24:S198–199.

209. Heller KN, Montgomery CL, Janssen PM, Clark KR, Mendell JR, Rodino-Klapac LR. AAV-mediated over-expression of human alpha7 integrin leads to histo-logical and functional improvement in dystrophic mice. *Mol Ther* 2013, 21:520–525.

210. Odom GL, Gregorevic P, Allen JM, Finn E, Chamberlain JS. Microutrophin delivery through rAAV6 increases lifespan and improves muscle func-tion in dystrophic dystrophin/utrophin-deficient mice. *Mol Ther* 2008, 16:1539–1545.

211. Shin JH, Bostick B, Yue Y, Hajjar R, Duan D. SER-CA2a gene transfer improves electrocardiographic per-formance in aged mdx mice. *J Transl Med* 2011, 9:132.

212. Lai Y, Zhao J, Yue Y, Wasala NB, Duan D. Partial restoration of cardiac function with ΔPDZ nNOS in aged mdx model of Duchenne cardiomyopathy. *Hum Mol Genet* 2014, 23:3189–3199.

213. Mendell JR, Sahenk Z, Malik V, Gomez AM, Flanigan KM, Lowes LP, Alfano LN, Berry K, Meadows E, Lewis S, et al. A phase I/IIa follistatin gene therapy trial for Becker muscular dystrophy. *Mol Ther* 2015, 23:192–201.

214. Xu R, Camboni M, Martin PT. Postnatal overexpres-sion of the CT GalNAc transferase inhibits muscular dystrophy in mdx mice without altering muscle growth or neuromuscular development: evidence for a utrophin-independent mechanism. *Neuromuscul Disord* 2007, 17:209–220.

215. Marshall JL, Crosbie-Watson RH. Sarcospan: a small protein with large potential for Duchenne muscular dystrophy. *Skelet Muscle* 2013, 3:1.

216. Huang LY, Halder S, Agbandje-McKenna M. Parvo-virus glycan interactions. *Curr Opin Virol* 2014, 7:108–118.

217. Hsu PD, Lander ES, Zhang F. Development and applications of CRISPR-Cas9 for genome engineer-ing. *Cell* 2014, 157:1262–1278.

218. Barrangou R, Doudna JA. Applications of CRISPR technologies in research and beyond. *Nat Biotechnol* 2016, 34:933–941.

219. Long C, Amoasii L, Mireault AA, McAnally JR, Li H, Sanchez-Ortiz E, Bhattacharyya S, Shelton JM, Bassel-Duby R, Olson EN. Postnatal genome editing partially restores dystrophin expression in a mouse model of muscular dystrophy. *Science* 2016, 351:400–403.

220. Tabebordbar M, Zhu K, Cheng JK, Chew WL, Widrick JJ, Yan WX, Maesner C, Wu EY, Xiao R, Ran FA, et al. In vivo gene editing in dystrophic mouse muscle and muscle stem cells. *Science* 2016, 351:407–411.

221. Dogra C, Changotra H, Wergedal JE, Kumar A. Reg-ulation of phosphatidylinositol 3-kinase (PI3K)/Akt and nuclear factor-kappa B signaling pathways in dystrophin-deficient skeletal muscle in response to mechanical stretch. *J Cell Physiol* 2006, 208:575–585.

222. Bibee KP, Cheng YJ, Ching JK, Marsh JN, Li AJ, Keeling RM, Connolly AM, Golumbek PT, Myerson JW, Hu G, et al. Rapamycin nanoparticles target defective autophagy in muscular dystrophy to enhance both strength and cardiac function. *FASEB J* 2014, 28:2047–2061.

223. Pauly M, Daussin F, Burelle Y, Li T, Godin R, Fauconnier J, Koechlin-Ramonatxo C, Hugon G, Lacampagne A, Coisy-Quivy M, et al. AMPK activa-tion stimulates autophagy and ameliorates muscular dystrophy in the mdx mouse diaphragm. *Am J Pathol* 2012, 181:583–592.

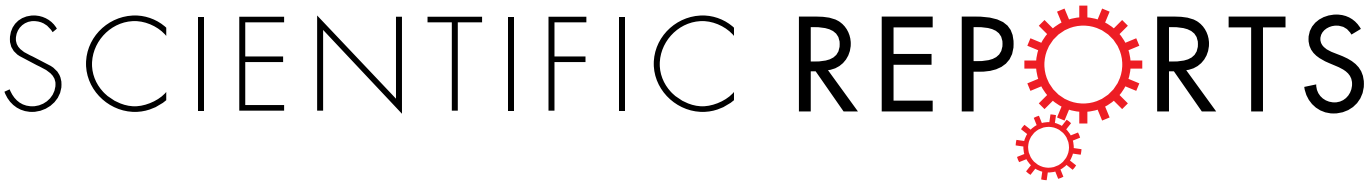

OPEN

Received: 8 November 2016
Accepted: 13 February 2017
Published online: 10 March 2017

CRISPR-Cas9 cleavage efficiency correlates strongly with target-sgRNA folding stability: from physical mechanism to off-target assessment

Xiaojun Xu[1], Dongsheng Duan[2] & Shi-Jie Chen[1]

The CRISPR/Cas9 complex, a bacterial immune response system, has been widely adopted for RNA-guided genome editing and transcription regulation in applications such as targeted genome modification and site-directed mutagenesis. However, the physical basis for its target specificity is not fully understood. In this study, based on a statistical mechanical analysis for the whole ensemble of sgRNA-target complex conformations, we identify a strong correlation between Cas9 cleavage efficiency and the stability of the DNA-RNA (R-loop) complex structures, with a Pearson correlation coefficient ranging from 0.775 to 0.886 for the tested systems. The finding leads to quantitative insights into important experimental results, such as the greater Cas9 tolerance to single-base mismatches in PAM-distal region than to PAM-proximal region and the high specificity and efficiency for shorter protospacers. Moreover, the results from the genome-wide off-target assessments, compared with other off-target scoring tools, indicate that the statistical mechanics-based approach provides more reliable off-target analyses and sgRNA design. To facilitate the genome engineering applications, a new web-based tool for genome-wide off-target assessment is established.

The clustered regularly interspaced short palindromic repeats (CRISPR)/Cas9 system[1–9], as a simple but efficient genome editing tool, has attracted increasing attentions recently. The Cas9/sgRNA (single guide RNA) has recently been used for effective gene targeting in many organisms/cells. For example, CRISPR/Cas9 *in vivo* gene editing leads to improved muscle function in a mouse model of Duchenne muscular dystrophy (DMD)[10]. Such results have established CRISPR/Cas9-based genome editing as an effective tool for gene modification in skeletal and cardiac muscle, and as a therapeutic approach to treat neuromuscular disorders and potentially many other diseases. However, considerable off-target effects hinder the application of this technology and inspire development/improvement of this technology to enhance the safety and efficacy of the promised genetic disease treatment.

Recent experimental and theoretical studies[11–13] proposed a two-state model for Cas9/sgRNA binding and cleavage: PAM recognition and R-loop formation (see Fig. 1). PAM recognition is governed by the PAM sequence such as NGG for the Streptococcus pyogenes Cas9 (SpCas9) and the PAM-proximal sequences. The improved specificity[14] with an engineered Cas9 nucleases supports the importance of PAM recognition to the overall Cas9/sgRNA mechanism. Here, the design of the Cas9 nucleases is based on the crystal structure of spCas9 in complex with guide RNA and target DNA[15,16] and uses the strategy of charge neutralization in the PAM-interacting non-target strand groove.

The physical mechanism for the CRISPR activity is not fully understood and the accuracy for quantitative predictions for any given Cas9/target/sgRNA system is not always reliable. The targeting specificity of

[1]Department of Physics, Department of Biochemistry, and Informatics Institute, University of Missouri, Columbia, MO, USA. [2]Department of Molecular Microbiology and Immunology, Department of Neurology, School of Medicine; Department of Biomedical Sciences, College of Veterinary Medicine; and Department of Bioengineering, University of Missouri, Columbia, MO, USA. Correspondence and requests for materials should be addressed to S.-J.C. (email: chenshi@missouri.edu)

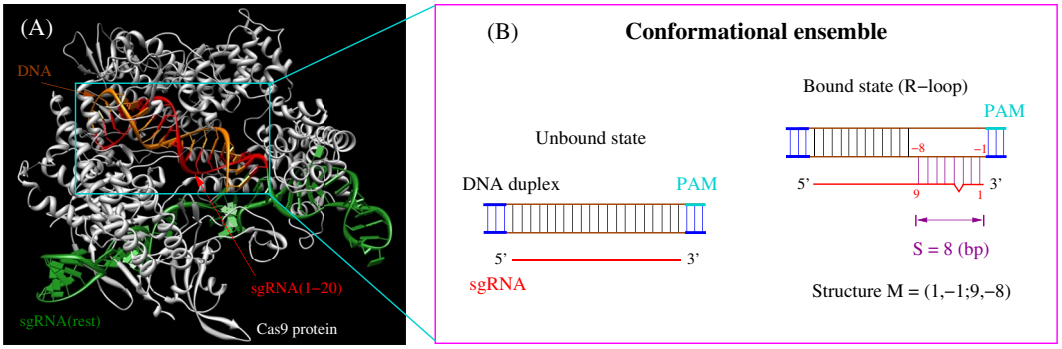

Figure 1. (**A**) The crystal structure of SpCas9 in complex with guide RNA and target DNA[15,16]. The sgRNA is tightly bound with the Cas9 protein. The first 20-nt of sgRNA (red) is base paired with the DNA target (orange) and the rest sgRNA nucleotides (green) have rich interactions with the Cas9 protein. As a result, we can only consider the DNA/RNA system (in the cyan box) to model the process of sgRNA binding to the DNA target site. (**B**) The competition between base stacking within the DNA and DNA-RNA hybrid base pairing/stacking results in the different DNA/RNA bound structures. In the unbound state, the target site maintains its original DNA-DNA base pairing within the chromatin. In the bound state, the sgRNA invades into the DNA duplex and forms the R-loop structure with the target DNA. The three-base pair DNA helix stretches on both ends of the R-loop are shown in blue. We allow a single-base bulge to be formed in the hybrid duplex. *S* denotes the length (number of base pairs) of the hybrid helix.

Cas9/sgRNA is regulated by the types of the PAM (protospacer adjacent motif) and the nature of mismatches in different regions of the protospacer in the target site. Many currently available tools are based on the mismatch information, such as the number and the position of mismatches, to find and evaluate potential off-target sites. For example, CROP-it[17] scores the potential off-target sites by dividing the protospacer into three segments with weight coefficients trained/optimized with the experimental (ChIP-Seq) data. CCTop[18] and Zhang's model (http://crispr.mit.edu/)[19] employ position-dependent weight coefficients in their off-target scoring algorithms. Recently, Doench *et al.*[20,21] developed a mismatch sequence- and position-dependent off-target scoring tool, namely, the Cutting Frequency Determination (CFD) score, with 240 fitting parameters. The recent findings of the off-target activity for sequences with more general insertions and deletions between target DNA and guide RNA[22] suggest the need for a new tool that can treat sequences beyond simple mismatches. Here we report such a new tool. This new computational tool is developed based on rigorous physical principles, can reproduce the previous experimental data, and can offer a general and consistent method for genome-wide off-target assessment and rational design of sgRNAs.

Quantitative predictions of the CRISPR activity require understanding of the physical mechanism. We reason that CRISPR-guided cleavage depends on the formation of active sgRNA-DNA state and such an active state may form an ensemble of structures. One of the distinctive features of our new method is the consideration of an ensemble (instead of a single structure as did in previous approaches) of active structures of the sgRNA-DNA complex. In our approach, we first identify the active sgRNA-DNA structures using experimentally determined CRISPR activity data. Based on the identified active structures, we establish a quantitative relationship between structure, stability, and the CRISPR activity using statistical mechanical analysis. The analysis further leads to a new predictive tool with two significant applications: (a) for a given target, to predict CRISPR activities for the different sgRNA sequences, and (b) for a given sgRNA, to provide genome-wide prediction for the potential off-target sites.

Methods

Test cases with single mutations. Recent experiments[14,19,23,24] showed that the CRISPR/Cas9 system can tolerate sgRNA-DNA mismatches and the gene editing efficiency is sensitive to the number, position and distribution of the mismatches. Zhang and his colleagues[14,19] chose four target sites within the human EMX1 gene (1, 2, 3, and 6) and one target site within the VEGFA(1) gene, and for each, generated a set of 57 different guide RNAs, which contains all the possible single-nucleotide substitutions in positions 1–19 directly 5′ of the requisite NGG PAM (see SI for an example). The 5′ guanine at position 20 is preserved, since the U6 promoter requires guanine as the first nucleotide of its transcript. These "off-target" guide RNAs were then assessed for cleavage activity at the on-target genomic locus. Qi *et al.*[23] and Liu *et al.*[24] studied mRFP(NT1) in E.coli MG1655 genome and the Renilla luciferase gene, respectively, with single-nucleotide substitutions (A ↔ U, G ↔ C) in positions 1–20 directly 5′ of the requisite NGG PAM. The data from these target sites provide ideal test cases for the investigation of sgRNA-DNA binding after PAM recognition. For this reason, we opt to use these published data in our analysis. Specifically, the data includes the target site DNA sequence, the perfectly matched sgRNA (without mismatch) and 57/20 sgRNAs that contain single mutation, and Cas9 cleavage efficiency from all seven target sites[14,19,23,24]. The protospacers in all the targets are 20-nt in length.

DNA-sgRNA structural ensemble. From the crystal structure of SpCas9 in complex with the guide RNA and the target DNA[15,16] (see Fig. 1A), we find that the sgRNA is tightly bound with the Cas9 protein, where the 20-nt single-stranded guide sequence is wrapped around by the Cas9. To access the target, the guide sequence of

sgRNA is likely in the single-stranded state before binding, which suggests that we can ignore the formation of the self-structure of the sgRNA in the sgRNA-DNA complex. Furthermore, the strong stability of DNA helix suggests that we can ignore DNA structural changes outside the R-loop region.

After PAM recognition (cyan in Fig. 1B), the sgRNA randomly searches for the binding sites on the target DNA strand for RNA-DNA hybridization, resulting in different sgRNA-DNA complex structures. A sgRNA-DNA bound state corresponds to all the structures where the sgRNA and the DNA are bounded by at least one base stack (minimum hybrid helix). The bound state includes partially as well as fully zipped (20-bp) DNA-RNA duplexes. Furthermore, as shown in Fig. 1B, we define a DNA-sgRNA binding mode "M" by the terminal base pairs of the duplex (See Fig. 1B). For example, M = (1, −1; 9, −8) in Fig. 1B denotes the duplex closed by terminal base pairs (1, −1) and (9, −8). We allow the formation of a single-nucleotide bulge[22] and the bulged nucleotide can be either on the RNA strand or on the DNA strand.

The sgRNA-DNA binding process involves competition between DNA-DNA and sgRNA-DNA base pairing. Complete DNA-DNA pairing results in the unbound state of the sgRNA-DNA system (Fig. 1B). The pairing of sgRNA with DNA causes the R-loop formation and changes the system from the unbound state to the bound state. The probability for sgRNA-DNA hybridization (binding) is determined by the free energy difference between the bound and the unbound states.

Free energy of the unbound state. In the unbound state, the free energy of the (separated) sgRNA and DNA is the sum of the (unbound) DNA and sgRNA: $\Delta G_{unbound} = \Delta G^{(DNA)} + \Delta G^{(RNA)}$. The DNA duplex free energy $\Delta G^{(DNA)}$ is the sum of the experimentally determined base pairing/stacking free energy parameters[25]. The free energy $\Delta G^{(RNA)}$ of the sgRNA, which is assumed to be a single-stranded random coil in the unbound state, is set to be zero as the reference state.

Free energy of the bound state. The DNA-sgRNA binding involves two steps: disruption of the DNA duplex and the subsequent DNA- sgRNA base pairing (R-loop formation). The free energy for a given bound state "M" is the sum of the free energy changes in the two steps: $\Delta G_M = \Delta G_M^{(DNA)} + \Delta G_M^{(hybd)}$, where $\Delta G_M^{(DNA)}$ and $\Delta G_M^{(hybd)}$ are the free energy changes in the DNA duplex and the sgRNA-DNA duplex, respectively. The sum over all the possible bound states gives the total bound free energy: $\Delta G_{bound} = \sum_M e^{-\Delta G_M/k_BT}$.

Folding stability. For the system shown in Fig. 1, there exist one unbound structure and 17,974 bound structures[26,27]. The sum of all the bound and the unbound states gives the total free energy ΔG_{tot} of the sgRNA/DNA system: $\Delta G_{tot} = -k_B\,Tln(e^{-\Delta G_{unbound}/k_BT} + e^{-\Delta G_{bound}/k_BT})$. The folding stability of the bound state "M" can be characterized by the free energy difference between the bound state "M" and the total state: $\Delta G_M^f = \Delta G_M - \Delta G_{tot}$, or, equivalently, the fractional population, which is the exponential of the free energy difference: $P_M = e^{-\Delta G_M^f/k_BT}$.

Search for functional structures. Not all the bound structures lead to successful Cas9 cleavage. To search for the active bound structures, we compute the total population of all the putative active structures:

$$P_{\text{active}} = \sum_{M,\text{active}} P_M \tag{1}$$

and test the correlation between the population P_{active} and the cleavage efficiency F using the Pearson correlation coefficient r(P_{active}, F). Here the Pearson correlation coefficient between parameters x and y is defined as

$$r(x, y) = \frac{\sum_{i=1}^{n}(x_i - \overline{x})(y_i - \overline{y})}{\sqrt{\sum_{i=1}^{n}(x_i - \overline{x})^2}\sqrt{\sum_{i=1}^{n}(y_i - \overline{y})^2}} \tag{2}$$

where $\overline{x} = \sum_{i=1}^{n} x_i/n$ and $\overline{y} = \sum_{i=1}^{n} y_i/n$ (the sample mean), n is the number of test systems (DNA/RNA sequences), x_i and y_i are the parameter values in the i-th test set.

A complication of the above analysis arises from the fact that not all the mismatch free energy parameters for the RNA-DNA hybrid helix are available[28]. To minimize the uncertainty in mismatches parameters in our search for the active structures, we use the forementioned published data sets[14,19,23,24], which involve at most one mismatch in each case, to search for the active structures. For these prototype systems, as an approximation, we simply assign zero free energy to a mismatched stack, which is less stable than a canonical base stack (usually with a negative free energy). Because the systems contain only a single mutation/mismatch, the free energy of the structures is mainly determined by the majority canonical base pairs/stacks rather than the single mismatch (see SI for details).

Assessment of off-target sites. To predict off-target sites for a given sgRNA, we need to account for the sequence-dependent energetic contributions from different mismatches, including tandem mismatches. To better assess genome-wide off-targets, we introduce nucleotide type and position-dependent mismatch parameters for DNA-RNA hybrid base pairs/stacks and one-bulge loop parameter in the DNA-RNA hybrid helix (see SI for details). We use the experimentally determined genome-wide off-target activity data[11,19,29,30] and a random search algorithm[31,32] to optimize the parameters. Specifically, for a given sgRNA, we sample all the possible targets in the genome and rank them according to the binding affinity of the functional sgRNA-DNA structures. By maximizing the Pearson correlation coefficient between the theoretically predicted binding affinity and the experimentally measured Cas9 cleavage efficiency on the different targets, we extract a set of mismatch parameters. As shown in the results section and the SI, the extracted parameters lead to great improvements in the predictions of Cas9 cleavage efficiency.

Target	ΔG^{helix}	$P_{full-zip}$	P_{active}	P_{bound}	CROP-it	CCTop	Zhang's model	CFD
EMX1.1	−0.208	−0.017	**0.798**	0.782	0.713	−0.693	0.74	0.719
EMX1.2	−0.072	0.029	**0.789**	0.532	0.658	−0.72	0.755	0.799
EMX1.3	0.188	0.015	**0.802**	0.387	0.72	−0.714	0.727	0.463
EMX1.6	0.503	−0.007	**0.831**	−0.046	0.755	−0.58	0.728	0.678
VEGFA.1	−0.074	0.148	**0.886**	−0.426	0.799	−0.637	0.724	0.736
Renilla	−0.132	0.359	**0.856**	0.201	0.781	−0.864	0.603	0.355
mRFP	−0.554	0.512	**0.775**	0.624	0.769	−0.759	0.451	0.674
Average	−0.050	0.148	**0.82**	0.293	0.742	−0.71	0.675	0.632

Table 1. Comparison between the current new method and four other existing methods; CROP-it[17], CCTop[18], Zhang's model[19], and CFD[21]. For each target, based on the 58/21 mutant and the unmutated sgRNA sequences, we evaluate the Pearson correlation between the experimentally determined SpCas9 cleavage efficiency[14, 19, 23, 24] and the computationally predicted (a) stability/population of the three functional structure candidates or (b) the CRISPR cleavage scores from other tools. In the table, ΔG^{helix} is the free energy of the fully-zipped hybrid helix. $P_{full-zip}$, P_{bound}, and P_{active} are the fractional populations of the fully-zipped (candidate 1), all the bound structures (candidate 2), and the active structures (candidate 3), respectively. The strong and consistent correlations for P_{active} indicates that the proposed active structures (candidate 3) are the functional structures for Cas9 cleavage after PAM recognition.

Results and Discussion

Putative sgRNA/DNA/Cas9 functional structures. We test three types of putative functional structures. The first candidate is the bound structure with the fully zipped 20 base pairs between the sgRNA and the DNA target, i.e., the bound structure (1, −1; 20, −20) in Fig. 1. We denote this candidate as the "full-zip" structure. The second candidate is the ensemble of all the bound structures, denoted as the "bound" structure. The third candidate is the hybrid helix starting immediately upstream of the PAM sequence containing the (1, −1) base pair and a helix no shorter than the minimum length of S_{min} base pairs. We denote this candidate as the "active" structures. As shown below, we find that the "active" structure (candidate 3 above) with $S_{min} = 7$ may be the functional structure.

Structure-activity correlation. We identify the functional structure as the one that yields the maximum structure-activity correlation r(P_{active}, F). As shown in Table 1, there exist no consistent correlation between the cleavage efficiency and the free energy of the fully zipped 20-bp structure (candidate 1 above). The finding is consistent with the result in the previous study[13]. In the tests for candidate 2 above (ensemble of all the bound structures), we find a correlation of 0.782 for the target of EMX1.1 and −0.426 for the target of VEGFA.1. The inconsistent results suggest that after PAM recognition, not all the bound structures can lead to efficient cleavage by the Cas9 protein.

In contrast, as shown in Table 1 and Fig. 2, there exists a strong and consistent correlation for candidate 3 above with $S_{min} = 7$. The Pearson correlation ranges from 0.775 to 0.886 with the average of 0.82 for the test cases, indicating that the proposed active structures are likely the functional structures for Cas9 cleavage.

The conclusion about the functional structures, derived from the correlation between structure (from theory) and activity (from experiment), is a result of the Cas9/DNA/sgRNA interactions in the sgRNA target recognition process. Previous studies[12, 13] suggested that after Cas9 binds to the PAM, the guide RNA invades into the PAM-adjacent protospacer DNA duplex, causing the formation of an R-loop motif immediately upstream of the PAM. During this strand invasion process, the guide RNA must displace the complementary strand of the protospacer. The competition between the invasion and the re-annealing of the DNA duplex results in a dynamic ("breathing") R-loop structure. PAM recognition and the resultant juxtaposition of the DNA duplex and sgRNA induce the base pairing of (1, −1) immediately upstream of the PAM sequence. To further promote the formation of the double-stranded breaks (DSBs) and cleavage for gene editing, a long hybrid helix (>7 base pairs) is required to stabilize the active structure. For the system shown in Fig. 1, there exist 269 such functional structures out of a total of 17,974 bound structures.

R-loop energy landscape and CRISPR activity. First, as shown in Fig. 3A, the unmutated sgRNA sequence shows a bumpy folding free energy landscape ΔG_M^f as a function of the different bound structures "M". Here, structure "M" is described by the length S of the sgRNA-DNA duplex zipped from the PAM site. Moreover, the different sgRNA-target systems show lacks a consistent S-dependence in the shape of the free energy landscape, suggesting a sensitive sequence dependence of the landscape. As a result, we expect that mutations in the sgRNA sequence may cause notable changes in CRISPR activity.

Second, to investigate the relationship between CRISPR efficiency and the different sgRNA-DNA structures, we evaluate the correlation coefficient $r(P_{active}, F)$ between the (theoretically predicted) fractional population P_M of a given sgRNA-DNA bound structure M (described by the helix length S) and the experimentally measured CRISPR cleavage efficiency. For each target, the correlation for a given M (helix length S) is an average over all the 58 sgRNA sequences, including one unmutated and $19 \times 3 = 57$ single-mutant sequences. The result leads to the following three conclusions (Fig. 3B). (1) Short helices with length $S < 7$ base pairs yield low or negative correlations. Such structures may be kinetically important as the initial steps in helix formation, however, the short-helix structures are not sufficiently stable and are unlikely the functional structures. (2) Long-helix structures alone

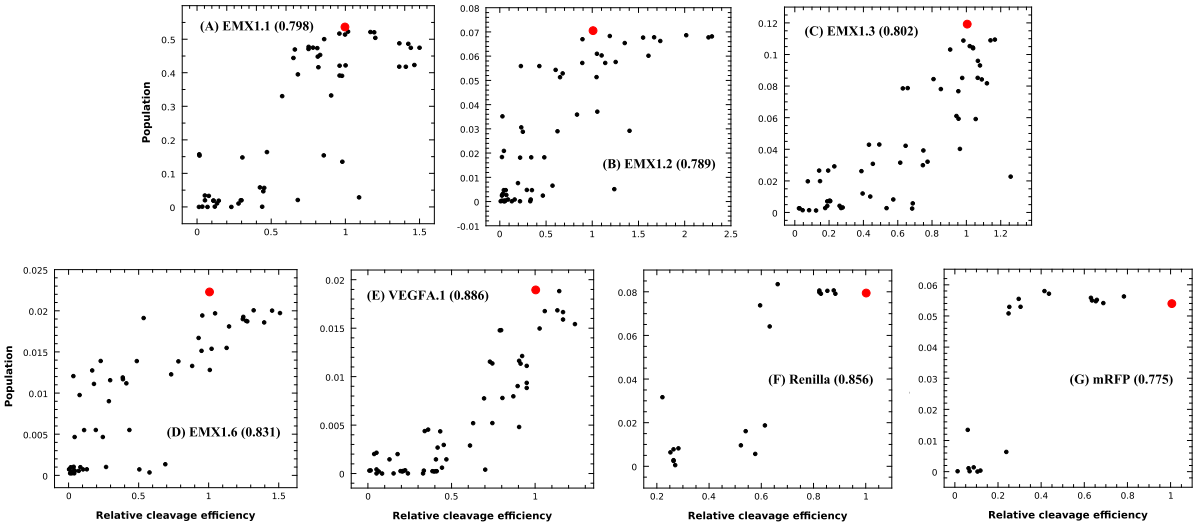

Figure 2. Pearson correlation between the relative cleavage efficiency and the fractional population of functional (active) structures, namely, R-loop structures that contain base pair (1, −1) and at least 7 base pairs in the hybrid helix, for (**A**) EMX1.1, (**B**) EMX1.2, (**C**) EMX1.3, (**D**) EMX1.6, (**E**) VEGFA.1, (**F**) Renilla, and (**G**) mRFP. The numbers in the brackets are the Pearson correlation coefficients. The red dots denote the data for the unmutated sgRNA sequences.

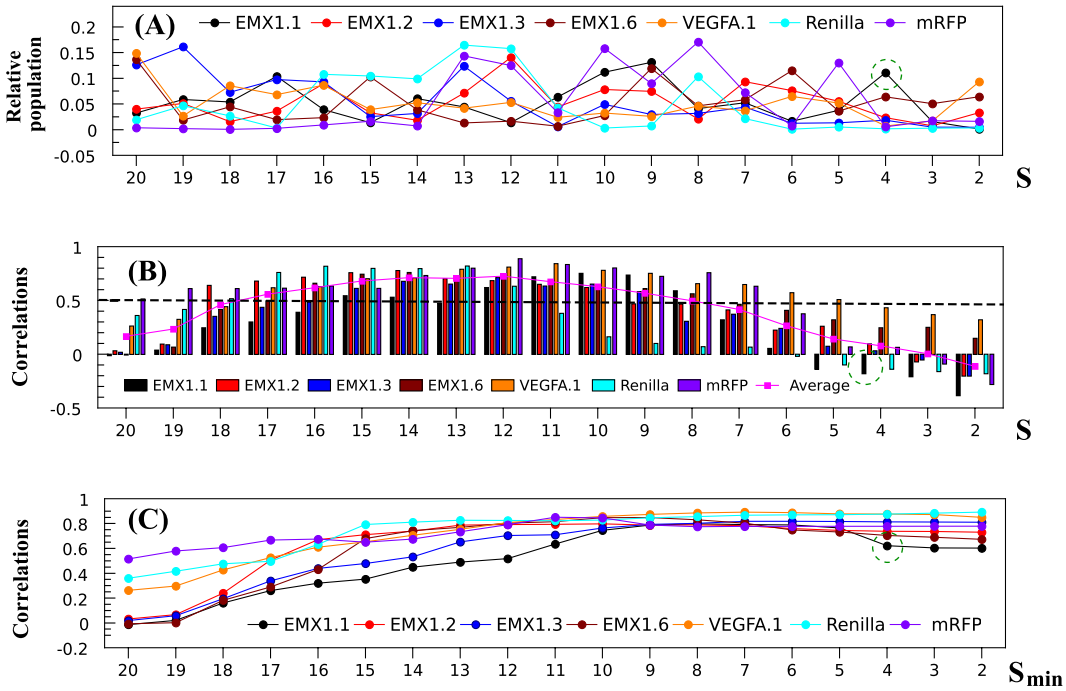

Figure 3. (**A**) Relative populations of the different sgRNA-DNA bound structures out of the total population of the bound structures. A sgRNA-DNA bound structure M is characterized by the helix length S base pairs measured from the (1, −1) base pair, as shown in Fig. 1B. For each target, we compute the population distribution P_M for the unmutated sgRNA sequence, and the relative population $P_M/e^{-G_{bound}/k_BT}$ (y-axis). (**B**) Correlation $r(P_M, F)$ between the population P_M of each individual bound structure M, which, as in (**A**), is characterized by the helix length S (in base pairs), and the CRISPR cleavage efficiency F for the given targets[13,18]. Here, for each target, for a given S, the correlation is evaluated based on all the 58 unmutated and mutated (single mismatch) sgRNA sequences. (**C**) Same as (**B**) except that the population for a given S_{min} is the sum over all the structures with the helix length longer than S_{min} base pairs. The sudden decrease at $S_{min} = 4$ base pairs (highlighted by the green circle) for EMX1.1 is caused by the negative correlation, shown in Fig. 3B.

may not always give high correlations. For example, structures of $S > 17$ base pairs show weak (<0.5) correlations. (3) The strongest correlation (>0.5) occurs to structures with helix length S from 8 to 17 base pairs. The above results suggest that an ensemble of R-loop with RNA-DNA hybrid helix length $S > 7$ base pairs may correspond to the functional structures.

To further confirm the above identified functional structure, we compute the correlation between the activity and the population of the different structure groups, namely, structures of helix length from S_{min} to 20 base pairs. As shown in Fig. 3C, the correlation reaches a plateau at S_{min} between 10 to 15 base pairs for the tested systems. The result indicate that for certain sgRNA and target sequences, a protospacer of length 15–20 bps might be sufficient to provide high cleavage efficiency[33,34].

Experiments suggest that the 20-nt long protospacer can be divided into two regions, the seed (PAM-proximal) region within 10 base pairs from the PAM and the non-seed (PAM-distal) region with 10 base pairs away from the PAM. Cas9 tolerates single-base mismatches in the non-seed region to a greater extent than in the seed region[19]. The position-dependent mismatch tolerance can also be explained by the statistical mechanical analysis above. Figure 3C shows the strong correlation between Cas9 cleavage and structures of helix length from 8 to 20 base pairs. When a single mismatch is introduced in the seed region, nearly all the functional structures contain the mismatch and hence the total cumulative population of these structures is greatly affected, resulting in a large change in the cleavage efficiency. However, if a single mismatch is introduced in the non-seed region, only a fraction of the functional structures contains the mismatch, thus, the impact to the total population of the functional structures is small. Therefore, mismatches in the non-seed region would have less impact on the CRISPR activity than mismatches in the seed region.

Prediction of off-target sites. To compare our method with the other existing methods, such as CROP-it[17], CCTop[18], Zhang's model[19], and CFD[21], we compute the correlation between the theoretical cleavage efficiency metric, such as the total population P_{active} of the functional structures in our current new method and the experimentally measured CRISPR efficiency. The test results shown in Table 1 for the aforementioned seven gene target systems, each with 58/21 sgRNA sequences, indicate that the different methods generally give reasonably consistent correlations except CCTop, which has negative correlations due to its specific scoring algorithm.

The unique feature of our approach is to account for the effect from not only the single "native" state with the fully zipped 20-bp sgRNA-DNA helix, but also the full spectrum of the functional states on the energy landscape, including the nonnative (bound and unbound) and partially folded sgRNA-DNA structures. The question, however, is whether these existing algorithms and our current new method can correctly assess the genome-wide off-target effects, which often involve multiple mismatches. Here, we use 24 cases obtained from four published data sets[11,19,29,30] to train the parameters and to test the reliability of the algorithms for off-target assessment. We also compare our new method with other existing methods[17–19,21].

Table 2 shows the test results for the above mentioned 24 cases. The tested sgRNAs have different numbers of off-targets, ranging from 9 to 5,957 genome-wide. For each sgRNA sequence, we calculate P_{active}, the total fractional population of the functional structures, for each scanned target. Sum over all the on- and off-targets gives the Pearson correlation coefficient for the given sgRNA sequence. We find that CROP-it[17] and CCTop[18] give similar performances, with most of the off-targets showing weak/no correlations. The algorithm by Hsu *et al.*[19] (Zhang's model) gives improved correlations, with 10 out of 24 cases showing strong (>0.5) correlations. Without the mismatch sequence dependence, CROP-it, CCTop, and the Zhang lab's scoring metrics may not correctly capture the effects of multiple-mismatches. For the CFD[21] scoring method, 17 out of 24 cases show strong (>0.5) correlations. Only 7 cases, with large numbers of off-targets, have the correlations below 0.5. The improvement of the performance may be attributed to the usage of the mismatch sequence- and position-dependent scoring functions. However, all four existing tools consider only mismatches in the full-length hybrid helix and cannot treat sgRNA/DNA sequences involving bulges and other loops in the sgRNA-DNA duplex[22].

The genome-wide test results (Table 2) support the conclusion that our new statistical mechanics-based algorithm provides improved off-target assessment. To further confirm the physical mechanism, namely, the relationship between the stability of the identified functional structures and the CRISPR activity, we test the algorithm at the different levels. As the lowest approximation, we first consider only the contributions from the canonical base pairs/stacks in our statistical mechanical analysis (SMA) (see SMAnone in Table 2). As shown in Table 2, 14 out of 24 cases show strong (>0.5) correlations. Without using any fitting parameters, the SMAnone scoring metric outperforms Zhang lab's model and reaches similar performance to CFD, which employs 240 fitted parameters. The results suggest that our algorithm may have captured the structure-function relationship for the Cas9/DNA/sgRNA system. For targets with large numbers of off-target sites, such as Nanog-sg3, which has 5,957 off-target sites, none of the scoring metrics can provide satisfactory correlation. To further increase the prediction accuracy, we introduce 261 energy parameters for the different mismatched base pairs as well as the position dependence of the mismatches. The parameters are estimated based on the optimization of the aforementioned correlation coefficient for the data listed in Table 2. The model with additional energy parameters (SMApara) gives improved predictions for the off-targets, where 20 out of 24 cases show strong correlations.

We also use seven cases obtained from three published data sets[10,35,36] to benchmark test the predictive power of our model. We note that these seven test cases are not included in the training set (24 cases in Table 2). As shown in Fig. 4, our statistical mechanical analysis-based models (without any parameter, SMAnone, and with additional energy parameters, SMApara) can have comparable or better performances than other non-physical algorithms, indicating the current models may possibly capture important aspects of the physical mechanism for CRISPR/Cas9 gene editing. Furthermore, with increasing amount of experimental data, our physical mechanism-based model, by incorporating more reliable parameters, may offer continuously improving predictions for off-target assessment and optimal sgRNA design.

Target	# of off-targets	CROP-it	CCTop	Zhang's model	CFD	SMA_{none}	SMA_{para}
From Hsu *et al.*[19]							
EMX1.1	9	0.799	−0.402	0.974	0.979	0.998	0.981
EMX1.3	33	0.227	−0.18	0.221	0.723	0.552	0.889
From Kuscu *et al.*[29]							
sgRNA1	50	0.327	−0.288	0.698	0.788	0.789	0.851
sgRNA2	17	0.466	−0.234	0.532	0.911	0.632	0.744
sgRNA3	41	0.195	−0.194	0.462	0.908	0.891	0.976
sgRNA4	484	0.077	−0.046	0.072	0.135	0.094	0.501
sgRNA5	52	0.343	−0.134	0.088	0.749	0.859	0.872
sgRNA6	1282	0.064	−0.026	0.228	0.251	0.233	0.301
sgRNA7	285	0.14	−0.039	0.614	0.673	0.216	0.639
sgRNA8	43	0.543	−0.171	0.641	0.812	0.548	0.501
sgRNA9	121	0.331	−0.062	0.825	0.804	0.861	0.812
sgRNA10	202	0.124	−0.169	0.773	0.76	0.777	0.579
sgRNA11	16	0.474	−0.148	0.643	0.649	0.642	0.628
sgRNA12	14	0.818	−0.009	0.82	0.832	0.818	0.818
From Tsai *et al.*[30]							
VEGFA(1)	22	0.448	−0.556	0.068	0.819	0.469	0.613
VEGFA(2)	151	0.298	−0.289	0.499	0.434	0.649	0.501
VEGFA(3)	60	0.332	−0.196	0.189	0.542	0.514	0.661
EMX1	16	0.352	−0.29	0.595	0.723	0.694	0.689
FANCF	9	0.375	−0.589	0.366	0.927	0.813	0.776
HEK293(4)	134	0.259	−0.131	0.404	0.379	0.177	0.501
From Wu *et al.*[11]							
Nanog-sg2	26	0.294	−0.335	0.428	0.808	0.311	0.502
Nanog-sg3	5957	0.065	−0.123	0.067	0.078	0.082	0.209
Phc1-sg1	2948	0.179	−0.263	0.163	0.207	0.176	0.342
Phc1-sg2	663	0.199	−0.168	0.245	0.271	0.186	0.394
Success rate*		3/24	2/24	10/24	17/24	14/24	20/24

Table 2. The Pearson correlations of six off-target scoring methods with the experimentally measured genome-wide off-target activities. Here, SMA_{none}, and SMA_{para} are the predicted scores (populations) from our statistical mechanical analysis (SMA)-based model without and with additional parameters, respectively. The experimental data is from the published papers. *Percentage of cases that show high (>0.5) correlation.

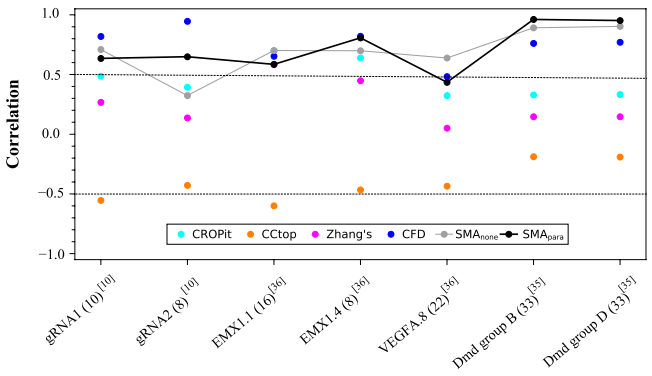

Figure 4. Tests of six off-target scoring methods using the experimentally measured genome-wide off-target activities. The numbers shown in the brackets are the number of the off-targets. The experimental data are from the corresponding published references. SMA_{none} and SMA_{para} are our models with and without parameters, respectively.

To implement the new algorithm described above, we have developed a user-friendly computational tool (VfoldCAS) to predict/rank off-target loci to facilitate the sgRNA design. The tool can be accessed at http://rna.

physics.missouri.edu/vfoldCAS. With the increasing amount of available experimental CRISPR data, the model is expected to provide off-target site predictions and sgRNA design with increasing accuracies.

Conclusions

Based on statistical mechanical principles and CRISPR gene editing efficiency data for different targets and sgRNAs, we explore the structure-based physical mechanism of the two-stage CRISPR gene editing process. The first stage is PAM recognition. This stage is determined by the PAM sequence and PAM/Cas9 interactions and chromatin accessibility. The second stage is the formation of the R-loop, namely, the target DNA/sgRNA bound structure. Different R-loop structures have different contributions to the overall cleavage efficiency. Through extensive theory-experimental comparisons we reveal a strong correlation between the population (stability) of the functional bound structures and the Cas9 cleavage efficiency. Such a correlation suggests that the folding stability of the functional structures plays an important role in the DNA targeting specificity of the CRISPR/Cas9 system. Specifically, we find that the major contribution comes from the bound structures which contain DNA-sgRNA helices of length 8–17 base pairs zipped from the PAM terminal. Our finding suggests that a full length (20 base pairs) RNA-DNA hybrid helix may not be mandatory for sgRNA-target recognition and Cas9 cleavage, and shorter protospacers can also ensure high targeting efficiency. Furthermore, the result supports the conclusion that Cas9 can tolerate mismatches in the PAM-distal (non-seed) region, although the perfect base-pairing in the PAM-proximal (seed) region is preferred.

From the kinetics point of view, the sgRNA-DNA hybrid helix can be quickly zipped up from the initially formed base pairs at the PAM binding site such as the (1, −1) base pair in Fig. 1B. However, from our statistical mechanical analysis, we find no correlation between the formation of the initial base pairs (a short hybrid helix) in the PAM-proximal region and CRISPR activity. The lack of correlation may stem from two possible reasons. First, as indicated in previous single-molecule DNA supercoiling experiments[12] and AFM imaging with kinetic Monte Carlo simulations[13], sgRNA-DNA helix folding kinetics involves a "breathing" process, where short-helix R-loop structures are transiently folded and unfolded. Second, Cas9 cleavage may require a sufficiently long hybrid helix for the double-stranded breaks. Therefore, as shown in Fig. 3B, the short-helix R-loop structures are unlikely functional and thus show low or negative correlations with CRISPR activity. Once the hybrid helix exceeds a threshold length, the sgRNA-DNA helix would proceed to zip up to perform the cleavage function.

Our current model, which uses the total population of the ensemble of functional R-loop structures zipped unidirectionally from the PAM-adjacent base pairs implicitly taken the kinetics pathway effect into account. In addition, as shown in Fig. 2, the unmutated sgRNA sequences have a high cleavage efficiency as expected, while some mutant sgRNAs even have better efficiency than the unmutated ones, suggesting possible additional effects, such as the 3D structure and the sequence-specific effects, beyond sgRNA-DNA base pairing. Further improvement of the model should consider the Cas9/PAM related structural features.

The identified physical mechanism leads to a new method for predicting CRISPR off-target sites and optimal design of sgRNAs for a given target. Unlike previous methods, which often involve ad hoc data fitting, this current new method is based on a rigorous physical mechanism. Thus, it can provide more accurate predictions. Indeed, tests with genome-wide data indicate that our new model gives more accurate predictions on off-targets than other existing scoring metrics. This new algorithm may offer an accurate method for optimal sgRNA design that can maximize activity and minimize off-target effects.

The new method reported here also has the unique ability to treat general R-loop structures. For instance, unlike previous methods, the current method considers contributions from bulge-looped structure. Further development of the method includes the consideration of a more complete ensemble of R-loop structures. Moreover, correct energy and entropy parameters are essential for the further development of the physical model. As more and more data become available, we expect a continuous increase in the number of available energy and entropy parameters. Chromatin accessibility can influence sgRNA-target binding. However, none of the currently available off-target site prediction tools can consider the spatial accessibility of the site in the 3D genome structure. Future model development should also consider additional potentially important factors such as the chromatin accessibility in PAM recognition and other possible effects such as the kinetic effects in R-loop formation and subsequent DNA/RNA hybridization, and the torque (twisting force induced by the DNA supercoiling)-regulated R-loop formation and disruption of the Cas9 cleavage efficiency.

References

1. Cong, L. *et al.* Multiplex genome engineering using CRISPR/Cas systems. *Science* **339(6121)**, 819–823 (2013).
2. Mali, P. *et al.* RNA-guided human genome engineering via Cas9. *Science* **339(6121)**, 823–826 (2013).
3. Hsu, P. D., Lander, E. S. & Zhang, F. Development and applications of CRISPR-Cas9 for genome engineering. *Cell* **157(6)**, 1262–1278 (2014).
4. Doudna, J. A. & Charpentier, E. Genome editing. The new frontier of genome engineering with CRISPR-Cas9. *Science* **346(6213)**, 1258096 (2014).
5. Shalem, O., Sanjana, N. E. & Zhang, F. High-throughput functional genomics using CRISPR-Cas9. *Nat Rev Genet* **16(5)**, 299–311 (2015).
6. Tsai, S. Q. & Joung, J. K. Defining and improving the genome-wide specificities of CRISPR-Cas9 nucleases. *Nat Rev Genet* **17(5)**, 300–312 (2016).
7. Xiong, X., Chen, M., Lim, W. A., Zhao, D. & Qi, L. S. CRISPR/Cas9 for Human Genome Engineering and Disease Research. *Annu Rev Genomics Hum Genet* **17**, 131–154 (2016).
8. Barrangou, R. & Doudna, J. A. Applications of CRISPR technologies in research and beyond. *Nat Biotechnol.* **34(9)**, 933–941 (2016).
9. Haeussler, M. *et al.* Evaluation of off-target and on-target scoring algorithms and integration into the guide RNA selection tool CRISPOR. *Genome Biol.* **17(1)**, 148 (2016).
10. Nelson, C. E. *et al. In vivo* genome editing improves muscle function in a mouse model of Duchenne muscular dystrophy. *Science* **351(6271)**, 403–407 (2016).
11. Wu, X. *et al.* Genome-wide bound of the CRISPR endonuclease Cas9 in mammalian cells. *Nat Biotechnol.* **32(7)**, 670–676 (2014).

12. Szczelkun, M. D. *et al.* Direct observation of R-loop formation by single RNA-guided Cas9 and Cascade effector complexes. *Proc Natl Acad Sci USA* **111(27)**, 9798–9803 (2014).
13. Josephs, E. A. *et al.* Structure and specificity of the RNA-guided endonuclease Cas9 during DNA interrogation, target bound and cleavage. *Nucleic Acids Res* **43(18)**, 8924–8941 (2015).
14. Slaymaker, I. M. *et al.* Rationally engineered Cas9 nucleases with improved specificity. *Science* **351(6268)**, 84–88 (2016).
15. Nishimasu, H. *et al.* Crystal structure of Cas9 in complex with guide RNA and target DNA. *Cell* **156(5)**, 935–949 (2014).
16. Anders, C., Niewoehner, O., Duerst, A. & Jinek, M. Structural basis of PAM-dependent target DNA recognition by the Cas9 endonuclease. *Nature* **513(7519)**, 569–573 (2014).
17. Singh, R., Kuscu, C., Quinlan, A., Qi, Y. & Adli, M. Cas9-chromatin binding information enables more accurate CRISPR off-target prediction. *Nucl Acids Res* **43(18)**, e118 (2015).
18. Stemmer, M., Thumberger, T., Del Sol Keyer, M., Wittbrodt, J. & Mateo, J. L. CCTop: an intuitive, flexible and reliable CRISPR/Cas9 target prediction tool. *PLoS One* **10(4)**, e0124633 (2015).
19. Hsu, P. D. *et al.* DNA targeting specificity of RNA-guided Cas9 nucleases. *Nat Biotechnol.* **31(9)**, 827–832 (2013).
20. Doench, J. G. *et al.* Rational design of highly active sgRNAs for CRISPR-Cas9-mediated gene inactivation. *Nat Biotechnol.* **32(12)**, 1262–1267 (2014).
21. Doench, J. G. *et al.* Optimized sgRNA design to maximize activity and minimize off-target effects of CRISPR-Cas9. *Nat Biotechnol.* **34(2)**, 184–191 (2016).
22. Lin, Y. *et al.* CRISPR/Cas9 systems have off-target activity with insertions or deletions between target DNA and guide RNA sequences. *Nucleic Acids Res.* **42(11)**, 7473–7485 (2014).
23. Qi, L. S. *et al.* Repurposing CRISPR as an RNA-guided platform for sequence-specific control of gene expression. *Cell* **152(5)**, 1173–1183 (2013).
24. Liu, Y. *et al.* Targeting cellular mRNAs translation by CRISPR-Cas9. *Sci Rep.* **6**, 29652 (2016).
25. SantaLucia, J. Jr. A unified view of polymer, dumbbell, and oligonucleotide DNA nearest-neighbor thermodynamics. *Proc Natl Acad Sci USA.* **95(4)**, 1460–1465 (1998).
26. Zhang, W. & Chen, S.-J. RNA hairpin-folding kinetics. *Proc Natl Acad Sci USA* **99(4)**, 1931–1936 (2002).
27. Xu, X. & Chen, S.-J. Kinetic mechanism of conformational switch between bistable RNA hairpins. *J Am Chem Soc.* **134**(30), 12499–12507 (2012).
28. Sugimoto, N. *et al.* Thermodynamic parameters to predict stability of RNA/DNA hybrid duplexes. *Biochemistry* **34(35)**, 11211–11216 (1995).
29. Kuscu, C., Arslan, S., Singh, R., Thorpe, J. & Adli, M. Genome-wide analysis reveals characteristics of off-target sites bound by the Cas9 endonuclease. *Nat Biotechnol.* **32(7)**, 677–683 (2014).
30. Tsai, S. Q. *et al.* GUIDE-seq enables genome-wide profiling of off-target cleavage by CRISPR-Cas nucleases. *Nat Biotechnol.* **33(2)**, 187–197 (2015).
31. Rastrigin, L. A. The convergence of the random search method in the extremal control of a many-parameter system. *Autom Remote Control* **24**, 1337–1342 (1963).
32. Solis, F. J. & Wets, R. J. B. Minimization by random search techniques. *Math Oper Res.* **6(1)**, 19–30 (1981).
33. Fu, Y., Sander, J. D., Reyon, D., Cascio, V. M. & Joung, J. K. Improving CRISPR-Cas nuclease specificity using truncated guide RNAs. *Nat Biotechnol.* **32(3)**, 279–284 (2014).
34. Zhang, J. P. *et al.* Different effects of sgRNA length on CRISPR-mediated gene knockout efficiency. *Sci Rep.* **6**, 28566 (2016).
35. Long, C. *et al.* Prevention of muscular dystrophy in mice by CRISPR/Cas9-mediated editing of germline DNA. *Science* **345(6201)**, 1184–1188 (2014).
36. Kleinstiver, B. P. *et al.* Engineered CRISPR-Cas9 nucleases with altered PAM specificities. *Nature* **523(7561)**, 481–485 (2015).

Acknowledgements

This research was supported by NIH grant R01-GM063732 (SC). DD is supported by NIH R01-AR69085 and Department of Defense MD150133.

Author Contributions

S.C. and D.D. conceptualized the project, X.X. and S.C. designed the study, X.X. performed the calculations, and X.X., S.C., and D.D. wrote the manuscript.

Additional Information

Supplementary information accompanies this paper at doi:10.1038/s41598-017-00180-1

Competing Interests: D.D. is a member of the scientific advisory board for Solid GT, LLC and an equity holder of Solid GT, LLC. The Duan lab has received research supports from Solid GT, LLC.

Publisher's note: Springer Nature remains neutral with regard to jurisdictional claims in published maps and institutional affiliations.

Research Article | Vol. 8, No. 3 | 1 Mar 2017 | BIOMEDICAL OPTICS EXPRESS 1271
Biomedical Optics EXPRESS

Heart structural remodeling in a mouse model of Duchenne cardiomyopathy revealed using optical polarization tractography [Invited]

Y. WANG,[1] K. ZHANG,[2] D. DUAN,[1,2] AND G. YAO[1,*]

[1]*Department of Bioengineering, University of Missouri, Columbia, MO 65211, USA*
[2]*Department of Molecular Microbiology & Immunology, University of Missouri, Columbia, MO 65211, USA*
[*]*yaog@missouri.edu*

Abstract: We investigated the heart structural remodeling in the mdx4cv mouse model of Duchenne cardiomyopathy using optical polarization tractography. Whole heart tractography was obtained in freshly dissected hearts from six mdx4cv mice. Six hearts from C57BL/6J mice were also imaged as the normal control. The mdx4cv hearts were significantly larger than the control hearts and had significantly higher between–subject variations in myofiber organization. While both strains showed classic cross-helical fiber organization in the left ventricle, the rate of the myocardial fiber orientation change across the heart wall was significantly altered in the right ventricle of the mdx4cv heart.

OCIS codes: (110.4500) Optical coherence tomography; (110.5405) Polarimetric imaging; (170.3880) Medical and biological imaging; (260.5430) Polarization.

References and links

1. D. Duan, "Challenges and opportunities in dystrophin-deficient cardiomyopathy gene therapy," Hum. Mol. Genet. **15**(2), R253–R261 (2006).
2. Y. J. Cheng, D. Lang, S. D. Caruthers, I. R. Efimov, J. Chen, and S. A. Wickline, "Focal but reversible diastolic sheet dysfunction reflects regional calcium mishandling in dystrophic mdx mouse hearts," Am. J. Physiol. Heart Circ. Physiol. **303**(5), H559–H568 (2012).
3. D. D. Streeter, Jr., H. M. Spotnitz, D. P. Patel, J. Ross, Jr., and E. H. Sonnenblick, "Fiber orientation in the canine left ventricle during diastole and systole," Circ. Res. **24**(3), 339–347 (1969).
4. P. A. Helm, L. Younes, M. F. Beg, D. B. Ennis, C. Leclercq, O. P. Faris, E. McVeigh, D. Kass, M. I. Miller, and R. L. Winslow, "Evidence of structural remodeling in the dyssynchronous failing heart," Circ. Res. **98**(1), 125–132 (2005).
5. D. Benoist, R. Stones, M. J. Drinkhill, A. P. Benson, Z. Yang, C. Cassan, S. H. Gilbert, D. A. Saint, O. Cazorla, D. S. Steele, O. Bernus, and E. White, "Cardiac arrhythmia mechanisms in rats with heart failure induced by pulmonary hypertension," Am. J. Physiol. Heart Circ. Physiol. **302**(11), H2381–H2395 (2012).
6. C. Mekkaoui, T. G. Reese, M. P. Jackowski, H. Bhat, and D. E. Sosnovik, "Diffusion MRI in the heart," NMR Biomed. (2015), doi:10.1002/nbm.3426.
7. F. J. Vetter, S. B. Simons, S. Mironov, C. J. Hyatt, and A. M. Pertsov, "Epicardial fiber organization in swine right ventricle and its impact on propagation," Circ. Res. **96**(2), 244–251 (2005).
8. Y. Wang and G. Yao, "Optical tractography of the mouse heart using polarization-sensitive optical coherence tomography," Biomed. Opt. Express **4**(11), 2540–2545 (2013).
9. Y. Wang, K. Zhang, N. B. Wasala, D. Duan, and G. Yao, "Optical polarization tractography revealed significant fiber disarray in skeletal muscles of a mouse model for Duchenne muscular dystrophy," Biomed. Opt. Express **6**(2), 347–352 (2015).
10. L. Azinfar, M. Ravanfar, Y. Wang, K. Zhang, D. Duan, and G. Yao, "High resolution imaging of the fibrous microstructure in bovine common carotid artery using optical polarization tractography," J. Biophoton. (2015), doi:10.1002/jbio.201500229.
11. Y. Wang, K. Zhang, N. B. Wasala, X. Yao, D. Duan, and G. Yao, "Histology validation of mapping depth-resolved cardiac fiber orientation in fresh mouse heart using optical polarization tractography," Biomed. Opt. Express **5**(8), 2843–2855 (2014).
12. C. Fan and G. Yao, "Full-range spectral domain Jones matrix optical coherence tomography using a single spectral camera," Opt. Express **20**(20), 22360–22371 (2012).
13. C. Fan and G. Yao, "Imaging myocardial fiber orientation using polarization sensitive optical coherence tomography," Biomed. Opt. Express **4**(3), 460–465 (2013).
14. Y. Wang, M. Ravanfar, K. Zhang, D. Duan, and G. Yao, "Mapping 3D fiber orientation in tissue using dual-angle optical polarization tractography," Biomed. Opt. Express **7**(10), 3855–3870 (2016).

#279545 https://doi.org/10.1364/BOE.8.001271
Journal © 2017 Received 27 Oct 2016; revised 27 Jan 2017; accepted 28 Jan 2017; published 1 Feb 2017

Biomedical Optics EXPRESS

15. B. Ciszek, D. Skubiszewska, and A. Ratajska, "The anatomy of the cardiac veins in mice," J. Anat. **211**(1), 53–63 (2007).
16. P. Agger, S. Lakshminrusimha, C. Laustsen, S. Gugino, J. R. Frandsen, M. Smerup, R. H. Anderson, V. Hjortdal, and R. H. Steinhorn, "The myocardial architecture changes in persistent pulmonary hypertension of the newborn in an ovine animal model," Pediatr. Res. **79**(4), 565–574 (2016).
17. T. A. Meyers and D. Townsend, "Early Right Ventricular Fibrosis and Reduction in Biventricular Cardiac Reserve in the Dystrophin-Deficient mdx Heart," Am. J. Physiol. Heart Circ. Physiol. **308**(4), H303–H315 (2015).
18. I. C. C. Barbin, J. A. Pereira, M. Bersan Rovere, D. de Oliveira Moreira, M. J. Marques, and H. Santo Neto, "Diaphragm degeneration and cardiac structure in mdx mouse: potential clinical implications for Duchenne muscular dystrophy," J. Anat. **228**(5), 784–791 (2016).
19. D. J. Stuckey, C. A. Carr, P. Camelliti, D. J. Tyler, K. E. Davies, and K. Clarke, "In vivo MRI characterization of progressive cardiac dysfunction in the mdx mouse model of muscular dystrophy," PLoS One **7**(1), e28569 (2012).

1. Introduction

Duchenne cardiomyopathy describes the dilated cardiomyopathy seen in later-stage Duchenne muscular dystrophy (DMD) patients. It is a leading cause of morbidity and mortality in DMD patients [1]. The mdx4cv mouse is one of the most commonly used DMD animal models where the dystrophin expression is blocked by a point mutation [1]. Mdx4cv mice develop a progressive cardiomyopathy that shares many features with the human disease [1]. Although mdx4cv mice have been studied extensively, the heart structural remodeling in this model has not been investigated in detail [2]. The heart is a highly adaptive organ and its structure may change in response to progressive deterioration of cardiac function. It is known that the myofibers in a healthy heart are organized in an exquisite and optimized structure [3], which was often altered in heart diseases as part of the pathological remodeling process [4, 5]. The knowledge of detailed myocardial fiber changes during disease progression is essential for understanding the intricate structure-function relationship in heart diseases.

The MRI based diffusion-tensor imaging (DTI) technology is the only practically available tool for imaging myocardial fiber structure in the whole heart [6]. However, in addition to its high system cost, the limited spatial resolution of DTI makes it extremely challenging for revealing detailed myocardial fiber structure in the small mouse hearts. A typical mouse heart has a diameter of ~6 mm with 1~2 mm thick ventricular wall and the myofiber orientation can change over 100° across the thin ventricular wall [6, 7]. Abrupt orientation changes of more than 50° were observed between different epicardial layers [7]. Therefore, a sufficient resolution is important for correctly imaging detailed fiber orientation changes in the ventricular wall of the heart.

Optical polarization tractography (OPT) is a newly developed method that can image high-resolution fiber organization in fibrous tissues [8–10]. It was based on the Jones matrix implementation of the polarization-sensitive optical coherence tomography (PSOCT). OPT uses Jones calculus to construct the depth resolved optic axis for measuring fiber orientation with microscopic resolution [11]. In this study, OPT was applied to image the myocardial fiber structures in freshly excised whole mouse hearts. The results revealed significant structural remodeling in the mdx4cv mouse model of Duchenne cardiomyopathy.

2. Methods

2.1 OPT system

The OPT method was implemented in a 0.85 μm wavelength spectral-domain Jones matrix PSOCT system which has been described in detail previously [12, 13]. Briefly, the system measures pixel-wise Jones matrix of the sample by using incident light with alternating right- and left-circular polarizations. For each incident polarization, the horizontally and vertically polarized components of the interference signals were detected using a custom spectrometer equipped with a 1024-pixel line scan camera running at 50k A-lines/sec. An iterative Jones calculus based algorithm was applied to extract the depth-resolved optic axis for mapping the

Biomedical Optics EXPRESS

fiber orientation [13]. The fiber orientation measured is between [-90°, 90°] and represents the projected orientations within the plane perpendicular to the incident light [8, 14], which is analog to the "helix" angle measured in DTI [2, 7]. The system has a 12.4 μm lateral resolution at the focus and a 5.9 μm axial resolution in tissue.

2.2 OPT imaging of a whole mouse heart

All animal experiments were approved by the institutional animal care and use committee. The freshly excised hearts from six 7-mo old male B6Ros.Cg-DMD$^{mdx\text{-}4cv}$/J mice (the "mdx" group) and six age-matched male C57BL/6J mice (the "BL6" group) were imaged using the OPT system. The procedure to image the whole heart tractography was described in details previously [8]. Briefly, the heart was mounted on a rotational stage via a 20-gauge needle passing through the long axis of the heart (between the apex and center of the base). The needle was fixed on the base of the stage and was aligned with the rotational axis. During imaging, the stage was rotated continuously over 360° at a speed of 1.25°/s while the light repeatedly scanned along the long axis of the heart (as the B-scan) using a galvanometer coupled with a telecentric lens (36 mm focal length). Each B-scan covered 8 mm with 2000 A-scans. A total of 3600 B-scans were acquired at a speed of 12.5 B-scans/s and took 288 s. The heart diameter was measured using a caliper.

The constructed 3D data set of fiber orientation had 280 × 2000 × 3600 pixels (in A × B × C scans) and covered a corresponding imaging area of 1.1mm × 8.0mm × 360°. The 2D "planar" tractography was first built at each *en face*s plane using Matlab streamline functions [8]. A 5 × 5 (pixels) median filter was applied to all processed B-scan images to improve signal-to-noise. The stack of the "planar" 2D tractography was then polar-transformed into the 3D coordinates from the measured heart diameter and heart surface [8]. The OPT results were visualized using the 3DSlicer software (www.slicer.org).

3. Results and discussion

Figure 1(a) shows intensity images of a BL6 and an mdx mouse heart. The BL6 heart appeared in a pear-like shape; whereas the mdx heart was bigger and close to a cylindrical shape. In all hearts tested, the mdx heart had an average diameter of 6.88 ± 0.48mm which was significantly larger (p = 0.013, Student's t-test) than the BL6 heart (6.15 ± 0.25 mm).

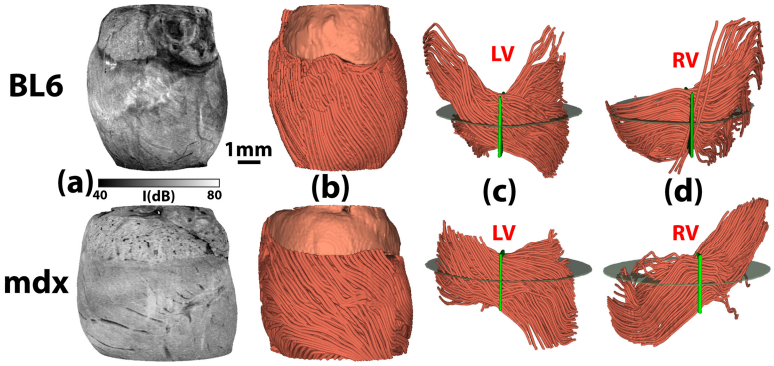

Fig. 1. (a) Intensity images of a BL6 heart (Visualization 1) and an mdx heart (Visualization 2). (b) The corresponding 3D tractography of the BL6 heart (Visualization 3) and the mdx heart (Visualization 4), both with the left ventricle (LV) facing front. Also shown are depth-resolved tractography showing myofibers passing through a 1.5 mm high region of interest (green plate) across (c) the LV (Visualization 5 and Visualization 6) and (d) the right ventricle (RV) (Visualization 7 and Visualization 8) of the BL10 and mdx hearts, respectively.

Figure 1(b) illustrates the global ventricular tractography of the same two hearts shown in Fig. 1(a). Since no clear optic axis data was obtained in the atrial and aorta tissues, they were shown in solid color. The fiber tractography shown in Fig. 1(b) was obtained at the 100 μm

Biomedical Optics EXPRESS

depth beneath the epicardium. The associated animations revealed the change of the fiber orientation of the entire heart. Overall, the fiber orientation appeared similar in the left ventricle (LV) of both the BL6 and mdx hearts, but quite different in the right ventricle (RV). To examine depth-resolved fiber orientation across the ventricular wall, Figs. 1(c) and 1(d) showed myocardial fibers that pass through a 1.5 mm high (along the B-scan) region of interest (ROI) located at the center of the LV and RV, respectively. The associated animations show the change of myofiber structure from the epicardium to the endocardium.

In both strains, the LV showed the classic "cross-helical" profile [3] (Fig. 1(c)). "Negatively orientated" fibers at the epicardium transitioned to circumferential at the middle of the ventricular wall, and became positively oriented toward the endocardium. However, the mdx heart appeared to have smaller helix angles and a smaller rate of orientation change over the LV wall than the BL6 heart. The myofibers in the BL6 RV had much less orientation changes across the heart wall than in the LV. The BL6 heart showed some "vertical" fibers close to the RV surface at the proximity of the right ventricle vein (RCV) [15]. This was not observed in the mdx heart. The RV of the mdx heart appeared to have more variations in fiber organization in the *en face* plane than the BL6 heart.

We further quantitatively analyzed the depth-resolved fiber organization in the hearts. To compensate for the variation in heart structure among different hearts, an evaluation "window" was defined in both the LV and RV based on common structural features including cardiac veins [15] observed in the intensity images of the mouse hearts (Fig. 2(a)). The vertical yellow dashed line was first drawn along the B-scan direction from the lowest boundary of the left atrium. This line ended at the intersection with the left cardiac vein (LCV) [15]. The middle point of this line was then identified as the center of the LV window ("Lc" in Fig. 2(a)). In addition, the white dashed line was drawn across the Lc along the C-scan direction. The intersection of this line with the RCV was selected as the center of the RV window ("Rc" in Fig. 2(a)). The two evaluation windows were then created by extending from their corresponding centers to reach a size of 2.8 mm × 70° (700 × 700 pixels, B × C) as illustrated as the blue boxes in Fig. 2(a). These windows were manually determined in all hearts and their coordinates were recorded for subsequent calculations.

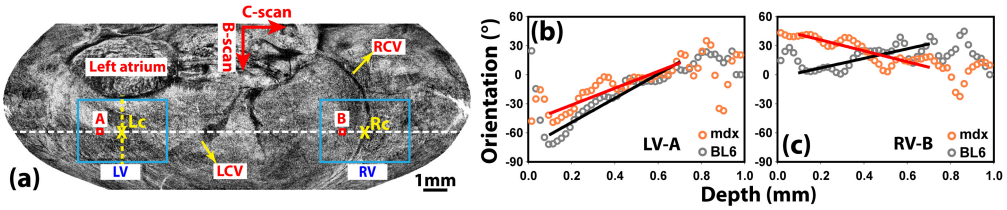

Fig. 2. (a) An illustration of the "window" in LV and RV (blue boxes) for quantitative analysis. LCV: left cardiac vein; RCV: right cardiac vein [15]. Also shown are example depth profiles of myocardial fiber orientation calculated at ROIs in the (b) LV and (c) RV as labeled in red boxes in (a). These sample data were obtained from the same hearts shown in Fig. 1.

Figures 2(b) and 2(c) show depth profiles of the fiber orientation at representative region-of-interests (ROIs) inside the LV and RV, respectively. The ROIs were marked as red boxes on the white dashed line in Fig. 2(a). The ROI size was 0.1 mm × 2.5° (25 × 25 pixels in B × C). The fiber orientation values were obtained using circular averaging within the ROI [10]. Consistent with the global tractography in Fig. 1, the depth-profiles of the fiber orientation in the LV showed the "cross-helical" transition from negative to positive orientation in both the BL6 and mdx hearts. An "inversed" transition (from positive to negative orientations) was observed in the BL6 heart within 100 μm from the epicardium; but this was not clear in the mdx heart (Fig. 2(b)). Such an inverse trend was also observed in our previous studies [11] and reported in a recent high resolution (9.4-T) DTI study of the larger ovine heart [16]. This was not reported in DTI studies of healthy mouse hearts [6], likely due to insufficient resolution. The fiber orientation of the BL6 RV was slightly positive with small changes

Biomedical Optics EXPRESS

across the ventricular wall. However, the mdx heart showed a significant "negative" trend of orientation changes over the depth.

Linear fitting was applied to calculate the "slope" of the orientation change between 0.1 and 0.7 mm in depth. Orientation data within the 0.1 mm from the heart surface were excluded in the fitting to avoid the "inverse" trend shown in Fig. 2(b). The fitted slopes were 124.9°/mm (R^2 = 0.91 and root-mean-square-error (RMSE) = 7.0°) in the BL6 LV and 86.8°/mm (R^2 = 0.81 and RMSE = 7.4°) in the mdx LV. For the RV curves (Fig. 2(c)), the obtained slopes were 49.5°/mm (R^2 = 0.61 and RMSE = 6.8°) in the BL6 heart and −56.5°/mm (R^2 = 0.70 and RMSE = 6.5°) in the mdx heart.

The "slope" of the fiber orientation change with depth was calculated for all the ROIs of the same size (0.1 mm × 2.5°) within the entire LV and RV evaluation windows. In other words, the depth profiles similar to those shown in Figs. 2(b) and 2(c) were constructed and linearly fitted for a total of 28 × 28 = 784 ROIs inside the evaluation window. The slope values can be color-coded for visualization (Fig. 3(a)). The image width of the mdx heart was wider along the C-scan direction because the mdx heart had a bigger diameter. More than 92.9% of the LV regions in both hearts had fitting R^2>0.6 or RMSE<10°. The slopes were relatively homogeneous in the LV of both the mdx and BL6 hearts; but the values were overall smaller in the mdx heart than the BL6 heart. The depth profiles in the RV showed more location-dependent variations in both hearts. However, the variations in the mdx heart were bigger. Only 68.8% of the mdx RV and 84.9% of the BL6 RV had fitting R^2>0.6 or RMSE<10°. Poorer linear fitting in the RV was also reported in previous DTI studies [5]. The fitting in the RV was also affected by the presence of the RCV as more abrupt orientation changes were observed at the proximity of the RCV.

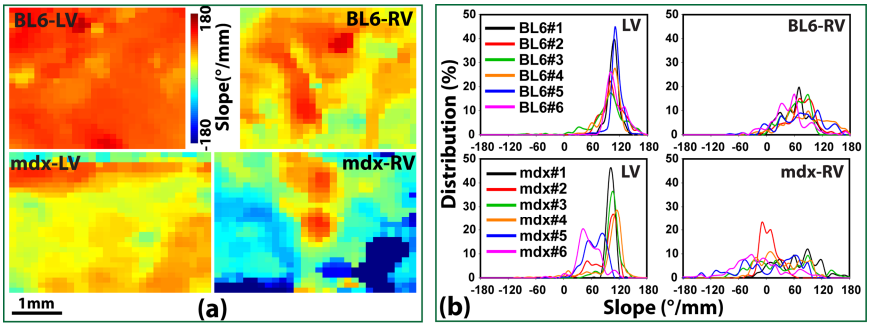

Fig. 3. (a) Examples of color-coded "slopes" of fiber orientation change with depth in the LV and RV of the same hearts shown in Fig. 2. (b) Distributions of the fiber orientation slopes obtained in all six BL6 hearts and six mdx hearts within the same LV and RV evaluation windows as defined in Fig. 2(a). BL6#1 and mdx#6 were the mice used in (a).

Figure 3(b) shows the distributions of the orientation slopes obtained in all experimental animals. The regions with fitting R^2<0.6 and RMSE>10° were not used in the calculation. Overall, the linear fitting in the mdx heart had R^2 = 0.81 ± 0.05 and RMSE = 8.19° ± 1.54° in the LV, and R^2 = 0.64 ± 0.10 and RMSE = 8.99° ± 1.28° in the RV. These fitting performance was similar to those of the BL6 heart: R^2 = 0.82 ± 0.03 and RMSE = 8.25° ± 0.47° in the LV, and R^2 = 0.68 ± 0.08 and RMSE = 8.51° ± 1.91° in the RV. The distributions in the BL6 LV were highly consistent and the rate of orientation change was 100 ~110°/mm at the peak position of the distribution. The distribution in the mdx LV varied among six mice with three hearts showing similar distributions as that of the BL6 heart; whereas the other three had broader distributions and a shift toward smaller slope values. Although the distributions in the RV were generally broader than that in the LV, the BL6 hearts still showed quite consistent distributions with positive slope values in more than 96.2% of the RV regions. However, all mdx RV curves showed much broader distributions with 38.8% of the mdx RV had negative slope values (−38.3 ± 34.0°/mm in average).

Biomedical Optics EXPRESS

Figure 4 shows the group comparison of the mean slope of the orientation change over depth obtained in all hearts. All the hearts showed "positive" slopes in the LV. The mdx group had smaller slope values (86.4°/mm ± 20.4°/mm) than the BL6 group (104.4°/mm ± 7.0°/mm) in the LV; but the difference did not reach statistical significance (p = 0.085, Student's t-test). However, the Levene's test indicated that the mdx group had a bigger variance in the slope data of the LV (p = 0.018). The group difference was more drastic in the RV where the variance was similar in both groups (p = 0.075, Levene's test). The group average of the slope was significantly smaller (p = 0.004, Student's t-test) in the mdx RV (20.3 ± 28.4°/mm) than in the BL6 RV (67.9 ± 12.6°/mm).

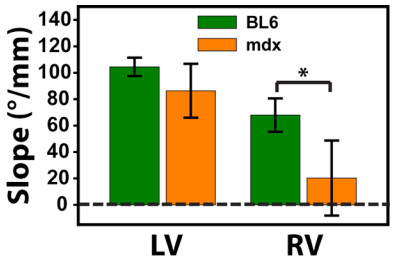

Fig. 4. A group comparison of the average rate of fiber orientation change with depth in the LV and RV of the six BL6 mice and six mdx mice. * p<0.01.

The severe structural remodeling observed in the RV of the 7-month-old mdx mouse is most likely caused by the diaphragm degeneration related pulmonary dysfunction [17, 18]. Deterioration of the respiratory function increases pulmonary vascular resistance which then leads to increased RV stress [17]. This process eventually results in tissue damage in the RV [17, 18]. The global heart structural remodeling can be a direct consequence of the myofiber damage in the RV. The large between-animal variations of the fiber organization observed in the LV of the mdx model may be indications of different disease progression in individual mice. More systematic studies are warranted to clarify the pathological process leading from local cardiac muscle damage to changes in the global heart structure.

The ~1.0 mm imaging depth achieved in this study was mainly limited by the 0.85 μm light source. The ventricular wall thickness of the 7-mo mouse heart is ~1.0 mm [19] and the RV wall is thinner than the LV wall. The 1.0 mm depth may not be sufficient to image through the entire LV wall. The imaging depth in heart can be improved by using a longer wavelength (e.g. 1.3 μm). The mdx hearts have similar ventricular wall thicknesses as the controls before 9-month of age [19]. Therefore the significantly different slope in fiber orientation changes over the depth cannot be caused by any differences in the wall thickness. It is important to note that this study only measured the helix angle of the 3D myocardial fiber located within the plane perpendicular to the incident light [2, 8]. Therefore, any orientation changes in planes that are parallel to the incident light were not detected. Imaging the true 3D fiber orientation is necessary to fully characterize the fiber structure changes, which can be realized using a variable-incident angle implementation of the OPT [14].

5. Conclusions

The OPT technology was applied to investigate the structural remodeling in the hearts of the mdx4cv mouse model of the Duchenne cardiomyopathy. OPT revealed significantly altered myocardial fiber organization in the hearts of 7-mo old mdx4cv mice in particular in the RV. This study demonstrated the potential of OPT as a useful imaging technique for studying high-resolution heart structural remodeling in small animal models of heart diseases.

Funding

This work was supported in part by the University of Missouri System Research Board and Department of Defense (MD150133).

COMMENTARY

A New Kid on the Playground of CRISPR DMD Therapy

Dongsheng Duan

Departments of Molecular Microbiology and Immunology and Neurology, School of Medicine, Department of Bioengineering, and Department of Biomedical Sciences, College of Veterinary Medicine, The University of Missouri, Columbia, Missouri.

DUCHENNE MUSCULAR DYSTROPHY (DMD) is the most common lethal muscle disease, affecting approximately 250,000 boys worldwide. The disease is caused by mutations in the *dystrophin* gene. Genetic approaches that can repair or replace the mutated gene may radically change the disease course and improve quality of life. Several mechanistically distinctive types of genetic manipulation strategies are currently being explored for treating DMD.[1,2] These include small molecule read-through of the nonsense stop codon, antisense oligonucleotide–mediated exon skipping of the RNA transcript, adeno-associated virus (AAV)–mediated gene replacement with a <4-kb *microdystrophin* gene and dual-AAV–mediated 6- to 8-kb *minidystrophin* gene therapy, transplantation of heterologous or genetically corrected autologous muscle stem cells, and clustered regularly interspaced short palindromic repeats (CRISPR)–mediated genome editing. Read-through strategy targets the translation step, and it only works for a sub-population of patients. Exon-skipping targets splicing and has to be designed personally for the specific mutation. Both read-through and exon-skipping treatments require repeated administration in order to achieve therapeutic benefits. One read-through drug has been approved in Europe, and one exon-skipping drug has been approved in the United States.[3–5] Dual AAV minidystrophin therapy has the potential to deliver a genetically optimized minigene that is derived from a naturally existing therapeutic gene in mildly affected Becker muscular dystrophy patients. Success has been achieved in the mouse model of DMD by local and systemic delivery.[6,7] AAV microgene therapy delivers a synthetic, highly abbreviated gene that encodes a protein about one-third the size of full-length dystrophin. Systemic microgene therapy has been conducted in the mouse and dog models, and a human trial is slotted for later this year.[8–11] Preclinical studies suggest that a single intravenous injection of an AAV microgene vector may provide lifelong protection in rodents.

CRISPR therapy is a new type of therapy that has emerged in the last few years.[12] It can remove the mutation from the genome. CRISPR therapy has two major components: an endonuclease called CRISPR-associated protein (Cas) and a guide RNA (gRNA) that directs the Cas to the target site for genome cutting. The Cas protein can be divided into two classes and five types.[13] Up to now, CRISPR therapy is mainly based on Cas9, a class 2, type II Cas protein. A flurry of papers published in the last 3 years have established the proof of principle for CRISPR DMD therapy using Cas9.[14–24] Collectively, these studies show effective editing of patient cells *in vitro* and mouse cells *in vivo*. Of high relevance to the development of CRISPR as a therapeutic modality for DMD, several groups delivered the gRNA and Cas9 expression cassette with AAV in mouse models of DMD. Encouragingly, treatment resulted in excellent restoration of dystrophin expression in skeletal muscle and the heart by immunostaining and western blot analysis. Physiological assays also demonstrated improvement of skeletal muscle function.[15–17,21]

A large collection of Cas endonucleases was discovered in the last couple of years.[25–28] Many of these newly emerged Cas proteins are capable of genome editing in eukaryotic cells. They represent a rich mine for CRISPR therapy. The unique properties of different Cas proteins offer unlimited opportunities to meet different therapeutic needs.

*Correspondence: Dr. Dongsheng Duan, Department of Molecular Microbiology and Immunology, One Hospital Drive, Columbia, MO 65212. E-mail: duand@missouri.edu

DOI: 10.1089/humc.2017.075

A study published in *Science Advances* on April 12 explored Cpf1, a class 2 type V Cas protein, for DMD therapy in induced pluripotent stem cells derived from a DMD patient and the mdx mouse model for DMD.[29] This is the first report demonstrating Cpf1 editing in a mammalian model of a human disease. Cpf1 creates sticky ends in the genome and favors pyrimidine-rich sequences. The Cpf1 gRNA is simpler than that of Cas9. The use of a different protospacer-adjacent motif sequence by Cpf1 expands versatility to genome editing. The authors showed that Cpf1 editing effectively restored the disrupted reading frame and yielded a near-full-length dystrophin protein. In induced pluripotent stem cells–derived cardiomyocytes, Cpf1 editing normalized the mitochondrial number and rescued the respiration rate. Re-implantation of Cpf1-corrected mdx zygotes in pseudopregnant females yielded mutation-corrected mice with normal muscle histology and improved muscle function. Off-target analysis suggests that Cpf1 is highly specific. It is also worth pointing out that in contrast to the published CRISPR strategy, which uses two gRNAs to direct Cas9 to two separate locations in the genome for mutation removal, Zhang *et al*. utilized a very creative approach by directing Cpf1 to cut the splicing acceptor site. This allows restoration of dystrophin expression by one cut, instead of two cuts, and hence may greatly improve the efficiency. Taken together, the results reported by Zhang *et al*. raise a high hope to complement existing Cas9 DMD therapy with Cpf1 (and likely other Cas proteins) for future clinical translation.[29]

It took about 8 years from the initial description of exon-skipping in mdx myoblasts to the first in-human clinical trial.[30,31] Similar time was taken from the report of the first engineered *micro-dystrophin* gene to the AAV-mediated local injection in DMD boys.[32,33] It remains to be seen whether CRISPR DMD therapy can follow the same path or may be on the fast track. However, it should be pointed out that there are significant roadblocks ahead of CRISPR therapy, such as off-target toxicity and the immunogenicity of bacteria-derived Cas protein. In the case of CRISPR DMD therapy, there are additional sets of challenges to overcome; for example: How long will therapy last? Will the immune reaction to the Cas protein eventually eliminate the treated dystrophin-positive muscle cells? Will CRISPR therapy improve heart function? Will gene editing effectively target muscle stem cells? Will AAV CRISPR cause any toxicity following long-term *in vivo* expression? Will CRISPR editing work in large mammals? For Cpf1, one still has to show that it can be used as a post-natal therapy for muscle diseases using viral and/or nonviral mediated gene transfer.[34]

ACKNOWLEDGMENTS

The author thanks Anna Azvolinsky, Rhonda Bassel-Duby, Shi-jie Chen, Chengzu Long, and Eric Olson for helpful discussion. DMD CRISPR therapy in the Duan lab is supported by the National Institutes of Health (AR-69085), Department of Defense (MD150133) and Hope for Javier.

AUTHOR DISCLOSURE

D.D. is a member of the scientific advisory board for Solid Biosciences and an equity holder of Solid Biosciences. The Duan lab has received research support from Solid Biosciences.

REFERENCES

1. Bengtsson NE, Seto JT, Hall JK, et al. Progress and prospects of gene therapy clinical trials for the muscular dystrophies. Hum Mol Genet 2016; 25:R9–17.
2. Duan D. Dystrophin gene replacement and gene repair therapy for Duchenne muscular dystrophy in 2016. Hum Gene Ther Clin Dev 2016;27:9–18.
3. Muntoni F, Fletcher S, Wilton S. Response to "Railroading at the FDA". Nat Biotechnol 2017;35: 207–209.
4. Mendell JR. Eteplirsen improves function and partially restores. Ann Neurol 2017;81:164–165.
5. Haas M, Vlcek V, Balabanov P, et al. European Medicines Agency review of ataluren for the treatment of ambulant patients aged 5 years and older with Duchenne muscular dystrophy resulting from a nonsense mutation in the dystrophin gene. Neuromuscul Disord 2015;25:5–13.
6. Lai Y, Yue Y, Liu M, et al. Efficient *in vivo* gene expression by trans-splicing adeno-associated viral vectors. Nat Biotechnol 2005;23:1435–1439.
7. Zhang Y, Yue Y, Li L, et al. Dual AAV therapy ameliorates exercise-induced muscle injury and functional ischemia in murine models of Duchenne muscular dystrophy. Hum Mol Genet 2013;22: 3720–3729.
8. Yue Y, Pan X, Hakim CH, et al. Safe and bodywide muscle transduction in young adult Duchenne muscular dystrophy dogs with adeno-associated virus. Hum Mol Genet 2015;24:5880–5890.
9. Bostick B, Shin J-H, Yue Y, et al. AAV-microdystrophin therapy improves cardiac performance in aged female mdx mice. Mol Ther 2011;19:1826–1832.
10. Gregorevic P, Allen JM, Minami E, et al. rAAV6-microdystrophin preserves muscle function and extends lifespan in severely dystrophic mice. Nat Med 2006;12:787–789.
11. Solid Biosciences. Press Release. https://solidbio.com/content/stepsforward-duchenne-muscular-dystrophy (last accessed May 24, 2017).
12. Zhang F. CRISPR-Cas9: prospects and challenges. Hum Gene Ther 2015;26:409–410.
13. Makarova KS, Wolf YI, Alkhnbashi OS, et al. An updated evolutionary classification of CRISPR-Cas systems. Nat Rev Microbiol 2015;13:722–736.

14. Long C, McAnally JR, Shelton JM, et al. Prevention of muscular dystrophy in mice by CRISPR/Cas9-mediated editing of germline DNA. Science 2014;345:1184–1188.

15. Long C, Amoasii L, Mireault AA, et al. Postnatal genome editing partially restores dystrophin expression in a mouse model of muscular dystrophy. Science 2016;351:400–403.

16. Nelson CE, Hakim CH, Ousterout DG, et al. *In vivo* genome editing improves muscle function in a mouse model of Duchenne muscular dystrophy. Science 2016;351:403–407.

17. Tabebordbar M, Zhu K, Cheng JK, et al. *In vivo* gene editing in dystrophic mouse muscle and muscle stem cells. Science 2016;351:407–411.

18. Ousterout DG, Kabadi AM, Thakore PI, et al. Multiplex CRISPR/Cas9-based genome editing for correction of dystrophin mutations that cause Duchenne muscular dystrophy. Nat Commun 2015; 6:6244.

19. Wojtal D, Kemaladewi DU, Malam Z, et al. Spell checking nature: versatility of CRISPR/Cas9 for developing treatments for inherited disorders. Am J Hum Genet 2016;98:1-–2.

20. Xu L, Park KH, Zhao L, et al. CRISPR-mediated Genome Editing Restores Dystrophin Expression and Function in mdx Mice. Mol Ther 2016;24:564–569.

21. Bengtsson NE, Hall JK, Odom GL, et al. Muscle-specific CRISPR/Cas9 dystrophin gene editing ameliorates pathophysiology in a mouse model for Duchenne muscular dystrophy. Nat Commun 2017; 8:14454.

22. Li HL, Fujimoto N, Sasakawa N, et al. Engineered nuclease mediated genetic correction in iPSCs derived from Duchenne muscular dystrophy patient. Mol Ther 2014;22:S124–S124.

23. Young CS, Hicks MR, Ermolova NV, et al. A Single CRISPR-Cas9 deletion strategy that targets the majority of DMD patients restores dystrophin function in hiPSC-derived muscle cells. Cell Stem Cell 2016;18:533–540.

24. Maggio I, Stefanucci L, Janssen JM, et al. Selection-free gene repair after adenoviral vector transduction of designer nucleases: rescue of dystrophin synthesis in DMD muscle cell populations. Nucleic Acids Res 2016;44:1449–1470.

25. Burstein D, Harrington LB, Strutt SC, et al. New CRISPR-Cas systems from uncultivated microbes. Nature 2017;542:237–241.

26. Abudayyeh OO, Gootenberg JS, Konermann S, et al. C2c2 is a single-component programmable RNA-guided RNA-targeting CRISPR effector. Science 2016;353.

27. Shmakov S, Abudayyeh OO, Makarova KS, et al. Discovery and functional characterization of diverse class 2 CRISPR-Cas systems. Mol Cell 2015;60:385–397.

28. Zetsche B, Gootenberg JS, Abudayyeh OO, et al. Cpf1 is a single RNA-guided endonuclease of a class 2 CRISPR-Cas system. Cell 2015;163:759–771.

29. Zhang Y, Long C, Li H, et al. CRISPR-Cpf1 correction of muscular dystrophy mutations in human cardiomyocytes and mice. Sci Adv 2017;3: e1602814.

30. Wilton SD, Lloyd F, Carville K, et al. Specific removal of the nonsense mutation from the mdx dystrophin mRNA using antisense oligonucleotides. Neuromuscul Disord 1999;9:330–338.

31. van Deutekom JC, Janson AA, Ginjaar IB, et al. Local dystrophin restoration with antisense oligonucleotide PRO051. N Engl J Med 2007;357: 2677–2686.

32. Yuasa K, Miyagoe Y, Yamamoto K, et al. Effective restoration of dystrophin-associated proteins *in vivo* by adenovirus-mediated transfer of truncated dystrophin cDNAs. FEBS Lett 1998;425:329–336.

33. Mendell JR, Rodino-Klapac LR, Rosales XQ, et al. Sustained alpha-sarcoglycan gene expression after gene transfer in limb-girdle muscular dystrophy, type 2D. Ann Neurol 2010; 68:629–638.

34. Zetsche B, Heidenreich M, Mohanraju P et al. Multiplex gene editing by CRISPR-Cpf1 using a single crRNA array. Nat Biotechnol 2017;35: 31–34.

Received for publication April 28, 2017;
accepted after revision May 8, 2017.

Published online: May 8, 2017.